

Potassium Hydride-mediated Hydrodesulfurization Catalyzed by Cobalt

by

Asama Vorapattanapong

A thesis submitted in partial fulfillment of the requirements for the degree of

Doctor of Philosophy

Department of Chemistry
University of Alberta

© Asama Vorapattanapong, 2018

Abstract

New triethylphosphoranimide-supported thiolate-capped clusters of cobalt and nickel were synthesized, isolated, and characterized as part of an investigation into homogeneous catalysts for the hydrodesulfurization of refractory organosulfur substrates. In particular, *p*-toluenethiolate and *i*-propylthiolate ligands were installed onto heterocubane phosphoranimide-supported cobalt and nickel halides *via* simple room temperature metathesis. The compounds were isolated, purified, and characterized principally by elemental analysis and X-ray crystallography.

The thiolate clusters, along with analogous phosphoranimide clusters capped by Cl, NPEt₃, and Me anions, were investigated as precatalysts for hydrodesulfurization (HDS) under mild conditions. All of these clusters, functioning as homogeneous catalysts, promote HDS under very mild reaction conditions (1 atm H₂ and 110 °C) in the presence of stoichiometric amount of KH to afford high conversion within 2 hours. Among these clusters, the chloride-capped cobalt cluster yields the highest conversion, giving a high yield of the fully desulfurized product. The high reactivity of the chloride-capped cluster led us to explore simple late transition metal halides (Fe, Co, Ni, and Cu) as precatalyst for our KH-mediated desulfurization. Surprisingly, these metal halides, likely function as heterogeneous catalysts, are also competent precatalysts, giving high conversions, albeit not as efficiently as the phosphoranimide-supported clusters.

As part of our investigation into the mechanism of the hydrodesulfurization reactions catalyzed by these heterocubane clusters, we have synthesized and partially characterized various phosphoranimide-supported cobalt hydride and sulfide clusters. The cobalt hydride and sulfide clusters were prepared from either the homoleptic cobalt bis(phosphoranimide) cluster or the simple chloride cluster using a range of hydride and sulfide sources. While these clusters were never isolated as pure materials, cobalt hydride and sulfide complexes were partially characterized *via* IR spectroscopy, as well as the characterization of the reaction by-products.

In addition to the synthesis of putative intermediates, the mechanistic roles of the transition metal and KH, along with the nature of the active catalysts, were investigated. Control experiments indicate that potassium hydride itself, as the sole reductant, remains competent for the “hydrogenolysis” of C–S bonds. Desulfurization by KH in the absence of hydrogen and catalyst can occur *via* two pathways: *ortho* deprotonation and nucleophilic aromatic substitution at the *ipso*-carbon of DBT. In addition to the nucleophilic hydride, the potassium cation plays an important role in activating the substrate by π -coordination. Augmenting the K^+ ion, the transition metal catalyst further promotes the desulfurization of DBT. In contrast, the presence of H_2 has only minimal effect on any of the KH-assisted desulfurization reactions.

Finally, the hydrogenolysis of C–S, C–O, C–N, and C–Br bonds of a range of heteroaromatic substrates were explored using catalytic $CoCl_2$ and KH under very mild reaction conditions (110 °C). Under these conditions, the system desulfurizes a range of diarylsulfides and promotes the hydrogenolysis of aromatic C–O, C–N, and C–Br bonds.

“We didn’t realize we were making memories, we just knew we were having fun.”

-Winnie the Pooh

This thesis is dedicated to N. Gelbara....

Acknowledgments

I would like to offer my sincerest gratitude to Professor Jeffrey M. Stryker for providing me with the opportunity to pursue my graduate research in his lab and also for his support and advice throughout the entire time. I would also like to extend my utmost appreciation to my supervisory committee and extended members for their guidance throughout my program.

I further extend my thanks to the current and past Stryker group members particularly, Dr. Robin Hamilton, Dr. Kseniya Revunova, Dr. Orain Brown, David Scott, Fiona Nkala, Aukse Brazianate, Jose Rodriguez, and Mark Aloisio, for their relentless help, support, and friendship. More importantly, I thank them for the countless coffee breaks over the past five years!

I would also like to acknowledge the chemistry services staff who have helped me through my numerous requests and questions, particularly, Wayne Moffat, Jennifer Jones, Katazhyna Haidukevich, Ema Stretenovic, Jeffrey Kwansny, Mark Miskolzie, Nupur Dabral, Dr. Bob McDonald, Dr. Mike Ferguson, and Jason Dibbs.

Lastly, I would like to thank my family and friends, particularly, my mom and dad, Ice, Akom, Hang Zhou, and Dorothea Mung, for their unyielding support and faith!

Table of Contents

Abstract.....	ii
Acknowledgments	v
List of Tables	xii
List of Figures.....	xiv
List of Schemes.....	xvii
List of Equations	xix
List of Abbreviations	xx
Prologue: Unconventional Approaches to Hydrodesulfurization	1
1. Catalytic Hydrodesulfurization: Heterogeneous Catalysts and Homogeneous Model Complexes.....	4
1.1 Introduction to hydrodesulfurization (HDS).....	4
1.1.1 Organosulfur complexes in crude oil	5
1.2 Heterogeneous catalysts for HDS.....	7
1.2.1 Catalyst structure	8
1.2.2 Binding modes of thiophenes, benzothiophenes, and dibenzothiophenes.....	11
1.2.3 Limitations and recent improvements in heterogeneous HDS catalysis	12
1.3 Homogeneous Organometallic Complexes for C–S Bond Activation	14
1.3.1 C–S bond cleavage by 2 nd and 3 rd row transition metal complexes and clusters	15
1.3.2 Modeling HDS using first-row transition metal complexes.....	17
1.4 Catalytic desulfurization with homogeneous complexes	25
1.4.1 Ir(triphos)H complex for catalytic desulfurization of DBT.....	25
1.4.2 Desulfurization of DBT using [Ni] and stoichiometric Grignard reagents	26

1.4.3 Stryker group's KH-mediated desulfurization	28
1.5 Conclusion.....	29
2. Rationale for Catalyst Design and the Syntheses of Transition Metal Phosphoranimide Clusters	30
2.1 Understanding polynuclear complexes	30
2.1.1 Heterogeneous catalysts and the discovery of clusters.....	30
2.1.2 Design and synthesis of low-coordinate transition metal clusters.....	33
2.2 Design of homogeneous polynuclear clusters for hydrodesulfurization	34
2.2.1 Phosphoranimide ligands for ancillary ligand free clusters.....	35
2.2.2 Syntheses of phosphoranimide ligands and metal clusters.....	38
2.2.3 Previous "Stryker group" transition metal phosphoranimide cluster synthesis	41
2.2.4 Syntheses of the Co heterocubane complexes.....	44
2.3 Results and Discussion.....	45
2.3.1 Synthesis of thiolate-capped cobalt and nickel triethylphosphoranimide heterocubane complexes	45
2.3.2 Synthesis of HDS reaction intermediates: sulfide- and hydride-capped phosphoranimide clusters of cobalt.....	51
2.4 Conclusion.....	61
3. Reactivity of Phosphoranimide-supported Heterocubane Clusters of Cobalt in Hydride-mediated Desulfurization	62
3.1 Previous HDS work using cobalt phosphoranimide complexes.....	62
3.2 Results and Discussion	65
3.2.1 Optimization of KH-mediated desulfurization of DBT by cobalt clusters 40 and 60	65
3.2.2 The reactivity of other neutral Co ²⁺ and Ni ²⁺ phosphoranimide clusters in KH-mediated desulfurization of DBT	66
3.2.3 Solvent effects on the tetranuclear cobalt triethylphosphoranimide clusters	71

3.2.4 Insights to the nature of the phosphoranimide cobalt clusters in hydride-assisted HDS	73
3.2.4.1 Identifying the nuclearity of the active catalyst.....	73
3.2.4.2 Homogeneity tests for cobalt catalysts derived from 40 , 53a , and 69	78
3.2.5 Hydride-mediated desulfurization of DBT catalyzed by cobalt (II) halides	80
3.2.6 KH-mediated, transition metal halide catalyzed desulfurization of DBT	81
3.3 Conclusion.....	82
4. Establishing the Role of the Base and Transition metals in KH-Mediated Hydrodesulfurization.....	84
4.1 Objectives.....	84
4.2 Results and Discussion	86
4.2.1 Control reactions to establish the role of the cobalt clusters, KH, and H ₂	86
4.2.2 Role of KH: Deprotonation and subsequent C–S bond cleavage of DBT	90
4.2.2.1 Other strong bases for the desulfurization of DBT promoted by cationic cobalt cluster 40	92
4.2.2.2 Potassium ion effect in KH-mediated desulfurization.....	93
4.2.3.3 Proposed HDS mechanism I : Ortho-deprotonation.....	97
4.2.3 Proposed Mechanism II : Nucleophilic aromatic substitution by KH.....	99
4.2.3.1 Desulfurization reactions with dialkyl dibenzothiophene	102
4.2.3.2 Synthesis of KD: further investigation into nucleophilic aromatic substitution by KH.....	103
4.2.3.3 Synthetic KH is not commercial KH	106
4.2.4 Role of the transition metal catalysts: oxidative addition “vs.” Lewis acid activation	108
4.2.4.1 Proposed mechanisms of cobalt-catalyzed, KH-mediated hydrodesulfurization....	110
4.2.5 Simple metal salt catalysis: the MX ₂ –KH system for deep desulfurization.....	115

4.2.6 Substrate scope for the CoCl ₂ –KH system.....	116
4.3 Conclusion.....	121
4.4 Concluding Remarks and Future Works.....	122
5. Experimental.....	124
5.1 General Procedures.....	124
5.2 Instrumentation.....	125
5.3 Experimental Procedures for Chapter 2.....	127
5.3.1 Synthesis of [CoCl(NPEt ₃) ₄ 53a	128
5.3.2 Synthesis of [CoMe(NPEt ₃) ₄ 60	129
5.3.3 Synthesis of [CoMe(NPEt ₃) ₄ PF ₆ 40	129
5.3.4 Synthesis of [Co(NPEt ₃) ₂] ₄ 69	130
5.3.5 Syntheses of [MSR(NPEt ₃) ₄	131
5.3.6 Characterization of intermediate Co–H clusters prepared from cationic methylcobalt cluster 40	133
5.3.6.1 Synthesis of the Co–H cluster.....	133
5.3.6.2 Analysis of the reactor volatiles using gas-phase FT-IR spectroscopy	133
5.3.6.3 Analysis of the solution of Co–H clusters using FT-IR spectroscopy.....	134
5.3.7 Synthesis and analysis of the Co–H intermediate prepared from [Co(NPEt ₃) ₂] ₄ 69 and H ₂	135
5.3.8 Synthesis of the Co–H cluster from [Co(NPEt ₃) ₂] ₄ 69 and 9-BBN.....	136
5.3.9 Synthesis of the Co–H cluster with [Co(NPEt ₃) ₂] ₄ 69 and HBPin.....	137
5.3.10 Synthesis of cobalt hydride cluster 77 using [CoCl(NPEt ₃) ₄ 53a and LiAlH ₄	138
5.3.11 Synthesis of cobalt deuteride cluster 154 using [CoCl(NPEt ₃) ₄ 53a and LiAlD ₄	139
5.3.12 Synthesis of cobalt sulfide cluster 80 from [Co(NPEt ₃) ₂] ₄ 69 and elemental sulfur	140

5.3.13 Synthesis of the trityl thiolate-capped cobalt cluster 84 using [CoCl(NPEt ₃) ₄ 53a	141
5.4 Experimental Procedures for Chapter 3	142
5.4.1 HDS reactions with cobalt cluster, hydrogen, and KH	142
5.4.2 TOF vs. concentration of cobalt clusters 40 and 69	144
5.4.3 Solution molecular weight determinations for cobalt clusters 40 and 69 by the Signer method	145
5.4.4 Homogeneity test for cobalt clusters 40 , 53a , and 69	148
5.4.5 HDS reactions with other transition metal halides, hydrogen, and KH	149
5.5 Experimental Procedures for Chapter 4	149
5.5.1 HDS reactions catalyzed by cobalt clusters 40 , 53a , and 69	149
5.5.2 Dibenzothiophene HDS promoted by KH in the presence and absence of H ₂	150
5.5.3 H ₂ production and detection during “hydrogen-free” HDS	151
5.5.4 Base-mediated HDS catalyzed by cationic cluster 40 : variation of the base	154
5.5.5 Potassium-ion effect: HDS reactions in the presence of 18-crown-6	155
5.5.6 Potassium-ion effects. Catalyst-free HDS reactions using other potassium sources	155
5.5.7 Isotopic labeling experiments: D ₂ and KD	156
5.5.7.1 Desulfurization under deuterium catalyzed by cobalt clusters 40 , 60 , and 69	156
5.5.7.2 Desulfurization under deuterium in the absence of transition metal source	159
5.5.8 HDS reactions of 4,6-dimethyl DBT promoted by KH in the presence and absence of homoleptic cluster 69	160
5.5.9 Syntheses of KH and KD	161
5.5.10 HDS reactions mediated by KD	162
5.5.10.1 KD-mediated HDS of DBT catalyzed by cobalt cluster 53a	162
5.5.10.2 HDS reaction of 4,6-Me ₂ DBT catalyzed by cobalt cluster 69	164

5.5.10.3 HDS reaction of DBT with KD in the absence of catalyst and hydrogen	166
5.5.10.4 KD-promoted HDS of 4,6-Me ₂ DBT in the absence of catalyst.....	168
5.5.12 Role of the transition metal catalyst.	175
5.5.12.1 In situ synthesis of Ni(DBT)(iPrAr ₂ Im) ₂ (127) and DBT desulfurization.....	175
5.5.12.2 Synthesis of manganese complex 6	176
5.5.12.3 Hydride-mediated HDS reaction of manganese complex 6	177
5.5.13 Kinetic profile of hydride-mediated desulfurization of DBT catalyzed by cobalt cluster 69	178
5.5.14 Hydride-mediated HDS of DBT in the presence of elemental sulfur.....	179
5.5.15 KH-promoted desulfurization of DBT catalyzed by various metal complex salts in the absence of hydrogen	179
5.5.16 Substrate scope for CoCl ₂ /KH system.....	180
References	184
Appendix	192

List of Tables

Table 1.1 Bond energy for different Y – S bond (Y = S or C).....	6
Table 2.1 Selected bond lengths and angles for cobalt heterocubane complex 61	49
Table 2.2 Selected bond lengths and angles for cobalt heterocubane complex 63	49
Table 2.3 Selected bond lengths and angles for nickel heterocubane cluster 62	51
Table 3.1 HDS reactions with [Co(NPEt ₃)Me] ₄ (60) and [Co(NPEt ₃)Me] ₄ PF ₆ (40).	63
Table 3.2 Catalytic HDS with phosphoranimido cobalt clusters 40 and 60 in the presence of stoichiometric potassium hydride yield high conversion of DBT to biphenyl.	66
Table 3.3 Desulfurization of transition metal thiolate heterocubane complexes.	68
Table 3.4 Hydride-mediated desulfurization promoted by phosphoranimide-supported cobalt clusters in toluene.	72
Table 3.5 Solution molecular weight of cluster 40	77
Table 3.6 Solution molecular weight of cluster 69	77
Table 3.7 Mercury puddle test for tetranuclear cobalt clusters 40 , 53a , and 69	79
Table 3.8 Desulfurization of DBT catalyzed by cobalt (II) halide.....	81
Table 3.9 Desulfurization of DBT catalyzed by late transition metal halides.....	82
Table 4.1 Control reactions of KH.....	85
Table 4.2 Control reactions using the cationic cobalt cluster 40	86
Table 4.3 Desulfurization reactions of DBT in the presence and absence different reagents. .	88
Table 4.4 Desulfurization of DBT in the presence of strong alkali metal bases.....	93
Table 4.5 Desulfurization in the presence of 18-crown-6.	94
Table 4.6 Desulfurization of DBT with ‘benign’ source of K ⁺ ion.....	95
Table 4.7 Desulfurization of DBT with synthesized and commercial KH.....	107
Table 4.8 Desulfurization of DBT catalyzed by cobalt (II) halide.....	109
Table 4.9 Desulfurization of DBT catalyzed by transition metal halide.....	116
Table 5.1 Mass of starting materials; yields of products for clusters 61–64	132
Table 5.2 HDS of dibenzothiophene as a function of cobalt cluster under 1 atm H ₂	143
Table 5.3 Changes in turnover frequency for hydride-mediated HDS reactions as a function of precatalyst concentration.	144
Table 5.4 Turnover frequency of hydride-mediated HDS as a function of the concentration of precatalyst cluster 69	145
Table 5.5 Amounts of standard and cationic cluster 40 and volumes of solvent for determination of solution molecular weight.	146
Table 5.6 Calculated and experimental molecular weights for 40 in solution.	147
Table 5.7 Amounts of standard and cationic cluster 69 and volumes of solvent for determination of solution molecular weight.....	147
Table 5.8 Calculated and experimental molecular weights for 69 in solution.	147
Table 5.9 Homogeneity tests for clusters 40 , 53a , and 69	148
Table 5.10 HDS reactions with other transition metal halides as the precatalyst.	149
Table 5.11 HDS reactions in the absence of KH.....	150
Table 5.12 Transition metal-free, potassium hydride mediated desulfurization of DBT.....	151
Table 5.13 Catalytic HDS reactions under hydrogen, as a function of the base.	154
Table 5.14 18-crown-6 inhibits catalytic hydrodesulfurization by potassium hydride.....	155

Table 5.15 Comparison of HDS reactivity of sodium hydride and potassium hydride.....	156
Table 5.16 KH-mediated desulfurization of 4,6-dimethyl DBT.	161
Table 5.17 Syntheses of KD and KH from potassium metal and naphthalene.	162
Table 5.18 Desulfurization of DBT with synthesized and commercial KH.....	169
Table 5.19 Aliquot HDS reactions catalyzed by homoleptic cluster 69	178
Table 5.20 Desulfurization of DBT in the absence of hydrogen.....	180
Table 5.21 Substrate scope for CoCl ₂ -KH system.	181

List of Figures

Figure 1.1 Crude oil is made up of a variety of organosulfur moieties. (R, R' = alkyl groups, n = number of alkyl substituents).....	6
Figure 1.2 Proposed surface structure of Co-Mo-S industrial catalyst.	10
Figure 1.3 Proposed mechanism for Co-Mo-S industrial catalyst.	11
Figure 1.4 Different bonding modes of aromatic substrates.	12
Figure 1.5 Reactivity of transition metal sulfides in the desulfurization of DBT.	13
Figure 1.6 Low-valent nickel cluster 13 readily cleaves the C–S bonds of DBT.	19
Figure 1.7 Pentanuclear nickel hydride cluster for desulfurization.....	22
Figure 1.8 Binding of the sulfur atom weakens the C–S bond.....	24
Figure 1.9 Ni catalyst for desulfurization of DBT.	27
Figure 1.10 The ethyl/iso-propyl ligand on the Ni center β -hydride eliminates to form Ni hydride complex.....	27
Figure 1.11 Cobalt and nickel catalysts for the KH-mediated desulfurization.	28
Figure 2.1 Industrial processes such as: (a) hydrodesulfurization that removes sulfur from crude oil use heterogeneous catalyst, (b) Claus process that converts H ₂ S to elemental sulfur, and (c) Contact process produces sulfuric acid from elemental sulfur.	30
Figure 2.2 Representation of naked and molecular clusters.....	32
Figure 2.3 Examples of polymetallic complexes 47 and 48	34
Figure 2.4 The phosphoranimide ligand has multiple binding modes.	35
Figure 2.5 Ethyl substituents lead to tetrameric heterocubane cluster 49 whereas bulky ^t butyl groups forms the dimeric μ^2 -phosphoranimide complex 50	37
Figure 2.6 Tolman cone angles for cyclopentadienyl and tri(^t butyl)phosphoranimide.....	37
Figure 2.7 A library of transition metal phosphoranimide clusters synthesized by the Stryker group members.	43
Figure 2.8 ORTEP diagrams of (a) [Co(NPEt ₃)(S ⁱ Pr)] ₄ 61 and (b) [Co(NPEt ₃)S(C ₆ H ₅ (CH ₃))] ₄ 63 . The thermal ellipsoids are shown at 30% probability, and hydrogen atoms are omitted for clarity. R ₁ (61) = 0.0438, R _w (61) = 0.1185, R ₁ (63) = 0.0351, R _w (63) = 0.1008.....	48
Figure 2.9 ORTEP diagrams of [Ni(NPEt ₃)(S ⁱ Pr)] ₄ (62). The thermal ellipsoids are shown at 30% probability, and hydrogen atoms are omitted for clarity. R ₁ = 0.0513, R _w = 0.1512.....	50
Figure 2.10 Heterolytic cleavage of H ₂ with metal heteroatom bond.	53
Figure 2.11 X-ray crystal structure of phosphoranimido borane complex 74 . The thermal ellipsoids are shown at 30% probability, and hydrogen atoms are omitted for clarity. R ₁ = 0.0512, R _w = 0.1447.....	55
Figure 2.12 The synthesis and preliminary solid-state structure report of pinacolboronate-capped cobalt cluster 76 . The thermal ellipsoids are shown at 30% probability, where hydrogen atoms and the ethyl substituents on the phosphoranimide are omitted for clarity. R ₁ = 0.0794, R _w = 0.2562.....	56
Figure 2.13 The synthesis of a bimetallic μ^2 -bridging sulfide complex.	58

Figure 2.14 The metathesis reaction between the chloride-capped cluster 53a and the KSCPh ₃ yields the tritylthiolate cluster 84 . The thermal ellipsoids are shown at 30% probability, and the hydrogen atoms and the ethyl substituents on the phosphoramidate are omitted for clarity. $R_1 = 0.0515$, $R_w = 0.1511$	60
Figure 3.1 Polynuclear clusters for the desulfurization of organosulfur compounds.	62
Figure 3.2 The cobalt heterocubane clusters adopt a pseudo-tetrahedral structure where a Co^{3+} center would have one vacant orbital (b).	64
Figure 3.3 TOF dependence on the concentration of cluster 40 . (Reaction conditions: 2.5 KH, 1 atm H ₂ , and 4 hours).	75
Figure 3.4 TOF dependence on the concentration of cluster 69 . (Reaction conditions: 2.5 KH, 1 atm H ₂ , and 2 hours).	75
Figure 4.1 The cobalt phosphoramidate clusters as precatalyst for HDS reactions.	84
Figure 4.2 ¹ H NMR spectrum of KH and DBT suspension heated for 2 hours at 110 °C.	92
Figure 4.3 Potassium cation presumably binds to the arene ring(s) or the sulfur atom of DBT.	96
Figure 4.4 Alkyl substituted DBT, especially at the 4 and 6 positions, are resistant to sulfur extrusion.	103
Figure 4.5 Secondary electron SEM images of synthesized and purified KH.	108
Figure 4.6 The conversion of DBT to biphenyl in 2 hours at 1 atm H ₂ and 110 °C using 0.5 mol% the bis(phosphoramidate) cobalt cluster 69	112
Figure 5.1 Gas-phase FT-IR spectrum of the volatiles from the reaction of cluster 40 and H ₂	134
Figure 5.2 The apparatus for the Signer method.	146
Figure 5.3 ¹ H NMR spectrum of KH/DBT suspension prior to heating (room temperature).	152
Figure 5.4 ¹ H NMR spectrum of KH and DBT suspension after heating for 2 h at 80 °C.	153
Figure 5.5 ¹ H NMR spectrum of KH and DBT suspension after heating for 2 h at 110 °C.	153
Figure 5.6 ¹ H and ² H NMR spectra of biphenyl from HDS reaction in the presence of KH, D ₂ , and catalyst 53a	157
Figure 5.7 ² H NMR spectrum of biphenyl from HDS reaction in the presence of KH, D ₂ , and catalyst 69	158
Figure 5.8 ² H NMR spectrum of biphenyl from HDS reaction in the presence of KH, D ₂ , and catalyst 40	158
Figure 5.9 ¹ H and ² H NMR spectra of 2-phenylthiophenol.	160
Figure 5.10 ¹ H and ² H NMR spectra of biphenyl.	163
Figure 5.11 ¹ H and ² H NMR spectra of 3,3'-dimethyl biphenyl.	165
Figure 5.12 ¹ H and ² H NMR spectra of biphenyl.	167
Figure 5.13 (a) The desulfurization of DBT using purified resulted in a red suspension. (b) When synthesized KH was used, the suspension has a blue color.	169
Figure 5.14 Secondary electrons SEM image of purified KH at magnification 5.00kx (scale: 1 μm).	170
Figure 5.15 Secondary electrons SEM image of purified KH at magnification 20.00kx (scale: 200 nm).	171
Figure 5.16 Secondary electrons SEM image of synthesized KH at magnification 5.00kx (scale: 1 μm).	172
Figure 5.17 Secondary electrons SEM image of synthesized KH at magnification 20.00kx (scale: 200 nm).	173

Figure 5.18 EDX plot of purified KH (a) vs. synthesized KH (b). 174

List of Schemes

Scheme 1.1	16
Scheme 1.2	16
Scheme 1.3	17
Scheme 1.4	18
Scheme 1.5	18
Scheme 1.6	19
Scheme 1.7	19
Scheme 1.8	20
Scheme 1.9	21
Scheme 1.10	23
Scheme 1.11	24
Scheme 1.12	25
Scheme 1.13	26
Scheme 1.14	27
Scheme 2.1	32
Scheme 2.2	38
Scheme 2.3	39
Scheme 2.4	39
Scheme 2.5	39
Scheme 2.6	40
Scheme 2.7	40
Scheme 2.8	41
Scheme 2.9	41
Scheme 2.10	44
Scheme 2.11	45
Scheme 2.12	47
Scheme 2.13	52
Scheme 2.14	54
Scheme 2.15	54
Scheme 2.16	55
Scheme 2.17	55
Scheme 2.18	57
Scheme 2.19	59
Scheme 2.20	59
Scheme 3.1	65
Scheme 3.2	69
Scheme 3.3	70
Scheme 3.4	74
Scheme 3.5	77
Scheme 3.6	78
Scheme 4.1	85
Scheme 4.2	90

Scheme 4.3	96
Scheme 4.4	98
Scheme 4.5	99
Scheme 4.6	99
Scheme 4.7	100
Scheme 4.8	101
Scheme 4.9	101
Scheme 4.10	103
Scheme 4.11	111
Scheme 4.12	111
Scheme 4.13	114
Scheme 4.14	114
Scheme 4.15	115
Scheme 4.16	120
Scheme 5.1	176

List of Equations

Equation 1.1	22
Equation 1.2	28
Equation 3.1	67
Equation 3.2	70
Equation 3.3	80
Equation 4.1	87
Equation 4.2	89
Equation 4.3	104
Equation 4.4	104
Equation 4.5	105
Equation 4.6	105
Equation 4.7	110
Equation 4.8	110

List of Abbreviations

Å	Angstroms
atm	Atmosphere
Bu	Butyl
cm ⁻¹	Wavenumbers
COD	1,5-Cyclooctadiene
Cp	Cyclopentadienyl
Cp*	Pentamethylcyclopentadienyl
Cy	Cyclohexyl
DBT	Dibenzothiophene
DCM	Dichloromethane
DFT	Density functional theory
DMSO	Dimethyl sulfoxide
e	Electron
equiv.	Equivalents
Et	Ethyl
FT	Fourier transform
g	Grams
h	Hours
HBPin	Pinacolborane
HDS	Hydrodesulfurization
HOMO	Highest occupied molecular orbital
IR	Infrared

kcal	Kilocalories
KDA	Potassium di-isopropyl amide
KTMP	Potassium tetramethylpiperidide
LDA	Lithium di-isopropyl amide
LiTMP	Lithium tetramethylpiperidide
L _n	Ligand
LUMO	Lowest unoccupied molecular orbital
M	Metal
Me	Methyl
MEDBT	4,6-Dimethyl dibenzothiophene
mg	Milligram
min	Minutes
mL	Millilitre
mmol	Millimole
mol	Moles
NHC	N-heterocyclic carbene
NMR	Nuclear magnetic resonance
Ph	Phenyl
pm	Picometers
ppm	Parts per million
Pr	Propyl
R	Generic alkyl/aryl substituent
RT	Room temperature

solv	Solvent
T	Temperature
^t Bu	Tert-butyl
THF	Tetrahydrofuran
TMS	Trimethylsilyl
TOF	Turnover frequency
tol	Toluene
<i>xs</i>	Excess
σ -BM	Sigma bond metathesis
σ -CAM	Sigma complex assisted metathesis
μ	Mu (bridging mode)
$^{\circ}\text{C}$	Degrees Celsius
ν	Nu (frequency)
η	Eta (hapticity)

Prologue: Unconventional Approaches to Hydrodesulfurization

Growing environmental concerns and regulatory pressures have led to a rise in the demand for new technologies to produce ultra-low sulfur transportation fuels.¹ The current state-of-the-art in hydrodesulfurization (HDS) processes relies on heterogeneous cobalt- or nickel-doped molybdenum catalysts,²⁻⁵ and is quite efficient for removing most of the organic sulfur entrained in hydrocarbon streams. However, the remaining sulfur in fuels is largely composed of polycyclic aromatic sulfur compounds, which present a considerable challenge for current HDS technologies, even when very harsh process conditions are employed. This makes refining crude oils with a high proportion of aromatic organosulfur constituents especially challenging; the bitumen sourced from Alberta's Oil Sands ranks as having among the highest concentrations of these thiophenic molecules worldwide.³ The industry has accepted that removing this last remaining sulfur in fuels (*i.e.*, "ultra-deep desulfurization") will require an entirely new approach, involving the use of new, carefully-designed classes of catalysts or more aggressive reducing agents.

Over the last four decades various academic research groups have designed homogeneous, polymetallic transition metal complexes, which are useful models for the active sites of industrial hydrotreatment catalysts, as well as excellent stoichiometric reagents for desulfurizing aromatic sulfur compounds.⁶⁻¹⁰ While these homogeneous complexes are highly reactive under mild conditions, after a single desulfurization reaction, they invariably form very strong M-S bond(s), which resist hydrogenolysis, thus limiting the method to stoichiometric reactivity.^{7, 11-12} The first chapter of this thesis will describe key discoveries in this area.

An unconventional approach to achieving ‘ultra-deep’ desulfurization is to use stoichiometric quantities of an alkali metal reagent in addition to, or in place of, hydrogen to improve the efficiency of the reaction. Since the 1970s, petroleum researchers led by ExxonMobil have filed multiple patents describing the use of alkali metals and alkali metal salts (MOH, MOR, and MH where M = Li, Na, K) to remediate high-sulfur feeds.¹³⁻²⁰ While these systems afford significant desulfurization, the methods require very forceful conditions (typically 34–340 atm H₂ and 260–500 °C) and are of limited practicality. A very recent report addresses the forcing conditions by simply switching to organosilanes as the stoichiometric reducing agent, allowing ultra-deep desulfurization of organosulfur model compounds to occur at relatively low temperatures and without hydrogen overpressure.²¹

The work described in this thesis seeks to combine these two promising areas of research. We first outline (Chapter 2) the synthesis of thermally robust, polymetallic clusters of the late first row metals (Co, Ni) as novel precatalysts for hydrodesulfurization. Following this, we demonstrate (Chapters 3 and 4) that these transition metal clusters, when combined with alkali metal hydrides – particularly KH – constitute the most effective HDS systems known to date, at least under comparably mild reaction conditions. While the initial discovery of this transition metal-promoted KH-mediated desulfurization system is credited to earlier researchers in the Stryker group and has been disclosed in patent filings,²²⁻²⁵ this research provides crucial clarification and updating of the original reports. In particular, we report basic mechanistic analysis that defines the role of each component of the system (catalyst, H₂, and KH). This has

permitted optimization of the catalyst and reaction conditions, as well as a more accurate mechanistic accounting of this potentially important discovery.

1. Catalytic Hydrodesulfurization: Heterogeneous Catalysts and Homogeneous Model Complexes

1.1 Introduction to hydrodesulfurization (HDS)

Gasoline consumption has steadily increased over the past decade.²⁶ In 2016, the United States consumed about 1.5 billion liters of gasoline per day.²⁷ However, burning fossil-based fuels has a detrimental environmental impact.²⁸ One particular concern is the conversion of the residual organic sulfur to noxious sulfur oxide gases (SO_x; X = 1, 2) during the combustion period. These sulfur oxides are responsible for inhibiting the proper functioning of catalytic converters in motor vehicles, leading to an increase in the emission of dangerous gases such as carbon monoxide and nitrogen oxides.¹ In addition, sulfur dioxide, a pungent and toxic gas, is a potent respiratory irritant, inhalation can lead to long term negative health effects.²⁹ Moreover, water and oxygen in the atmosphere react with sulfur dioxide to produce sulfuric acid, the leading cause of acid rain.³⁰ These concerns, taken together, have led to very stringent regulations on residual sulfur content allowed in fuel. For example, the United States Environmental Protection agency (US EPA) and the Environment and Climate Change Canada (ECCC) required the use of ultra-low sulfur fuel with no more than 12 ppm residual sulfur by early 2020; this is a total of 2 ppm lower than the current value of 14 ppm accepted.^{1, 31}

The bitumen found in Alberta's oil sands which represent one of the world's largest proven petroleum deposits, is viscous and contains high heteroatom (S, N, and O; Alberta: 7 %)³ and metal (Ni and V) concentrations. This results in the need for extensive upgrading and refining in order to convert this crude oil into fuels and peterochemicals.^{2, 32-33} The bitumen undergoes feed separation through distillation and removal of salts and sediments. Higher boiling point fractions, containing up to 6 wt % of sulfur, are subjected to a rigorous primary thermal

upgrading, converting it to lower molecular weight fractions and to a certain extent removing sulfur *via* thermal cracking, coking, and/or hydroconversion.^{1, 5, 7, 32, 34-35} The resulting oil has reduced viscosity and a lowered sulfur content, commercially described as sour medium crude. This medium crude requires additional upgrading by catalytic hydrodesulfurization in order to prevent deactivation of downstream catalysts^{2, 5, 36} and meet the government's stringent regulations on sulfur content.^{1, 31} Even after the crude oil undergoes these upgrading and refining processes, the sulfur content in gasoline produced using current technologies remains higher than 2020 target values.⁵

Hydrodesulfurization, or HDS, is the process that removes sulfur from the crude oil through hydrogenolysis of the C–S bonds, typically over a heterogeneous cobalt-molybdenum sulfide catalyst.^{32, 36} However, current industrial catalyst systems suffer from several drawbacks. HDS requires high temperature (>300 °C) and high hydrogen pressure (≥ 100 atm). The process is costly and energy intensive, as well as simultaneously converting a substantial percentage of the feed to coke, a toxic, valueless commodity.^{7, 37} In addition, “deep” desulfurization remains an issue, where the catalytic removal of the most refractory organosulfur compounds is inefficient.^{6-7, 32, 35} Thus, more efficient catalysts are required to meet the current and future regulations.

1.1.1 Organosulfur complexes in crude oil

In addition to aromatic and alkyl chain hydrocarbons of broad molecular weight distribution, crude oil also contains a variety of sulfur compounds, ranging from alkyl thiols and ethers to hydrocarbon-substituted condensed polycyclic thiophenes, as illustrated in Figure 1.1.

Current catalytic technology easily removes thiols, thioethers, light aromatic sulfides, and disulfides.^{5, 7} Due to the lower bonding energy of *sp*³-hybridized C–S and S–S bonds (Table 1.1),³⁸ some of these organosulfur moieties are removed during the thermal cracking process, during which the crude oil is heated above 400 °C. Sulfur from thiols, sulfides, and disulfides is completely extruded as H₂S during the catalytic hydrotreatment process. On the contrary, the aromatic C–S bonds of thiophenes, benzothiophenes, dibenzothiophenes, and alkyl-substituted analogues, particularly those found in the asphaltene fraction, remain unaffected by thermal cracking^{2, 5, 32} and, to a large extent, by catalytic hydrotreatment.^{7, 32, 36}

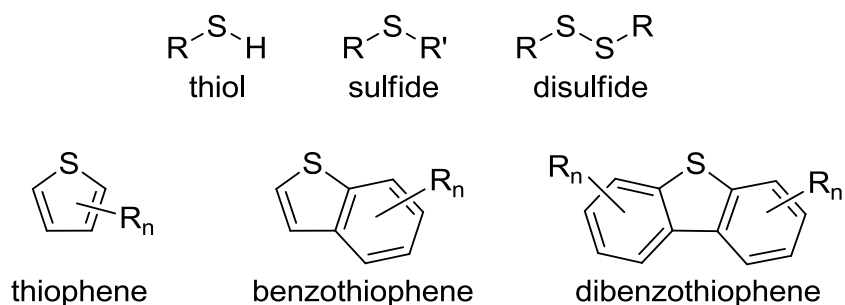


Figure 1.1 Crude oil is made up of a variety of organosulfur moieties. (R, R' = alkyl groups, n = number of alkyl substituents).⁷

Table 1.1 Bond energy for different Y – S bond (Y = S or C).³⁸

Bond	Bond Energy (kcal/mol)
S – S	65
C – S	73
C = S	136

The strength of the C–S bond varies dramatically with the hybridization of the carbon center (Table 1.1). The *sp*²-hybridized C–S bonds of thiophenic compounds are also constrained within the aromatic systems, resulting in very strong C–S bonds. To remove this sulfur, catalytic hydrogenation is used to partially saturate the aromatic sulfur compounds, which weakens the C–S bonds and removes the persistent sulfur. However, hydrogenation of polycyclic aromatic systems requires forceful conditions.^{5, 39} In addition, aromatic compounds are beneficial in fuels; thus, saturating the aromatic hydrocarbons with H₂ is not only expensive but unnecessary for fuel quality.⁴⁻⁵

More efficient catalysts are required for deep and ultra-deep desulfurization, allowing HDS-refined petroleum to meet environmental regulation.^{1, 31} The removal of sulfur from these refractory compounds from heavy oils and bitumen remains an issue for the efficient production of transportation fuels.

1.2 Heterogeneous catalysts for HDS

Current commercial HDS relies on heterogeneous catalysts typically composed of molybdenum or tungsten sulfide, doped with promoters such as cobalt or nickel. The catalysts are usually dispersed on high surface area γ -alumina or other inert supports. Bimetallic CoMo or NiMo formulations are most common, but tri-metallic CoNiMo catalysts are also used to increase the efficiency of desulfurization and promote hydrodenitrogenation.⁴⁰ These catalysts are typically prepared *via* impregnation of the support with the metal precursors, followed by high temperature calcination, sulfidation, and activation. The procedure involves adsorption of

ammonium molybdate (or tungstenate) and cobalt (or nickel) nitrate solutions onto high surface area alumina, silica-alumina, or silica, followed by heating in air at high temperature (400–600 °C). Well-dispersed metal oxide clusters bonded to the support are obtained upon the thermal decomposition of the precursor salts.^{7, 34}

A stable and active catalyst is produced by sulfiding the oxide precatalyst.^{7, 34} Sulfidation occurs *in situ* by exposing the oxide precatalyst to a mixture of hydrogen and high-sulfur feed, typically spiked with simple organosulfur compounds (*e.g.*, dimethyl disulfide).^{34, 41} Alternatively, *ex situ* preparation involves using H₂S to replace the organosulfur feed for pre-sulfiding the precatalyst.³⁴

1.2.1 Catalyst structure

The chemical structure of the sulfided catalyst, particularly characterization of the active sites, is important for understanding and improving catalyst reactivity. However, heterogeneous catalysts are challenging to characterize because of the non-uniformity of the metal species on the surface, and the corresponding diversity of the catalytically active site(s). As such, the exact structures of most heterogeneous catalysts, including those used for HDS, are often not well defined and/or only partially understood. Surface analysis techniques such as EXAFS and Mossbauer spectroscopy provide some insight into the structure of the active sites.^{32, 42} In the case of HDS catalysts, two different structures are proposed for the unpromoted MoS₂ or WS₂ catalyst phases. Type I metal sulfide structures consist of a well-dispersed monolayer of molybdenum or tungsten sulfide on the surface of the alumina support. The metals are not fully sulfided; strong M–O–Al (M = W or Mo) bonds are retained. The Type II structure consists of

multiple layers of fully sulfided metals. The edge sites are the active sites for HDS in both Type I and II precatalysts. The sulfided slabs become unsaturated under catalytic conditions by hydrogenolysis of the weakest metal-sulfide bond(s).³⁴

The most dramatic improvement in the HDS activity of MoS₂ (or WS₂) crystallites is achieved by introducing of cobalt or nickel “promoter” atoms. Four structural models have been proposed to explain the synergistic effects between the promoter and primary catalyst.^{34, 43} The *monolayer model* is based on the Type I structure of the unpromoted catalyst; the MoS₂ (or WS₂) exists as a monolayer on alumina. Nickel or cobalt atoms are believed to stabilize this Mo or W layer.^{34, 44} The *‘intercalation’ model* suggests that the molybdenum or tungsten is sandwiched between two layers of sulfur, which is further decorated with unsaturated nickel or cobalt atoms.⁴⁵ Moreover, the *pseudo-intercalation model* suggests that the important cobalt or nickel atoms are located at the edge sites of the MS₂ (M = Mo, W) layers.³⁴

The *“remote control” model* posits the presence of multiple discrete layers of molybdenum or tungsten sulfide decorated with a CoS_x phase.^{32, 34} The close proximity between catalyst and promoter atoms results in synergistic binding and activation of hydrogen and substrates. Specifically, hydrogen “spillover” (transfer) is proposed, where the cobalt sulfide clusters serves to promote hydrogenation at nearby molybdenum sulfide sites. Reduction by hydrogen spillover creates coordinative unsaturated sites (CUS) on the molybdenum surface for hydrogenolysis of the C–S bonds.^{32, 34}

The most accepted modern structural model is that of bimetallic Co-Mo-S active sites proposed by Topsøe, *et al.* In this model, MoS₂ crystallites on the alumina surface are decorated at the edge sites with cobalt at various concentrations.^{32, 46} Metallic cobalt and cobalt sulfides are also found as discrete clusters on the surface of and intercalated into the alumina (Figure 1.2).³⁴ In this model, the bimetallic “corner sites” of the Co-Mo-S surface serve as the active site for hydrodesulfurization.^{32, 46}

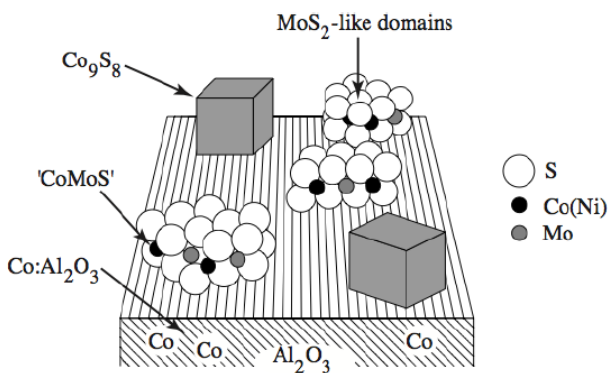


Figure 1.2 Proposed surface structure of Co-Mo-S industrial catalyst.³⁴

The sulfur is most weakly bound to the cobalt atom at the bimetallic “corner site.”^{32, 46} It is proposed that, under hydrogen, the cobalt sulfide loses H₂S, creating a vacant bimetallic coordination site (Figure 1.3). Although the precise mechanism of C–S bond activation is not known, organosulfur compounds can bind to this vacant site and undergo hydrodesulfurization.^{7,}

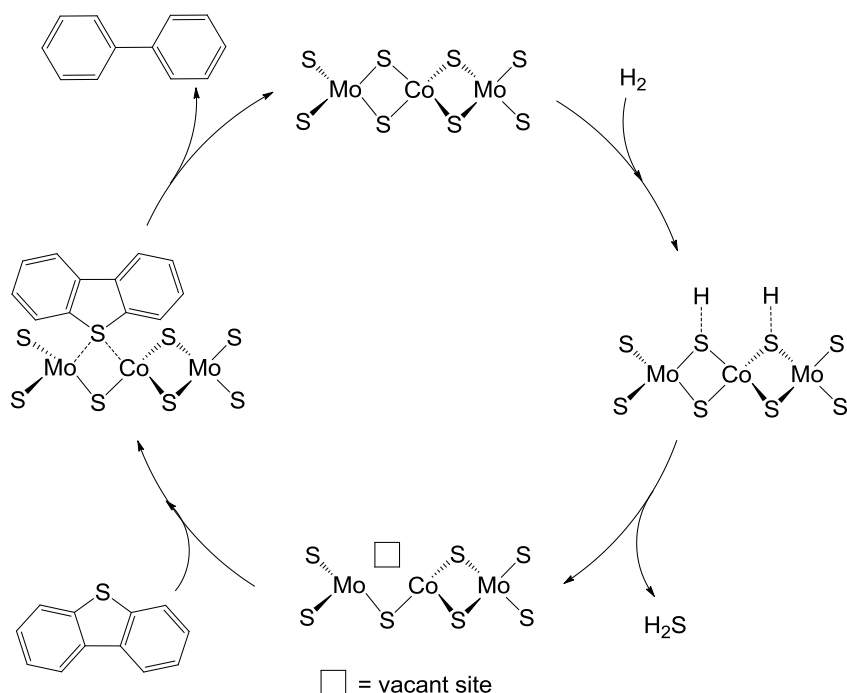


Figure 1.3 Proposed mechanism for Co-Mo-S industrial catalyst.⁷

1.2.2 Binding modes of thiophenes, benzothiophenes, and dibenzothiophenes

The generally accepted mechanism for catalytic HDS begins with binding of the organosulfur substrates on the heterogeneous catalyst surface, leading to C–S bond activation and desulfurization. For substrate binding, at least one vacant site on the metal is required.⁷ Chemisorption experiments on the catalyst surface and supporting theoretical calculations indicate that the number of coordinatively unsaturated sites available to the substrate induces different substrate binding modes. Thiophene, benzothiophene, and dibenzothiophene bind in an η^1 -mode *via* the sulfur lone pair when only one coordination site is available (Figure 1.4, η^1 -S). The η^1 -S binding mode is proposed to be directly involved in sulfur extrusion.⁴⁸ Steric effects from the alkyl substituents (at positions 2- and 5- of thiophene; 4- and 6- of DBT) potentially inhibit η^1 -S binding. This correlates with the lower desulfurization activity of catalysts toward the alkylated sulfur heterocycles.⁴⁹⁻⁵⁰

Multi-site coordination (η^2 -S, C=C) is possible when two accessible vacant sites are available.⁵¹ A further increase in π -hapticity of the substrates is possible when three vacant sites are available; the resulting η^5 - and η^6 -arene coordination is thought to lead to hydrogenation of the aromatic ring.^{48, 51-52} The η^5 - or η^6 -coordination mode is particularly important for alkylated sulfur heterocycles, which typically require hydrogenation prior to desulfurization.^{7, 50}

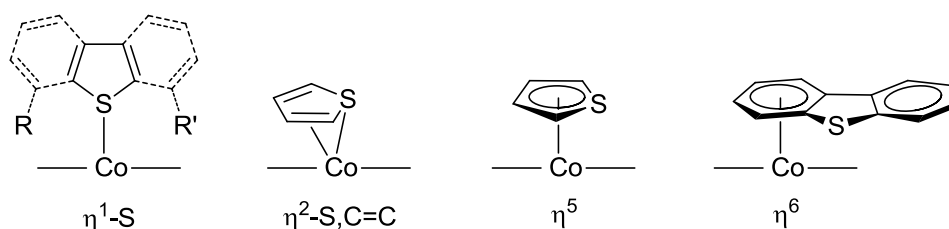


Figure 1.4 Different bonding modes of aromatic substrates.⁷ (R, R' = H, Me)

1.2.3 Limitations and recent improvements in heterogeneous HDS catalysis

A variety of transition metals have been investigated for hydrogenation activity because of its importance in deep hydrodesulfurization. For instance, a nickel-doped catalyst is usually used, which provides higher hydrogenation activity.^{7, 34} Noble metal catalysts (Pt and Pd) also show high hydrogenation activity and have attracted much research interest.⁵³ However, these metals are very costly and are easily poisoned by sulfur.

Other transition metals have been explored for reactivity towards C–S bond activation, and a strong correlation between activity and the periodic trends among the metal elements is evident. Pecoraro *et al.*,⁵⁴ Vissers *et al.*,⁵⁵ and Ledoux *et al.*⁵⁶ established this dependence by plotting reactivity *vs.* metal position on the Periodic Table, obtaining a classic volcano plot for

the simple sulfides (Figure 1.5).⁷ The plot shows that second- and third-row transition metals show a volcano-type distribution in reactivity, with second- and third-period elements in Groups 8 and 9 being most active in the desulfurization of DBT. In contrast, first-row transition metals overall show significantly lower activity towards C–S bond cleavage.^{7, 35} The volcano plot arises from variations in metal sulfide bond energies as a function of position in the period. Topsøe *et al.* propose that higher desulfurization activity is correlated with higher surface energies (and lower surface stability) of the metal sulfide.³² Alternatively, Toulhoat, *et al.*, suggest that higher desulfurization activity is attributed to the “optimum” M–S bond strengths found among groups 8 and 9.⁵⁷ This reflects Sabatier’s principle: metal sulfides of intermediate bond strength are most active in desulfurization.^{7, 58}

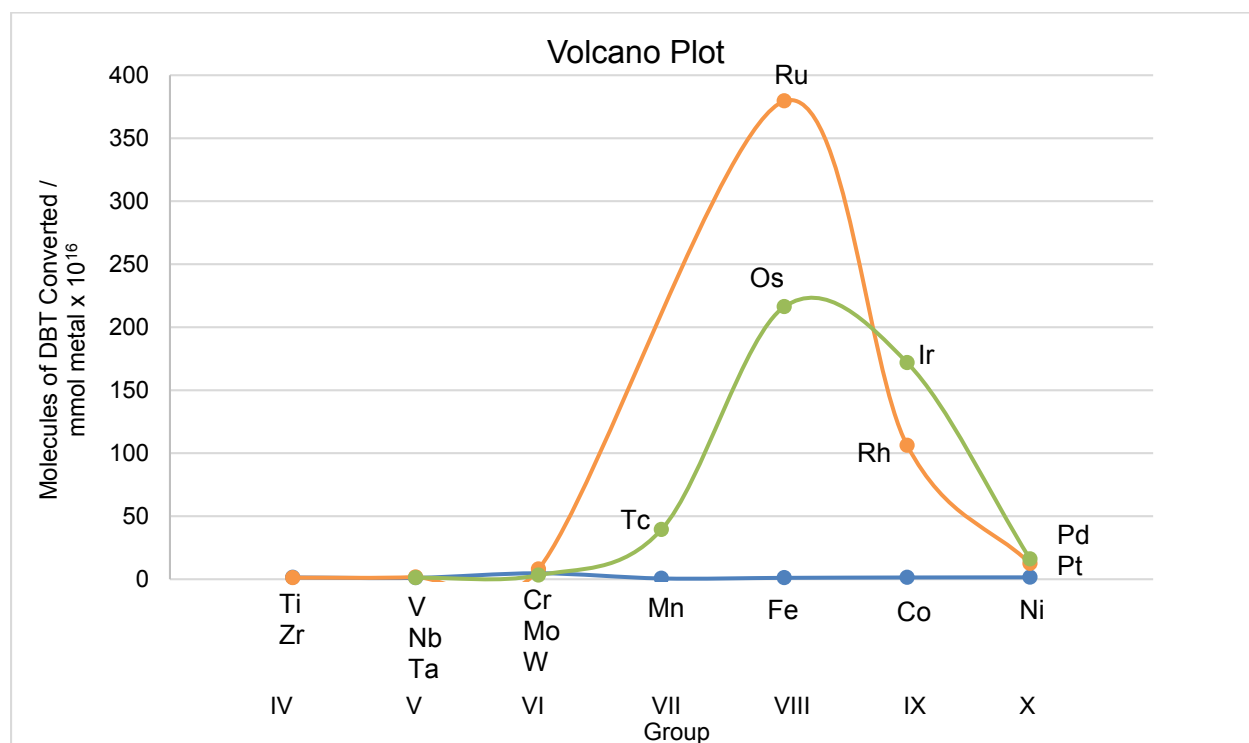


Figure 1.5 Reactivity of transition metal sulfides in the desulfurization of DBT. (Adapted from Ref [54])

Besides the choice of transition metal, a range of other strategies have been reported for improving HDS activity of the catalysts. One of the approaches is the addition of chelating agents such as ethylenediaminetetraacetic acid (EDTA) and cyclohexanediaminetetraacetic acid (CyDTA), during impregnation of the catalyst. The chelating agent strongly binds to the cobalt atoms and prevent the formation of the inactive Co_9S_8 phase during sulfidation. Thus, after thermal decomposition of the chelating agents, the cobalt atoms are well dispersed, increasing promoting effects.⁵⁹⁻⁶¹ Alternatively, changing the support, especially using a mixed support, *e.g.*, $\text{TiO}_2\text{-SiO}_2$, instead of alumina, also leads to improved desulfurization activity.⁶²⁻⁶⁴

1.3 Homogeneous Organometallic Complexes for C–S Bond Activation

Studying heterogeneous catalysts has provided valuable insights into substrate adsorption/desorption, catalyst decomposition, and basic mechanistic pathway. However, more detailed analysis is limited by the non-uniform surface of supported catalysts.^{5-7, 32, 35, 65} Alternatively, investigation of homogeneous transition metal complexes, existing as discrete molecules, provides structural and reactivity details, as well as mechanistic information typically inaccessible through studying heterogeneous systems. This improvement in characterization can lead to rational design of more active homogeneous – and heterogeneous – catalysts.^{7, 35, 66-74}

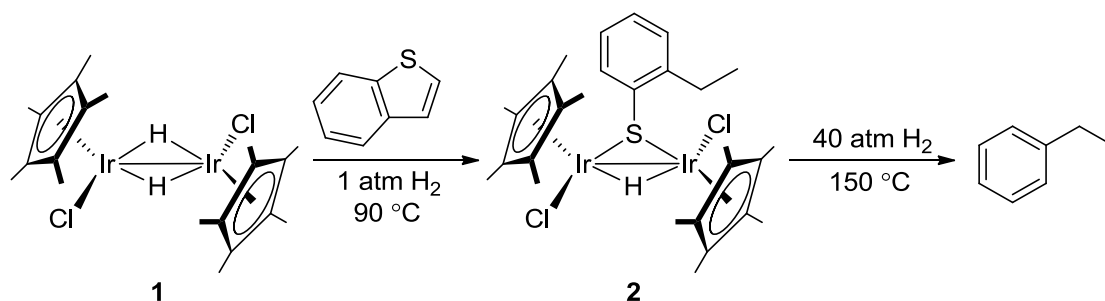
Many homogeneous transition metal complexes have been studied to model the active sites of industrial HDS catalysts. From the investigation of homogeneous complexes, it is clear that a range of low-valent transition metal complexes readily cleave C–S bonds in sulfur

heterocycles under relatively mild conditions.^{7, 35, 66-74} Comprehensive reviews of the topic have been reported;^{7, 35} this selective review is intended to be instructional. This discussion is principally limited to those involving first-row transition metal complexes and reactions of aromatic sulfur compounds.

1.3.1 C–S bond cleavage by 2nd and 3rd row transition metal complexes and clusters

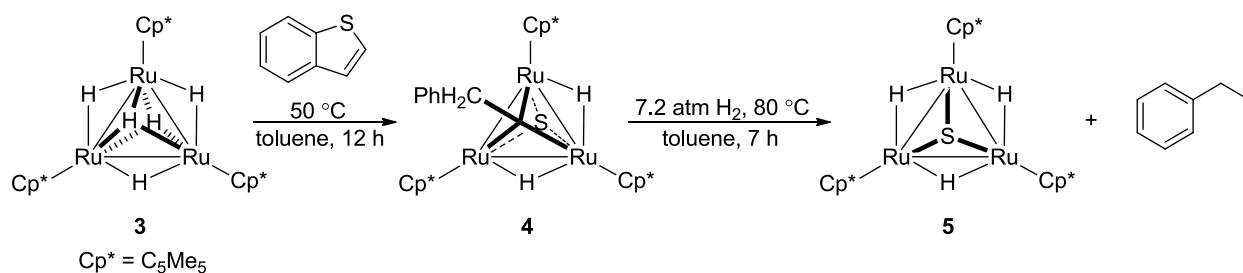
Second- and third-row transition metals complexes have been widely used to activate the C–S bonds of thiophenes at relatively mild temperatures. Of these, organo-molybdenum^{70, 75-76} and -tungsten^{70, 77-78} compounds are common because they contain the same metals as the commercial catalysts. Other second- and third-row organotransition metal compounds, including complexes based on Re,⁷⁹⁻⁸⁰ Ru,⁸¹⁻⁸² Rh,^{72, 83} Ir,⁸⁴⁻⁸⁵ and Pt^{73, 86} are also competent for activating the C–S bonds in these refractory compounds. From these studies, it is clear that low-valent coordinatively unsaturated mononuclear complexes readily insert into the C–S bond of aromatic organosulfur compounds; however, complete desulfurization typically requires multiple metal centers that function cooperatively.

Vicic and Jones provide a good example of this point, albeit using a third-row metal. Cooperative activity between two iridium centers in the bimetallic hydride complex **1** results in complete desulfurization of thiophene and benzothiophene (Scheme **1.1**).^{7, 87} Isolation of the bridging thiolate intermediate **2** suggests that the μ^2 -sulfur coordination of the thiolate leads to the second C–S bond cleavage. The μ^2 -sulfide binding motif weakens the C–S bond, facilitating hydrodesulfurization.

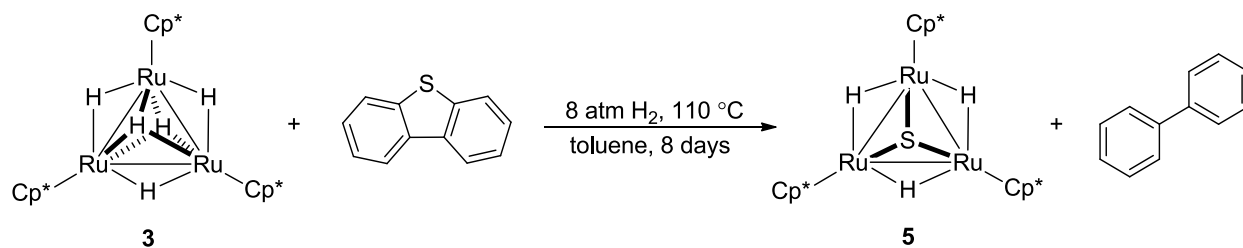


Scheme 1.1^{7, 87}

Another important illustration of cooperative activity is the stoichiometric desulfurization of benzothiophene by tri-ruthenium hydride **3**, reported by Suzuki and coworkers.⁸⁸ Hydride **3** mediates the desulfurization of benzothiophene (Scheme 1.2) and dibenzothiophene (Scheme 1.3). For benzothiophene, a μ³-sulfide **4** is formed thermally. In the presence of H₂, hydrogenolysis of the Ru–C bond liberates the sulfur-free product. As observed with the iridium μ²-thiolate dimer **2**, a bridging sulfur atom leads to the complete desulfurization of both benzothiophene and dibenzothiophene.⁸⁸



Scheme 1.2

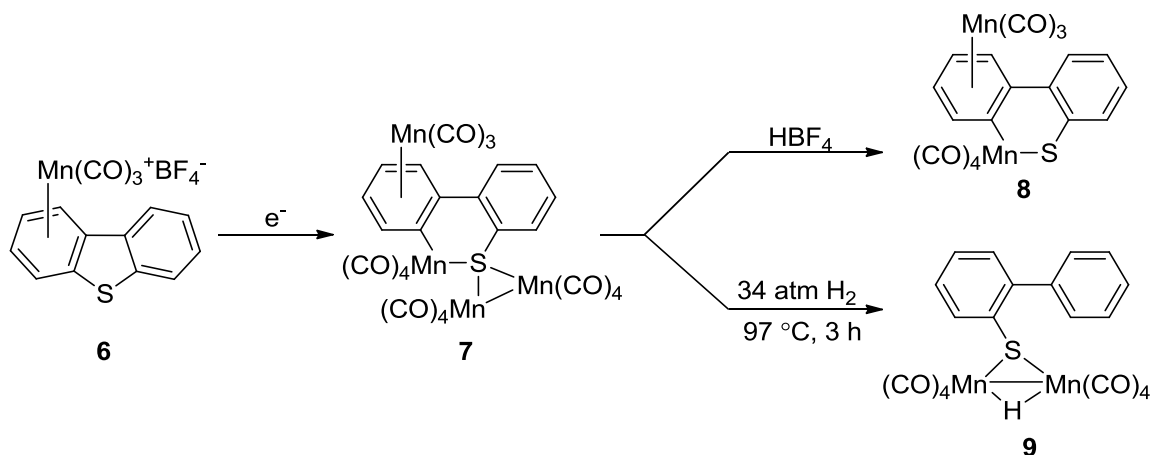


Scheme 1.3

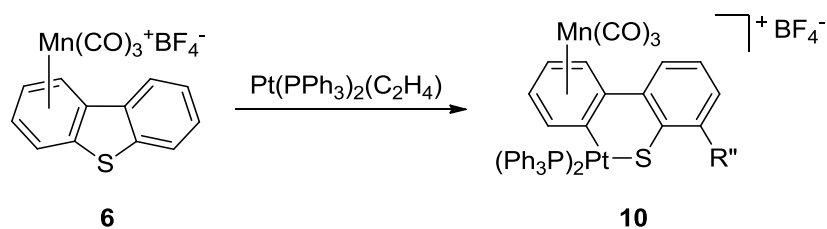
1.3.2 Modeling HDS using first-row transition metal complexes

Second- and third-row transition metals are rare, toxic, and expensive.⁸⁹ Moreover, many second- and third-row metals form strong metal–sulfur bonds, resulting in the harsh conditions required to effect catalyst turnover.^{7, 35} First-row transition metals are earth-abundant, inexpensive, and more environmentally friendly than second- and third-row elements.⁸⁹ With a greater emphasis on environmental footprint, cost, and bulk availability concerns, first-row transition metals are of particular interest for use in industrial catalysis and other applications.⁹⁰

Late first-row metal complexes readily insert into the C–S bonds of organosulfur compounds. Sweigart and coworkers demonstrated that the C–S bond of DBT is activated by η^6 -coordination of the Mn(CO)₃⁺ fragment to the aromatic π -system.⁹¹ The C–S bond of the DBT-derived manganese π -complex **6** is weakened by this π -coordination. Upon one-electron reduction by cobaltacene or Na/Hg amalgam, the unsaturated Mn(CO)₄ fragment activates the C–S bond of DBT to afford polymetallic manganese complex **7** (Scheme 1.4). The addition of a proton source to manganese cluster **7** leads to the thiametallacycle **8**, while heating manganese cluster **7** under hydrogen results in hydrogenolysis of the Mn–C bond. Similarly, low-valent platinum, which does not readily react with free DBT, inserts to the C–S bond of the cationic manganese complex **6**, forming hetero-bimetallic cluster **10** (Scheme 1.5).⁹²

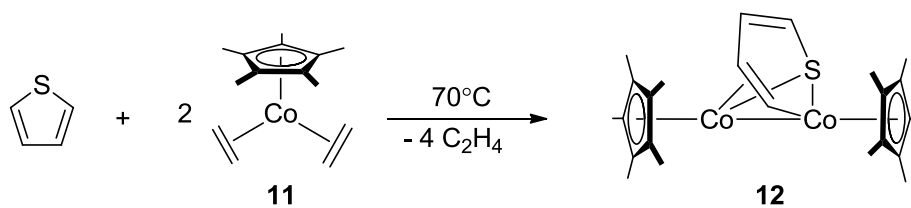


Scheme 1.4



Scheme 1.5

More electron-rich metal complexes readily cleave C–S bonds without coordinative pre-activation by a Lewis acid. For example, Jones and coworkers reported that half-sandwich cobalt complex **11** inserts into aromatic C–S bonds under mild conditions (Scheme 1.6).⁹³ In this case, *two* cobalt centers are required to activate the C–S bond of thiophene, giving dinuclear “flyover” complex **12**. A similar bimetallic cobalt complex is obtained when half-sandwich cobalt complex **11** reacts with dibenzothiophene.⁹



Scheme 1.6

Low-valent nickel also readily cleaves the C–S bonds of thiophenic molecules. For example, dinuclear NHC complex **13** (Figure 1.6) inserts into the C–S bond of DBT under ambient conditions to form the thiametallacycle **14** (Scheme 1.7).^{74, 94} The monomeric thiametallacycle does not react further, in contrast to other nickel thiametallacycles (discussed below).

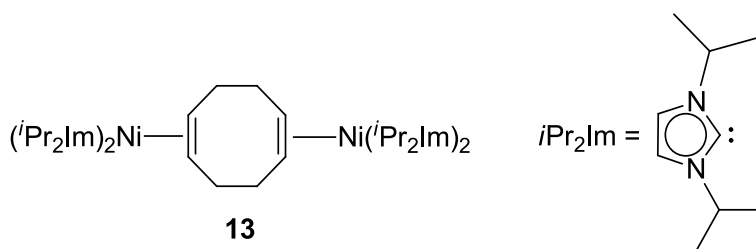
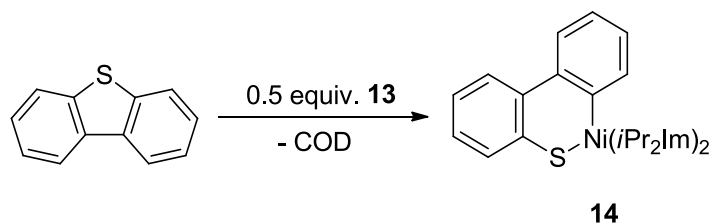
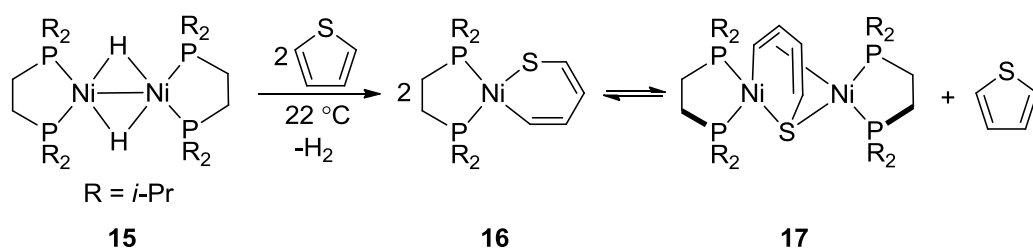


Figure 1.6 Low-valent nickel cluster **13** readily cleaves the C–S bonds of DBT.⁹⁵

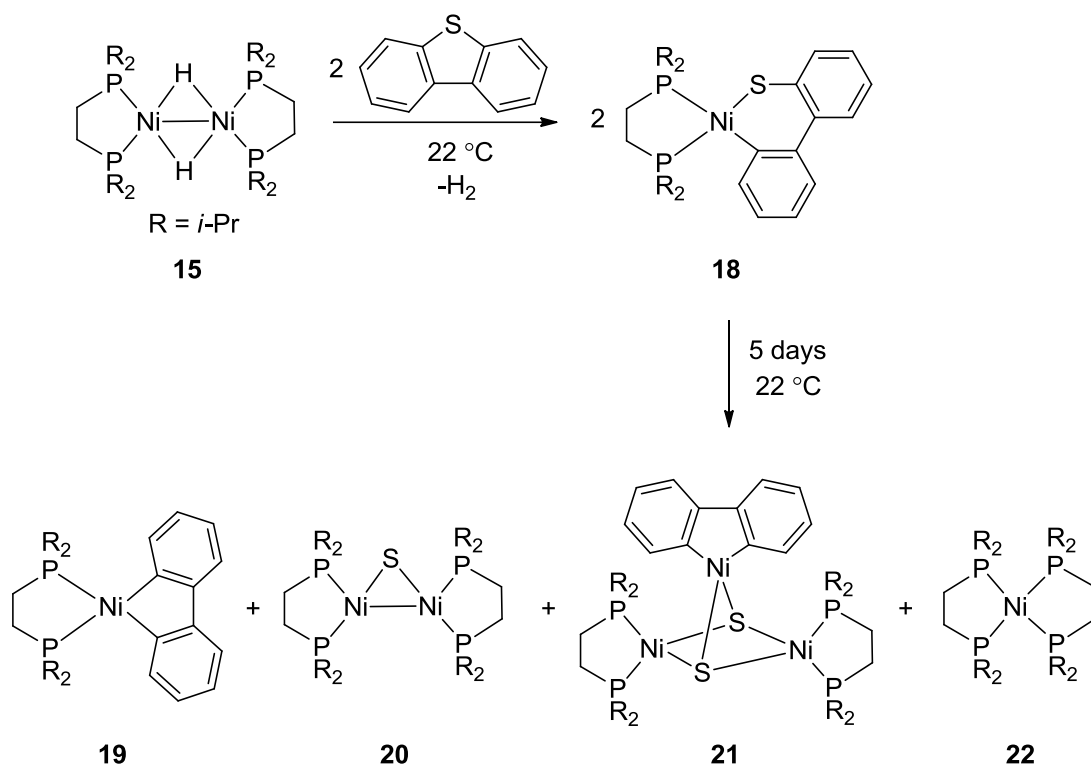


Scheme 1.7

As in the second- and third-row, synergistic cooperation in first-row polymetallic clusters is vital for stoichiometric desulfurization of organosulfur compounds. In fact, the *first* first-row transition metal compound to fully desulfurize thiophenic molecules is the bimetallic nickel(I) hydride complex **15**.^{11, 74, 94, 96} This compound adds oxidatively at the C–S bond of thiophene, benzothiophene, and dibenzothiophene (Schemes **1.8** and **1.9**), initially forming monomeric thianickelacycles **16** and **18**. Monomeric thianickelacycle **16** exists in equilibrium with bimetallic cluster **17**, a common binding motif for first-row transition metals.

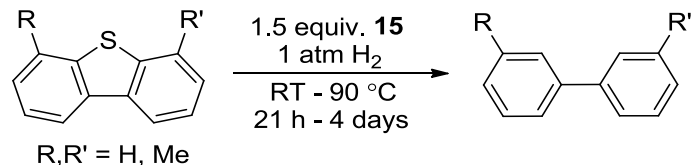


Scheme 1.8



Scheme 1.9

Thianickelacycle **18**, formed by cleavage of DBT, transforms very slowly to multiple Ni-containing products (Scheme **1.9**).^{11, 74, 96} The isolation of polymetallic clusters **20** and **21** implies the importance of cooperative activation for desulfurization. Despite the facile desulfurization to form μ -sulfide clusters, the Ni–S bond of the bimetallic μ -sulfido complexes **20** and **21** does not undergo hydrogenolysis, rendering the desulfurization reaction stoichiometric. Though limited, bimetallic nickel hydride **15** is very reactive, desulfurizing even sterically hindered 4,6-dialkyl-DBT under relatively mild conditions (Equation **1.1**). This was the first example of hydrodesulfurization mediated by a first-row transition metal complex.



Equation 1.1

An even more reactive polymetallic nickel complex was recently disclosed by Shoshani and Johnson.⁸¹ These authors report hydrodesulfurization of 4,6-dimethyl-DBT, by phosphine-supported pentanuclear polyhydride complex **23** (Figure 1.7). While Vicic's phosphine nickel complex **15** requires heating at 90 °C for 21 hours, pentanuclear cluster **23** desulfurizes DBT and its 4,6-dialkyl analogues *at room temperature over 3 hours*. In addition to μ^4 -bridging sulfide **24**, a simple Ni(I) phosphine capped with an η^6 -toluene ligand (**25**) is obtained, along with other paramagnetic Ni sulfide species (Scheme 1.10). While the desulfurization is not catalytic, yielding only two equivalents of hydrocarbon per cluster, pentanuclear cluster **23** represents a tremendous advance in the use of polymetallic complexes. Multiple metals at the active site can make the desulfurization of even the most refractory C–S bonds facile.⁹⁷

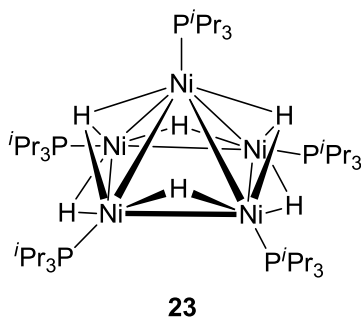
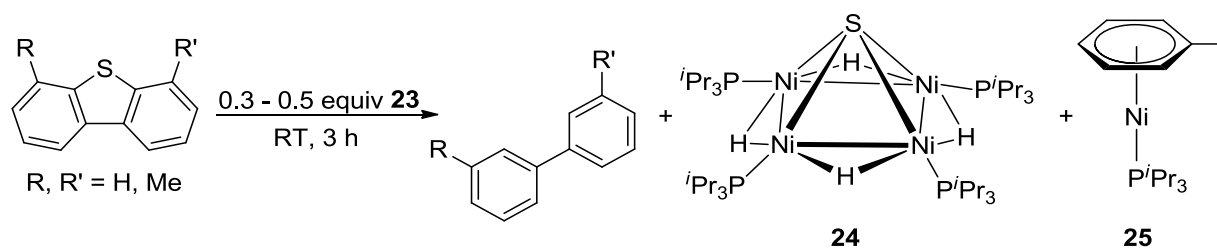
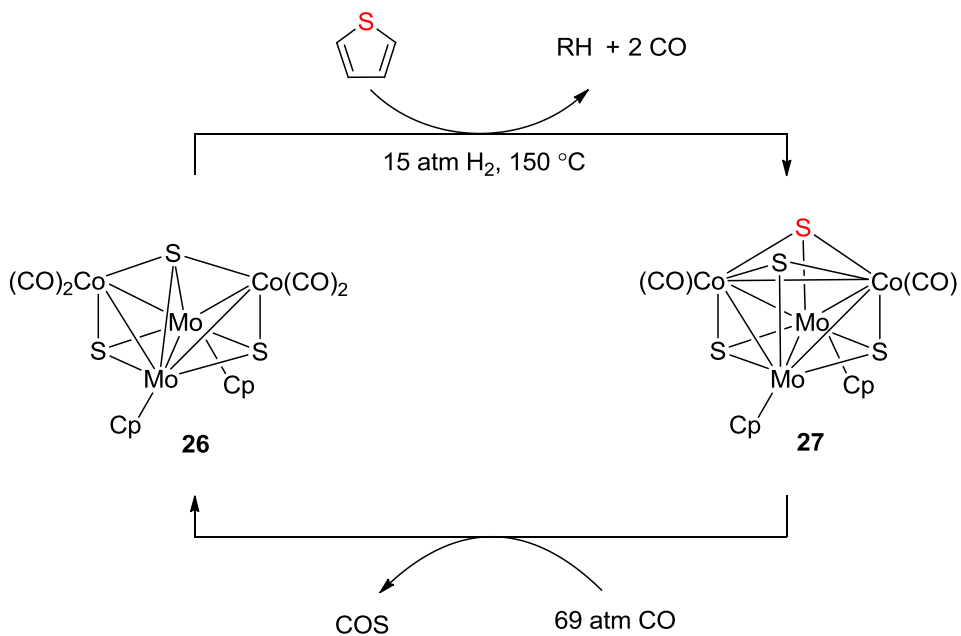


Figure 1.7 Pentanuclear nickel hydride cluster for desulfurization.⁹⁷



Scheme 1.10

An older, but very important example of a molecular cluster that mimics the active site of CoMoS catalysts is found in the work of M. David Curtis and coworkers.^{71, 98} Curtis' model system was the first and most direct model of industrially-relevant cobalt-promoted MoS₂ catalysts. The homogeneous bimetallic cluster **26** mediates stoichiometric desulfurization of thiophene under mild conditions (Scheme **1.11**), generating μ^3 -bridging sulfide cluster **27** and the hydrocarbon. High pressure of carbon monoxide (69 atm) facilitates the regeneration of the Mo-Co-S cluster **26**, although the sulfur is extruded as carbonyl sulfide, not hydrogen sulfide. However, desulfurization of thiophene occurs only when the CO pressure is below 28 atm. At higher pressures, CO saturates the cluster, preventing substrate binding. Thus, the catalytic desulfurization using molybdenum cobalt sulfide cluster **26** is not possible.



Scheme 1.11

Based upon kinetic and mechanistic studies, Curtis and coworkers showed the importance of multi-site substrate binding. The triply-bridging sulfide significantly weakens the C–S bond, lowering the bond dissociation energy to ~ 20 kcal/mole (Figure 1.8).⁹⁸ The μ^3 -bonding motif emphasizes the significance of polymetallic clusters and cooperative activation in desulfurization.

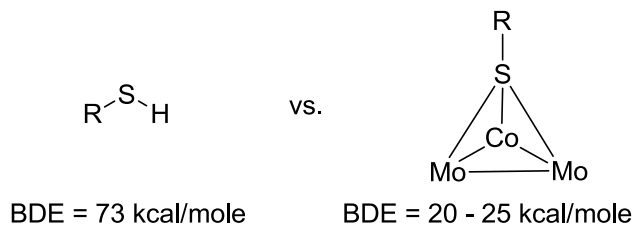
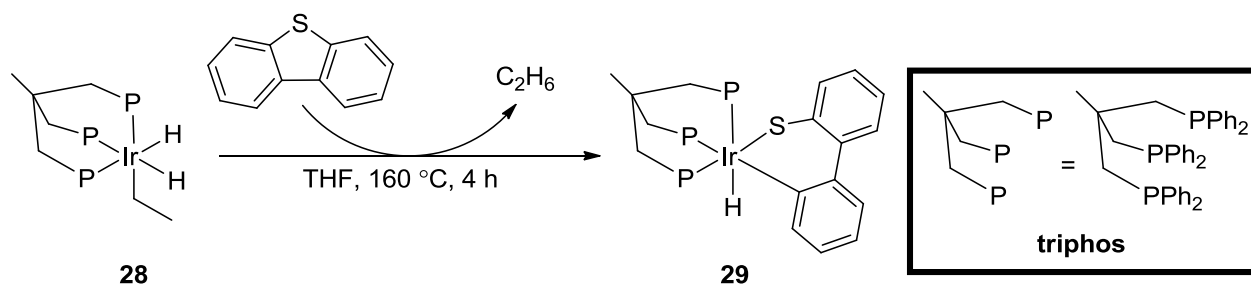


Figure 1.8 Binding of the sulfur atom weakens the C–S bond. (R = aliphatic.)⁹⁸

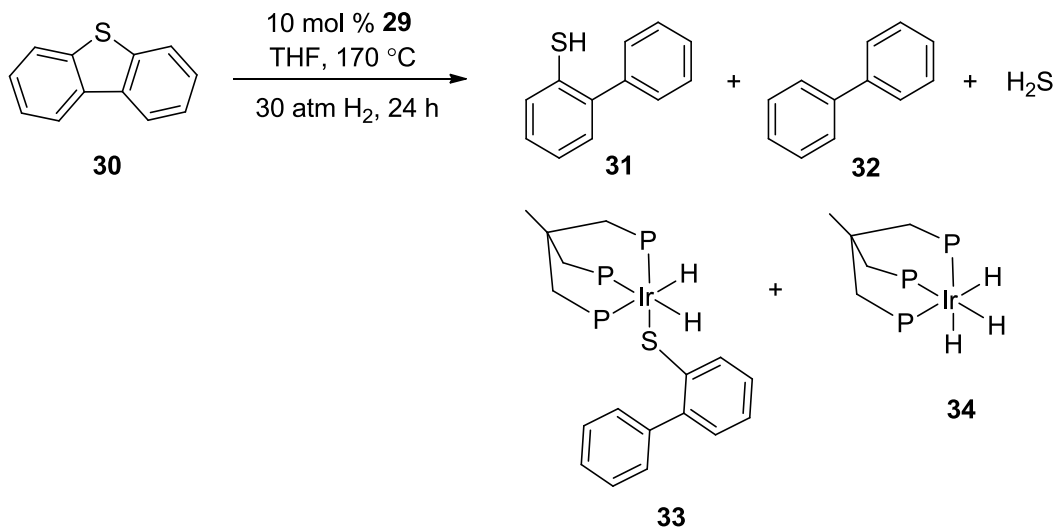
1.4 Catalytic desulfurization with homogeneous complexes

1.4.1 Ir(triphos)H complex for catalytic desulfurization of DBT

Although catalytic desulfurization by homogeneous transition metal complexes is limited, the reaction can be achieved using precious second- or third-row metals. Bianchini, Sanchez-Delgado, *et al.* reported the first examples of *catalytic* desulfurization of DBT, using homogeneous iridium complex **28**.⁸⁵ The complex selectively cleaves the C–S bond of DBT at 160 °C, giving thiametallacycle complex **29** (Scheme 1.12). Thiametallacycle **29** *catalyzes* the desulfurization of DBT at elevated temperature and hydrogen pressure, yielding a mixture of 2-phenylthiophenol **31** (48 %), biphenyl **32** (10 %), and unquantified H₂S, along with two Ir intermediates, **33** and **34** (Scheme 1.13). A similar Rh(triphos)H complex was found to catalyze the desulfurization of thiophene and benzothiophene under identical conditions.⁹⁹⁻¹⁰⁰ Despite the successful catalytic desulfurization, neither Ir nor Rh are suitable for use as industrial catalysts.¹⁰¹



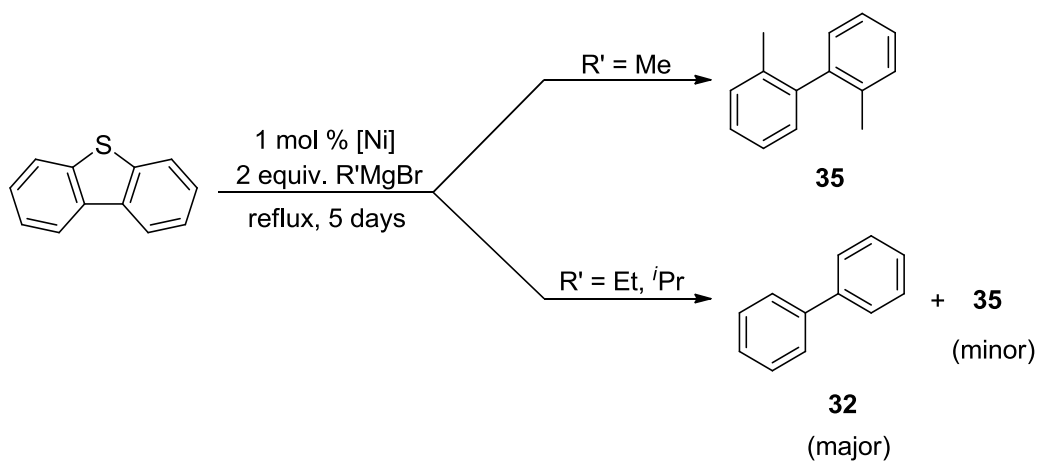
Scheme 1.12



Scheme 1.13

1.4.2 Desulfurization of DBT using [Ni] and stoichiometric Grignard reagents

Catalytic desulfurization using a first-row metal has only been accomplished by using a strongly reducing Grignard reagent in place of hydrogen (Scheme 1.14).¹⁰² A range of Ni(I), Ni(II), and Ni(0) sources are competent for catalytic desulfurization of dibenzothiophene in the presence of excess Grignard reagent (Figure 1.9). The use of MeMgCl resulted in desulfurization with simultaneous cross-coupling to form 2,2'-dimethylbiphenyl **35**. However, when using ethyl or isopropyl Grignard as the reductant, *hydrodesulfurization* is obtained, arising from β -hydride elimination of the alkylnickel intermediate **38** (R' = Et, *i*Pr) (Figure 1.10).¹⁰² The mild conditions and nickel catalysts are attractive; however, long reaction times and the use of costly and pyrophoric Grignard reagents in excess make the system irrelevant to large-scale industrial applications.



Scheme 1.14

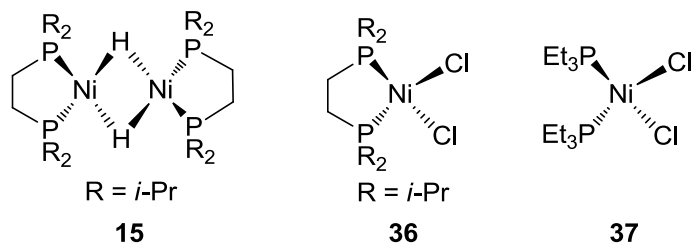


Figure 1.9 Ni catalyst for desulfurization of DBT.¹⁰²

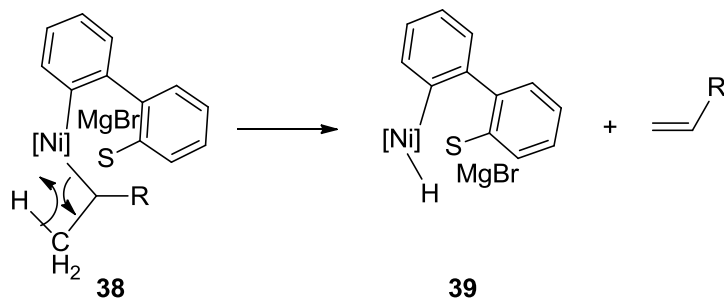
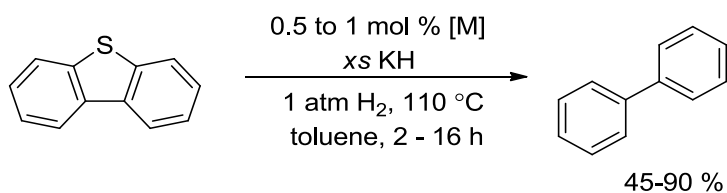


Figure 1.10 The ethyl/iso-propyl ligand on the Ni center β -hydride eliminates to form Ni hydride complex. (R = H or Me)¹⁰²

1.4.3 Stryker group's KH-mediated desulfurization

The Stryker group has reported KH-mediated desulfurization of DBT (Equation 1.2) catalyzed by low-valent cobalt and nickel cluster catalysts **40** and **41** (Figure 1.11).¹⁰³⁻¹⁰⁴ High conversion of DBT to biphenyl is observed at 110 °C and under atmospheric hydrogen pressure. The catalyst system is versatile, showing a broad substrate scope, including 4,6-dimethyl-DBT.^{22-23, 105} The remainder of this dissertation is concerned with the development, understanding, and optimization of this novel catalytic reaction and class of first-row metal catalysts, phosphoramidate-supported polymetallic clusters.



Equation 1.2

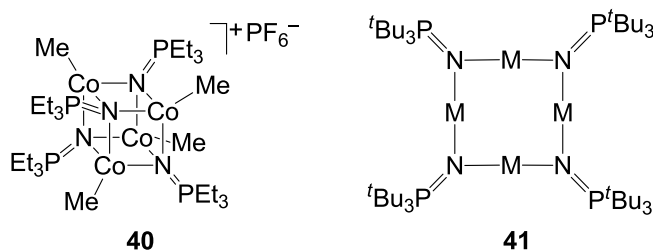


Figure 1.11 Cobalt and nickel catalysts for the KH-mediated desulfurization.^{22-23, 105}

1.5 Conclusion

Industrial catalysts remain inefficient for hydrodesulfurization of refractory organosulfur heterocycles. The investigation of homogeneous organometallic complexes to model commercial heterogeneous catalysts has revealed that polymetallic, electron-rich transition metal clusters provide the cooperative binding and activation necessary for facile desulfurization. However, steric encumbrance in such clusters can inhibit substrate coordination. The Stryker group has designed a series of coordinatively unsaturated first-row metal clusters as potential new catalysts for base-promoted hydrodesulfurization. These low valent precatalysts are discussed in greater detail in the following chapter.

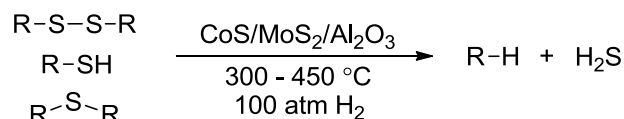
2. Rationale for Catalyst Design and the Syntheses of Transition Metal Phosphoranimide Clusters

2.1 Understanding polynuclear complexes

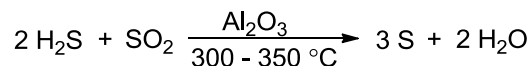
2.1.1 Heterogeneous catalysts and the discovery of clusters

As discussed in Chapter 1, heterogeneous catalysts are ubiquitous in industrial chemical processes.⁴² Diverse industries, ranging from the production of inorganic and organic fine chemicals to crude oil refining and commodity petrochemicals, rely on heterogeneous catalysts.^{42, 53, 106-107} Hydrodesulfurization of crude oil (Figure 2.1a) requires heating the petroleum feed over a bed of cobalt and molybdenum sulfide supported on alumina.^{42, 108} Further, heterogeneous catalysts drive the Claus process (Figure 2.1b), which uses alumina to convert the toxic hydrogen sulfide byproduct to elemental sulfur.^{42, 107-109} Finally, a heterogeneous vanadium pentoxide catalyst is used to convert elemental sulfur into sulfuric acid (Figure 2.1c).¹¹⁰

a) Hydrodesulfurization



b) Claus process



c) Contact process

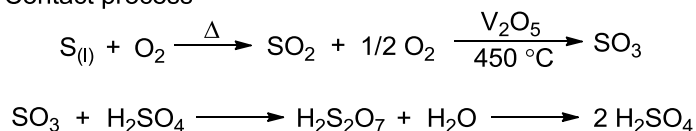


Figure 2.1 Industrial processes such as: (a) hydrodesulfurization that removes sulfur from crude oil use heterogeneous catalyst, (b) Claus process that converts H₂S to elemental sulfur, and (c) Contact process produces sulfuric acid from elemental sulfur.

Heterogeneous catalysts generally feature high stability under harsh conditions, high productivity (if not selectivity), and simple separations of catalysts from products. The mechanism and activity of most heterogeneous catalysts, however, remain poorly understood. Although the investigation of homogeneous mononuclear catalysts is more straightforward, the results offer little benefit for understanding heterogeneous catalysts due to the drastic structural differences. Mononuclear complexes lack the cooperative metal–metal interactions observed on surface catalysts and cannot model synergistic interactions, presumed to be central to the functioning of heterogeneous catalysts. For modelling the active sites of solid state catalysts, discrete homogeneous clusters of interacting metals, incorporating multiple metal sites are more appropriate.^{106, 111-117}

In 1964, Cotton described clusters as a group of metal atoms (three or more) with substantial metal–metal bonding.¹¹⁷⁻¹¹⁸ However, the current definition has expanded to include compounds containing a group of two or more metals with any electronic or magnetic interactions.¹¹⁶ This definition covers a broader class of polynuclear complexes comprising highly diverse structures, nuclearities, oxidation states, and catalytic activities.^{112, 116, 119-121} Transition metal clusters may be homo- or heterometallic and can be further divided into two broad structural categories: (1) *naked* clusters and (2) *molecular* clusters. *Naked* metal clusters are unsupported by ligands, and exist only in an inert medium or isolated in a solid matrix (*e.g.*, **42**, Figure 2.2).^{115, 122} Molecular clusters are similarly polynuclear, but stabilized by ancillary ligands. Depending on the extent of metal–metal interactions, molecular clusters can be further sub-categorized as either molecular metal clusters or polymetallic *complexes*. In molecular metal clusters, the metals engage in direct metal–metal bonding/magnetic interaction (*e.g.*, **43** and **44**),

but unlike the naked clusters, molecular clusters are stabilized by terminal and, frequently, bridging ligands. In contrast, polymetallic complexes are multi-metal clusters lacking direct metal–metal bonding (e.g., **45**).^{106, 112, 115-116, 119-121, 123}

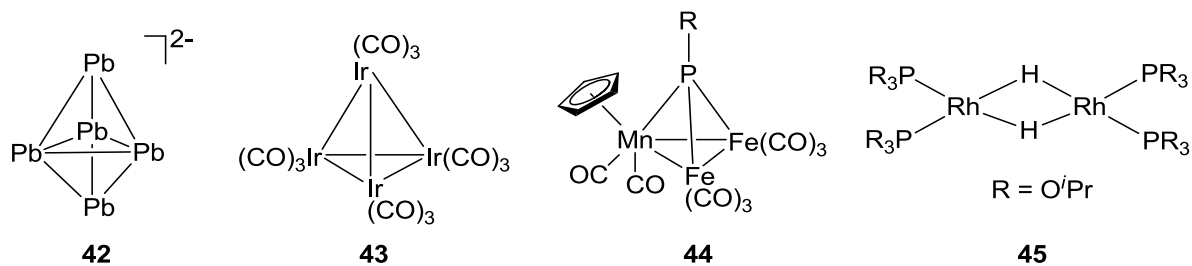
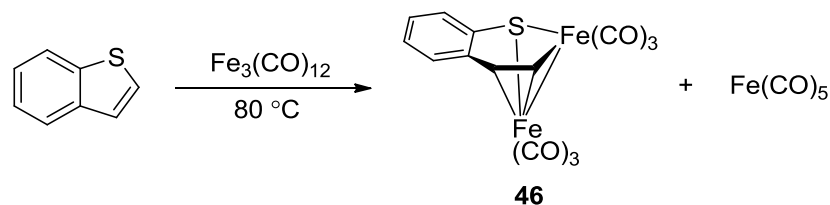


Figure 2.2 Representation of naked and molecular clusters.

Synergic interactions among multiple metal centers potentially result in beneficial catalytic properties. Multiple binding sites, present in some cluster, can lower substrate activation energies and stabilize fragments created during the transformation. In addition, multiple binding sites can provide enhanced selectivity control in some reactions.^{112, 115-116, 119-120} For instance, triiron dodecacarbonyl complex oxidatively adds the refractory C–S bond of benzothiophene upon heating to form the bridging organothiolate ligand stabilized by two Fe centers (**46**, Scheme 2.1).¹²⁴⁻¹²⁵



Scheme 2.1

2.1.2 Design and synthesis of low-coordinate transition metal clusters

For the design of *chemically* reactive polymetallic clusters, coordinatively unsaturated and sterically accessible metal centers are key. The reactivity of many polymetallic clusters is limited by coordinative saturation, where ancillary ligands or other metals occupy all potential metal binding sites.^{106, 111-112, 118, 126} Consequently, cleavage of a metal–metal or metal–ligand bond is required before substrate binding, but this can lead to the loss of structural integrity and eventual disintegration of the cluster and nanoparticle formation. A better alternative is to construct clusters comprised of low-coordinate transition metals, with persistent vacant coordination sites. In this case, no prior transformation or structural reorganization of the cluster is necessary for catalysis.^{106, 116, 127-128}

The design and synthesis of low-coordinate transition metals clusters is not without difficulties.^{112, 121, 127-128} Careful selection of ligands is critical to create coordinative unsaturation or high ligand lability while maintaining the integrity of the cluster.¹²⁷ Most often, bulky ligands are used to enforce low-coordination, but the resulting steric crowding can severely inhibit substrate binding (**47**, Figure 2.3).¹²⁰ The use of *bridging* ligands provides a means to synthesize coordinatively unsaturated clusters while avoiding steric crowding around each metal center (**48**, Figure 2.3).^{121, 127-128}

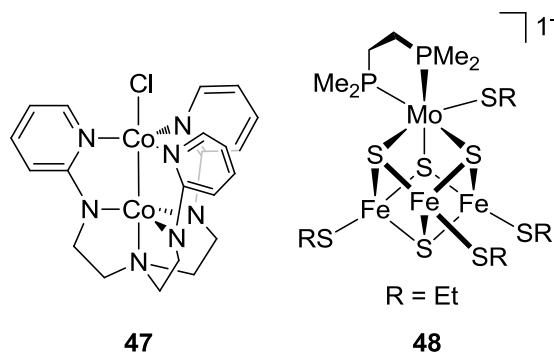


Figure 2.3 Examples of polymetallic complexes **47**¹²⁰ and **48**¹²⁷.

2.2 Design of homogeneous polynuclear clusters for hydrodesulfurization

The Stryker group is interested in the synthesis of *ancillary ligand-free low-coordinate* first-row transition metal clusters for the hydrodesulfurization of refractory organosulfur compounds. We are particularly interested in the middle to late first-row transition metals, *i.e.* manganese, iron, cobalt, nickel, and copper, because of their low relative costs, lower toxicity, and general abundance in the earth's crust.⁸⁹ To ensure facile reactivity, the polynuclear clusters are designed to enforce electronic and coordinative unsaturation at the metal atoms. Similar to the proposed active sites for industrial CoMoS catalysts, the clusters described here feature *single-atom ligand bridges* between the metal centers. This configuration is advantageous, maintaining the metal atoms in close proximity for cooperative activation and hydrogenolysis of the C–S bonds in refractory organosulfur compounds.

2.2.1 Phosphoranimide ligands for ancillary ligand free clusters

Anionic trialkylphosphoranimide ligands, $[\text{R}_3\text{PN}]^-$ (Figure 2.4) inherently nucleate polynuclear clusters.¹²⁹ Electronically isolobal to the cyclopentadienyl anion, the phosphoranimide can donate up to six electrons from a single nitrogen atom, formally making one σ -bond and up to two π -bonds.¹³⁰⁻¹³² Phosphoranimide ligands are also isoelectronic to dianionic silylamides, *e.g.* $[\text{R}_3\text{SiN}]^{2-}$, and alkoxides. Many main group and transition metal phosphoranimide complexes are known, prepared by many synthetic routes.¹³¹

The versatile bonding modes of the phosphoranimide ligand is very attractive for cluster synthesis, since a single ligand can bind to as many as three metal atoms.¹³¹ The terminal phosphoranimide ligand, bound to a single metal center, can donate six, four, or two electrons (bonding modes **A** or **B**; Figure 2.4). For six-electron donation (**A**), the metal–ligand bond is short and strong, with a nearly linear M–N–P angle. For four (or two)-electron bonding (mode **B**), the M–N bond is longer, leading to a non-linear M–N–P angle. These two bonding modes are typically observed for phosphoranimide ligands bound to a high oxidation state metal.

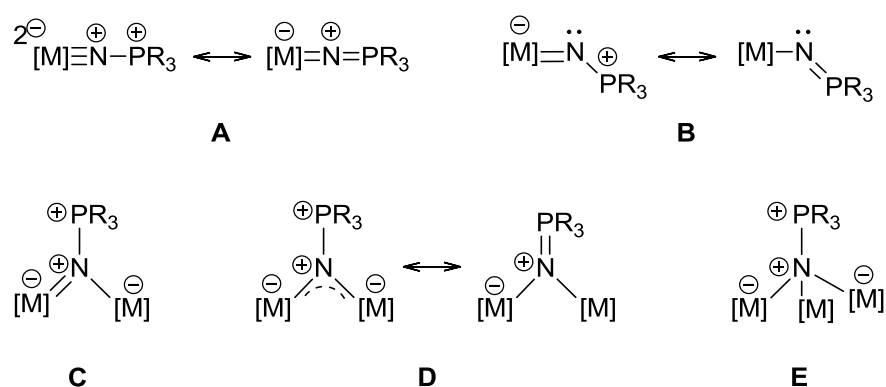


Figure 2.4 The phosphoranimide ligand has multiple binding modes.

The phosphoranimide ligand can also bond to multiple, lower-valent metal centers. Doubly-bridging phosphoranimide ligands can bind unsymmetrically (**C**, Figure 2.4) or, more commonly, symmetrically (**D**). Bridging the phosphoranimide lengthens the M–N bond and decreases the M–N–P bond angle.¹³¹ Typically, bimetallic clusters feature two μ^2 -bridging phosphoranimide ligands. Trimetallic six-electron bonding (mode **E**) is most common, observed in a range of later metal heterocubane clusters, with each μ^3 -phosphoranimide ligand occupying the corner sites of a cubic structure. In such structures, the M–N–M bond angles are acute and the metal centers adopt a distorted tetrahedral structure.¹³¹⁻¹³³

The electronic and steric properties of phosphoranimide ligands can be tuned by varying the substituents on phosphorus. Electron-donating substituents (ethyl, ^tbutyl) stabilize formally pentavalent phosphorus, decreasing net electron donation from the nitrogen atom to the phosphorus atom. The reduced N→P electron donation renders the phosphoranimide nitrogen more nucleophilic. This results in a longer N–P bond and shorter, stronger M–N bond.¹⁰³ The steric bulk of the phosphorus substituents also influences the nuclearity of the clusters.¹³¹ Smaller substituents, *e.g.* methyl and ethyl, readily accommodate up to three metal centers, generally forming heterocubane structure (**49**, Figure 2.5).¹³²⁻¹³⁷ Bulky substituents, *e.g.* ^tbutyl, can lead to the formation of mononuclear,¹³⁸⁻¹⁴⁰ binuclear,^{103, 141-143} or coplanar tetranuclear clusters^{25, 104, 144} (**50**, Figure 2.5), but restricts bridging to μ^2 -coordination.

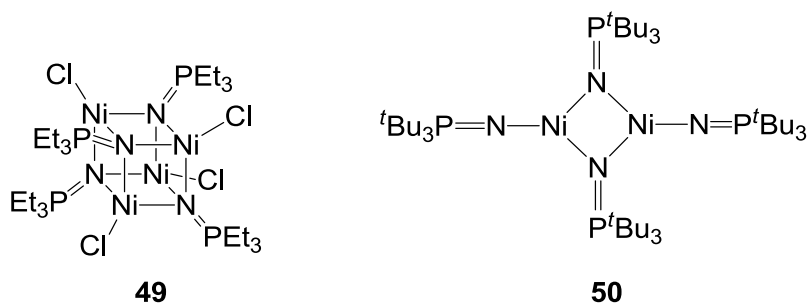


Figure 2.5 Ethyl substituents lead to tetrameric heterocubane cluster **49** whereas bulky ^tbutyl groups forms the dimeric μ^2 -phosphoramidate complex **50**.

Although steric bulk controls the hapticity of the phosphoramidate ligand, the large substituents are displaced from the metal center by the two-atom N–P linkage, maintaining reasonable steric accessibility to the metal. By comparison, the cyclopentadienyl anion occupies a similar coordination volume, according to Tolman cone angles (Figure 2.6).^{140, 145} However, the distance between the metal center and the large substituents is greater in the phosphoramidate ligand (2.2 Å for M–Cp vs. 3.4 Å for M–N–P). The N–P bond of the phosphoramidate is a “molecular spacer” between the metal center and the phosphine moiety, an important feature in our cluster design.¹⁰³

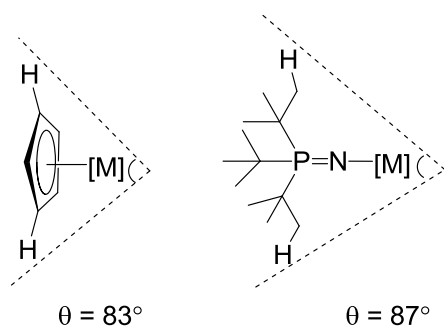
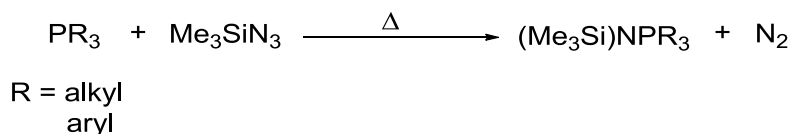


Figure 2.6 Tolman cone angles for cyclopentadienyl and tri(^tbutyl)phosphoramidate.

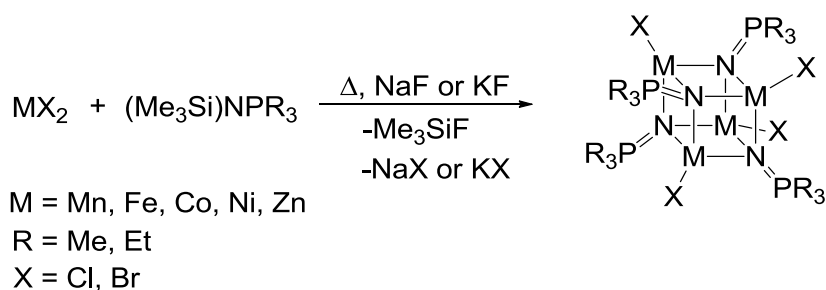
2.2.2 Syntheses of phosphoranimide ligands and metal clusters

The phosphoranimide ligand can be synthesized by multiple routes, which can be divided into two main categories: Staudinger-type oxidation of phosphines using silylazide^{129, 131} and Dehnicke's dihalophosphorane reaction with a metal amide.¹⁴⁶ We have adapted the latter for large scale synthesis of polynuclear clusters, due to its applicability over a wide range of phosphines, and easy metathesis with transition metal halides.¹⁴⁷

Dehnicke first described the synthesis of phosphoranimide ligand by a Staudinger-type oxidation of the phosphine using trialkylsilyl azide at elevated temperature, giving the neutral silylphosphoranimide in high yield (Scheme 2.2).¹²⁹ However, azide reagents are very toxic, expensive, and potentially explosive, limiting the method to small-scale syntheses.¹⁴⁸ For low molecular weight silylphosphoranimides, the molten silylphosphoranimide reacts directly with many transition metal halides in the presence of excess fluoride (Scheme 2.3). The very strong Si-F bond is the thermodynamic driving force for complete metathesis of the phosphoranimide and metal salts. The absence of fluoride leads only to dative silylphosphoranimide bonding. The direct metathesis of the silylphosphoranimide ligand is impossible for most alkyl- and all aryl-substituted silylphosphoranimides, which do not melt at accessible temperatures.^{131, 134-137}

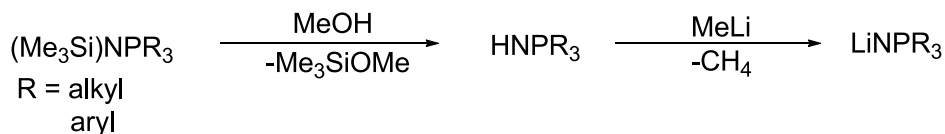


Scheme 2.2

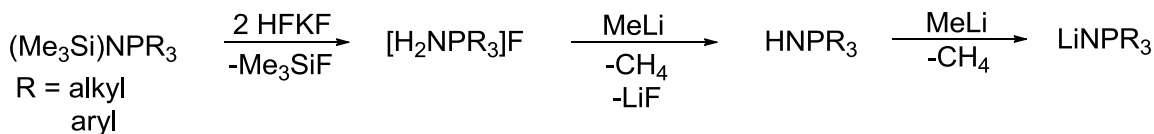


Scheme 2.3

Synthesis of halide-capped transition metal phosphoranamide complexes bearing large alkyl or aryl substituents requires prior hydrolysis of the silylphosphoranamide, followed by deprotonation (Scheme 2.4). The resulting lithium salt is added to a metal halide and the ensuing metathesis reaction forms the metal phosphoranamide complex.^{131, 149} An improved procedure for the hydrolysis of the silylphosphoranamide replaces methanol with potassium hydrogen bifluoride for simpler isolation of the intermediate phosphoranimine (Scheme 2.5).¹⁵⁰

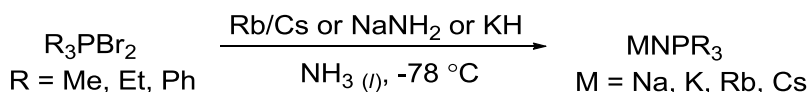


Scheme 2.4

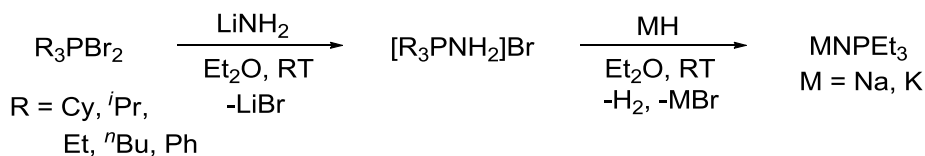


Scheme 2.5

Dehnicke and coworkers also reported an alternative, azide-free synthesis of phosphoranimides salt by the reaction of dihalophosphorane with an alkali metal amide.¹⁴⁶ Initially, Cs or Rb amides were used, generated *in situ* from the metals in liquid ammonia. The nucleophilic amide ion displaces halide from the dihalophosphorane; subsequent *in situ* deprotonation produces the alkali metal phosphoranimide (Scheme 2.6). Sodium amide and potassium hydride can be used in place of the dissolving metal to give the sodium and potassium phosphoranimide salts, respectively.¹⁴⁶ More conveniently, our current method avoids the use of ammonia by using commercial lithium amide in diethyl ether, giving the phosphoraniminium salt, which is easily deprotonated by using sodium- or potassium hydride (Scheme 2.7).¹⁵⁰

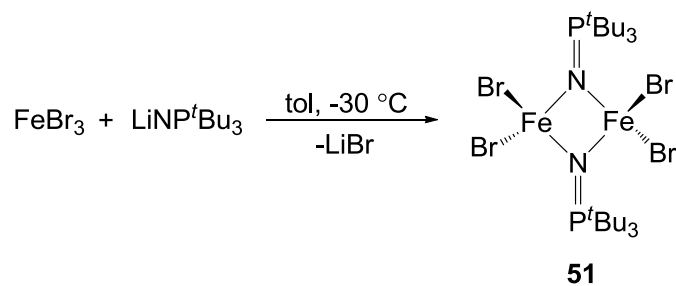


Scheme 2.6



Scheme 2.7

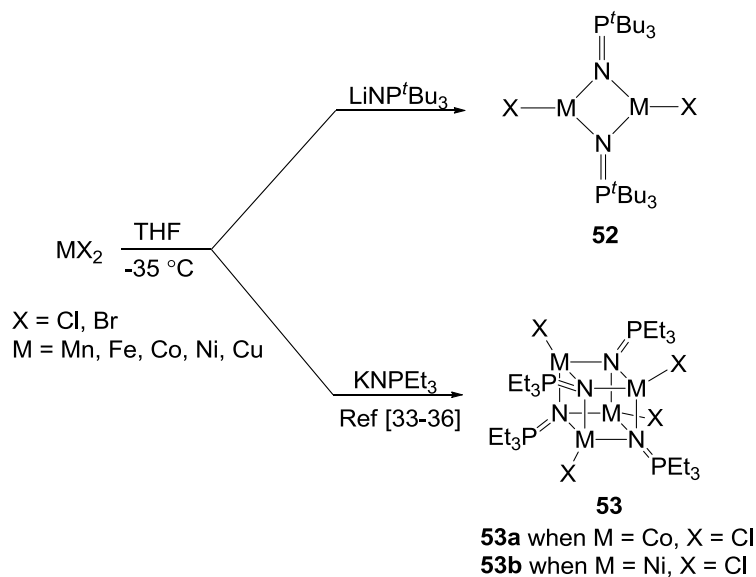
Anionic metathesis provides a highly convenient and general method for installing the phosphoranimide ligand on various transition metal compounds. Stephan, *et al.*, first demonstrated the simplicity of this metathesis reaction in a limited study of iron, obtaining dimeric complex **51** from ferric bromide and lithium tri(*n*-butyl)phosphoranimide (Scheme 2.8).¹⁴²



Scheme 2.8

2.2.3 Previous “Stryker group” transition metal phosphoramidate cluster synthesis

Our research group has used low-temperature metathesis to build a large library of phosphoramidate-supported metals clusters. Several of these compounds are precatalysts for hydrodesulfurization in the presence of stoichiometric base, as well as for hydrosilylation and hydrogenation. Halide-capped bi- and tetranuclear clusters **52**¹⁴² and **53**¹³⁴⁻¹³⁷ are useful starting points for the preparation of structurally varied polymetallic precatalysts.



Scheme 2.9

Replacement of the halides with terminal phosphoranimide ligands provides homoleptic bisphosphoranimide complexes **54** and **55** (Mn^{24} , Fe^{151} , $\text{Co}^{103, 151}$, and Ni^{24} ; Figure 2.7), which react readily with hydrogen to form active hydride catalysts. Homoleptic clusters **54** and **55** are typically prepared directly from the metal halide and two equivalents of the phosphoranimide anion, without isolating the intermediate halide-capped cluster. Hydrocarbyl-capped heterocubane clusters of $\text{Mn}^{24, 152}$, $\text{Fe}^{151-152}$ and Co^{103} **56** were reported by Dehnicke and, later, by Stryker, *et al.*, from the reaction of an anionic alkylating agent. Methyl lithium can be used to prepare the Mn and Fe compounds,¹⁵² but the analogous cobalt alkylation required the use of dimethylmagnesium in dioxane, taking advantage of the Schlenk equilibrium and precipitation of insoluble $\text{MgCl}_2 \cdot \text{dioxane}$ (see Scheme 2.11, below).¹⁰³ Methyl-capped bimetallic tri(*t*-butyl)phosphoranimide clusters **57** of Mn^{24} and Fe^{151} are prepared by initial treatment of the metal halide with MeLi, followed by addition of the tri(*t*-butyl)phosphoranimide salt. Allyl-capped binuclear clusters of Fe^{153} , Co^{153} and $\text{Ni}^{25, 153}$ (**58**) are also prepared in this fashion.

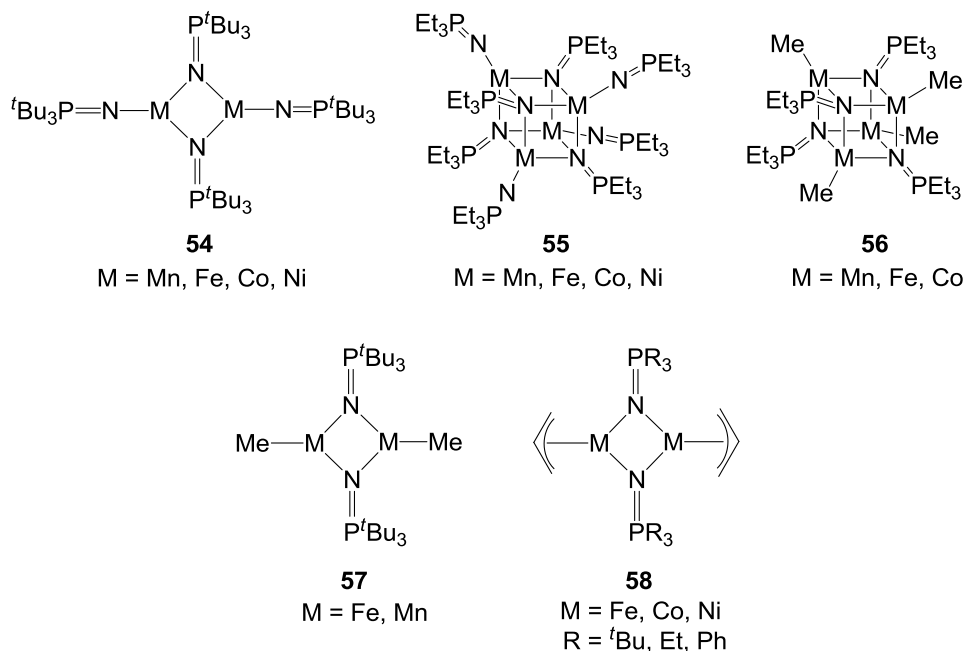
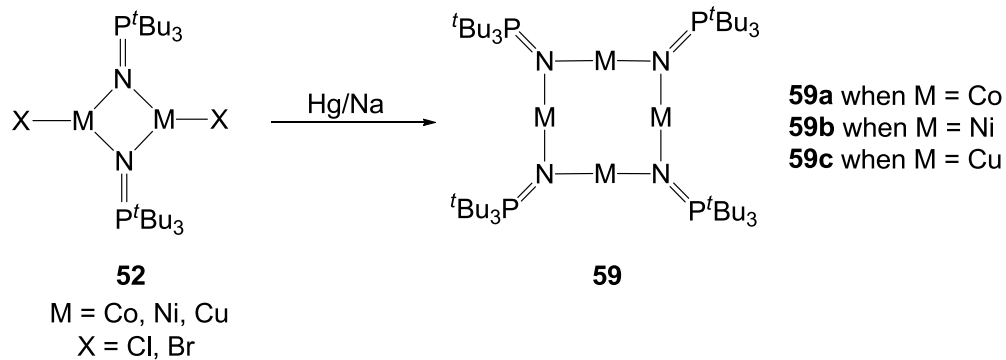


Figure 2.7 A library of transition metal phosphoranamide clusters synthesized by the Stryker group members.

Bunquin and Brown in the Stryker group isolated structurally unprecedented *linear, two-coordinate* tetranuclear clusters of Co (**59a**)¹⁴⁴ Ni (**59b**),^{25, 144} and Cu (**59c**)²⁴ from the reduction of dimeric **52** using sodium amalgam or other alkali metal (Scheme **2.10**). These homoleptic clusters feature four co-planar monovalent metal ions in an extremely low coordination environment.^{24-25, 104, 144} Reduction of halide-capped heterocubane clusters affords pentane-soluble amorphous powders, which are highly reactive, but not structurally characterized.¹⁰⁴



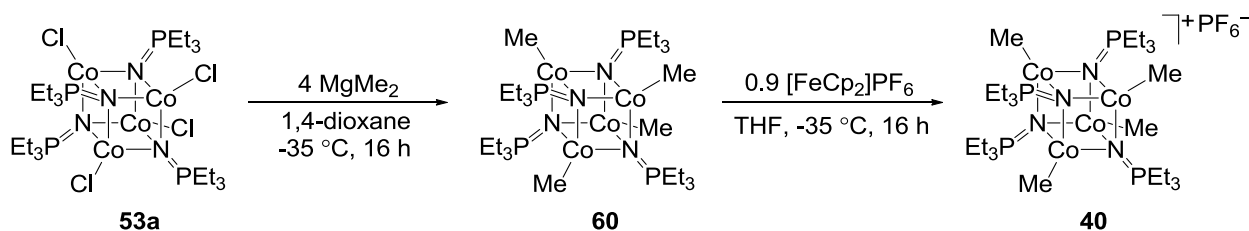
Scheme 2.10

2.2.4 Syntheses of the Co heterocubane complexes

For this thesis, triethylphosphoranimide-supported heterocubane clusters of Co and Ni are the most pertinent structural motifs. Dr. Houston Brown first studied methyl-capped cobalt phosphoranimide cluster **60** (Scheme 2.11) as a precatalyst for HDS,¹⁰³ anticipating that the M–C bonds would readily undergo hydrogenolysis to form the active metal–hydride catalyst.¹⁵⁴⁻¹⁵⁵ Unfortunately, cobalt cluster **60** undergoes hydrogenolysis only slowly under high hydrogen pressure (see chapter 3), implying that hydrogenolysis of Co(II)–Me bonds is not facile.¹⁰³

For reasons fully described in chapter 3, one-electron oxidation of methyl-capped cluster **60** yields an isostructural, mixed-valence cluster with tremendously enhanced reactivity (Scheme 2.11). The resulting cationic cobalt cluster **40** activates hydrogen rapidly at low pressure and temperature, and provides a superior catalyst for hydrodesulfurization reactions mediated by stoichiometric potassium hydride. DFT calculations performed by collaborators¹⁵⁶ indicate that the LUMO in the cationic cluster **40** is lower in energy than in the neutral cluster **60**, accounting generally for the difference in hydrogenolysis reactivity. The mixed-valence cluster **40** also

catalyzes the hydrogenolysis of strong C–O bonds, again in the presence of stoichiometric KH.¹⁰³



Scheme 2.11

2.3 Results and Discussion

2.3.1 Synthesis of thiolate-capped cobalt and nickel triethylphosphoranimide heterocubane complexes

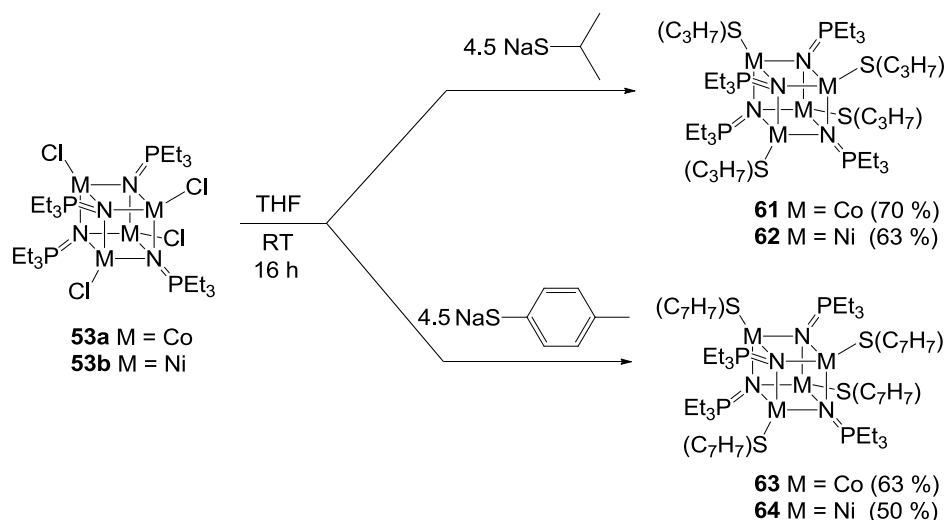
To diversify the library of potential polymetallic precatalysts, we explored the synthesis of thiolate-capped tetranuclear complexes for use in hydrodesulfurization. The basic lone pair on the sulfur atom can, in principle, assist in the heterolytic activation of hydrogen, a mechanistic pathway unavailable to alkyl ligands. Transition metal thiolate complexes in biological systems are known to activate molecular hydrogen, presumably through heterolytic cleavage.¹⁵⁷⁻¹⁵⁸ Importantly, transition metal thiolate complexes model one of the putative intermediates in catalytic hydrodesulfurization, valuable for probing the rate and mechanism of M–S bond hydrogenolysis.⁷ More importantly, the μ^2 -sulfido metal complexes, the syntheses described fully below, also represent one of the intermediates in the HDS reactions (see chapter 1). Indeed, several studies have shown that hydrogenolysis of this M–S bond is generally the rate limiting

step of the catalytic cycle for HDS,^{5, 7, 158} and a working understanding of the mechanism of this process in our system is greatly desired.

For this study, two electronically distinct alkylthiolates were selected. The isopropyl substituent is electron-donating, making the lone pair on sulfur more basic, which we posited should lead to facile heterolytic hydrogen activation. Conversely, the electron-withdrawing *p*-toluene substituent leads to a more polarized, weaker metal–sulfur interaction, which may promote M–S bond hydrogenolysis. The *p*-toluenethiolate ligand is particularly attractive because it is structurally similar to the 2-phenylthiophenolate intermediate presumably formed during the hydrodesulfurization of DBT.

These metal thiolate compounds were prepared from the metathesis reaction of the chloride-capped heterocubane clusters of cobalt and nickel (**53a,b**) with the sodium thiolate salts (Scheme **2.12**). Alternative routes for the preparation of transition metal thiolate complexes include protonolysis of M–Y bonds (Y = C, N, O) using a neutral thiol or oxidative addition of disulfides.¹⁵⁴ However, for our purposes, the room temperature metathesis reaction proved to be most convenient (Scheme **2.12**). A slight excess of the thiolate salt is required to ensure complete substitution; analytically pure thiolato complexes **61–64** were isolated by titration into a 1 : 1 mixture of hexane and toluene. X-ray quality single crystals of clusters **61–63** were obtained from cold, saturated THF solutions. The solid-state structures of compounds **61–63** all reveal the familiar M₄N₄ distorted heterocubane core, with each pseudotetrahedral metal capped by a terminal thiolate ligand. Despite our best efforts, X-ray quality crystals of *p*-toluenethiolate-

capped nickel cluster **64** have not been obtained; however, a heterocubane structure analogous to the other clusters is confidently proposed.



Scheme 2.12

The Co–N bonds in 2-propanethiolate cluster **61** (2.1011(3) Å, Table 2.1) are longer than those observed in all other phosphoranimide-supported heterocubane clusters of cobalt (Figure 2.8a). Despite this slightly expanded Co₄N₄ core, the Co–N–Co and N–Co–N bond angles in cluster **61** are nearly identical to those observed in the chloride- or methyl-terminated clusters.^{103, 135} A distorted tetrahedral symmetry characterizes each cobalt center, featuring three smaller N–Co–N bond angles of 92.59(11)° and an obtuse N–Co–S bond angle of 129.41(9)°, deviating significantly from the ideal bond angles in a tetrahedral complex (109.5°). The Co–S bond length for the terminal 2-propanethiolate ligand (2.2535(12) Å) is well within measured values for terminal Co–SR bonds.¹⁵⁹⁻¹⁶⁰ The bond distance between pairs of cobalt atoms (2.7692(8) Å) precludes a direct Co–Co bond interaction, which typically involves an internuclear distance of 2.4–2.6 Å.¹⁶¹⁻¹⁶² Despite the absence of direct metal–metal bonding, the cobalt atoms interact

strongly through the single-atom bridges, as supported by DFT calculations performed on similar heterocubane clusters.¹⁵⁶

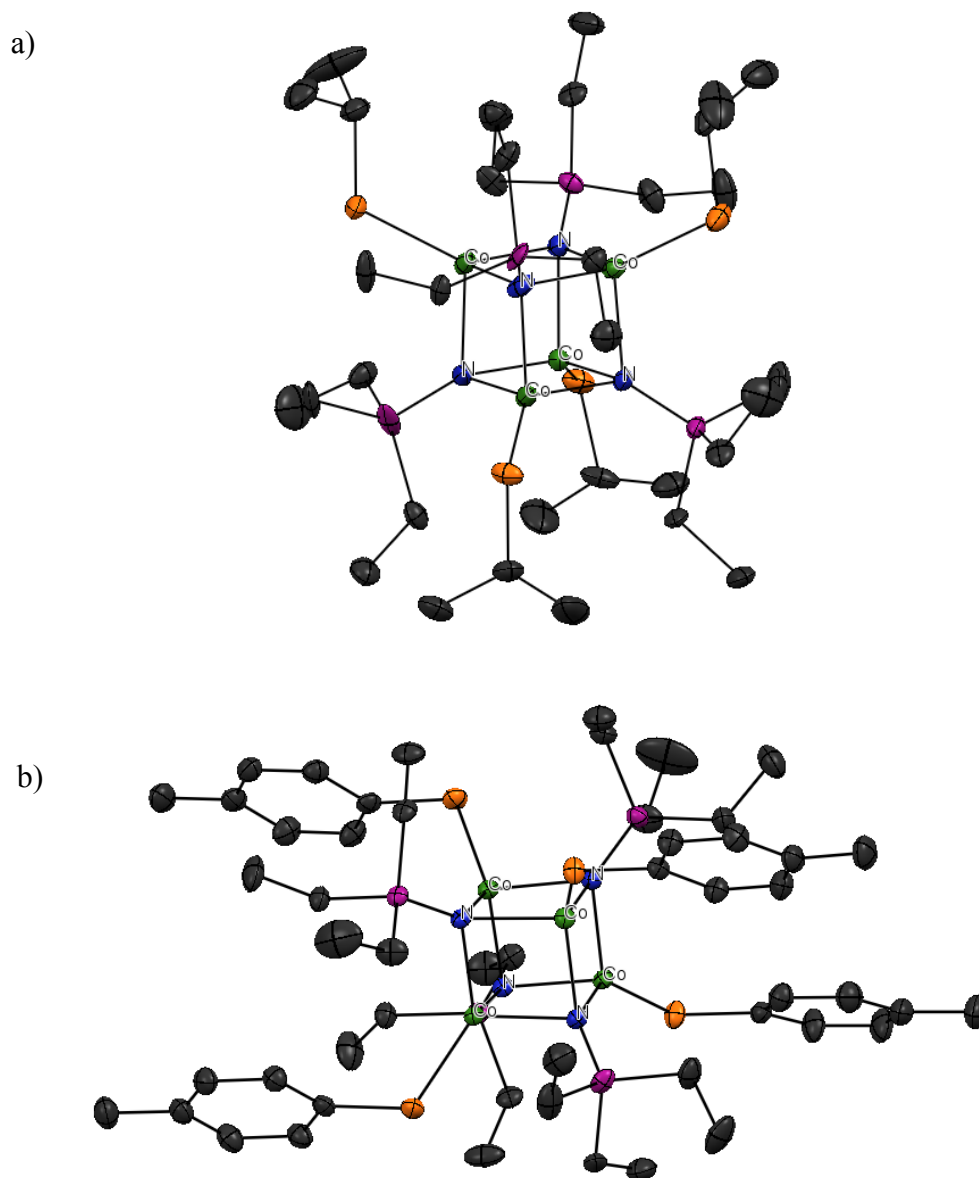


Figure 2.8 ORTEP diagrams of (a) [Co(NPET₃)(S'Pr)]₄ **61** and (b) [Co(NPET₃)S(C₆H₅(CH₃))]₄ **63**. The thermal ellipsoids are shown at 30% probability, and hydrogen atoms are omitted for clarity. R_1 (**61**) = 0.0438, R_w (**61**) = 0.1185, R_1 (**63**) = 0.0351, R_w (**63**) = 0.1008.

Table 2.1 Selected bond lengths and angles for cobalt heterocubane complex **61**.

[Co(NPEt ₃)(S ^{<i>i</i>} Pr)] ₄ 61			
	Bond length (Å)		Bond angle (°)
Co••Co	2.7692(8)	Co–N–Co	87.93(11)
Co–N	2.1011(3)	N–Co–N	92.59(11)
N–P	1.584(3)	Co–S–C	111.79(15)
Co–S	2.2535(12)		
S–C	1.823(5)		

Key bond metrics for cobalt *p*-toluenethiolate cluster **63** are nearly identical to those of 2-propanethiolate cluster **61**. The Co–N bond lengths of the *p*-toluenethiolate complex **63** are slightly shorter (2.0418(15) Å), but the Co–N–Co and N–Co–N bond angles of 87.22(6)° and 92.43(6)° (Table 2.2), respectively, remain unchanged. The shorter Co–N bonds in cluster **63** can be attributed to the electron-withdrawing *p*-toluene substituent and, consequently, weaker Co–S bond. However, this observation must be interpreted with caution. The Co–S bond length of both thiolate-capped complexes **61** and **63** are nearly identical, raising the question of whether the electronic nature of the hydrocarbon substituent on the sulfur has any measurable effect on the Co–S or Co–N bond lengths. Crystal packing forces in the solid state are more likely to account for the slight difference between the two structures.

Table 2.2 Selected bond lengths and angles for cobalt heterocubane complex **63**.

[Co(NPEt ₃)(SC ₇ H ₇)] ₄ 63			
	Bond length (Å)		Bond angle (°)
Co••Co	2.8443(1)	Co–N–Co	87.22(6)
Co–N	2.0418(15)	N–Co–N	92.43(6)
N–P	1.5950(15)	Co–S–C	114.79(1)
Co–S	2.2616(5)		
S–C	1.781(2)		

The heterocubane core of the corresponding nickel 2-propanethiolate cluster **62** (Figure 2.9) is isostructural with the Ni₄N₄ core of the starting chloride-capped nickel phosphoranimide cluster **53b** reported by Dehnicke, *et al.*¹³⁴ The Ni–N bond length (2.028(3) Å) and Ni–N–Ni and N–Ni–N bond angles (91.53(12)° and 88.53(12)° respectively; Table 2.3) are nearly identical to the reported values of the parent halide cluster **53b**.¹³⁴ Similar to the cobalt thiolate clusters, the nickel centers of thiolate complex **62** have a distorted tetrahedral symmetry with smaller N–Ni–N bond angles of 88.53(12)° and obtuse N–Ni–S bond angle of 111.63(18)°. The Ni–S bond (2.2444(11) Å) of thiolate cluster **62**, are slightly shorter than the Co–S bonds of the heterocubane clusters **61** and **63**, but are within the range assigned to terminal nickel thiolate bonds.¹⁶⁰

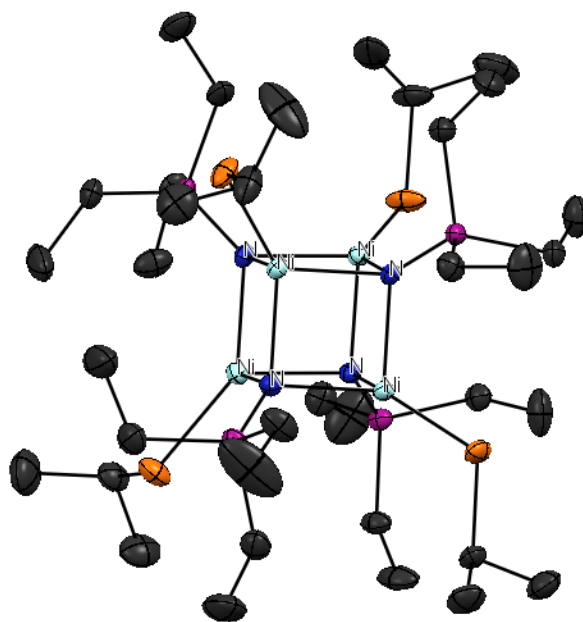


Figure 2.9 ORTEP diagrams of [Ni(NPEt₃)(S'Pr)]₄ (**62**). The thermal ellipsoids are shown at 30% probability, and hydrogen atoms are omitted for clarity. R₁ = 0.0513, R_w = 0.1512.

Table 2.3 Selected bond lengths and angles for nickel heterocubane cluster **62**.

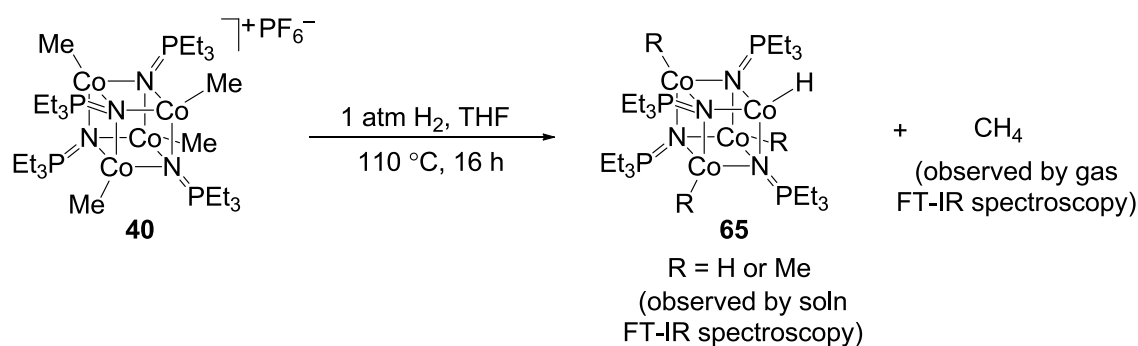
[Ni(NPEt ₃)S(C ₆ H ₅ (CH ₃))] ₄ 62			
Bond length (Å)		Bond angle (°)	
Ni••Ni	2.9123(8)	Ni–N–Ni	91.53(12)
Ni–N	2.028(3)	N–Ni–N	88.53(12)
N–P	1.586(3)	Ni–S–C	111.63(18)
Ni–S	2.2444(11)		
S–C	1.894(6)		

2.3.2 Synthesis of HDS reaction intermediates: sulfide- and hydride-capped phosphoranimide clusters of cobalt

The synthesis and characterization of the phosphoranimide-supported cobalt hydrido and sulfido clusters were targeted as part of our probe into the mechanism of the hydrodesulfurization reaction (*vide infra*). Such complexes are widely accepted to be intermediates in catalytic HDS reactions, with the latter critical to catalyst turnover.⁷ Dr. Houston Brown initially demonstrated that cationic cobalt cluster **40** reacts with molecular hydrogen (1 atm) at room temperature, as evidenced by a color change from green to light brown.¹⁰³ Solution UV-Vis spectroscopy confirmed this reaction, with a significant change in the shape of the absorbance spectrum of **40** observed upon exposure to hydrogen. However, an FT-IR spectrum of the solid isolated from this reaction did not reveal absorbance bands diagnostic for the presence of Co–H bonds.¹⁰³

Following up on these initial results, a solution of cluster **40** was heated to 110 °C for 16 h under hydrogen (Scheme **2.13**), which also resulted in a color change from green to dark brown. Gas-phase FT-IR spectrum of the volatiles in the headspace of the reactor established the presence of methane, formed from hydrogenolysis of at least one Co–Me bond (see

experimental). Furthermore, FT-IR spectroscopy of the remaining dark brown solution revealed a weak but sharp absorbance at 1900 cm^{-1} corresponding to a terminal Co–H bond.^{155, 163} This reaction does not, however, lead to the isolation of a structurally characterized hydride cluster.



Scheme 2.13

Hydrogenolysis of metal–heteroatom bonds (N, O, and S), *via* heterolytic activation pathway, presumably proceeds through a four-center transition state (e.g., **66**, Figure 2.10) leading to transfer of a proton with concomitant formation of the metal–hydride **67**.¹⁶⁴ This pathway is mechanistically distinct from σ -bond metathesis because it relies on the overlap between the filled non-bonding orbital of the ligand and the σ^* -orbital of dihydrogen, resulting in a highly polarized, cooperative cleavage of the H–H bond.¹⁶⁴⁻¹⁶⁵ In this pathway, no open coordination site on the metal is necessary. An external Brønsted base, not bound to the metal, can also assist in heterolytic activation of the hydrogen molecule, but an open coordination site for hydrogen must be present.¹⁶⁶ The terminal ligand of the homoleptic bis(phosphoranimide)cobalt cluster **69** (see Scheme 2.14, below) provides an ideal basic site for cluster activation by heterolytic activation. Bis(phosphoranimido) cluster **69**, initially prepared

by Dr. Houston Brown, remained unexplored until this work. Chapters 3 and 4 of this document provide a full discussion of this hydrogenolysis.¹⁰³

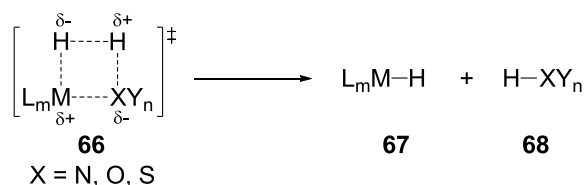


Figure 2.10 Heterolytic cleavage of H₂ with metal heteroatom bond.

Hydrogenolysis of the Co–N bond(s) in bisphosphoranimide cluster **69** presumably leads to a cobalt hydride and phosphoranimine (**71**, Scheme 2.14). Upon treatment at 110 °C under hydrogen and removal of unreacted starting material, the IR spectrum of the remaining THF-soluble fraction shows a weak absorption at 2197 cm⁻¹, suggesting the presence of a Co–H bond.^{155, 163} Unfortunately, neither free nor coordinated triethylphosphoranimine (**71**) was detected by either IR or NMR spectroscopy. In contrast, Dr. Orain Brown in the Stryker group detected liberated ^tBu₃PNH (**72**, Scheme 2.15) *via* ³¹P NMR spectroscopy, upon hydrogenolysis of bimetallic nickel tri(^tbutyl)phosphoranimide complex **50** under similar conditions.²⁴ However, in this case, rapid decomposition of the nickel hydride intermediate(s) preclude the observation of the Ni–H bond by IR spectroscopy. Taken together, these experiments nonetheless suggest that the terminal M–N bonds of the phosphoranimide-supported clusters undergo hydrogenolysis to form the metal hydride intermediates. This makes cobalt bisphosphoranimide cluster **69** an attractive precatalyst for the base-promoted HDS reactions (see Chapter 3).

The superficially analogous reaction using HBpin instead of 9-BBN unexpectedly yielded pinacolboronate-capped cobalt complex **76** (Figure 2.12) as the only crystalline product, albeit in indeterminate yield. The borane, in this case, is insufficiently electrophilic to react irreversibly at the nitrogen lone pair, leading to a more complex transformation of unknown mechanism. The origin of the unexpected oxygen in this process remains undetermined.

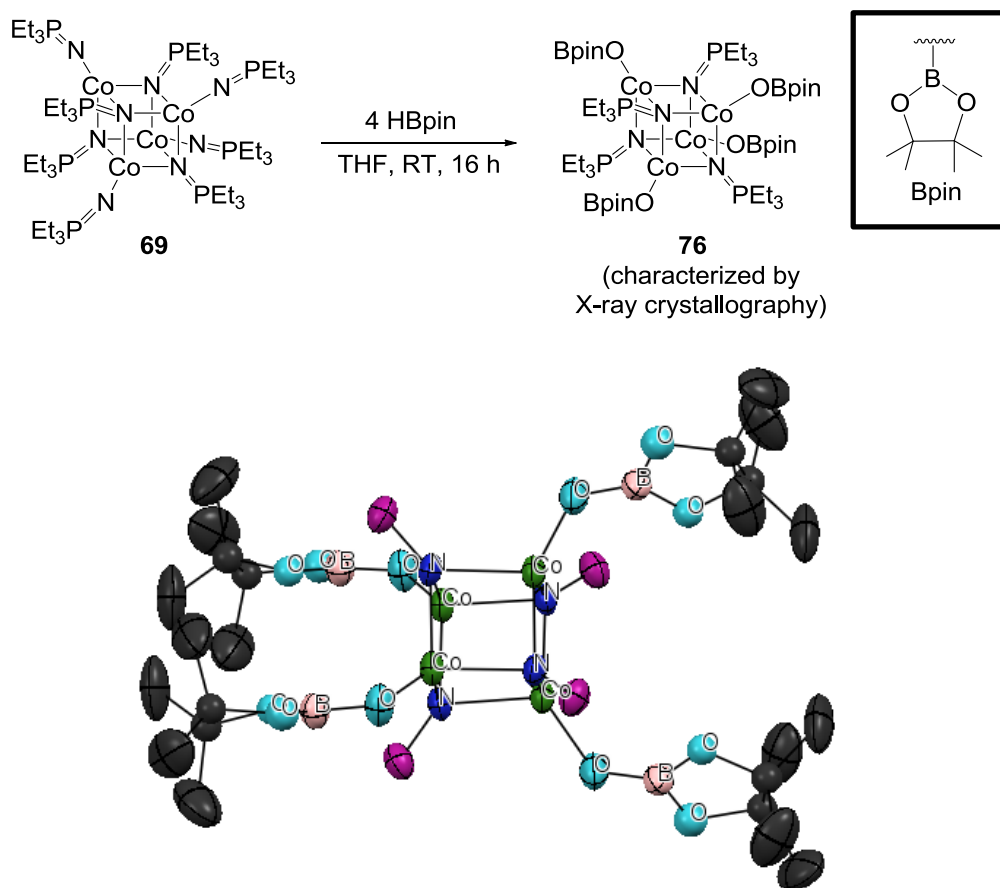
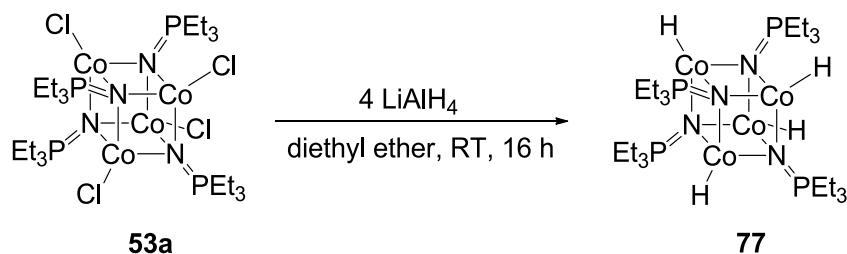


Figure 2.12 The synthesis and preliminary solid-state structure report of pinacolboronate-capped cobalt cluster **76**. The thermal ellipsoids are shown at 30% probability, where hydrogen atoms and the ethyl substituents on the phosphoranime are omitted for clarity. $R_1 = 0.0794$, $R_w = 0.2562$.

Following many unsuccessful attempts to isolate metal hydride complexes derived from the cobalt bisphosphoranime cluster, we attempted a more direct approach, despite a long

history of evident failures. Although the reaction of potassium hydride with chloride cluster **53a** does not proceed at an appreciable rate, both K-selectride and Superhydride reduce the cluster to colloidal Co(0). In contrast, the reaction with lithium aluminum hydride may provide cobalt (terminal) hydride complex **77** (Scheme 2.18), as characterized by elemental analysis and IR spectroscopy ($\nu_{\text{M-H}} = 2048 \text{ cm}^{-1}$). Unfortunately, recrystallization failed to afford X-ray quality crystals. In addition, to confirm the formation of this cobalt hydride complex, the reaction between chloride-capped cluster **53a** and lithium aluminum deuteride was investigated. The cobalt deuteride complex was characterized by IR spectroscopy, showing a lower M–D frequency ($\nu_{\text{M-D}} = 1722 \text{ cm}^{-1}$) as expected. This strongly suggests the formation of the cobalt hydride (and deuteride) complexes from the reaction of cluster **53a** and lithium aluminum hydride (and deuteride).



Scheme 2.18

The preparation of isolable cobalt sulfide clusters presented similar challenges. As highlighted in Chapter 1, stoichiometric desulfurization of organosulfur compounds by metal complexes invariably leads to metal sulfide intermediates, with strong hydrogenolysis-resistant M–S bonds.⁷ Deliberate synthesis of sulfided derivatives of our phosphoranimide-supported precatalysts provides the opportunity to develop conditions under which these metal–sulfide bonds more readily undergo hydrogenolysis. Dominique Hebert, of the Stryker group, pioneered

this work, preparing and characterizing μ^2 -sulfido iron tri(*t*-butyl)phosphoranimide complex **79** (Figure 2.13), using elemental sulfur as an oxidant.¹⁵¹ Analogous complexes of cobalt and nickel were prepared, but could not be isolated as crystalline compounds.

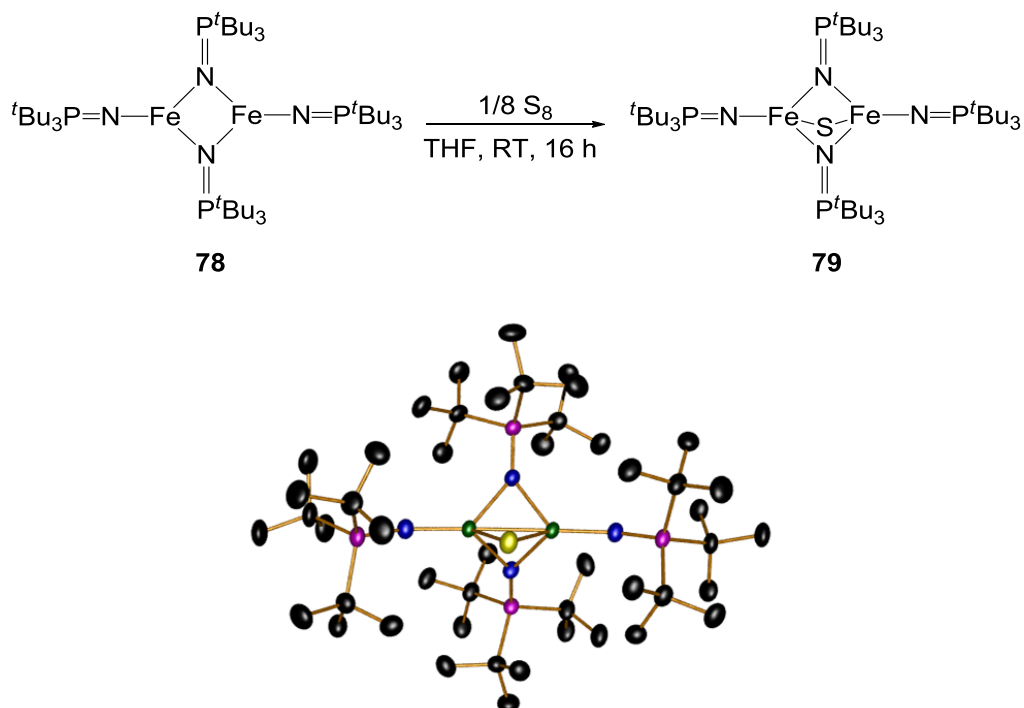
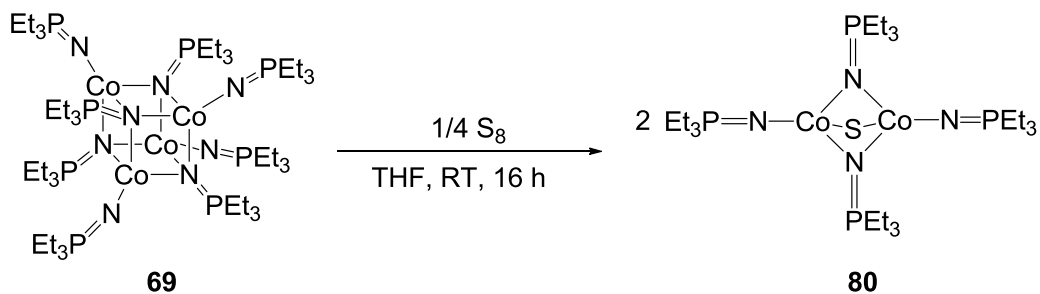


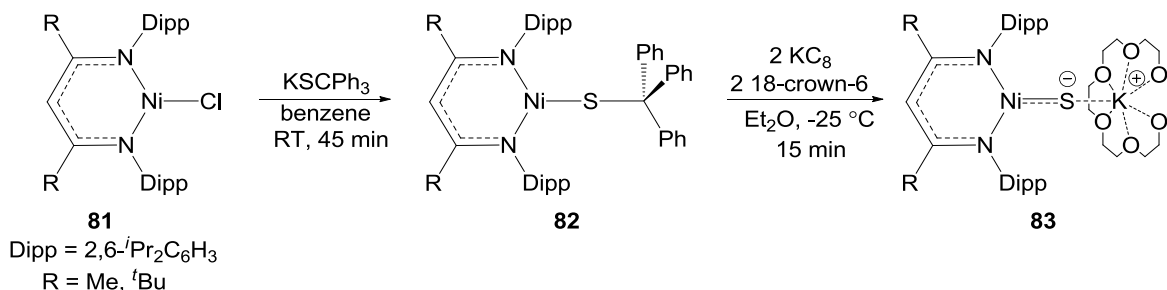
Figure 2.13 The synthesis of a bimetallic μ^2 -bridging sulfide complex.¹⁵¹

Using Hebert's method,¹⁵¹ a sulfided cobalt bisphosphoranimide cluster could be prepared from the reaction of cobalt bis(triethylphosphoranimide) complex **69** with elemental sulfur (Scheme 2.19). The reaction is poorly reproducible and single crystals could not be obtained, but combustion analysis is consistent with the expected μ^2 -sulfide complex **80**. An alternative synthetic method is clearly required.



Scheme 2.19

Hayton, *et al.*, reported an alternative method to isolate a ‘terminally’ bound Ni sulfide (complex **83**) *via* reductive dealkylation of the tritylthiolate complex.¹⁶⁹ The reduction of tritylthiolate Ni complex **82** with KC₈ in the presence of 18-crown-6 cleaves the weaker C–S bond rather than the Ni–S bond (Scheme 2.20). The nominally terminal sulfide complex (**83**) formed is actually capped by a potassium crown ether complex.



Scheme 2.20

We adapted this method by preparing the tritylthiolate-capped cobalt phosphoramidate cluster **84** (Figure 2.14) from chloride-capped cobalt cluster **53a** and KSCPh₃. Incomplete substitution of the chloride by the tritylthiolate ligand is evident in the solid-state structure of the “purified” cluster **79**, even after prolonged reaction times (16 h). We attribute this to the steric interactions between the phenyl substituents of the tritylthiolate and the ethyl substituents of the

phosphoranimide ligands. Unfortunately, reduction of this dithiolato cluster by KC_8 in the presence of 18-crown-6 led to an intractable mixture of products, in spite of careful control of stoichiometry and reaction conditions.

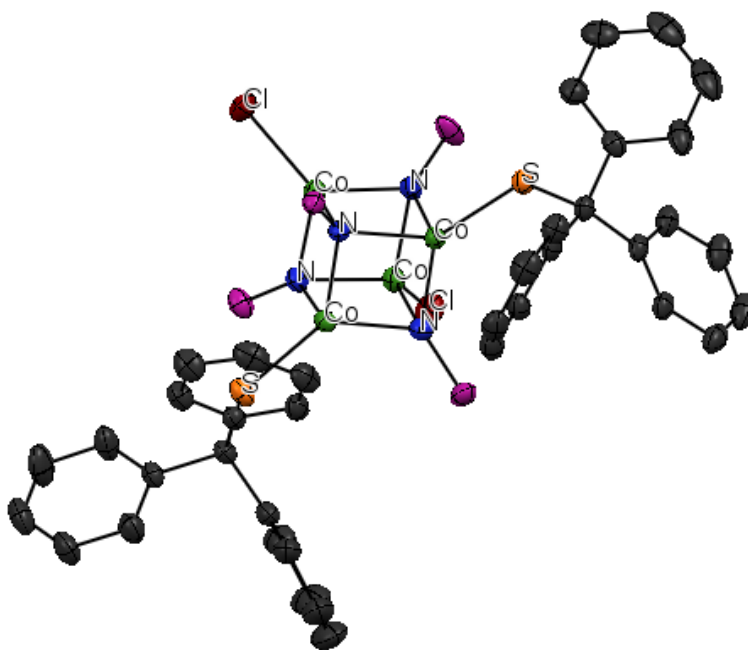
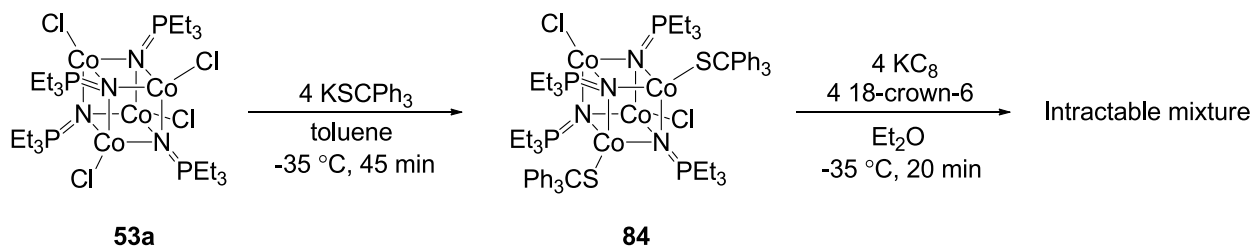


Figure 2.14 The metathesis reaction between the chloride-capped cluster **53a** and the KSCPh_3 yields the tritylthiolate cluster **84**. The thermal ellipsoids are shown at 30% probability, and the hydrogen atoms and the ethyl substituents on the phosphoranimide are omitted for clarity. $R_1 = 0.0515$, $R_w = 0.1511$.

2.4 Conclusion

Novel thiolate-capped cobalt and nickel phosphoranimide clusters have been prepared and structurally characterized. The 2-propanethiolate- and *p*-toluenethiolate-capped clusters were synthesized straightforwardly by metathesis using sodium thiolate. The solid-state structures confirmed the terminal binding of the thiolate to the metal centers, which are peripheral to the heterocubane core.

Phosphoranimide-supported cobalt hydride and μ^2 -sulfido clusters were prepared and partially characterized, providing opportunities for mechanistic investigations and precatalyst optimization. The syntheses are challenging and plagued by reproducibility issues, particularly on larger scale. Furthermore, solid-state characterization of key complexes remains incomplete.

In subsequent chapters, the hydride-mediated HDS activity of phosphoranimide-supported cobalt and nickel heterocubane clusters are described in detail. In addition, the precise role of these transition metal clusters in the desulfurization reaction will be examined.

3. Reactivity of Phosphoranimide-supported Heterocubane Clusters of Cobalt in Hydride-mediated Desulfurization

3.1 Previous HDS work using cobalt phosphoranimide complexes

The Stryker group is interested in polynuclear clusters of the late first-row metals as precatalysts for deep and ultra-deep hydrodesulfurization under mild reaction conditions. The phosphoranimide-supported clusters described in Chapter 2 (Figure 3.1) display promising HDS activity, catalyzing the desulfurization of DBT under mild conditions (1–34 atm H₂ and 110–200 °C) in the presence of stoichiometric strong base, particularly KH and KO^tBu.^{24-25, 103-104, 150} This dissertation is primarily concerned with the hydride-mediated HDS reactions catalyzed by triethylphosphoranimide-supported cobalt clusters. We are focused on understanding the nature of the active catalyst as well as the precise role of KH in the desulfurization reactions. This chapter briefly surveys a range of cobalt precatalysts, as well as examines the nature of the active catalyst. Chapter 4 follows with a comprehensive mechanistic discussion on the role of the hydride and the transition metal in the cleavage of C–S bonds in dibenzothiophenes.

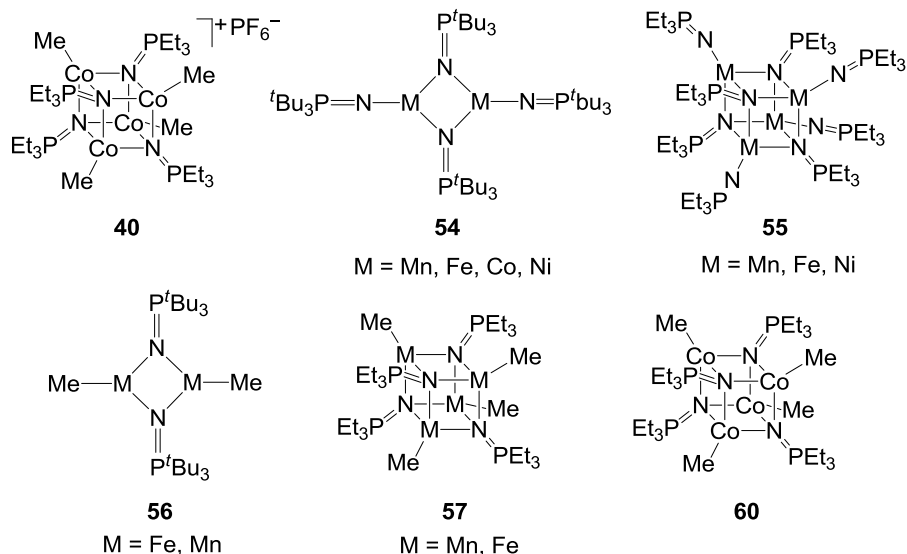
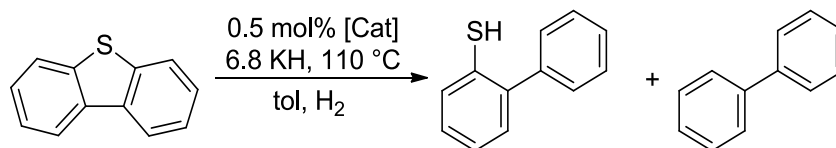


Figure 3.1 Polynuclear clusters for the desulfurization of organosulfur compounds.

The neutral methyl-capped cluster **60** and its mixed-valence cationic derivative **40** (Figure 3.1) were both investigated as precatalysts for hydride-mediated desulfurization reactions. The mixed valence tetranuclear cluster **40** promotes rapid desulfurization of DBT, in the presence of excess potassium hydride, at unprecedentedly mild conditions: 110 °C and 1 atm of H₂ pressure.¹⁰³ In contrast, the activity of the related neutral cluster is more subdued; methylcobalt cluster **60** only functions as a catalyst under high hydrogen pressure (34 atm H₂) and, even then, only achieves maximum turnover frequency (TOF) of 4.06 C–S bond cleavages per hour at this temperature (Table 3.1, entries 1–3). For comparison, the cationic cluster **40** was reported to achieve 95 C–S bond cleavages h⁻¹ with DBT under ambient pressure (entry 4).

Table 3.1 HDS reactions with [Co(NPEt₃)Me]₄ (**60**) and [Co(NPEt₃)Me]₄PF₆ (**40**).¹⁰³



Entry	[Cat]	H ₂ (atm)	Time (h)	TOF ^a (h ⁻¹)
1	60	1	17	0.00
2	60	34	1.2	0.00
3	60	34	2.0	4.06
4	40	1	0.5	95.00

KH is purified according to procedure outlined in the experimental section. ^aTurnover frequency (TOF) is defined as moles per C–S bond cleavage per mole of catalyst per hour.

The reason for the disparity in reactivity between the two clusters becomes clear by considering the electronic structure(s) of the constituent cobalt ions. In the neutral methylcobalt cluster **60**, each high-spin d^7 Co^{2+} center exists in a distorted tetrahedral environment in which all the d-orbitals are either fully or partially occupied. The absence of a vacant orbital impedes the coordination of hydrogen (a, Figure 3.2); thus, the only available pathway to cleave the Co–Me bond, forming the active Co–H catalyst, is *sigma*-bond metathesis (σ –BM) (a, Scheme 3.1).¹⁷⁰ In contrast, the oxidized cluster **40** has one Co atom formally in the +3 oxidation state, creating a vacant, low-lying orbital in the cluster for H_2 coordination (b, Figure 3.2). This Co– H_2 *complex* weakens the H–H bond, allowing the more facile σ -*complex assisted metathesis* (σ –CAM) reaction to proceed, forming the active Co–H intermediate (b, Scheme 3.1).¹⁷¹

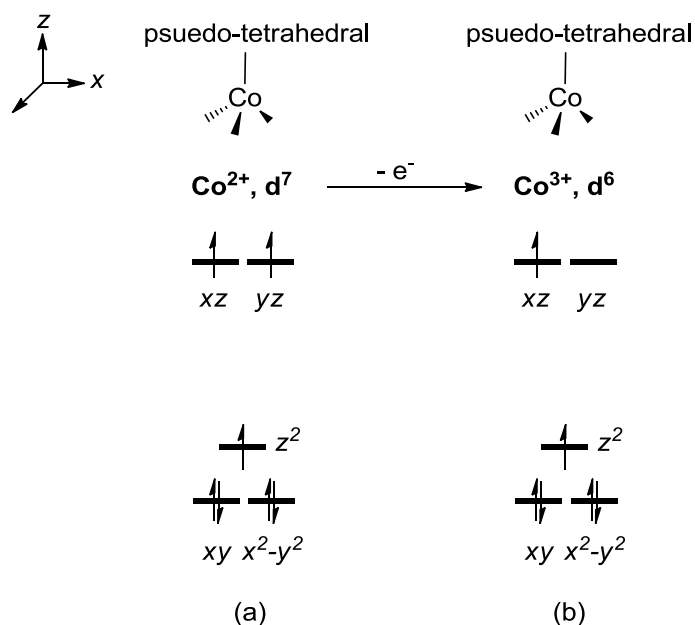
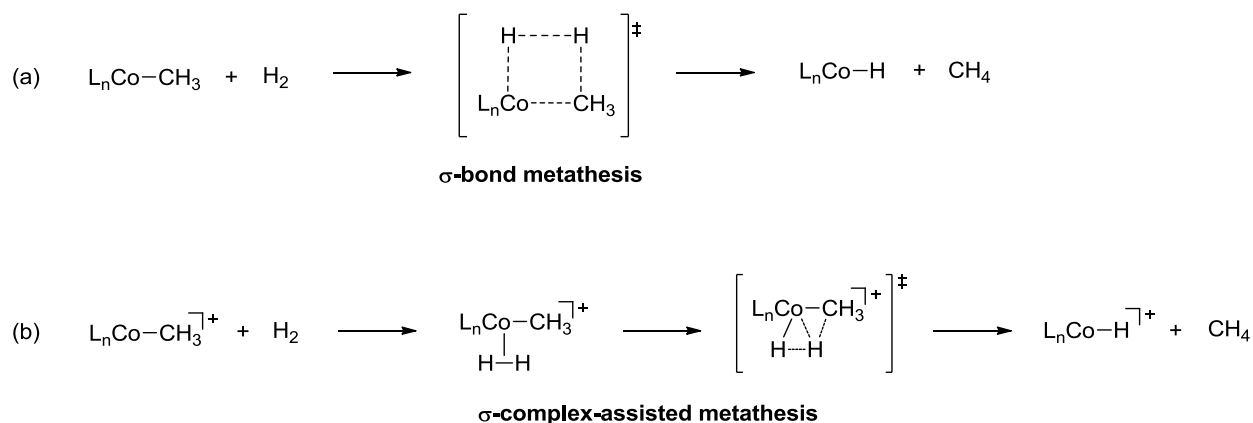


Figure 3.2 The cobalt heterocubane clusters adopt a pseudo-tetrahedral structure where a Co^{3+} center would have one vacant orbital (b).¹⁰³



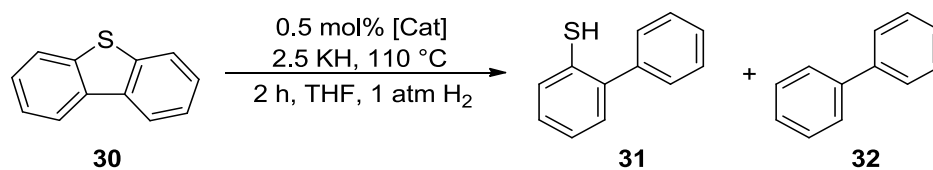
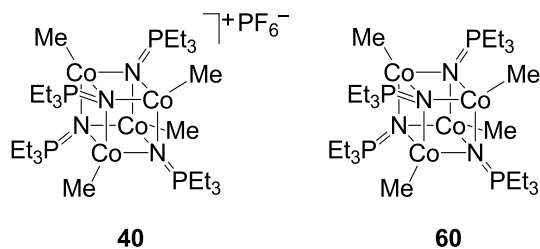
Scheme 3.1

3.2 Results and Discussion

3.2.1 Optimization of KH-mediated desulfurization of DBT by cobalt clusters **40** and **60**

More recent experiments raised questions regarding the reactivity of the tetranuclear cobalt phosphoranimide clusters **40** and **60**. In the original report, the mixed-valence cluster **40** promotes quantitative desulfurization of DBT after just one hour using 6.8 equivalents of KH.¹⁰³ However, under nominally identical conditions, we observed at best 63% conversion of DBT to a mixture of biphenyl and 2-phenylthiophenol (Table 3.2, entry 1). Quantitative conversion of DBT can be obtained only by increasing the reaction time, and even then, the fraction of 2-phenylthiophenol is significant (35%, entry 2). Furthermore, the neutral methylcobalt complex **60**, previously reported to be inactive under mild conditions (see Table 3.1), catalyzes hydride-mediated HDS at 110 °C and 1 atm of H₂ (Table 3.2, entry 5), though the yield of biphenyl is low. This unexpected, albeit inefficient, desulfurization activity led us to speculate that other neutral Co²⁺ phosphoranimide clusters may also be well-suited as HDS precatalysts.

Table 3.2 Catalytic HDS with phosphoranimido cobalt clusters **40** and **60** in the presence of stoichiometric potassium hydride yield high conversion of DBT to biphenyl.



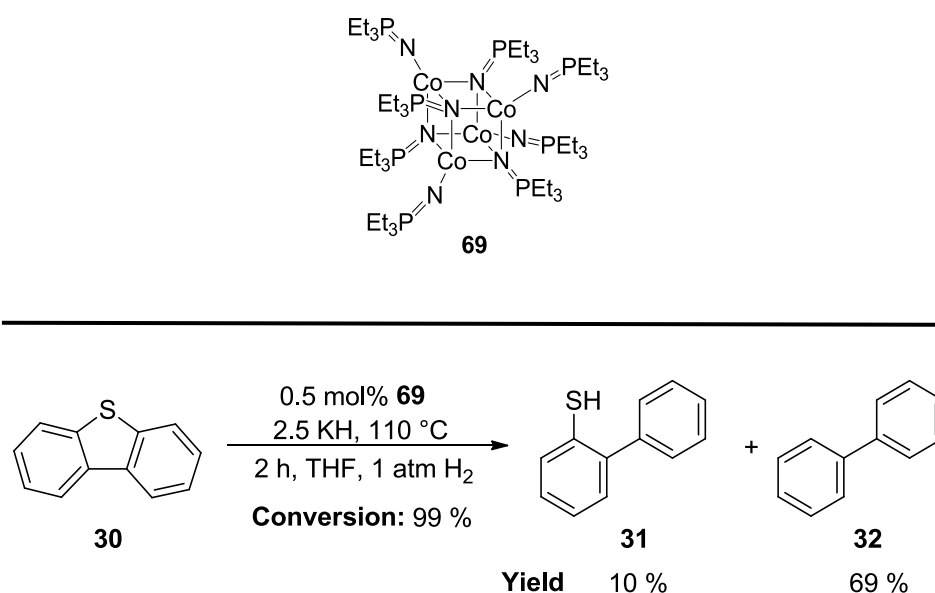
Entry	[Cat] ^a	Conversion (%) ^b	31 (%)	32 (%)
1	40	63 ^{c,d}	29	14
2	40	100	35	45
3	60	97	59	17

Conversions and yields are calculated based on the results from gas chromatography using n-dodecane as the internal standard. KH was purified according to the procedure outlined in the experimental section. ^a0.5 mol% of the cluster. ^bConversion is calculated based on the amount of DBT recovered. If the conversion is not equal to total yield, there are also unrecovered materials (see experimental section). ^c6.8 equivalents of KH was used. ^dReaction time: 1.38 h.

3.2.2 The reactivity of other neutral Co²⁺ and Ni²⁺ phosphoranimide clusters in KH-mediated desulfurization of DBT

In the end, all of the tetranuclear phosphoranimide-supported Co²⁺ clusters described in Chapter 2 proved to be effective precatalysts for potassium hydride-mediated desulfurization. The nature of terminal ligand has a significant impact on the reactivity. Bisphosphoranimido cobalt cluster **69**, which has terminal phosphoranimide ligands, was first synthesized by Dr. Houston Brown, but its HDS activity was not assessed.¹⁰³ This we proceeded to do.

Bis(phosphoranimide) cluster **69** proved to be an excellent precatalyst; the desulfurization of DBT proceeds efficiently, with near-quantitative conversion of the starting material (Equation **3.1**). The product distribution from the reaction catalyzed by the homoleptic cluster **69** favors biphenyl more so than when either neutral or cationic cluster **60** or **40** is used (Equation **3.1** cf. Table **3.2**, entries 2, 5).

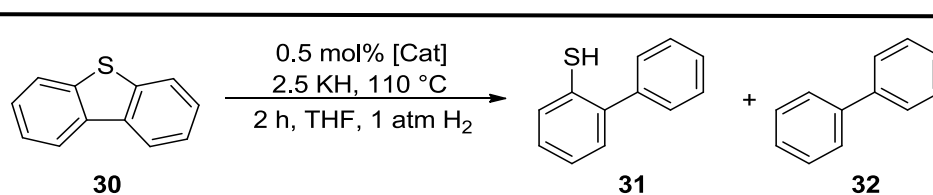
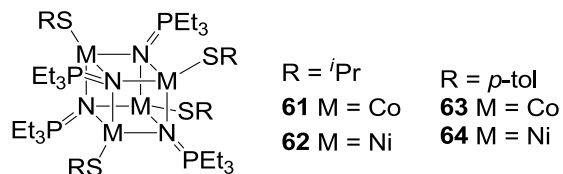


Equation 3.1

Similarly, tetranuclear phosphoranimide-supported thiolate clusters **61–64** also promote the desulfurization of DBT in the presence of KH (Table **3.3**). The thiolato cobalt complexes **61** and **63** convert the majority of DBT to biphenyl, but significant quantities (16–32 %) of the partially desulfurized product are also observed (entries 1–2). Surprisingly, the analogous thiolate-capped nickel clusters **62** and **64** are not as efficient for HDS (entries 3–4), affording high conversion of DBT, but mostly to 2-phenylthiophenol. This contrasts to reactivity of the

thiolate-capped cobalt clusters **61** and **63**, and the reasons for this are not clear. Dr. Orain Brown in this group has reported the opposite trend for KO^tBu-mediated desulfurization of DBT: nickel precatalysts are excellent, while cobalt is completely inactive.²⁴

Table 3.3 Desulfurization of transition metal thiolate heterocubane complexes.

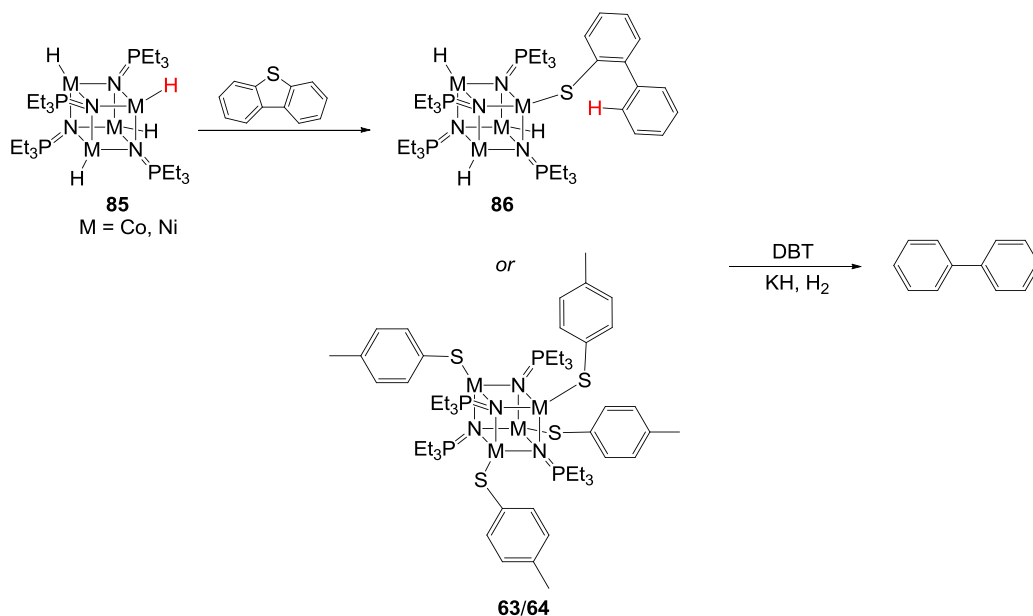


Entry	[Cat] ^a	Conversion (%) ^b	31 (%)	32 (%)
1	61	95	32	52
2	63	91	16	64
3	62	100	93	1
4	64	100	87	1

Conversions and yields are calculated based on the results from gas chromatography using *n*-dodecane as the internal standard. KH was purified according to the procedure outlined in the experimental section. ^a0.5 mol% of the cluster. ^bConversion is calculated based on the amount of DBT recovered. If the conversion is not equal to total yield, there are also unrecovered materials (see experimental section).

The fact that thiolate-capped clusters **61–64** catalyze desulfurization reveals that the metal–sulfur bonds of these complexes react with hydrogen under our conditions. As was also the case for the bisphosphoranimido cluster **69**, the hydrogenolysis of the M–S bonds is proposed

to proceed *via* heterolytic activation of dihydrogen. Other transition metal thiolate complexes also react with hydrogen in this fashion.^{157-158, 160, 172} The successful catalysis by the *p*-toluenethiolate complexes **63** and **64** in particular suggests that similar 2-phenylthiophenolate complexes (**85**, Scheme 3.2) are reasonable intermediates in the HDS reaction. Hydrogenolysis of either of these complexes (**63/64** or **86**) forms an active metal hydride that goes on to promote full desulfurization (Scheme 3.2). It should be noted that while these thiolate complexes are excellent models for possible intermediates; they do not at all represent the resting ‘sulfided’ state of the catalyst, the hydrogenolysis of which presents great difficulty. Further, while the thiolate clusters are useful precatalysts for HDS, further exploration of their reactivity was suspended, in favor of other, more active, phosphoranimide-supported clusters.



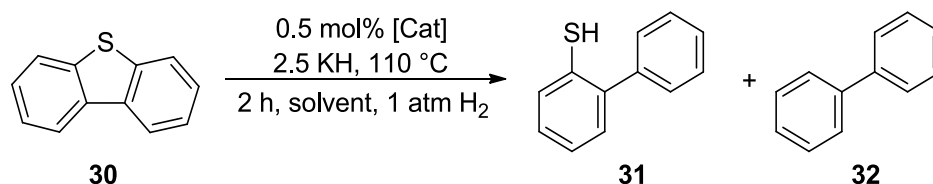
Scheme 3.2

The Dehnicke heterocubane cluster **53a**, which is an intermediate in the synthesis of the phosphoranimide-supported cobalt clusters discussed above, was itself a remarkably active

3.2.3 Solvent effects on the tetranuclear cobalt triethylphosphoranimide clusters

For the chloride-capped cobalt cluster **53a** and other tetranuclear phosphoranimide-supported cobalt precatalysts, THF is the best solvent for hydride-mediated HDS. The chloride cluster and the cationic methylcobalt cluster **40** are soluble in THF, but only sparingly soluble in toluene; the dramatic difference in reactivity observed is unsurprising (Table 3.4, entries 1–4). However, there are no notable differences in the solubilities of the neutral methylcobalt cluster **60** and the bisphosphoranimide cluster **69** in THF and toluene, yet the difference in reactivity persists (entries 5–8). Precatalyst solubility is therefore not the sole reason for the lower activity of the cobalt clusters in toluene when compared to THF.

Table 3.4 Hydride-mediated desulfurization promoted by phosphoranimide-supported cobalt clusters in toluene.



Entry	[Cat] ^a	Solvent	Conversion (%) ^c	31 (%)	32 (%)
1	53a ^b	THF	100	3	96
2	53a	tol	44	12	13
3	40 ^b	THF	100	35	45
4	40	tol	39	18	7
5	60 ^b	THF	97	59	17
6	60	tol	16	0	2
7	69 ^b	THF	99	10	69
8	69	tol	59	38	17

Conversions and yields are calculated based on the results from gas chromatography using n-dodecane as the internal standard. KH was purified according to the procedure outlined in the experimental section. ^a0.5 mol% of the cluster. ^bThese results appear above in this chapter. ^cConversion is calculated based on the amount of DBT recovered. If the conversion is not equal to total yield, there are also unrecovered materials (see experimental section).

Instead, it appears that the solubility of key intermediates and, perhaps, of the KH itself, is a more important determinant of optimal solvent. Hydrogenolysis of the C–S single bond of DBT generates 2-phenylthiophenol **31**, which in the presence of excess base is rapidly converted to the potassium 2-phenylthiophenolate. In polar solvents such as THF, the thiophenolate salt has some solubility, but in a low polar medium, *e.g.*, toluene, an insoluble precipitate forms. Further desulfurization of the thiophenolate salt in toluene is therefore inhibited and a high proportion of

2-phenylthiophenol **31** is obtained upon acidic workup. Similar to the thiophenolate, KH is more soluble in THF than in toluene,¹⁷⁵ thus, affecting the reactivity resulting in lower conversion of DBT in toluene.

Another potential inhibitory effect of toluene is competitive π -coordination to the cobalt center or to the potassium cation. Coordination of DBT to either the cobalt catalyst or to K^+ ions may be crucial for C–S bond cleavage, and a π -electron rich solvent such as toluene is likely to compete for these coordination sites, suppressing HDS. Chapter 4 of this thesis presents a more complete investigation of the importance of π -coordination for HDS.

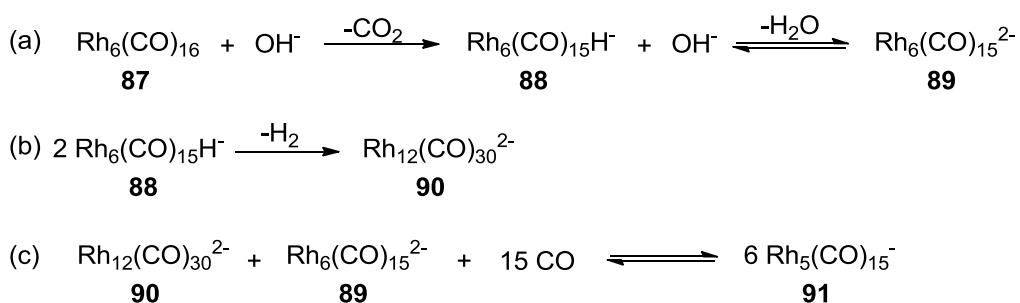
3.2.4 Insights to the nature of the phosphoranimide cobalt clusters in hydride-assisted HDS

Our study of selected tetranuclear triethylphosphoranimide-supported cobalt clusters provided valuable insight into the nature of the active catalyst involved in this HDS reactions. Much of the discussion that follows is limited to cationic cobalt cluster **40** and neutral cobalt bisphosphoranimide **69**; however, the insights readily transfer to the other heterocubane cobalt clusters.

3.2.4.1 Identifying the nuclearity of the active catalyst

Polymetallic clusters similar to those discussed in this thesis are known to undergo structural reorganization to generate active catalysts under many reaction conditions. Relevant cluster transformations include ligand dissociation/isomerization, agglomeration, and fragmentation.¹⁷⁶ Any of these processes can occur in the heterocubane cobalt clusters under HDS conditions.

A convenient method to assess the activation pathway for a particular cluster, is to evaluate the dependency of the turnover frequency (TOF) on the initial concentration of the precatalyst cluster.¹⁷⁶ If the active catalyst is generated by cluster agglomeration, the TOF increases with increasing initial concentration. In contrast, an inversely proportional relationship is observed when fragmentation is the activating pathway. For example, with rhodium cluster **87** (a, Scheme 3.4) used in Reppe hydrogenation of benzaldehyde, higher initial concentrations of the rhodium complex **87** resulted in *lower* turnover frequencies.¹⁷⁷ This clearly suggests that the active catalyst(s) is a specie(s) from the fragmentation of cluster **87**, however, the exact nuclearity of the active catalyst cannot be determined from this evaluation alone. In independent studies by Vidal *et al.* and Chini *et al.*, rhodium complex **87**, in basic medium, transforms, agglomerates, and fragments into different species as shown in Scheme 3.4.¹⁷⁸⁻¹⁷⁹ The authors further suggest that rhodium clusters **88** and/or **89** are/is likely the active catalyst(s).¹⁷⁷ It should also be noted that this kinetic result requires that the active species be in equilibrium with the parent cluster for reliable interpretation.



Scheme 3.4

In our determination, the relationship between TOF and concentration for cobalt complexes **40** and **69** strongly suggests that the clusters fragment to generate the active species under the reaction conditions. For both clusters, increasing the concentration leads to a lower turnover frequency (Figures 3.3 and 3.4). While this information clearly suggests fragmentation of the clusters, the size of the fragments formed cannot be determined. For this purpose, the Signer determination¹⁸⁰ of the solution molecular weight of the clusters is more useful.

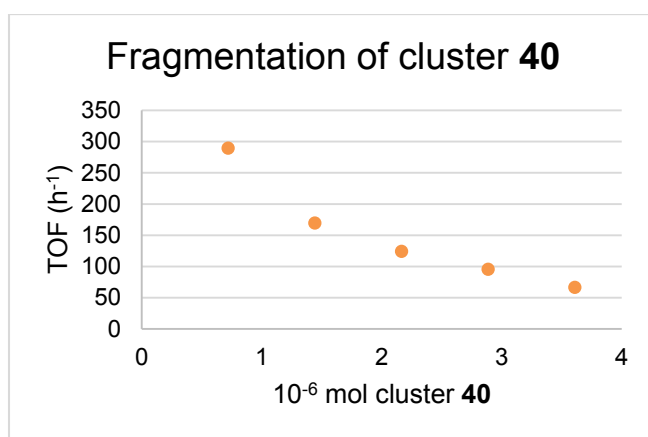


Figure 3.3 TOF dependence on the concentration of cluster **40**. (Reaction conditions: 2.5 KH, 1 atm H₂, and 4 hours)

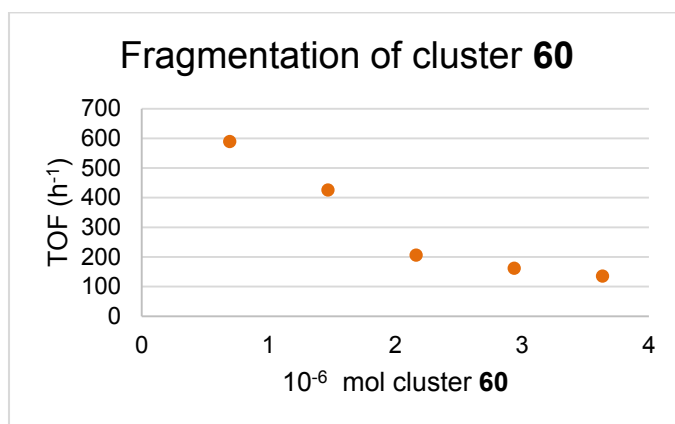


Figure 3.4 TOF dependence on the concentration of cluster **69**. (Reaction conditions: 2.5 KH, 1 atm H₂, and 2 hours)

The Signer method relies on the equilibration of solvent vapors between two solutions, one containing a reference compound of known molecular mass and the other containing a sample under investigation.¹⁸⁰ Because of the dependence of the vapor pressure on the concentration of the solutions, the molarity or molecular weight of the unknown can be determined by recording the final volume of each solution and using these values in the appropriate equation:

$$M_1 = \frac{W_1}{W} \times \frac{V}{V_1} \times M \quad (\text{a})$$

where M_1 and M are the molecular weights of the unknown and standard, respectively, W_1 and W are the masses in grams of the unknown and the standard used in the experiment, and V_1 and V are the final volumes in mL.¹⁸¹⁻¹⁸²

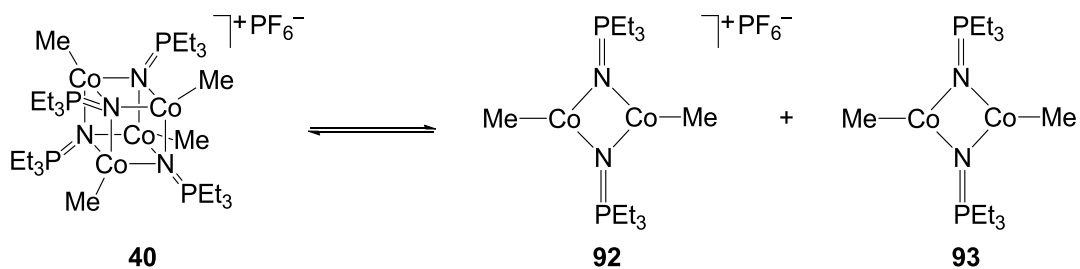
From these measurements, the molecular weight of the compound in solution was determined to be approximately half the molecular weight of the respective parent heterocubane clusters (Tables 3.5 and 3.6). It should be noted that the molecular weight measurements were not conducted under typical HDS reaction conditions. Nevertheless, the calculated molecular weights, along with the qualitative data obtained from the TOF studies together suggest that the cobalt clusters **40** and **69** fragment into reactive dimers, as shown in Schemes 3.5 and 3.6.

Table 3.5 Solution molecular weight of cluster **40**.

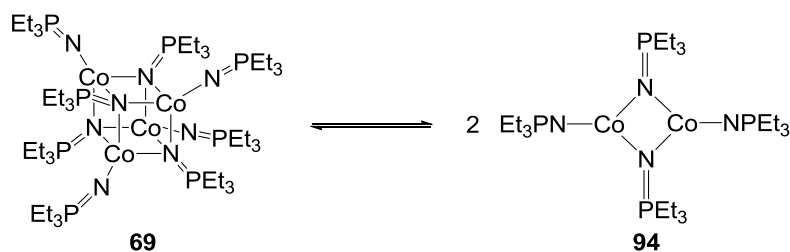
	Molecular weight (g/mol)
Heterocubane	969.5
Dimer	484.7
Calculated from Signer method	464

Table 3.6 Solution molecular weight of cluster **69**.

	Molecular weight (g/mol)
Heterocubane	1293.0
Dimer	646.5
Calculated from Signer method	620



Scheme 3.5



Scheme 3.6

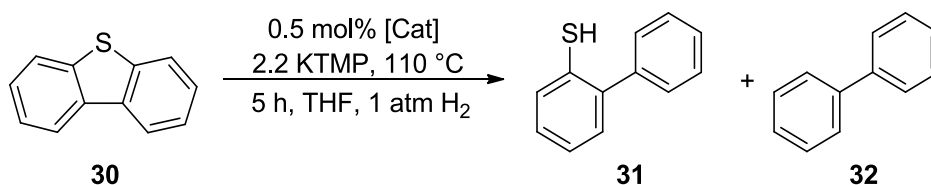
3.2.4.2 Homogeneity tests for cobalt catalysts derived from **40**, **53a**, and **69**

The facile fragmentation of heterocubane cobalt clusters **40** and **69** prompted further investigation into whether or not the active catalyst remains homogeneous under the reaction conditions. Cluster fragmentation and the associated cleavage of metal–metal or metal–ligand bonds can easily lead to the formation of heterogeneous metal species.¹⁸³ The mercury puddle test is the most common and convenient experiment to test the homogeneity of the active catalyst.¹⁸⁴ Elemental mercury forms amalgams in the presence of heterogeneous particles of many metals, leading to suppression of catalytic activity. However, mercury poisoning experiments do not provide definitive confirmation that the catalyst is heterogeneous. Some heterogeneous metal catalysts do not form amalgams with mercury. Conversely, elemental mercury can also react with some homogeneous transition metal complexes, inducing decomposition and/or inhibition of catalytic activity.¹⁸⁴⁻¹⁸⁷

The efficiency of cobalt-catalyzed desulfurization reaction decreases only slightly in the presence of excess mercury (300 equivalents per metal; Table 3.7). This implies that under the reaction conditions (110 °C, 1 atm H₂), the active catalysts remain homogeneous at shorter reaction times. For this investigation, potassium tetramethylpiperidide (KTMP) was used as the stoichiometric base, excluding the possibility of background desulfurization caused by KH.

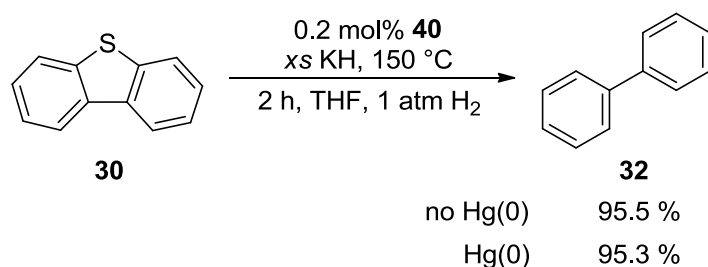
Potassium hydride alone desulfurizes DBT to some extent (see Chapter 4); KTMP is minimally reactive toward with DBT (entries 7, 8). Earlier mercury tests conducted by Houston Brown also pointed to the homogeneity of the cationic cluster **40**; however, his reactions were not controlled for KH reactivity and require cautious interpretation (Equation 3.3).¹⁰³

Table 3.7 Mercury puddle test for tetranuclear cobalt clusters **40**, **53a**, and **69**.



Entry	[Cat] ^a	Eq. of Hg(0) per Co atom	Yield	
			31 (%)	32 (%)
1	40	0	13	16
2	40	300	6	8
3	53a	0	6	13
4	53a	300	3	10
5	69	0	14	15
6	69	300	10	5
7	-	0	0	2
8	-	300	0	3

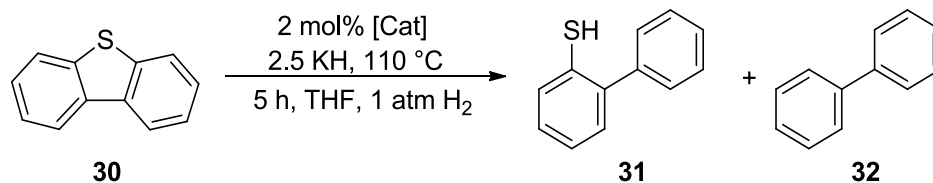
Conversions and yields are calculated based on the results from gas chromatography using n-dodecane as the internal standard. ^a0.5 mol% of the cluster.



Equation 3.3

3.2.5 Hydride-mediated desulfurization of DBT catalyzed by cobalt (II) halides

Preassembled phosphoranimide cobalt(II) clusters are not exclusive catalysts for HDS; simple cobalt(II) halides *without supporting ligands* are also remarkably active for the hydride-mediated desulfurization of DBT. Both CoCl₂ and CoBr₂ promote the desulfurization of DBT in the presence of KH, with near-stoichiometric conversion to a mixture of 2-phenylthiophenol and biphenyl observed after 5 h (Table 3.8, entries 1–2). The most active phosphoranimide cobalt clusters achieve the same conversion in just 2 h (entry 3), with higher selectivity for biphenyl. However, the simplicity of the cobalt halide precatalyst system cannot be ignored. The slower reactivity and low selectivity of simple cobalt halide precatalysts are most likely the result of the heterogeneity of this particular catalyst system.

Table 3.8 Desulfurization of DBT catalyzed by cobalt (II) halide.

Entry	[Cat] ^a	Conversion (%) ^d	31 (%)	32 (%)
1	CoCl ₂	99	41	44
2	CoBr ₂	97	56	30
3	53a ^{b,c}	100	3	96

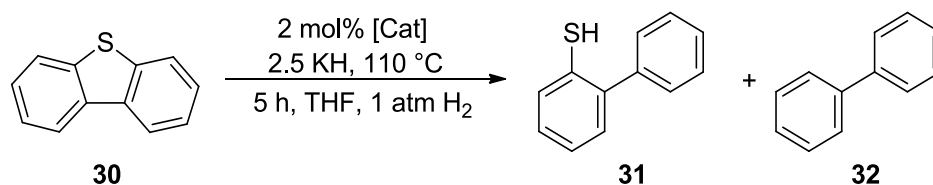
Conversions and yields are calculated based on the results from gas chromatography using n-dodecane as the internal standard. KH was purified according to the procedure outlined in the experimental section. ^a2 mol% of the metal center or 0.5 mol% per 4 metal centers. ^bThe reaction is reported in Equation 3.2. ^cReaction time: 2 h. ^dConversion is calculated based on the amount of DBT recovered. If the conversion is not equal to total yield, there are also unrecovered materials (see experimental section).

3.2.6 KH-mediated, transition metal halide catalyzed desulfurization of DBT

The unexpected activity of cobalt halides led us to explore other simple late transition metal halide salts as precatalysts for KH-mediated desulfurization. All mid-to-late first-row transition metal halides (Fe to Cu) promote desulfurization of DBT under mild conditions, with uniformly high conversions observed (Table 3.9), suggesting most of the reactivity is inherent to KH rather than the catalyst. Cobalt remains the metal of choice, leading to higher proportions of biphenyl (Table 3.8, entries 1 and 2), with FeCl₂ surprisingly rating the next most efficient precatalyst (Table 3.9, entry 1). Very little biphenyl is produced using CuBr₂ as the precatalyst, but the conversion of DBT to 2-phenylthiophenol is still appreciable (Table 3.9, entry 7). Zero-valent metal particle (heterogeneous) catalysts are likely formed from each of these metal halide precatalysts, by *in-situ* metathesis with KH, followed by decomposition of the metal hydride

intermediates. Once formed, the precise role of these metal particles in the desulfurization reaction remains unclear; however, the following chapter explores this issue.

Table 3.9 Desulfurization of DBT catalyzed by late transition metal halides.



Entry	[Cat] ^a	Conversion (%) ^b	31 (%)	32 (%)
1	FeCl ₂	98	58	35
2	NiCl ₂	96	76	14
3	NiBr ₂	100	63	19
4	CuCl ₂	98	73	16
5	CuBr ₂	78	75	1

Conversions and yields are calculated based on the results from gas chromatography using n-dodecane as the internal standard. KH was purified according to the procedure outlined in the experimental section. ^a2 mol% of the metal center or 0.5 mol% per 4 metal centers. ^bConversion is calculated based on the amount of DBT recovered. If the conversion is not equal to total yield, there are also unrecovered materials (see experimental section).

3.3 Conclusion

The desulfurization of DBT proceeds efficiently in the presence of stoichiometric KH and catalytic phosphoranimide-supported heterocubane clusters of cobalt and nickel (**40**, **53a**, **60–64**, and **69**). Clusters capped by chloride or terminal phosphoranimide proved to be most efficient under these conditions, affording the highest yields of the fully desulfurized hydrocarbon.

Remarkably, even simple late transition metal halide salts are also competent in catalyzing the desulfurization of DBT, albeit at lower selectivity.

To determine the nature of the cobalt clusters under reaction conditions, both kinetic and solution MW experiments were investigated. The relationships between the TOF and catalyst concentration along with the solution molecular weights strongly suggest that cobalt heterocubane clusters readily fragment into dimers in solution. Nevertheless, the fragmentation of these clusters does not lead to the rapid formation of heterogeneous catalysts, as supported by the retention of high desulfurization activity despite the presence of elemental mercury. Although, slow transformation is suggested by inhibition observed at longer reaction times.

Thus far, we have discovered that a broad range of late first-row transition metal sources are competent precatalysts for hydride-mediated HDS. Despite these successful desulfurization reactions, understanding the respective roles of the stoichiometric base and transition metal are critical to a determination of the mechanism of KH-mediated HDS. In the following chapter, the specific role of the potassium hydride and the metal, as well as the proposed mechanisms will be examined and discussed in some detail.

4. Establishing the Role of the Base and Transition metals in KH-Mediated Hydrodesulfurization

4.1 Objectives

In the previous chapter, we established that phosphoranamide-supported cobalt heterocubane clusters (Figure 4.1) promote hydrodesulfurization of refractory organosulfur compounds in the presence of stoichiometric potassium hydride under mild conditions. In this chapter, distinguishing the roles of the transition metal and hydride base is discussed, as part of a larger effort to determine the mechanism of the hydride-mediated HDS reaction.

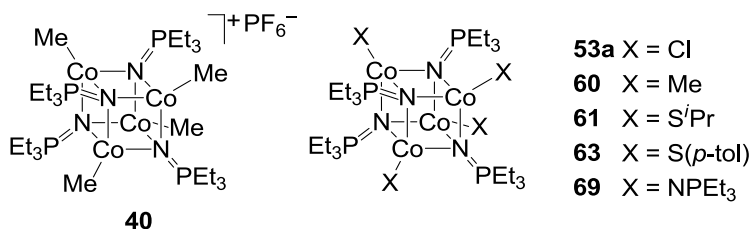
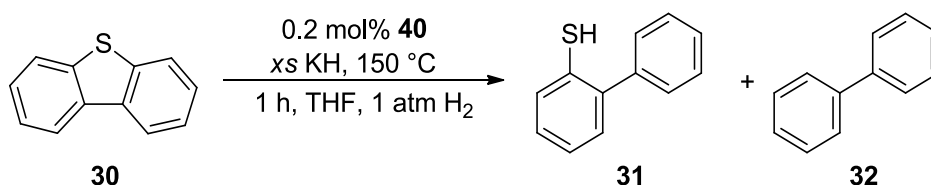


Figure 4.1 The cobalt phosphoranamide clusters as precatalyst for HDS reactions.

Previous members of this group established that the combination of transition metal, H₂, and KH are essential for the desulfurization of DBT under mild conditions (Table 4.1, entry 1).^{103, 144} If any component is excluded, only minimal conversion of DBT is observed (entries 2–4). From these results, it was proposed that desulfurization of DBT proceeds *via* a classic mechanism, involving insertion of the transition metal into the C–S bonds of DBT, followed by hydrogenolysis to liberate biphenyl, and formation of sulfided cobalt. Ideally, reaction of this sulfided cobalt compound with hydrogen would regenerate the active catalyst and concomitantly

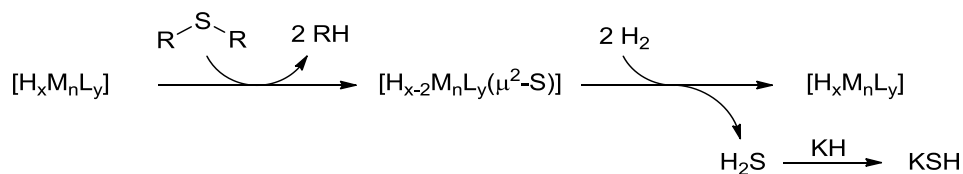
liberate H₂S which can be sequestered by the reaction with a strongly basic scavenger such as KH (Scheme 4.1).

Table 4.1 Control reactions of KH.¹⁰³



Entry	40	H ₂	KH	31 (%)	32 (%)
1	✓	✓	✓	0	68
2	✓	✓	✗	0	stoichiometric
3	✓ ^a	✗ ^b	✓	0	stoichiometric
4	✗	✓	✓	0	0

KH is purified according to procedure outlined in the experimental section. Conversions are obtained using GC-MS analysis. ^a5 mol% **40**. ^bH₂ added to activate the cluster.

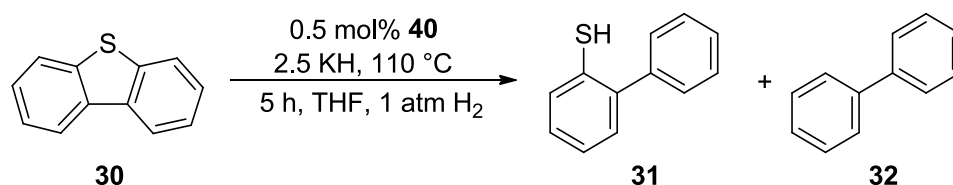


Scheme 4.1

The earlier results contrast those discussed here. While the mixture of catalyst, H₂, and KH is *optimal* for desulfurization, significant C–S bond activation is observed when the transition metal is excluded (Table 4.2, entry 3) and even when KH alone is used (entry 4). These observations necessitated a more thorough examination of control reactions, to develop an

understanding of the role(s) played by each reagent in the cobalt-catalyzed, hydride-mediated hydrodesulfurization system.

Table 4.2 Control reactions using the cationic cobalt cluster **40**.



Entry	40	H₂	KH	31 (%)	32 (%)
1	✓	✓	✓	27	58
2	✓	✓	✗	0	trace
3	✗	✓	✓	58	0
4	✗	✗	✓	63	1

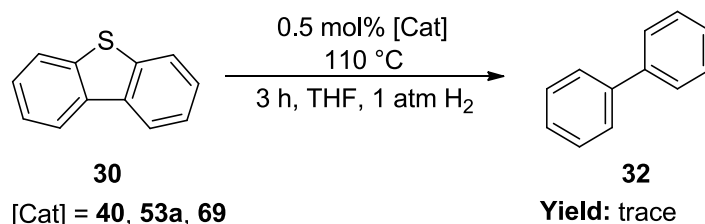
Conversions and yields are calculated based on the results from gas chromatography using n-dodecane as the internal standard. KH was purified according to the procedure outlined in the experimental section.

4.2 Results and Discussion

4.2.1 Control reactions to establish the role of the cobalt clusters, KH, and H₂

We began our series of control reactions by establishing the reactivity of the transition metal catalyst alone. Only sub-stoichiometric (per mole of precatalyst) desulfurization is observed when the cobalt cluster is exposed to DBT and hydrogen (Equation 4.1), indicating that, at least under our reaction conditions, the transition metal is not active for catalytic C–S bond hydrogenolysis. Dr. Houston Brown reported slightly better activity in analogous

experiments, with stoichiometric desulfurization obtained from the reaction of the cationic cluster **40** with DBT and H₂ in the absence of KH (Table 4.1, entry 1). These results establish that the transition metal indeed cleaves the C–S bonds of DBT, but H₂ is neither competent or necessary to promote turnover of the sulfided catalyst.

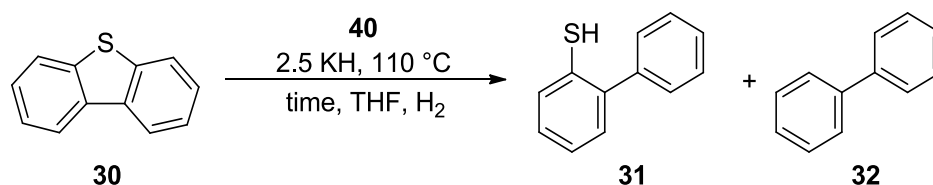


Equation 4.1

We further challenged this hypothesis by excluding H₂ from an otherwise typical reaction. In contrast to the claim that H₂ was imperative, we found that the combination of stoichiometric KH and catalytic cobalt cluster **40** is sufficient for desulfurizing DBT (Table 4.3, entry 1 vs. 2). Furthermore, excluding both H₂ and the transition metal reveals that KH alone is a sufficiently powerful reductant, cleaving at least one C–S bond in DBT to form 2-phenylthiophenol under identical reaction conditions (entry 3). This clearly shows that the hydride is not simply a basic scavenger, or even a turnover promoter, but instead the dominant reductant for the first carbon-sulfur bond hydrogenolysis. The ‘KH only’ method even yields some desulfurization of DBT to biphenyl at higher temperature or prolonging the reaction time (entries 4–5). The presence of added H₂ has a minimal effect on this KH-induced C–S bond cleavage (entries 6–8). While this ‘KH only’ method pales in comparison to the efficiency of the ternary [Co]/KH/H₂ desulfurization system, these results clearly establish that much of what was

earlier reported was stoichiometric KH-mediated desulfurization ‘promoted’ by the transition metal and *assisted* by H₂.

Table 4.3 Desulfurization reactions of DBT in the presence and absence different reagents.



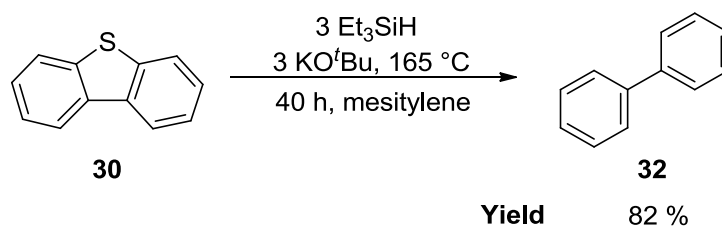
Entry	40 (mol%)	Time (h)	H ₂ (atm)	Conversion (%) ^b	31 (%)	32 (%)
1	0.5	2	0	99	39	38
2	0.5	2	1	100	35	45
3	0	5	0	72	63	1
4	0	16	0	99	78	10
5 ^a	0	5	0	100	79	11
6	0	5	1	74	58	0
7	0	16	1	93	89	2
8	0	16	34	93	81	1

Conversions and yields are calculated based on the results from gas chromatography using n-dodecane as the internal standard. KH was purified according to the procedure outlined in the experimental section. ^aReaction temperature: 130 °C. ^bConversion is calculated based on the amount of DBT recovered. If the conversion is not equal to total yield, there are also unrecovered materials (see experimental section).

In hindsight, this reactivity of KH with DBT is not entirely surprising, despite the mild conditions. The use of alkali metal salts, particularly sodium hydride, in hydrodesulfurization reactions is precedented.¹³⁻²⁰ In 1977, Baird and Bearden (ExxonMobil) disclosed through a

patent that treatment of high-sulfur petroleum feedstocks with excess NaH at high temperature (370–437 °C) and high H₂ pressure (34–100 atm) led to substantial desulfurization.¹³ In addition, the inventors noted that in the absence of H₂, NaH alone still desulfurizes the petroleum feedstock, albeit with lower efficiency, indicating that potassium hydride can readily function as the sole reductant in desulfurization reactions.

Recently, Grubbs *et al.* reported the hydrodesulfurization of refractory organosulfur substrates using excess potassium tert-butoxide and triethylsilane as the hydride source (Equation 4.2).²¹ This system affords high conversion (>80 % yield) at much lower temperatures (165 °C) than the NaH/hydrogen system, but the reaction is slow, requiring 40 h to achieve reasonable conversion. Under hydrogen rather than silane, no conversion is obtained under these conditions.²⁴



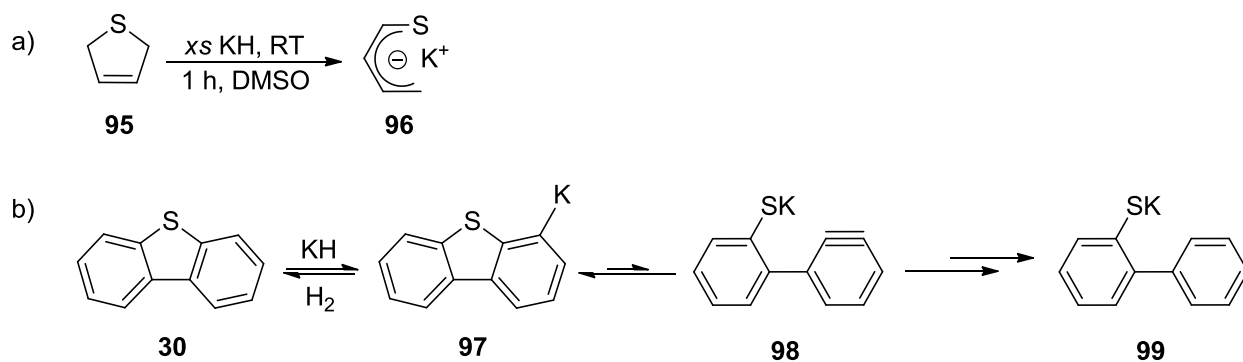
Equation 4.2

What our discoveries show is that, by using KH/H₂ (instead of NaH/H₂ or KO^tBu/silane) *along with* a transition metal catalyst, the hydrodesulfurization of dibenzothiophene proceeds under vastly milder reaction conditions (110 °C and 2–5 h, see Table 4.3). Having realized this, we became interested in understanding the mechanism of KH-mediated desulfurization in greater detail, with the intention of optimizing the process. The remainder of this chapter will outline our

attempts to (1) understand the specific role(s) of KH, (2) explore the effects of added H₂ in this system, and finally, (3) examine the origin of the promotional effect of the transition metal catalyst on the uncatalyzed reaction.

4.2.2 Role of KH: Deprotonation and subsequent C–S bond cleavage of DBT

Any consideration of the role of potassium hydride must include a discussion of its potential to act both as a strong Brønsted base and a source of nucleophilic hydride. The strong basicity of KH is well established;¹⁸⁸⁻¹⁸⁹ a variety of organic substrates *e.g.* alcohols, amines, and even weakly acidic hydrocarbons, are deprotonated by this reagent.¹⁸⁹ One particularly relevant example of the basicity of KH is the deprotonation-induced C–S bond cleavage of 2,5-dihydrothiophene (**95**, Scheme 4.2, a), reported by Gamero-Melo, *et al.*¹⁹⁰ The ring-opened potassium thiapentadienyl **96** is a model for the 2-phenylthiophenolate potassium salt we propose is formed from the deprotonation of the C–H bonds at the 4-/6- positions of DBT (Scheme 4.2, b).



Scheme 4.2

The energy profiles for the deprotonation of 2,5-dihydrothiophene and DBT are different in important ways however. Deprotonation of 2,5-dihydrothiophene and subsequent C–S bond cleavage is irreversible, forming a stable potassium thiapentadienyl complex **96**. In contrast, *ortho*-deprotonation of DBT that leads to the C–S bond cleavage of DBT forms an unstable aryne intermediate (**98**) which is in equilibrium with a more stable DBT anion **97**. While the formation of the aryne intermediate (**98**) is unfavorable, when formed, the aryne intermediate can undergo nucleophilic addition by either the anionic sulfur atom or the hydride. Nucleophilic addition of the hydride to the aryne intermediate **98**, then, leads the formation of 2-phenylthiophenolate **99**.

To investigate *ortho* C–H deprotonation of DBT by purified KH, we monitored the reaction of the two reagents by ¹H NMR spectroscopy in THF-d₈ solution. Between room temperature and 80 °C, the reaction mixture is a gray suspension and the ¹H NMR spectrum reveals only resonances attributable to unreacted DBT (see experimental, Chapter 5). On heating to 110 °C however, the appearance of the KH/DBT suspension changes from gray to a deep-red, which is typical for DBT desulfurization reactions conducted at scale. The ¹H NMR spectrum of this mixture shows a small resonance at 4.55 ppm, diagnostic for soluble H₂ (Figure 4.2),¹⁹¹ and the aromatic region contains broad new resonances, likely from the potassium thiolate salt or the potassium anion of DBT formed from the deprotonation of DBT.

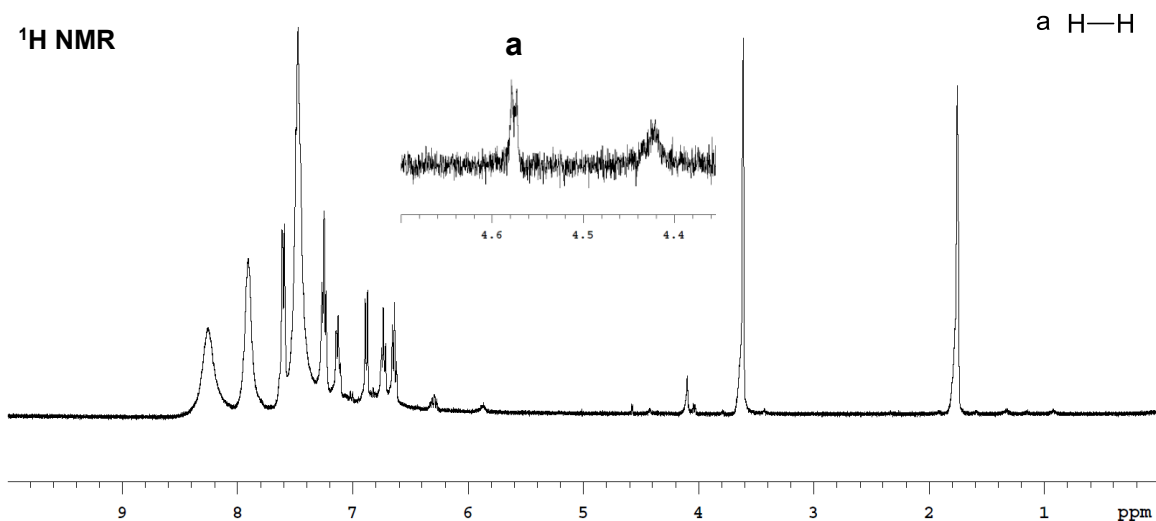


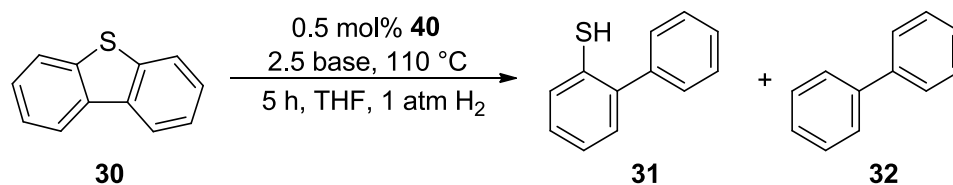
Figure 4.2 ^1H NMR spectrum of KH and DBT suspension heated for 2 hours at 110 °C.

4.2.2.1 Other strong bases for the desulfurization of DBT promoted by cationic cobalt cluster **40**

To independently confirm the importance of C–H deprotonation for C–S bond hydrogenolysis, other strong bases were screened in place of KH. These reactions were conducted in the presence of the cationic cobalt cluster **40** to ensure high conversion. Sodium hydride, with a (theoretically) identical basicity to KH, affords very little conversion, but gives only biphenyl (Table 4.4, entry 1 vs. 2). Similarly, strong soluble bases, such as lithium di(*iso*-propyl)amide (LDA) and lithium tetramethylpiperide (LiTMP) are ineffective (entries 3 and 5), yet the potassium analogues, KDA and KTMP, function reasonably well (entries 4 and 6). Tertiary alkoxides, however, do not promote C–S bond cleavage in DBT, even when the potassium salt is used (entries 7 and 8). Two clear points emerge from these data: (1) A strong base ($\text{p}K_{\text{a}} \geq 27$) is required to promote C–S bond cleavage, and (2) *potassium ions are*

indispensable for promoting the desulfurization of DBT under mild conditions. Both further confirm that the role of KH is certainly not limited to sequestering H₂S, with the hydride anion reversibly deprotonating DBT, promoted, specifically, by potassium counterions.

Table 4.4 Desulfurization of DBT in the presence of strong alkali metal bases.



Entry	Base	pK _a ^a	31 (%)	32 (%)
1	NaH	36	0	2
2	KH	36	27	58
3	LDA	36	1	3
4	KDA	36	37	11
5	LiTMP	36	1	4
6	KTMP	36	18	14
7	NaO ^t Bu	27	0	0
8	KO ^t Bu	27	0	0.7

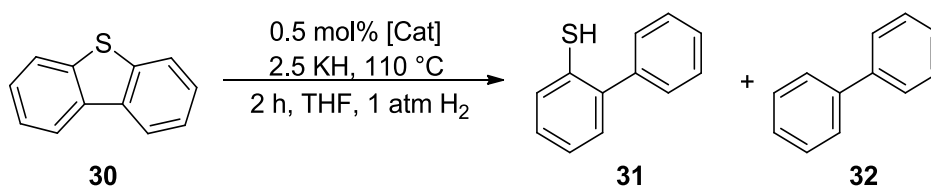
Conversions and yields are calculated based on the results from gas chromatography using n-dodecane as the internal standard. The amount of catalyst used: 0.5 % per cluster or 2% per metal center. ^aThe pK_a values (in DMSO) are from Ref [192].

4.2.2.2 Potassium ion effect in KH-mediated desulfurization

This potassium ion effect is intriguing, warranting further investigation and discussion. We assessed the importance of K⁺ binding by conducting cobalt-catalyzed reductions in the

presence of 18-crown-6. Unsurprisingly, chelation of the K^+ ions to the crown ether effectively suppresses the potassium effect, evidenced by the very low conversions of DBT (Table 4.5, entries 1–2 *cf.* entries 3–4). If basicity were the sole consideration, then chelation should have made a more aggressive base and/or hydride, leading to accelerated reactivity.^{175, 189, 193} Instead, the hydride-mediated desulfurization relies as much on the promotional effect of potassium cations as it does on the hydride anions.

Table 4.5 Desulfurization in the presence of 18-crown-6.



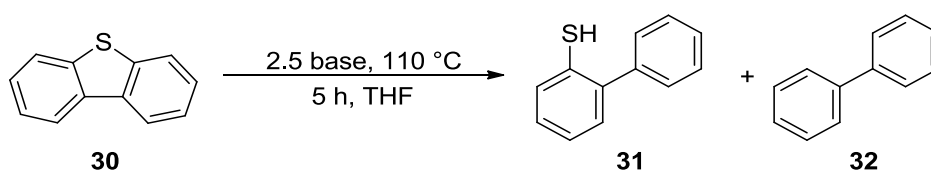
Entry	[Cat]	18-crown-6 (equiv.)	31 (%)	32 (%)
1	40	0	35	45
2	69	0	10	69
3	40	2.5	1	4
4	69	2.5	5	1

Conversions and yields are calculated based on the results from gas chromatography using n-dodecane as the internal standard. KH was purified according to the procedure outlined in the experimental section.

To confirm the independence of this ‘ K^+ counter-ion effect’ from the hydride anion, an external ‘benign’ source of soluble potassium was added to the sodium hydride-mediated desulfurization of DBT. While NaH is nearly ineffective for the desulfurization of DBT (Table 4.6, entry 1), by simply adding a source of K^+ ions (*via* KO^tBu), the C–S bond cleavage reaction

occurs with efficiency exceeding that of KH alone (entry 2 vs. entry 3). A control reaction confirms that KO^tBu alone is not responsible for the desulfurization (entry 4).²⁴ Potassium *tert*-butoxide in the reaction mixture likely reacts with NaH, existing in equilibrium with KH and NaO^tBu, as seen in the reaction of *n*-BuLi and KO^tBu.¹⁹⁴ Potassium hydride formed *in situ*, then, proceeds to cleave the C–S bonds of DBT.

Table 4.6 Desulfurization of DBT with ‘benign’ source of K⁺ ion.

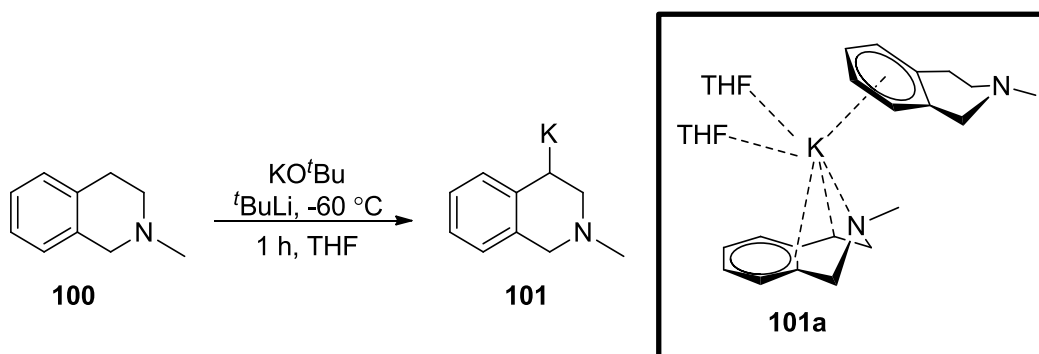


Entry	Base	KO ^t Bu (equiv.)	31 (%)	32 (%)
1	NaH	0	0	1
2	KH	0	63	1
3	NaH ^a	2.5	88	1
4	KO ^t Bu ^{b,c}	-	0	0

Conversions and yields are calculated based on the results from gas chromatography using *n*-dodecane as the internal standard. ^aReaction time: 2 hours. ^bReaction in the presence of 1 atm H₂. ^cRef [24].

A similar reactivity-enhancing potassium-ion effect has been reported for various organic reactions.^{21, 195-196} The origin is often linked to the greater enthalpic stability of cation- π complexes preferentially formed between K⁺ ions and arene rings, as compared to Na⁺ or Li⁺ ions.¹⁹⁵ For example, Strohmman and coworkers reported that K⁺ is crucial in the deprotonation of benzylic C–H bonds in 2-phenylethylamine **100** by *tert*-butyllithium to form metalated

intermediate **101** (Scheme 4.3).¹⁹⁶ The deprotonation only proceeds in the presence of KO^tBu, partly attributable to the increased stabilization of the intermediate by larger K⁺ ion compared to Li⁺ only. In addition to this, the counterion exchange between KO^tBu and ^tBuLi forms a stronger base, ^tBuK, which deprotonates 2-phenylethylamine more rapidly.



Scheme 4.3

In our case, potassium cations can interact with DBT *via* several binding modes (η^6 -, η^5 -arene, or η^1 -S), as shown in Figure 4.3. Coordination of the arene ring(s) to K⁺ acidifies the C–H bond *ortho* to the sulfur atom,¹⁹⁵ facilitating deprotonation. Potassium cations in η^5 -coordination mode also lower the activation energy for nucleophilic *ipso*-substitution of DBT by the hydride ion, an alternative mechanistic pathway (see discussion below).¹⁵⁶

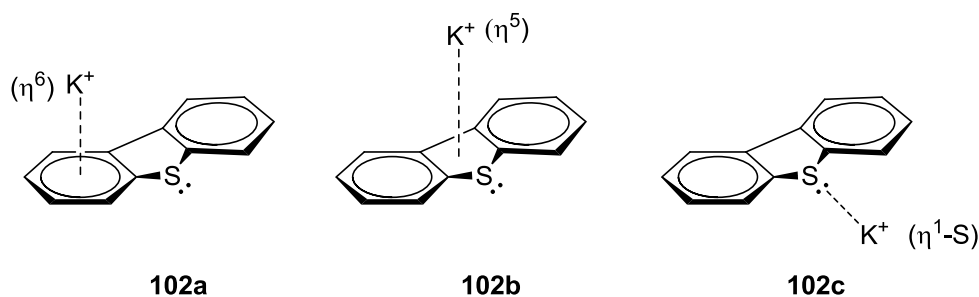
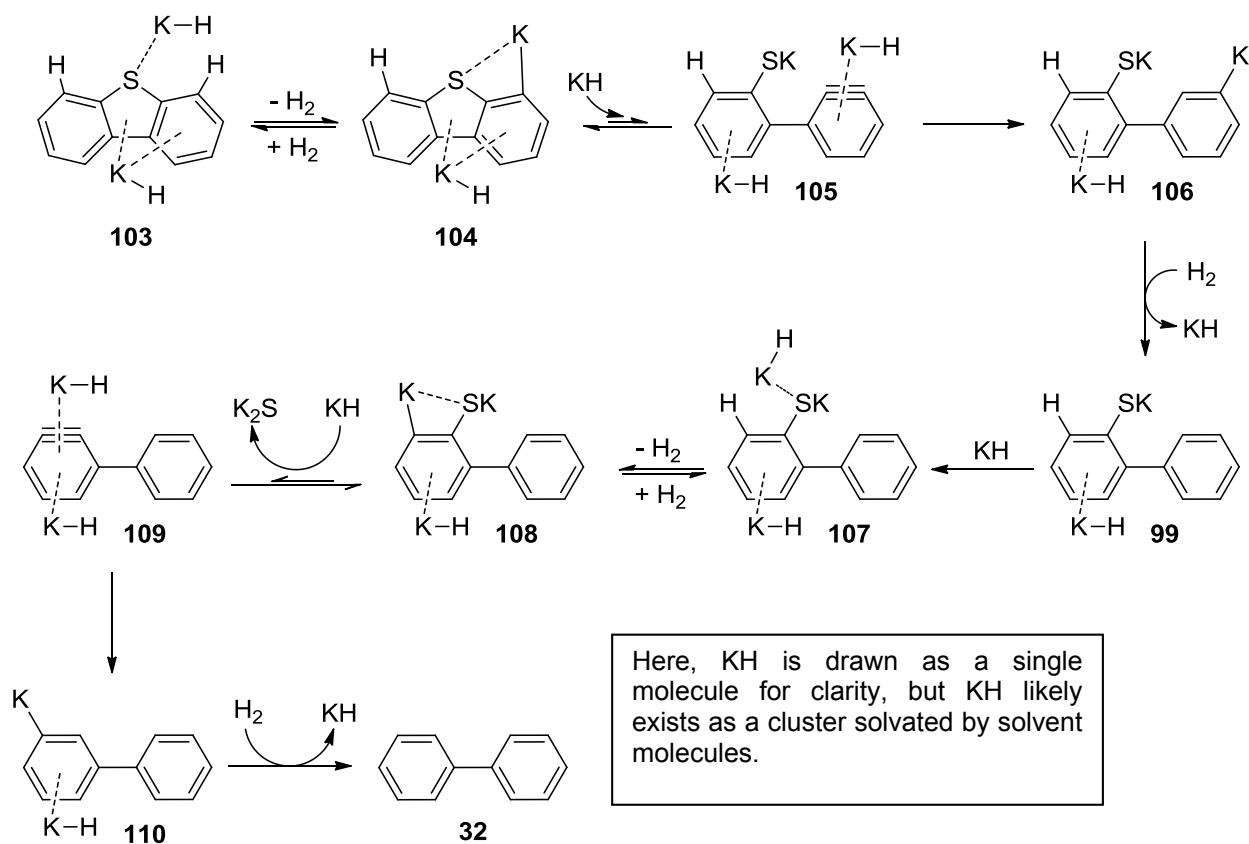


Figure 4.3 Potassium cation presumably binds to the arene ring(s) or the sulfur atom of DBT.

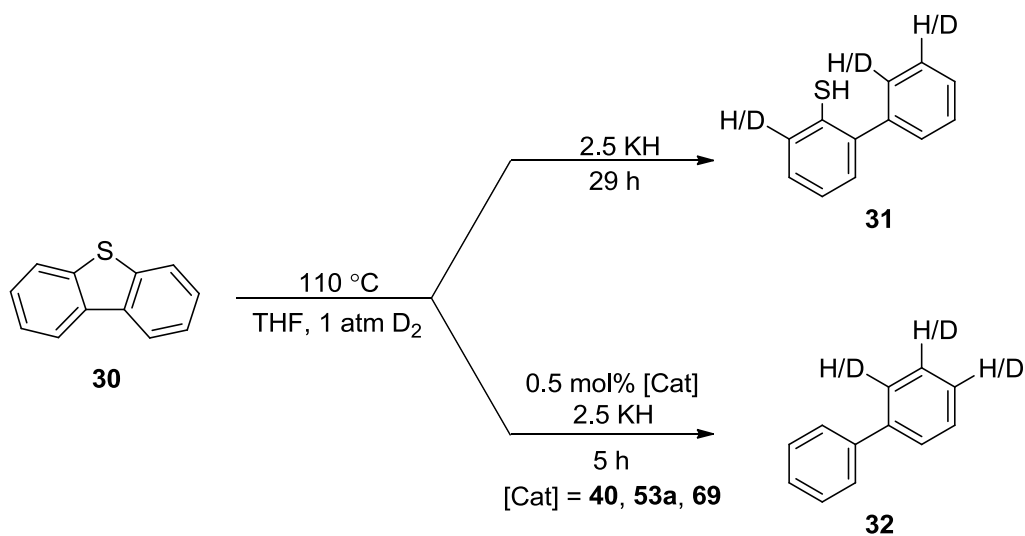
4.2.3.3 Proposed HDS mechanism I: *Ortho*-deprotonation

By considering the strong basicity of KH and the pronounced K^+ ion effect, a preliminary mechanistic proposal can be constructed for the hydride-mediated desulfurization of DBT. π -coordination of a K^+ ion to DBT (complex **103**) activates the substrate by rendering the C–H bonds more acidic toward *ortho*-deprotonation by hydride ion (Scheme **4.4**). The resulting anionic DBT complex **104** can then undergo C–S bond cleavage to form an aryne complex **105**, also stabilized by at least one K^+ ion. The existence of the aryne intermediate has not been independently verified, but if it is formed, it will be in equilibrium with anionic complex **104**. Subsequently, hydride addition (**106**) and protonation, produce the partially desulfurized intermediate potassium thiophenolate complex **99**. Repetition of the process leads to the second C–S bond cleavage, to afford biphenyl.



Scheme 4.4

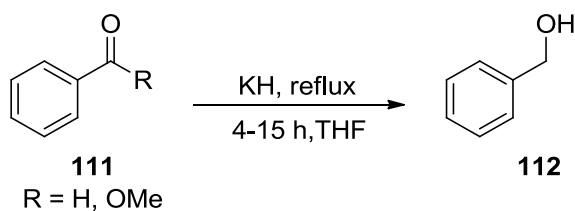
The source of protons in this reaction is likely molecular hydrogen, which is added to the reaction vessel or formed in low concentration from the deprotonation of DBT. Deuterium labelling studies confirm this equilibrium exchange; deuterium incorporation is observed at the 2'-, 3-, and 3'-positions of 2-phenylthiophenol during KH-promoted desulfurization of DBT under D₂ gas (Scheme 4.5, top). In the presence of a transition metal catalyst, deuterium is incorporated at the 2-positions of biphenyl, along with extensive H/D exchange at both 3- and 4-positions (Scheme 4.5, bottom). Deuterium incorporation in both reactions suggests that H₂ is the likely source of the protons required in the reaction shown in Scheme 4.4.



Scheme 4.5

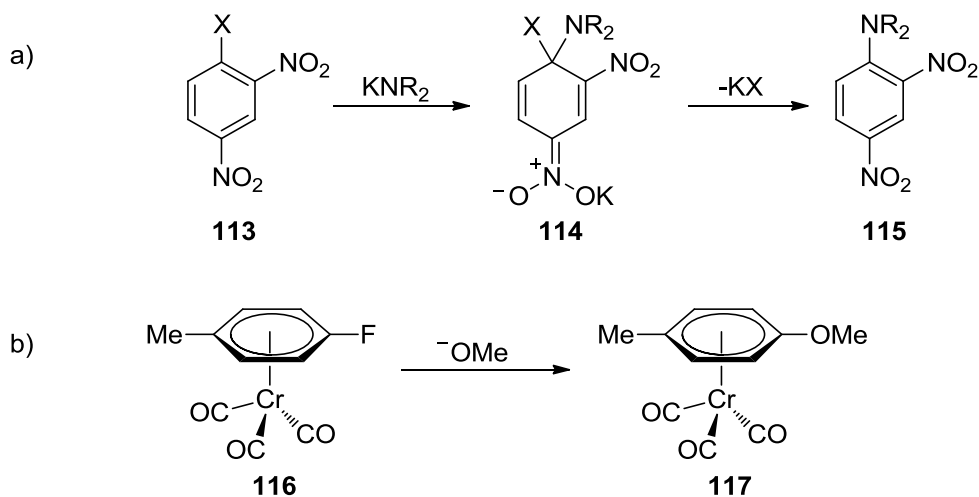
4.2.3 Proposed Mechanism II: Nucleophilic aromatic substitution by KH

Potassium hydride can react with DBT by an entirely different mechanism, based upon the nucleophilicity of the hydride ion. KH is a potent source of nucleophilic hydride,¹⁸⁸⁻¹⁸⁹ reducing haloboranes, ketones, aldehydes, carbon-halide bonds, as well as Y-Y bonds (Y = Si, Sn, Ge).¹⁸⁹ For instance, KH reduces the carbonyl functionality in both benzaldehyde and methyl benzoate (**111**, Scheme 4.6), yielding benzyl alcohol **112**.¹⁹⁷ For KH-mediated desulfurization of DBT, the hydride can react at the C-S bond by *nucleophilic aromatic substitution* pathway, leading to *ipso*-substitution of the thiolate substituent by hydride.

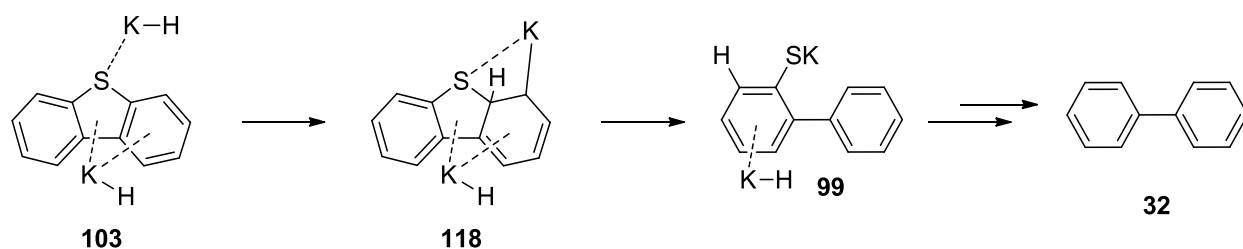


Scheme 4.6

Nucleophilic aromatic substitution (S_NAr) reactions are common in organic syntheses and strongly promoted by the presence of electron-withdrawing group(s) *ortho* or *para* to the leaving group (e.g. complex **113**, Scheme 4.7, a).¹⁹⁸⁻²⁰⁰ The reaction typically proceeds in two steps, with the initial addition of nucleophile to form a stabilized Meisenheimer complex (**114**), followed by elimination of the leaving group.¹⁹⁹⁻²⁰⁰ For more electron-rich aromatic systems, π -coordination of the arene to a Lewis acidic transition metal complex (e.g., chromium tricarbonyl) activates the arene ring towards nucleophilic substitution (Scheme 4.7, b).²⁰⁰⁻²⁰¹ In our case, the transition metal catalyst can function in this role, but in the absence of catalyst, we propose that the potassium ion– π interaction induces this activation, promoting *ipso*-substitution of DBT by the hydride (Scheme 4.8).



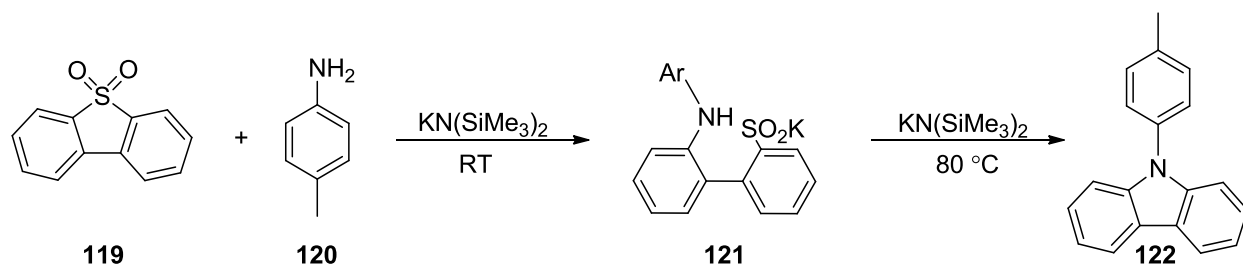
Scheme 4.7



Here, KH is drawn as a single molecule for clarity, but KH likely exist as a cluster solvated by solvent molecules.

Scheme 4.8

Carbon-sulfur bond cleavage *via* S_NAr of dibenzothiophene-5,5-dioxide (**119**) is known, and offers some mechanistic insights.²⁰² Interestingly, Osuka *et al.*, report that the nucleophilic substitution of dibenzothiophene-5,5-dioxide (**119**) by toluidine (**120**) requires *excess* strong potassium base (Scheme 4.9). The nucleophilic substitution does not occur using DBT; the sulfone is much more reactive. Nevertheless, this adds credence to the potential for potassium ion coordination to be essential to activate DBT itself toward desulfurization by KH. In our system, KH, a stronger and smaller nucleophile than the anilide anion, would react more readily with DBT, with or without further activation.



Scheme 4.9

Importantly, Osuka *et al.* show that nucleophilic substitution/ring opening of dibenzothiophene-5,5-dioxide is facile, proceeding at room temperature, while the second C–S bond cleavage requires heating to 80 °C (Scheme 4.9).²⁰² This is similar to what we observed in our ‘KH only’ desulfurization, where KH alone can cleave the first C–S bond of DBT, but the second C–S bond cleavage only proceeds efficiently when a transition metal is added (see Table 4.3, entry 1 *vs.* 3).

4.2.3.1 Desulfurization reactions with dialkyl dibenzothiophene

To distinguish among competing mechanistic proposals (*ortho* deprotonation/aryne *vs.* *ipso* substitution) for the desulfurization of DBT induced by KH, the reduction of 4,6-dimethyldibenzothiophene (**123**, Figure 4.4) was investigated. For this substrate, *ortho* deprotonation is eliminated from consideration; any HDS reactivity should proceed exclusively by nucleophilic substitution. In the event, potassium hydride does not react with 4,6-dimethyl dibenzothiophene (MEDBT) under comparable conditions, giving only a trace of the substituted 2-phenylthiophenol **125**. This leads instinctively to the conclusion that *ortho* deprotonation is the more relevant mechanistic proposal. However, deactivation of the arene ring by electronic and steric effects arising from methyl substituents would also inhibit *ipso* substitution in this case.²⁰³ Upon addition of a cobalt catalyst, 4,6-dimethyl DBT undergoes HDS at a rate comparable to that observed for DBT (Scheme 4.10). This reaction is assumed to proceed by *ipso* substitution. However, the presence of the transition metal creates entirely new mechanistic possibilities. More definitive experimentation is required to distinguish among them.

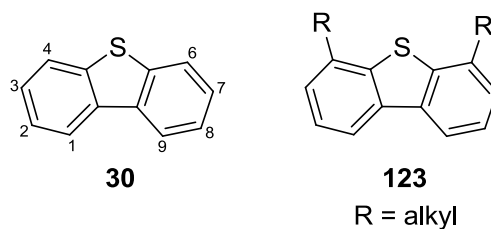
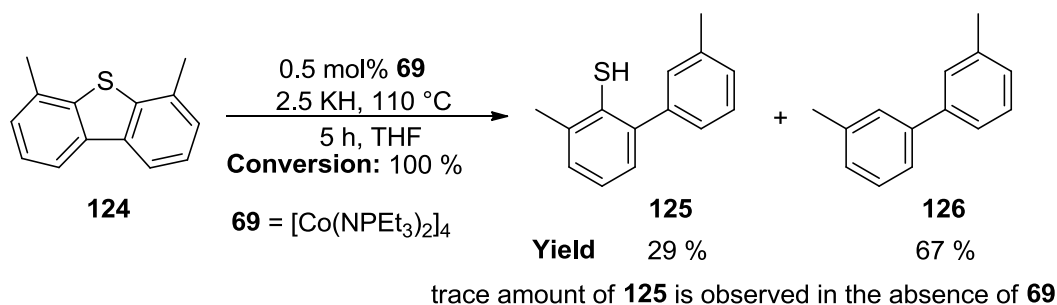


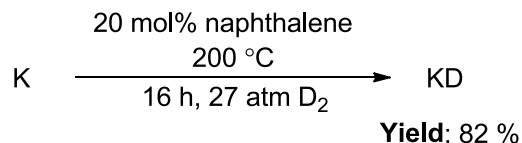
Figure 4.4 Alkyl substituted DBT, especially at the 4 and 6 positions, are resistant to sulfur extrusion.



Scheme 4.10

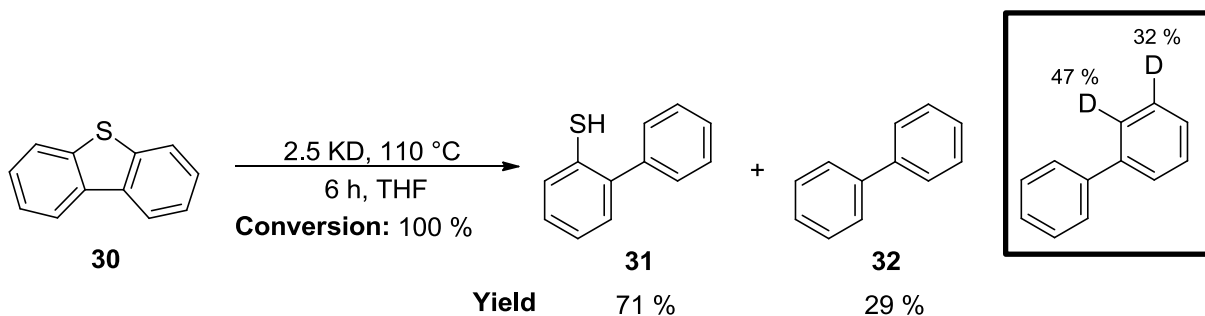
4.2.3.2 Synthesis of KD: further investigation into nucleophilic aromatic substitution by KH

Deuterium labelling studies offer the most direct method for studying the mechanism of KH-mediated C–S bond cleavage. By using potassium deuteride in place of KH and determining the extent and position of deuterium incorporation in the products and recovered starting material, a proposed mechanism can be deduced. Potassium deuteride is not commercially available. Our attempts to prepare it by adapting the synthetic method reported for KH (200 °C, molten potassium, and 27 atm D₂)¹⁸⁹ proved futile. Instead, an alternative method, reported by Bank, *et al.*, for preparing NaH was adapted, giving a good yield of pure KD.²⁰⁴ The addition of catalytic naphthalene to potassium metal under D₂, followed by heating to 200°C produced KD in 82 % isolated yield (Equation 4.3). Unreacted elemental potassium is easily removed from the crude product by addition of fresh naphthalene in THF at reflux.



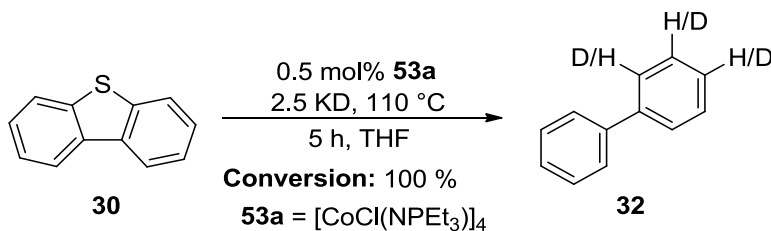
Equation 4.3

Using KD, the incorporation of deuterium into the HDS terminal product biphenyl was determined. Synthesized KD outperformed purified commercial KH, reacting with DBT very efficiently (100% conversion), producing biphenyl in 29% yield, as determined by GC analysis (Equation 4.4 vs. Table 4.3, entry 5). The ^2H NMR spectrum of the isolated biphenyl shows deuterium incorporation at the 2- and 3-positions, with 47 % and 32 % D incorporation, respectively. The high incorporation at the 2-positions (50 % is theoretical maximum) strongly suggests that the C–S bond cleavages occur *via* direct nucleophilic aromatic substitution ($\text{S}_{\text{N}}\text{Ar}$) by the deuteride ion. The lower incorporation of deuterium at the 3- and 3'-positions is attributable to background acid-base H/D exchange, but may also indicate that the *ortho*-deprotonation/aryne pathway or an alternative single-electron transfer pathway,²⁰⁵ are viable. The uncatalyzed desulfurization of 4,6-Me₂-DBT using KD does not proceed to an appreciable conversion as observed with the reaction of the substrate with KH alone, providing no useful information.

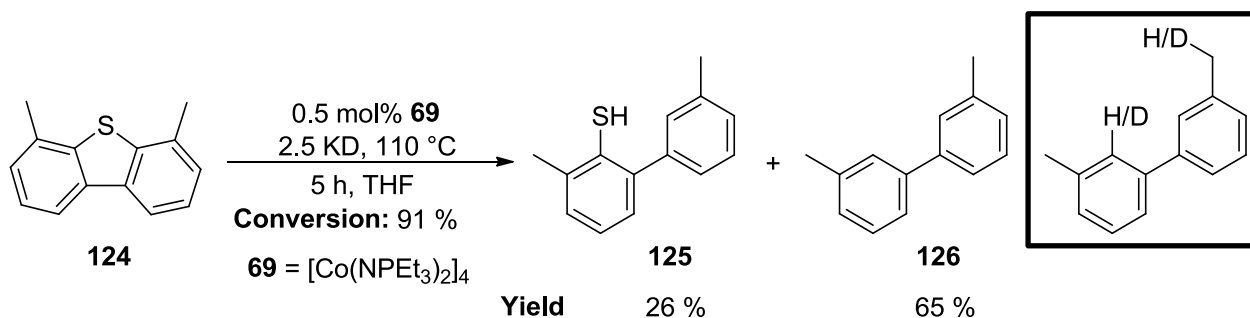


Equation 4.4

Transition metal-catalyzed KD-mediated desulfurization is very efficient, but provides even less mechanistic guidance. *For the first time, however, quantitative conversion of DBT to biphenyl is obtained after 5 hours at 110 °C, using KD and the simple tetrachlorocobalt cluster 53a* (Equation 4.5). The ^2H NMR spectrum of the biphenyl reveals extensive deuterium incorporation at the 2-, 3-, and 4-positions, precluding reasonable mechanistic inferences without further experimentation. The cobalt-promoted desulfurization of 4,6-Me₂-DBT by KD is similarly efficient (91% conversion, 65% fully desulfurized hydrocarbon, Equation 4.6). The ^2H NMR spectrum of the isolated 3,3'-dimethylbiphenyl **126** shows deuterium incorporation at the 2-position, again supporting a nucleophilic substitution as the dominant reaction pathway. Interestingly, deuterium incorporation is also observed at the benzylic positions, presumably through reversible deprotonation and reprotonation by H–D.



Equation 4.5



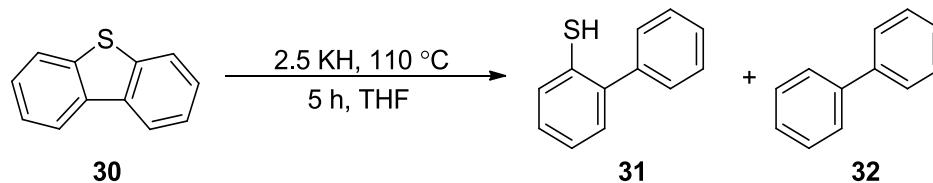
Equation 4.6

4.2.3.3 Synthesized KH is not commercial KH

The higher desulfurization activity of KD in comparison to commercial KH prompted direct investigation into this disparity (see Table 4.3, entries 3 and 6; *cf.*, Equation 4.3). Three lots of potassium hydride were compared under otherwise identical reaction conditions: hexane-washed commercial KH, purified commercial KH, and pure synthesized KH. Hexane-washed KH was obtained by repeated rinsing of purchased KH with anhydrous hexanes to remove the paraffin oil. The purified commercial KH was obtained from this material by treatment with 20 mol% naphthalene in THF at reflux to remove entrained elemental potassium. The synthesized KH was obtained using the method described above for KD (see experimental).

The synthesized KH is superior for desulfurization, when compared to either commercial samples. Near-quantitative conversion of DBT and the highest conversion to biphenyl (20%) is obtained with this material (Table 4.7, entry 1). In contrast, purified commercial KH and hexane-washed KH lead to lower and very low conversions, with only trace amounts of full desulfurization obtained under otherwise identical conditions (entries 2–3). The possibility that trace amounts of transition metal(s) impurities might be responsible for the higher activity of synthesized KH was excluded by EDX spectroscopy (energy-dispersive X-ray spectroscopy), only K, and low concentrations of C and O were detected in the KH samples.

Table 4.7 Desulfurization of DBT with synthesized and commercial KH.



Entry	KH	31 (%)	32 (%)
1	Synthesized	77	20
2	Purified ^a	63	1
3	Hexane-washed	26	1

Conversions and yields are calculated based on the results from gas chromatography using n-dodecane as the internal standard. ^aThe result appear above. ^bPurified KH is commercially bought and purified with the addition of 20 mol% naphthalene in THF and heated at reflux.

Micrographs produced by scanning electron microscope (SEM) of synthesized KH reveal smaller, more uniform particles of KH, with an qualitative average size of around 200 nm (Figure 4.5, left). In contrast, particles of purified, commercial KH are both larger and more polydisperse (Figure 4.5, right). Since the reactivity of KH largely occurs at the surface of the crystallites, smaller particle size leads to higher surface area, and thus, higher reactivity.²⁰⁶⁻²⁰⁷

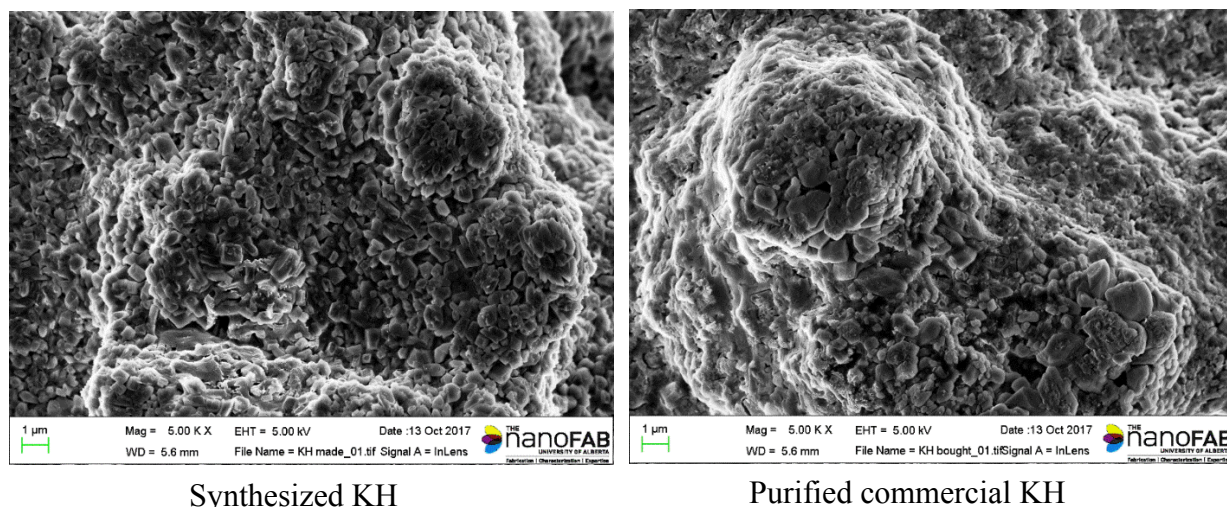
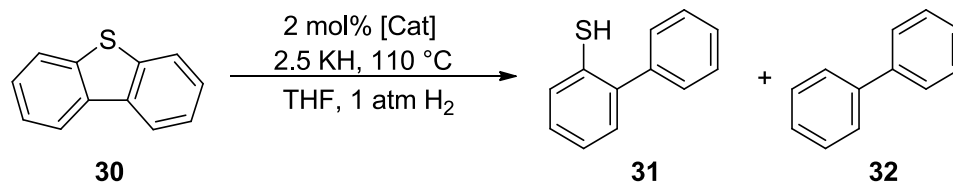


Figure 4.5 Secondary electron SEM images of synthesized and purified KH.

4.2.4 Role of the transition metal catalysts: oxidative addition “vs.” Lewis acid activation

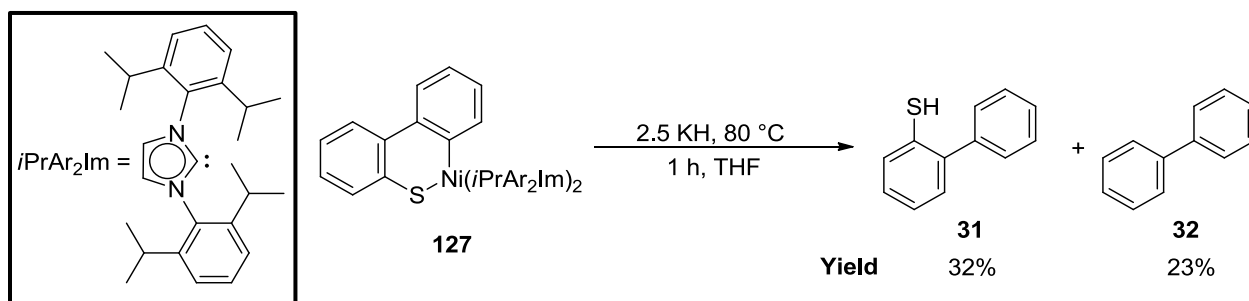
While KH alone desulfurizes DBT, there is a dramatic rate enhancement in the reaction when a transition metal catalyst is present. Although the specific transition metal precatalyst used is not inconsequential (homogeneous *vs.* heterogeneous, preassembled clusters *vs.* simple metal halides, Table 4.8), nearly every cobalt source provides some enhancement. This raises questions regarding the composition of the active catalyst and the precise role of the transition metal(s) in KH-promoted HDS. Two key roles can be envisioned for the low-valent catalyst: (1) oxidative insertion of the metal atom into the C–S bond of DBT, leading to hydrogenolysis and eventual desulfurization,^{7, 95, 100} and alternatively, (2) the transition metal π -coordinates to the arene ring of DBT, weakening the C–S bond towards hydride-mediated cleavage.⁹¹⁻⁹² A combination of both (1) and (2), or an entirely distinct mechanistic pathway is also possible.

Table 4.8 Desulfurization of DBT catalyzed by cobalt (II) halide.

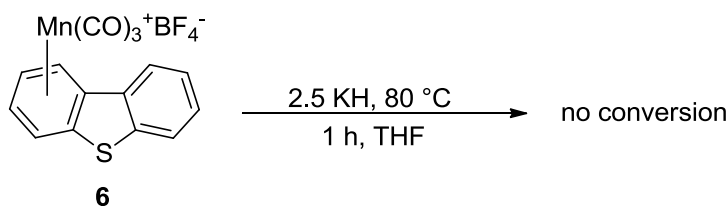
Entry	[Cat] ^a	Time (h)	Conversion (%)	31 (%)	32 (%)
1	53a ^b	2	100	3	96
2	CoCl ₂	5	99	41	44
3	CoBr ₂	5	97	56	30

Conversions and yields are calculated based on the results from gas chromatography using n-dodecane as the internal standard. KH was purified according to the procedure outlined in the experimental section. ^a2 mol% of the metal center or 0.5 mol% per 4 metal centers. ^b**53a** = [CoCl(NPEt₃)₄].

As a rudimentary probe of the role of the transition metal, two homogeneous precatalyst complexes known to interact with DBT in distinct ways were used for KH-mediated desulfurization in the absence of hydrogen. Under conditions where no background desulfurization by KH is observed, nickel NHC complex **127**,⁹⁵ known to readily insert into the C–S bond of DBT (Equation 4.7), was added to the reaction mixture. In the presence of this Ni complex, substantial desulfurization is observed (23 % conversion to biphenyl). On the other hand, manganese tricarbonyl DBT cation **6**, known to coordinate DBT in an η^6 -*hapticity*, has no promotional effect on KH-mediated C–S bond activation (Equation 4.8).⁹¹ While not conclusive, these results suggest that the oxidative cleavage of the C–S bond by the transition metal catalyst is most important, more so than catalyst/arene π -coordination.



Equation 4.7

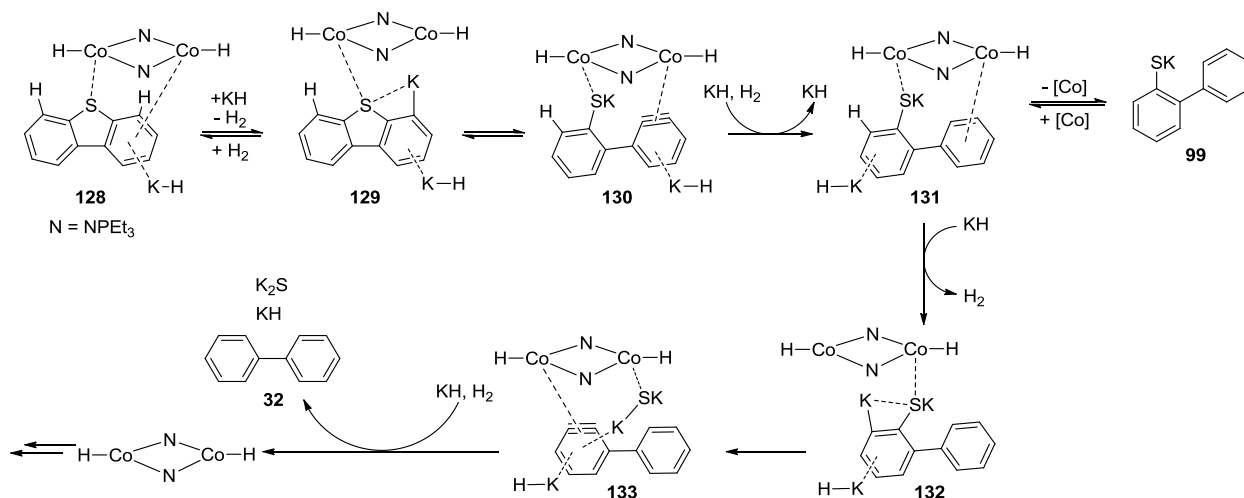


Equation 4.8

4.2.4.1 Proposed mechanisms of cobalt-catalyzed, KH-mediated hydrodesulfurization.

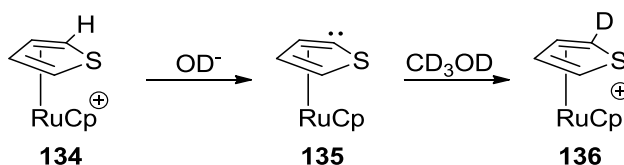
Similar to the potassium cation (see Figure 4.3), the transition metal can bind η^5 or η^6 to the arene ring or η^1 to the sulfur atom of DBT, activating the substrate towards deprotonation and/or nucleophilic substitution by KH. In the metal-catalyzed KH deprotonation (Scheme 4.11), the coordination of a hypothetical cobalt hydride cluster, formed during precatalyst activation, (see Chapter 2), to DBT further lowers the activation energy for deprotonation of C–H bonds. This accounts for the extensive H/D exchange (see Scheme 4.5 above) as well as accelerated desulfurization activity in transition metal-catalyzed HDS reactions (see Chapter 3). Angelici and Sauer observed a similar C–H bond activation of a thiophene molecule which is π -coordinated to a ruthenium complex (**134**, Scheme 4.12).^{203, 208} Because of this π -coordination, a comparatively

weak base ($\text{OD}^- \text{pK}_a(\text{DMSO}) = 32$)¹⁹² easily deprotonates the C–H bonds of thiophene (normal $\text{pK}_a(\text{DMSO}) = 32.5$)²⁰⁹ at the 2- and 5-positions (*e.g.*, **135**). Subsequent deuteration results in H/D exchange.



Here, the cluster was drawn as a dimer for clarity, but both dimeric or heterocubane cluster can presumably catalyze the reaction.

Scheme 4.11



Scheme 4.12

Coordination of the cobalt cluster to DBT leads to facile deprotonation of the *ortho* C–H bonds by KH, cleaving the C–S bond with concomitant formation of an unstable arylene intermediate **105** (see Scheme 4.4 above). The catalyst intercepts the arylene (**130**),²¹⁰ stabilizing the intermediate and promoting hydride addition and protonation by H₂ to yield cobalt thiolate

intermediate **131** (Scheme 4.11). The ring-opened substrate, potassium 2-phenylthiophenolate, can dissociate from the cobalt and give 2-phenylthiophenol upon acidic work-up.

The reaction kinetic profile of the hydride-assisted hydrodesulfurization of DBT catalyzed by homoleptic cluster **69** supports this intermediate dissociation of the thiolate salt. At 110 °C and 1 atm H₂, the concentration of dibenzothiophene precipitously decreases to near zero within the first 15 minutes (Figure 4.6), converting DBT to 2-phenylthiophenol (~70 %).

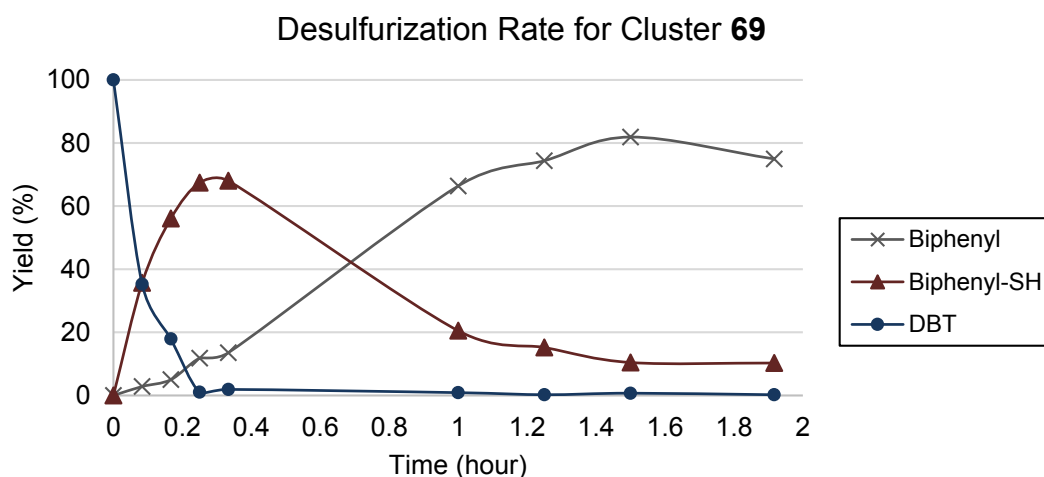
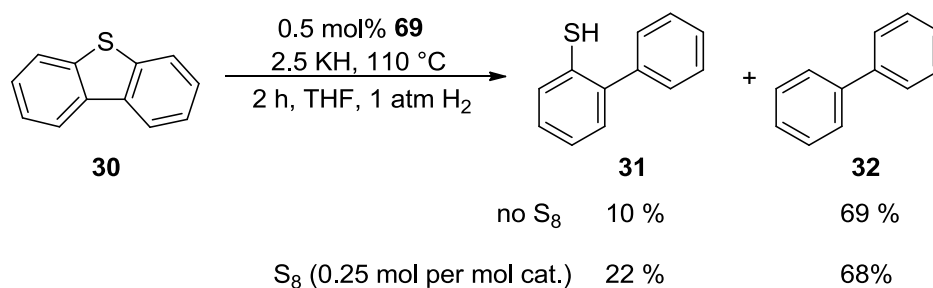


Figure 4.6 The conversion of DBT to biphenyl in 2 hours at 1 atm H₂ and 110 °C using 0.5 mol% the bis(phosphoranimide) cobalt cluster **69**.

Recoordination of the 2-phenylthiophenolate to the catalyst leads eventually to full desulfurization. This could follow the benzyne hypothesis, as the second equivalent of KH can deprotonate the *ortho*-C–H bond, generating anionic intermediate **132** (Scheme 4.11). Coordination of the sulfur atom to cobalt is likely necessary to polarize and weaken the remaining C–S bond for elimination by KH. This accounts for the more efficient

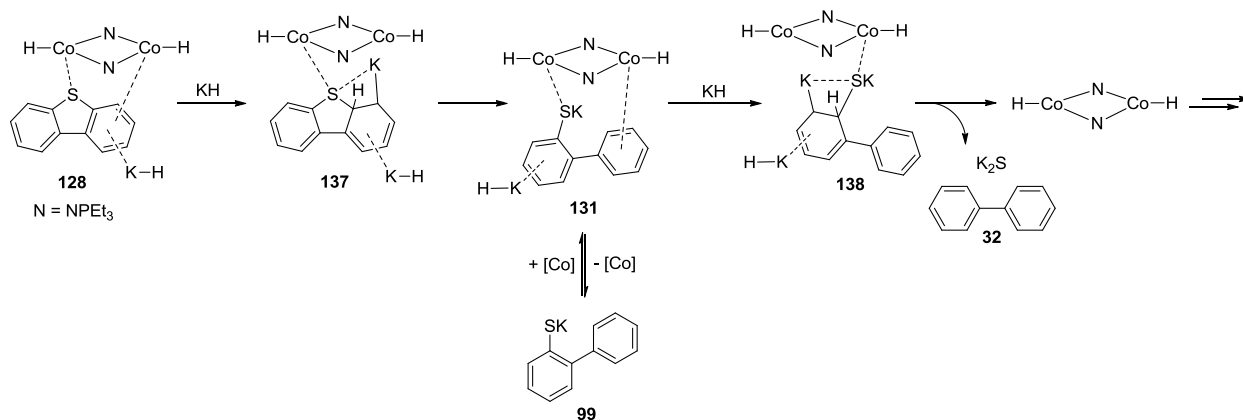
hydrodesulfurization observed in the presence of the transition metal source (see Table 4.3, entry 1 vs. 3). The cleavage of the C–S bond forms a second cobalt-stabilized aryne intermediate (**133**), which is finally converted to biphenyl. Potassium sulfide (K₂S) is, theoretically, the only byproduct from this reaction, but we have not confirmed this; the byproduct could conceivably be KSH. In this hydride-mediated HDS mechanism, the cobalt atoms form only dative bonds to sulfur, accounting for the high catalytic activity. This contrasts to homogeneous transition metal complexes and catalyst that form stable, hydrogenolysis-resistant M–S clusters during attempted hydrodesulfurization. This leads to only stoichiometric reactivity.⁷ If, however, formal Co–S bonds are formed under these reaction conditions, the excess KH in the reaction mixture can, apparently, regenerate Co–H bond(s) from the sulfide by KH metathesis.

To investigate the ease of regeneration of the active catalyst from sulfided cobalt, we deliberately added elemental sulfur to the HDS reaction, anticipating *in situ* formation of a stable cobalt sulfide cluster (see discussion in Chapter 2). If the Co–S bond resists hydrogenolysis under the reaction conditions, a suppression of desulfurization activity would be expected. However, the desulfurization activity should not be affected if the active catalyst is regenerated by the reaction of the cobalt sulfide with KH. In the event, this is observed: the activity of the homoleptic cluster **69** toward desulfurization is maintained despite the addition of sulfur, affording high conversion (99 %) and high yield of biphenyl (Scheme 4.13).

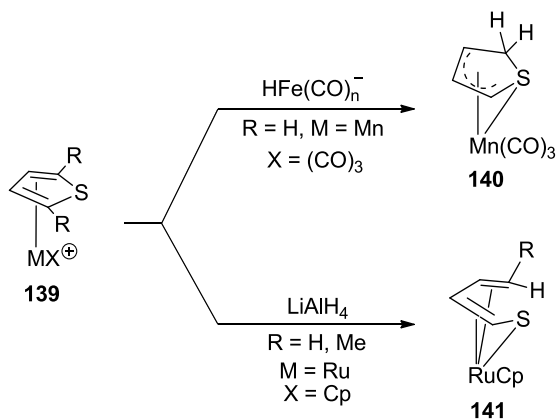


Scheme 4.13

The η^5 -, η^6 -, or η^1 -coordination of DBT or 2-thiophenolate **99** to the catalyst promotes nucleophilic aromatic substitution by KH or a cobalt hydride intermediate (Scheme **4.14**). Coordination to the metal(s) withdraws electron density from the substrate π -system, making the *ipso* carbon more electrophilic.^{201, 203, 211-212} Angelici, *et al.*, observed a similar hydride addition to η^5 -thiophene complexes of Mn²¹¹ and Ru²¹³ (Scheme **4.15**) using a mild external hydride source. Interestingly, this hydride addition produces the η^4 -thioallyl complex **140**; no C–S bond cleavage is observed.²¹¹ This accounts for the absence of KH-mediated desulfurization in η^6 -DBT Mn(CO)₃⁺ complex (**6**, Equation **4.7**). In contrast, nucleophilic addition of LiAlH₄ to the analogous Ru complex **139** leads to the C–S bond cleavage of thiophene.²¹³



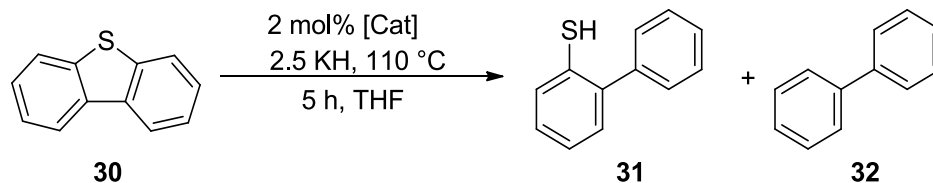
Scheme 4.14



Scheme 4.15

4.2.5 Simple metal salt catalysis: the $\text{MX}_2\text{-KH}$ system for deep desulfurization

Among the more important discoveries reported in this thesis is the use of simple first-row transition metal halide salts together with KH as a simple, highly convenient system to catalyze deep desulfurization (Table 4.9). These reactions do not require added H_2 ; in fact, the reactions can be inhibited by high concentrations of H_2 in the reactor. The conversions are *uniformly* high (>99 %) for all mid-to-late first-row metal halides (Fe to Cu) and biphenyl is the major product in all cases (Table 4.9). Iron and cobalt halides are most effective, giving near-quantitative conversion of DBT to biphenyl (entries 1–3). Ironically, as HDS precatalysts, these metal halides outperform the polymetallic phosphoramidate clusters synthesized from them. While the Grubbs $\text{KO}^t\text{Bu/silane}$ system for HDS is impressive,²¹ the present *hydrogenolysis* method is superior in terms of simplicity, atom economy, mildness of reaction conditions, and cost of reductant.

Table 4.9 Desulfurization of DBT catalyzed by transition metal halide.

Entry	[Cat] ^a	Conversion (%)	31 (%)	32 (%)
1	FeCl ₂	100	15	80
2	CoCl ₂	100	11	84
3	CoBr ₂	100	12	76
4	NiCl ₂	100	14	76
5	NiBr ₂	100	18	72
6	CuCl ₂	100	28	63
7	CuBr ₂	99	31	62

Conversions and yields are calculated based on the results from gas chromatography using n-dodecane as the internal standard. KH was purified according to the procedure outlined in the experimental section. ^aThe amount of catalyst used: 2 % per metal center or 0.5 % per 4 metal centers (equivalent to 4 metal centers of the clusters).

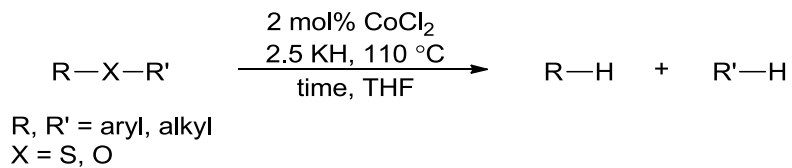
4.2.6 Substrate scope for the CoCl₂-KH system

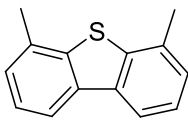
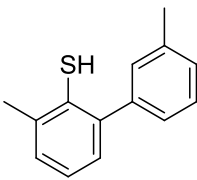
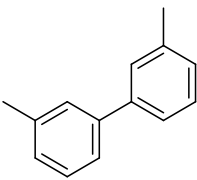
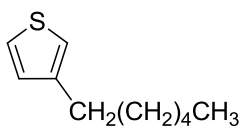
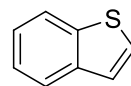
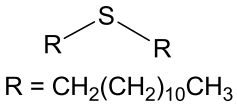
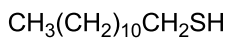
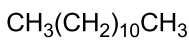
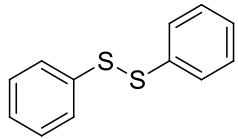
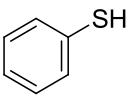
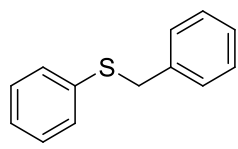
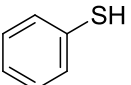
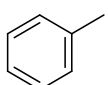
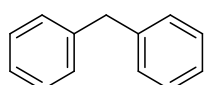
Using this convenient catalyst/reagent system (CoCl₂ and KH), we briefly investigated the desulfurization of a range of sulfur-containing substrates representative of the typical organosulfur molecules found in crude oil. As expected, the desulfurization of dimethyl DBT is not as efficient as observed for DBT (Table 4.10, entry 1 vs. Table 4.9, entry 2). This mirrors the trend observed in the industrial HDS reactors, where 4,6-dialkyl DBT remains in the hydrocarbon stream even after aggressive hydrotreatment conditions.¹⁵⁶ In contrast, organosulfur molecules such as thiophene and benzothiophene typically undergo facile C-S bond activation

using industrial catalysts as well as many homogeneous transition metal complexes.^{51, 68, 93, 125, 203, 208, 213-214} Surprisingly, in our case, no C–S bond cleavage is observed for either thiophene or benzothiophene (Table 4.10, entries 2–3). The likely reason for this observation is the absence of an extended aromatic system (< 3 conjugated aromatic rings) in either of these substrates, which is necessary for the facile coordination of the K⁺ or the transition metal in desulfurization reaction pathway (entry 1 vs. entry 4). Binding of the potassium cation or the transition metal to larger polycyclic aromatic compounds is generally more favorable, thus explaining higher reactivity towards DBT and dimethyl DBT.

While higher reactivity is observed with polycyclic aromatic systems, some desulfurization activity is observed with organosulfur compounds containing acyclic sulfur atoms, albeit for unique reasons. The S–S bond cleavage observed for diphenyl disulfide (Table 4.10, entry 5), is likely due to thermal processes with some acceleration provided by the transition metal, the C–S bonds remain untouched however. The C_{aryl}–S bond in phenyl benzyl sulfide is not cleaved either, instead, thiophenol and toluene are formed by activation of the weaker benzylic C–S bonds. Some C–C coupling products such as diphenyl methane are also obtained (entry 6). The C_{aryl}–S bond of thioanisole also remains intact, with cleavage occurring exclusively at the C_{sp3}–S bond forming thiophenol (entry 7). The selective cleavage of the C_{sp3}–S bond is likely due to the fact that thiophenolate is a better leaving group. In addition, nucleophilic addition to an C_{sp3}–S bond occurs more readily than the nucleophilic aromatic substitution.

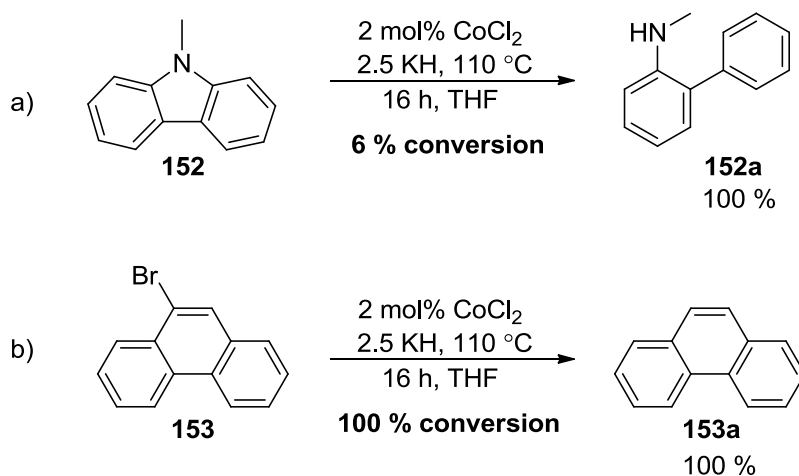
Table 4.10 Desulfurization and C–O bond hydrogenolysis of a variety of substrates.



Entry	Substrate	Time (h)	Conv. (%)	Product Selectivity (%)		
1	 124	5	74	 125 71%	 126 29%	
2	 142	5	0			
3	 143	5	0			
4	 144 R = CH ₂ (CH ₂) ₁₀ CH ₃	5	5	 144a 66%	 144b 34%	
5	 145	5	65	 145a 100%		
6	 146	5	100	 146a 32%	 146b 10%	 146c 58%

Entry	Substrate	Time (h)	Conv. (%)	Product Selectivity (%)
7	 147	5	100	 147a 100 %
8	 148	16	100	 148a 42 % 148b 3 % 148c 20 % 148d 15 % 148e 11 % 148f 9 %
9	 149	16	40	 149a 51 % 149b 49 %
10	 150	16	86	 150a 55 % 150b 45 %
11	 151	16	100	 151a 100 %

Conversions are obtained from GC-MS analysis. KH was purified according to the procedure outlined in the experimental section.



Scheme 4.16

The CoCl_2/KH system is not limited to C–S bond cleavage. Phenoxathiin undergoes both C–S and C–O bond activation, to provide both phenol and thiophenol among other products (Table 4.10, entry 8). Benzene is obtained from the complete defunctionalization of the substrate. The C–S bond cleavage is unsurprising, but the C–O bond activation was encouraging and led us to explore deoxygenation of other aryl ether substrates. Such deoxygenation reactions could find application in the depolymerization and deoxygenation of lignin, necessary for biomass valorization. Under similar reaction conditions (reaction run for 16 h), the CoCl_2/KH cleaves the C–O bonds of aryl ether compounds to form phenols along with a hydrocarbon fragment (Table 4.10, entries 9–11). No complete deoxygenation is observed, thus limiting this system, in its current state, to partial depolymerization of lignin. Even C–N bonds, which typically pose a significant challenge for industrial hydrotreatment catalysts, are cleaved using the CoCl_2/KH system. Only a single C–N bond of 9-methylcarbazole is cleaved however, with full denitrogenation expected to require much more forceful conditions (Scheme 4.16, a). Finally, preliminary results reveal that C–X bonds succumb to defunctionalization using the CoCl_2/KH

method. Stoichiometric conversion of 9-bromophenanthrene to phenanthrene is affected under our standard reaction conditions (Scheme 4.16, b). Taken together these are preliminary studies indicate that this CoCl_2 and KH system, may well developed as a convenient, highly effective, and general method for defunctionalization of diverse organic molecules, even if the cost and handling challenges of KH limit the scale.

4.3 Conclusion

We have demonstrated that potassium hydride in THF is a remarkably active reducing agent, promoting C–S bond cleavage in DBT, under mild conditions and in the absence of both H_2 or a transition metal source. Given sufficient time or elevated temperatures, this reaction will proceed to give the desulfurized product, biphenyl. Adding any first-row transition metal including our phosphoranimide-supported clusters, or even simple transition metal halides will dramatically increase the efficiency of this KH-mediated desulfurization reaction, to quickly afford near-quantitative conversion of DBT to biphenyl. While added H_2 can participate in this reaction, it is certainly not necessary and has no promotional effect on the C–S bond cleavages in either the ‘KH only’ or the transition metal/KH systems.

The complete mechanism of the KH-mediated desulfurization remains to be determined. Nevertheless, we have discovered several important steps of this KH-mediated desulfurization of DBT. While the hydride is required, the potassium ion of the base is equally important, promoting the C–S bonds cleavage by binding to the arene ring and/or the sulfur atom of the substrate. The transition metal adopts a similar role to the potassium ion, which further promotes

the KH-mediated desulfurization reactions. The actual desulfurization reaction appears to proceed by a nucleophilic aromatic substitution mechanism involving a metal- π coordinated organosulfur molecule. Aliphatic C–S bonds are also cleaved, albeit with less efficiency. While there is clear evidence that the potassium hydride deprotonates the C–H bonds of DBT (and other substrates), it is not clear that this is either a relevant or dominant pathway for C–S bond cleavage, requiring further confirmation. Finally, KH along with a simple metal halide, CoCl_2 , has emerged as a simple, general system for the activation of a range of carbon heteroatom bonds with C–O, C–N and C–Br bonds all showing promising reactivity under our conditions.

4.4 Concluding Remarks and Future Works

The chapters in this dissertation have described the hydride-mediated desulfurization of DBT by a series of phosphoranimide-supported cobalt clusters at unprecedentedly mild reaction conditions (1 atm H_2 and 110 °C). Further investigation of this base-assisted reactions using the transition metal halides emphasizes the importance of KH in our reactivity. More importantly, it has provided us with the simplest and atom-economic conditions, where preliminary examination of the limited substrate scope affords promising reactivity towards C–S, C–O, C–N, and C–Br bonds cleavage.

While the transition metal halides and KH system is useful for C–S and C–O bond hydrogenolysis, its application in industry remains limited. The requirement of stoichiometric amount of KH is not only hazardous due to its sensitivity to moisture, but is also costly. In particular, the use of potassium hydride for petroleum or biomass upgrading poses potential risk

due to high water content in the crude mixture. Therefore, development of new and more active catalytic system, where H_2 is the sole reductant is our priority. In our hydride-mediated C–X bonds (where X = O, S) hydrogenolysis, one of the important steps is the $K^+-\pi$ complexation, promoting the cleavage of these bonds. The synthesis of the cobalt precatalyst with potassium atoms incorporated would possibly eliminate the use of stoichiometric amount of potassium promoter.

Nevertheless, the $CoCl_2/KH$ system can be optimized for further application in small scale desulfurization, deoxygenation, denitrogenation, and dehalogenation. A wider range of substrates should be examined to explore for both the tolerance of and reactivity towards different functional groups. In addition, future investigation of Lewis acids is required to address the challenges in complete cleavage of C–X bond (X = O, N) hydrogenolysis.

5. Experimental

The following general procedures, descriptions of instrumentation, and some syntheses (cobalt clusters **40**, **53a**, **60**, and **69**) are adapted from previous Stryker group members.

5.1 General Procedures

All chemicals were purchased from Alfa Aesar, Thermo Fisher Scientific, Sigma Aldrich, or Strem Chemicals and used without further purifications unless stated otherwise. Commercially purchased potassium hydride was washed with excess anhydrous hexanes to remove the paraffin oil (hexane-washed KH) and dried under vacuum. Potassium hydride (KH) was then further purified to remove traces of potassium metal by stirring under reflux overnight in dry THF containing 20 mol% naphthalene. After heating, the purified KH was collected by vacuum filtration and washed three times with 10 mL portions of anhydrous THF and dried under vacuum. All HDS reactions use this purified KH, unless indicated otherwise.

All air- and moisture-sensitive manipulations were executed using standard Schlenk techniques on an N₂/vacuum double manifold or inside an MBraun Labmaster sp glove box under N₂ atmosphere, with the oxygen level maintained below 5 ppm. Hexanes, toluene, diethyl ether, and dichloromethane were dispensed from Pure Process Technology free-standing solvent purification systems (SPS). THF was distilled from Na/benzophenone and 1,4-dioxane from Na under N₂. Solvents inside the glove box were tested with a THF solution of Na/benzophenone (1 drop of a diluted THF solution to 2 mL solvent) to ensure dryness and the absence of O₂. All glassware were dried in the oven (> 150 °C) overnight or flame dried under vacuum before use.

For heating, medium-wall sealed glass vessels (also unofficially called glass bomb) were inserted into an aluminum dry-block adapter plate heated using an Ika stir/heat plate with digital temperature control. Care should be taken to ensure: (1) the glass vessel is fully inserted into the dry-block and (2) the temperature probe of the stir/heat plate is inserted into the dry-block to prevent over heating the glass bomb. In addition, to increase the safety measures and prevent glass shards exiting the fumehood, a blast shield is placed in front of the aluminum dry-block adapter and stir/heat plate. The maximum temperature safe for the catalytic reactions in these glass vessels with different solvents are as follow: (1) THF: 130 °C and (2) toluene: 150 °C. High pressure steel autoclaves were heated in silicone oil baths maintained on Ika stir plates with digital temperature control. Low temperature reactions were cooled in an isopropanol/dry ice bath (−78 °C), ice/water bath (0 °C), or by using a Neslab Cryocool with Cryotrol temperature control (for overnight reactions). For elemental analysis, purified samples were dried on a high vacuum line ($<10^{-5}$ Torr), equipped with a three-stage silicone oil diffusion pump.

5.2 Instrumentation

FT-IR, GC-MS, and CHNS combustion analyses were performed by the staff of the Analytical and Instrumentation Laboratory in the Chemistry Department at the University of Alberta. Air-sensitive IR spectroscopy was performed on a Nicolet Magna 750 FT-IR spectrometer or a Nicolet 8700 FT-IR spectrometer operated by OMNIC Spectra Software. Air-sensitive IR samples were prepared inside the dry box as a cast film on two 25 x 4 mm KBr salt plates sandwiched together, sealed and separated by nitrile elastomer O-rings.

Tandem gas chromatography-mass spectrometry was performed using a Hewlett Packard GCD series G1800A GC-MS, with HP 5870 or 5971 mass detectors. The column used was an Agilent DB-5 MS 25m x 0.25 mm x 0.25 micron film thickness. The MS reference library was provided by NIST/EPA/NIH 2011 Mass Spectral Library, with the NIST11 software package.

Elemental analysis (CHNS) of air-sensitive samples was performed in duplicate using a Carlo Erba EA11-0 Elemental analyzer. Inside the dry box, 1-2 mg of the compound (pre-dried on a high vacuum line, $<10^{-5}$ Torr) was placed inside a pre-weighed tin boat and folded into a small cube. The folded boat is inserted into another tin boat and again folded to inhibit exposure to air and moisture.

^1H , ^{31}P , and ^2H NMR spectroscopy were performed in standard 5 mm NMR tubes sealed with plastic caps. The spectra were obtained using Varian/Agilent 400 MHz spectrometers at 27 °C.

X-ray crystal structure determinations and data collection were performed by the X-ray Crystallography Laboratory at the University of Alberta. Crystallographic data were collected using a Bruker DB or PLATFORM diffractometer, both equipped with SMART APEX II CCD area detectors.

Reaction product analysis was performed using gas chromatography with flame ionization detection (GC-FID) on Agilent 6890N gas chromatograph with a HP-5 (5% phenyl)-methylpolysiloxane capillary column (Agilent). Yields were calculated based on the calibration

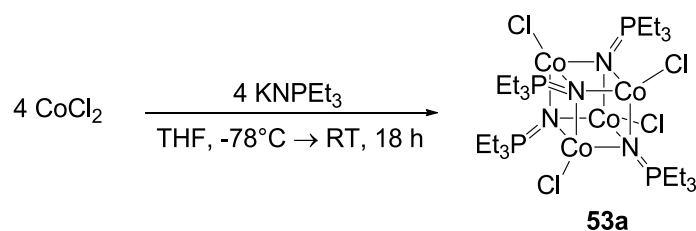
curve using *n*-dodecane as the internal standard. Calibration curves of dibenzothiophene, 4-phenylthiophenol, and biphenyl were created with varying the concentration of the analyte with standard *n*-dodecane, included as an appendix. GC-MS results were obtained using Agilent 6850 gas chromatograph equipped with an Agilent HP-5 (5% phenyl)-methypolysiloxane capillary column.

Scanning electron micrographs and energy-dispersive x-ray data are obtained by the Nano Fabrication and Characterization facility at the University of Alberta. The micrographs and EDX data were collected using the Zeiss Sigma field emission scanning electron microscope with Oxford AZtecSynergy system for EDS and EBSD acquisition.

5.3 Experimental Procedures for Chapter 2

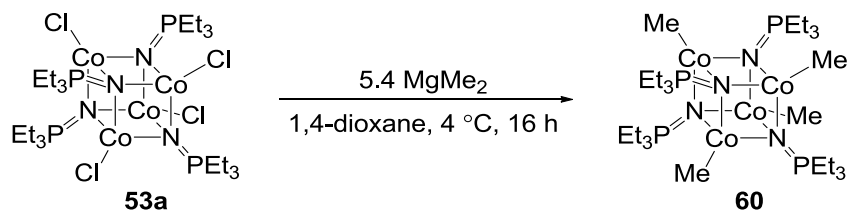
The triethylphosphoranimide ligand (KNPEt₃) and chloride-capped nickel phosphoranimide cluster **53b** were prepared according to the method reported in the theses of the previous Stryker group members.^{25, 103-104} Dimethyl magnesium was prepared according to previously reported procedure.²¹⁵

5.3.1 Synthesis of $[\text{CoCl}(\text{NPEt}_3)]_4$ **53a**



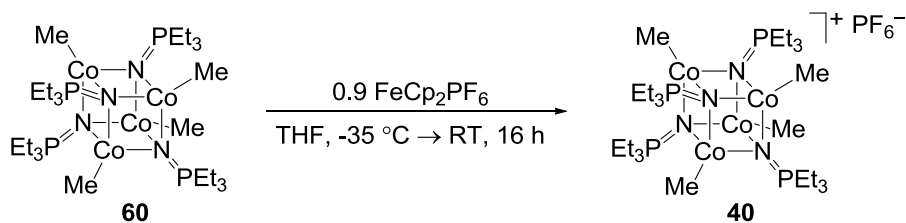
This synthesis was adapted from the method previously reported by Dr. Brown.¹⁰³ Inside the dry box, CoCl_2 (1.15 g, 8.85 mmol) and THF (~75 mL) were added into a pre-dried 250-mL Schlenk flask equipped with a Teflon-coated stir bar. In another 250-mL Schlenk flask, KNPEt_3 (1.48 g, 8.67 mmol) was dissolved in THF (80 mL). On the Schlenk line, the CoCl_2 suspension was cooled to -78°C by immersion in an isopropyl/dry ice bath. With vigorous stirring, the KNPEt_3 solution was slowly added to the flask under a constant flow of N_2 , resulting in blue-green suspension. The mixture was stirred -78°C for 2h, then, allowed to slowly warm to room temperature. At room temperature, the suspension was stirred for additional 16 h. Under reduced pressure, the THF was removed, leaving a green powder. Dichloromethane (~60 mL) was added to the flask and stirred for 10 min to extract the product. The green solution was transferred to a Schlenk frit and filtered through Celite. The flask was washed with 3x10 mL portions of dichloromethane (DCM) until the wash solution was colorless. Under reduced pressure, the DCM was removed, resulting in green powder. Inside the dry box, the solid was washed with 3x10 mL portions of pentane to again yield pale green powder. After drying under high vacuum, the known product, $[\text{CoCl}(\text{NPEt}_3)]_4$ (1.59 g, 1.75 mmol, 81 %), was characterized by elemental analysis: C: 31.85, H: 6.68, N: 5.97. Expected elemental analysis values: C: 31.81, H: 6.67, N: 6.18.

5.3.2 Synthesis of $[\text{CoMe}(\text{NPEt}_3)]_4$ **60**



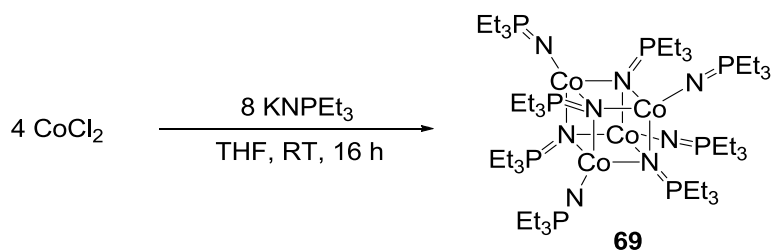
This synthesis was adapted from the method previously reported by Dr. Brown.¹⁰³ In the dry box, $[\text{CoCl}(\text{NPEt}_3)]_4$ (0.19 g, 0.21 mmol) was weighed into a 5-dram vial equipped with a Teflon stir bar and dissolved in dry 1,4-dioxane (~1 mL). In another 5-dram vial, $\text{MgMe}_2 \cdot (\text{C}_4\text{H}_8\text{O}_2)_{0.65}$ (0.11 g, 0.95 mmol) was dissolved in 1,4-dioxane (~1 mL). Both vials were cooled to 4 °C in the dry box freezer. With vigorous stirring, the $\text{MgMe}_2 \cdot (\text{C}_4\text{H}_8\text{O}_2)_{0.65}$ solution was added dropwise to the solution of $[\text{CoCl}(\text{NPEt}_3)]_4$, transforming the blue-green solution to dark green. The mixture stirred at room temperature for 16 h. The solvent was removed under reduced pressure, resulting in a mixture of white and green powders. The green $[\text{CoMe}(\text{NPEt}_3)]_4$ was extracted using hexane and filtered twice through Celite plugs. Hexane was removed under reduced pressure, affording green, microcrystalline $[\text{CoMe}(\text{NPEt}_3)]_4$ (0.12 g, 0.14 mmol, 67 %). The product was confirmed with elemental analysis: C: 40.77, H: 8.89, N: 6.80. Expected elemental analysis values: C: 40.79, H: 8.80, N: 6.80.

5.3.3 Synthesis of $[\text{CoMe}(\text{NPEt}_3)]_4\text{PF}_6$ **40**



This synthesis was adapted from the method previously reported by Dr. Brown.¹⁰³ In the dry box, [CoMe(NPEt₃)₄] (0.13 g, 0.15 mmol) was weighed into a 5-dram vial equipped with a Teflon stir bar and dissolved in dry THF (~1 mL). In another 5-dram vial, ferrocenium hexafluorophosphate (0.048 g, 0.15 mmol) was suspended in THF (~1 mL). The ferrocenium hexafluorophosphate suspension was added dropwise to the vigorously-stirred solution of [CoMe(NPEt₃)₄], resulting in a dark green solution. The mixture was allowed to warm to room temperature and stirred for 16 h. The solvent was removed, resulting in dark green, oily solid. The solid was washed with hexane (~20 mL) until the washes were colorless. After drying under reduced pressure, the crude product was dissolved in THF (~3 mL) and filtered through a Celite plug. The final product [CoMe(NPEt₃)₄]PF₆ (0.11 g, 0.12 mmol, 79%) was dried under reduced pressure to yield powdery, green solid. After drying under high vacuum, the product was found to be pure based on elemental analysis data: C: 34.96, H: 7.33, N: 5.47. Expected elemental analysis values: C: 34.69, H: 7.49, N: 5.78.

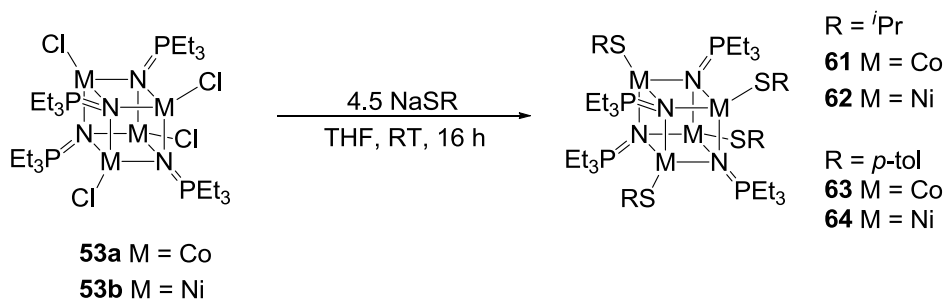
5.3.4 Synthesis of [Co(NPEt₃)₂]₄ **69**



This synthesis was adapted from the method previously reported by Dr. Brown.¹⁰³ In the dry box, CoCl₂ (0.12 g, 0.94 mmol) was weighed into a 5-dram vial equipped with a Teflon stir bar and suspended in dry THF (~1 mL). In another 5-dram vial, two equivalents of KNPEt₃ (0.34 g, 1.9

mmol) was dissolved in THF (~2 mL). The THF solution of KNPEt₃ was added dropwise to the vigorously-stirred suspension of CoCl₂, resulting in a dark green solution. The mixture was allowed to stir at room temperature for 16 h. The solvent was removed under reduced pressure, resulting in green and white powders. The green product was extracted into hexane and filtered through a Celite plug. The dark green filtrate was cooled to -35 °C in the dry box freezer for 1 h, after which the solution was passed through another Celite plug. Hexane was removed, leaving a dark green powder of homoleptic cobalt cluster **69** (0.24 g, 0.18 mmol, 78 %). The product was dried under high vacuum and characterized by elemental analysis: C: 44.05, H: 9.23, N: 8.43. Expected elemental analysis values: C: 44.59, H: 9.35, N: 8.67. This synthesis was also performed at a larger scale (~400 mg).

5.3.5 Syntheses of [MSR(NPEt₃)₄]



Inside the dry box, a 5-dram vial equipped with a Teflon stir bar was charged with cluster **53a/b** and THF (~1–2 mL). In another 5-dram vial, the sodium thiolate was dissolved in 2 mL of THF. The sodium thiolate solution was added dropwise to the solution of the cluster with vigorous stirring, during which time the color slowly transformed from blue/green to dark olive-green. The solution was left to stir for 16 h at room temperature, after which the THF was removed

under reduced pressure, revealing a dark olive-green powder. The product was extracted into a mixture of hexane and toluene (1 : 1) and filtered twice through Celite plugs. The solvents were removed under reduced pressure, resulting in dark olive-green solid. The product was further dried under high vacuum and characterized by elemental analysis. X-ray quality crystals of each product, except Ni cluster **64**, were obtained by from cold (-35 °C) THF solution of the clusters. Details of the crystal structure determination of clusters **61**, **63**, and **62** are provided in Appendix I, II, and III, respectively.

Table 5.1 Mass of starting materials; yields of products for clusters **61–64**.

Entry	Cluster	53a/b (g, mmol)	NaSR (g, mmol)	Yield (g, mmol, %)	CHNS data	Expected CHNS values
1	61	0.20, 0.22	0.096, 0.98	0.16, 0.15, 70	C: 40.53 H: 8.07 N: 4.70 S: 11.53	C: 40.60 H: 8.33 N: 4.26 S: 12.04
2	62	0.038, 0.038	0.016, 0.17	0.028, 0.026, 63	C: 40.59 H: 8.13 N: 4.89 S: 11.07	C: 40.64 H: 8.34 N: 5.27 S: 12.05
3	63	0.39, 0.43	0.22, 1.5	0.36, 0.28, 66	C: 49.76 H: 7.00 N: 4.22 S: 9.85	C: 49.68 H: 7.06 N: 4.46 S: 10.20
4	64	0.074, 0.071	0.047, 0.32	0.044, 0.035, 50	C: 50.01 H: 7.33 N: 4.24 S: 8.46	C: 49.72 H: 7.06 N: 4.46 S: 10.21

5.3.6 Characterization of intermediate Co–H clusters prepared from cationic methylcobalt cluster **40**

5.3.6.1 Synthesis of the Co–H cluster

Inside the glove box, a resealable, medium-walled glass vessel equipped with a Teflon-coated stir bar was charged with [CoMe(NPEt₃)₄PF₆] (**40**, 0.063 g, 0.065 mmol) and THF (10 mL), resulting in a green solution. The reactor was sealed with a Teflon cap. Outside the glove box, the solution was frozen in liquid nitrogen and placed under vacuum for 10 min. After warming up to room temperature, the vessel was pressurized with hydrogen to 1 atm over a period of 3 minutes. The vessel was resealed and heated at 110 °C for 16 h during which the green solution transformed to dark brown.

5.3.6.2 Analysis of the reactor volatiles using gas-phase FT-IR spectroscopy

The sidearm of the glass reactor was stoppered with a Teflon septum and purged with a high flow of N₂ for 10 minutes to remove air. The Teflon cap was opened to allow the volatiles to enter the side arm. With a gas-tight syringe, a sample of the volatiles in the headspace was removed and injected into a quartz gas cell (path length: 8 cm) purged with a flow of N₂ prior to the injection. The IR spectrum obtained is shown in Figure **5.1**. The FT-IR spectrum shows absorptions at 2900 cm⁻¹ (s, br), 1550 cm⁻¹ (w, br), 1300 cm⁻¹ (w), 1050 cm⁻¹ (m), and 920 cm⁻¹ (w).

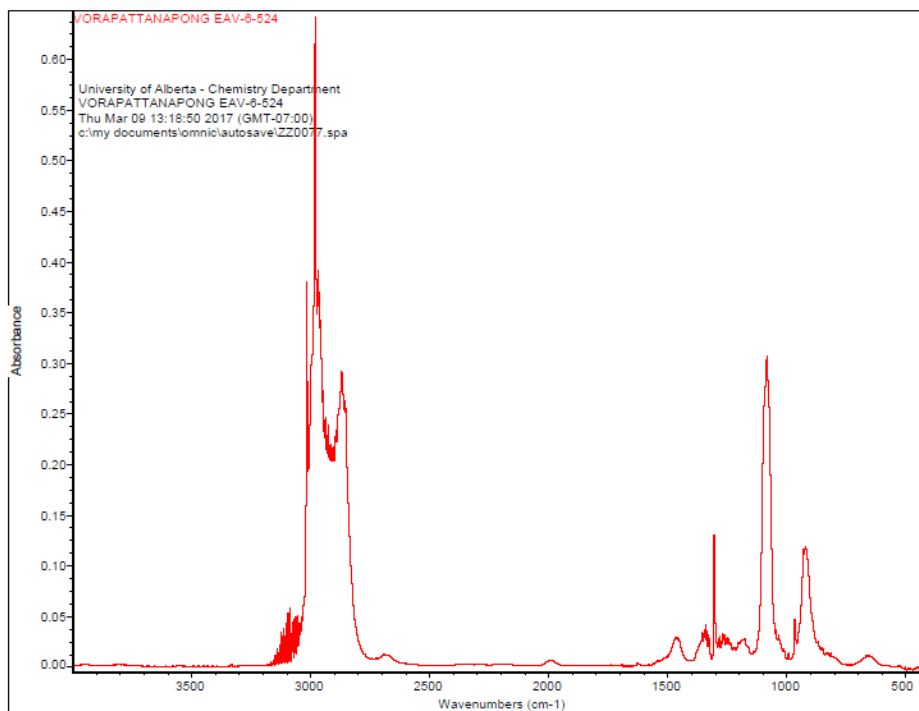
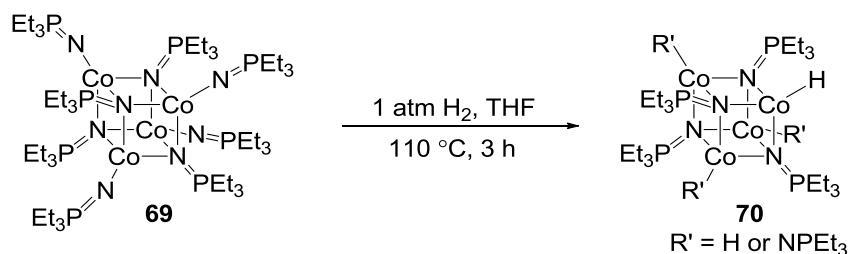


Figure 5.1 Gas-phase FT-IR spectrum of the volatiles from the reaction of cluster **40** and H₂.

5.3.6.3 Analysis of the solution of Co–H clusters using FT-IR spectroscopy

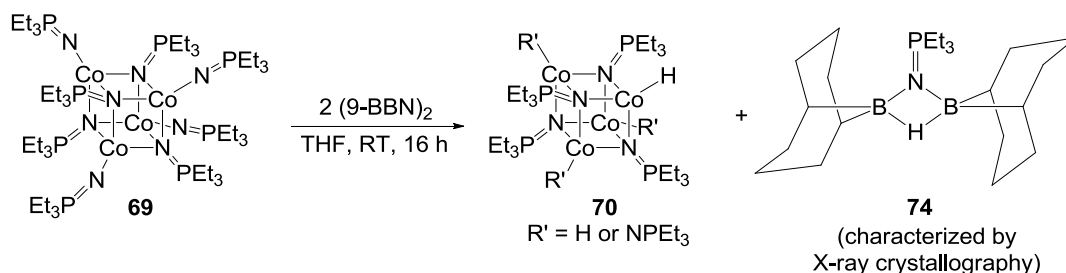
A cast file of the sample was prepared inside the glove box on KBr plates, as described in section 5.2. The FT-IR spectrum (see Appendix VII) shows absorptions at 3319 cm⁻¹ (m, br), 2919 cm⁻¹ (m), 1900 cm⁻¹ (w), 1409 cm⁻¹ (s, br), and 839 cm⁻¹ (s).

5.3.7 Synthesis and analysis of the Co–H intermediate prepared from $[\text{Co}(\text{NPEt}_3)_2]_4$ **69** and H_2



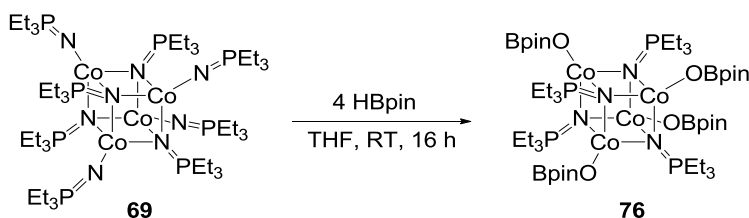
The cobalt hydride cluster was prepared using the same procedure outlined in section 5.3.6.1, using $[\text{Co}(\text{NPEt}_3)_2]_4$ **69** (0.032 g, 0.025 mmol) dissolved in THF (4 mL). After the dark green solution was heated under hydrogen for 16 h, a dark brown solution was obtained. Inside the glove box, the solution was transferred to a 5-dram vial, where the solvent was removed under reduced pressure to yield a dark brown, oily solid. The crude product was washed with hexane (~5 mL) until the wash was colorless, leaving a dark brown solid. From the wash, hexane was removed to yield green, oily solid. To the hexane-insoluble portion, THF (~1 mL) was added to extract the product, which was filtered through a Celite plug and dried under reduced pressure, giving a green oily solid. For the dark brown solid, THF was added to dissolve the crude and filtered through a Celite plug. Both the hexane-soluble and THF-soluble fractions were analyzed by FT-IR spectroscopy (see Appendix VII). IR-spectrum for THF-soluble fraction: 2929 cm^{-1} (m), 2197 cm^{-1} (w), 1409 cm^{-1} (m), 1126 cm^{-1} (s), and 764 cm^{-1} (m). IR-spectrum for hexane-soluble fraction: 2931 cm^{-1} (m), 1456 cm^{-1} (m), 1214 cm^{-1} (m), 1085 cm^{-1} (s), and 761 cm^{-1} (m). No resonances that correspond to either coordinated or free phosphoramidate were observed in the ^{31}P NMR spectra of either the hexane-soluble or THF-soluble fractions, each dissolved in d^6 -benzene.

5.3.8 Synthesis of the Co–H cluster from $[\text{Co}(\text{NPEt}_3)_2]_4$ **69** and 9-BBN



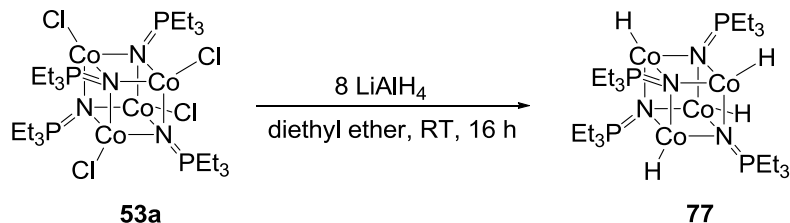
Inside the glove box, a 5-dram vial equipped with a stir bar was charged with $[\text{Co}(\text{NPEt}_3)_2]_4$ **69** (0.093 g, 0.072 mmol) and THF (1 mL), affording a dark green solution. In another 5-dram vial, 9-BBN (0.26 g, 0.14 mmol) was dissolved in THF (2 mL). The solution of 9-BBN was added to a vigorously stirred solution of cluster **69**, transforming the dark green solution to olive green. The solution was left to stir at room temperature for 16 h. The THF was removed under reduced pressure, revealing a mixture of dark green and white solids. The product was extracted with hexane and filtered through two Celite plugs. A portion of the green solution was transferred to another 5-dram vial, where the solution was cooled to $-35\text{ }^\circ\text{C}$ to obtain X-ray quality crystals. For the remaining solution, hexane was removed under reduced pressure, revealing olive-green solid. The solid was dried under high vacuum and submitted for CHN analysis: C: 68.53, H: 11.30, N: 2.21. Expected elemental analysis values for cluster **70** (where R' = H): C: 46.77, H: 9.50, N: 7.64. Elemental analyses suggest that the primary fraction is a mixture of cobalt hydride cluster **70** and byproduct **74**. From the THF solution cooled to $-35\text{ }^\circ\text{C}$ mentioned above, X-ray quality crystals of the byproduct were obtained. Details of the crystal structure determination of byproduct **74** are provided in Appendix IV.

5.3.9 Synthesis of the Co–H cluster with $[Co(NPEt_3)_2]_4$ **69** and HBPin



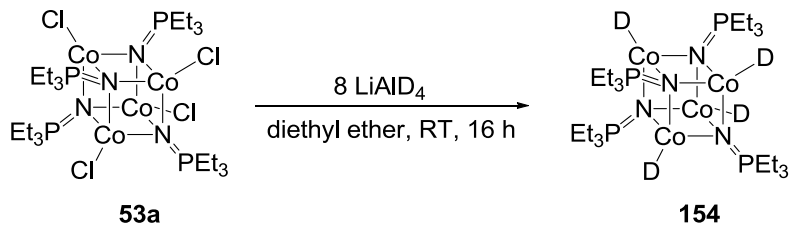
In the dry box, $[Co(NPEt_3)_2]_4$ **69** (0.016 g, 0.013 mmol) was weighed into a 5-dram vial equipped with a Teflon stir bar and dissolved in dry THF (~1 mL). Pinacol borane (0.0064 g, 0.050 mmol) and THF (~1 mL) were added into another 5-dram vial. The THF solution of pinacol borane was added dropwise to the solution of cluster **69**, which immediately transformed from dark green to dark brown. After 16 h stirring at room temperature, THF was removed under reduced pressure, giving a brown, oily solid. The product was extracted with hexane and filtered through two Celite plugs. The brown solution was analyzed using FT-IR spectroscopy (see Appendix VII): 3446 cm^{-1} (m, br), 2968 cm^{-1} (vs), 1497 cm^{-1} (vs), 1215 cm^{-1} (s), 1157 cm^{-1} (vs), 1081 cm^{-1} (vs), and 763 cm^{-1} (m). X-ray quality crystals of cluster **76** were grown from hexane at $-35\text{ }^\circ\text{C}$. Details of the crystal structure determination of byproduct **76** are provided in Appendix IV.

5.3.10 Synthesis of cobalt hydride cluster **77** using $[\text{CoCl}(\text{NPEt}_3)]_4$ **53a** and LiAlH_4



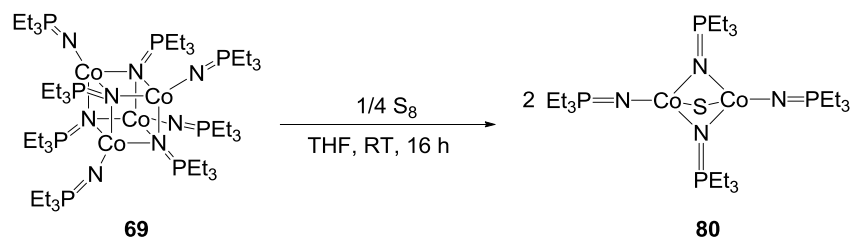
In the glove box, a 5-dram vial equipped with a stir bar was charged with $[\text{CoCl}(\text{NPEt}_3)]_4$ **53a** (0.18 g, 0.19 mmol) and diethyl ether (1 mL), affording a green solution. LiAlH_4 (0.069 g, 1.8 mmol) and diethyl ether (1 mL) were added to another 5-dram vial. The grey suspension of LiAlH_4 was added to a vigorously stirred solution of cluster **53a**, transforming the green solution immediately to a brown suspension. The solution was left to stir at room temperature for 16 h. THF was removed under reduced pressure, revealing a mixture of green and brown solids. The product was extracted with diethyl ether and filtered through two Celite plugs, resulting in a brown solution. The solvent was removed under reduced pressure, leaving a brown solid. The product was dried under high vacuum and submitted for CHN analysis: C: 37.44, H: 7.67, N: 4.09. Expected elemental analysis values for cobalt hydride cluster **77**: C: 37.51, H: 8.39, N: 7.2. FT-IR (ether) (see Appendix VII): 3366 cm^{-1} (m, br), 2926 cm^{-1} (s), 2048 cm^{-1} (m), 1456 cm^{-1} (s), 1383 cm^{-1} (m), 1048 cm^{-1} (s), 762 cm^{-1} (s), and 410 cm^{-1} (m).

5.3.11 Synthesis of cobalt deuteride cluster **154** using $[\text{CoCl}(\text{NPEt}_3)]_4$ **53a** and LiAlD_4



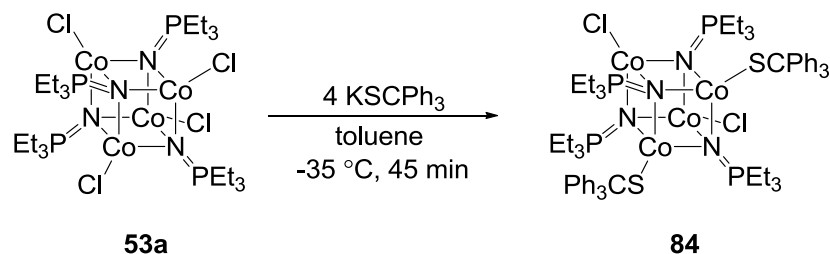
In the glove box, a 5-dram vial equipped with a stir bar was charged with $[\text{CoCl}(\text{NPEt}_3)]_4$ **53a** (0.052 g, 0.057 mmol) and diethyl ether (1 mL), affording a green solution. LiAlD_4 (0.020 g, 0.47 mmol) and diethyl ether (1 mL) were added to another 5-dram vial. The grey suspension of LiAlH_4 was added to a vigorously stirred solution of cluster **53a**, transforming the green solution immediately to a brown suspension. The solution was left to stir at room temperature for 16 h. THF was removed under reduced pressure, revealing a mixture of green and brown solids. The product was extracted with diethyl ether and filtered through two Celite plugs, resulting in a brown solution. The solvent was removed under reduced pressure, leaving a brown solid. FT-IR (ether) (see Appendix VII): 3416 cm^{-1} (m, br), 2928 cm^{-1} (s), 2246 cm^{-1} (w), 1722 cm^{-1} (w), 1456 cm^{-1} (s), 1383 cm^{-1} (m), 1148 cm^{-1} (s), and 775 cm^{-1} (m).

5.3.12 Synthesis of cobalt sulfide cluster **80** from $[\text{Co}(\text{NPEt}_3)_2]_4$ **69** and elemental sulfur



In the glove box, a 5-dram vial equipped with a stir bar was charged with $[\text{Co}(\text{NPEt}_3)_2]_4$ **69** (0.024 g, 0.019 mmol) and THF (1.5 mL), affording a dark green solution. Elemental sulfur (0.0013 g, 0.0051 mmol) and THF (1 mL) were added into another 5-dram vial. The yellow suspension of S_8 was added to a vigorously stirred solution of cluster **69**, transforming the green solution to olive-green. The solution was left to stir at room temperature for 16 h. THF was removed under reduced pressure, revealing a green, oily solid. The product was extracted with hexane and filtered through two Celite plugs. The solvent was removed under reduced pressure, again affording a green oily solid (0.019 g, 0.028 mmol, 74 %). The product was dried under high vacuum and submitted for CHNS analysis: C: 42.26, H: 8.71, N: 7.65, S: 5.83. Expected elemental analysis values for cluster **80**: C: 42.48, H: 8.91, N: 8.26, S: 4.73.

5.3.13 Synthesis of the trityl thiolate-capped cobalt cluster **84** using $[\text{CoCl}(\text{NPEt}_3)]_4$ **53a**

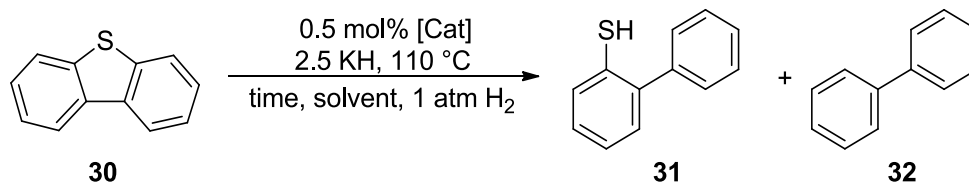


In the glove box, a 5-dram vial equipped with a stir bar was charged with $[\text{CoCl}(\text{NPEt}_3)]_4$ **53a** (0.041 g, 0.046 mmol) and toluene (1 mL), affording a green solution. In another 5-dram vial equipped with a stir bar, KSCPh_3 (0.057 g, 0.182 mmol) was dissolved in toluene (1.5 mL). Both vials were cooled to $-35\text{ }^\circ\text{C}$ for 1 h inside the glove box freezer. After 1 h, the green solution of cluster **53a** was added to a vigorously stirred colorless solution of KSCPh_3 . The solution was left to stir at room temperature for 1 h, giving a green solution with white precipitate. The suspension was filtered through a Celite plug, affording an olive green solution. Toluene was removed under reduced pressure and the product then extracted with a mixture of hexane and toluene (3 : 1). The solution was passed through two Celite plugs. A fraction of the solution was cooled to $-35\text{ }^\circ\text{C}$ to obtain single crystals. Details of the crystal structure determination are provided in Appendix VI. For the remaining fraction, the solvents were removed under reduced pressure, giving olive-green powder (0.047 g, 0.034 mmol, 80 %). The product was dried under high vacuum and submitted for CHNS analysis: C: 45.71, H: 6.59, N: 4.65, S: 2.73. Expected elemental analysis values for **84**: C: 45.06, H: 6.60, N: 4.89, S: 2.80.

5.4 Experimental Procedures for Chapter 3

5.4.1 HDS reactions with cobalt cluster, hydrogen, and KH

In the glove box, the specified cobalt cluster (2 mol% per metal/0.5 mol% per cluster, 0.0036 mmol), potassium hydride (0.072 g, 1.8 mmol), dibenzothiophene (0.13 g, 0.73 mmol), and solvent (10 mL) were added to a resealable, medium-walled glass vessel equipped with a Teflon-coated magnetic stir bar. The vessel was sealed with a Teflon cap. Outside the glove box, the vessel was cooled by immersion in liquid nitrogen until the suspension was frozen. The vessel was then evacuated for 10 min. After 10 min, the suspension was allowed to warm to room temperature and flushed with 1 atm H₂ for 3 minutes. The vessel was resealed and heated to 110 °C for the indicated time. Afterward, the reaction mixture was cooled to room temperature, and the suspension was quenched with 10 % HCl solution until the solution was acidic. The organic layer was extracted with ether and filtered through a Florisil plug. Then, the organic layer was dried over MgSO₄ and filtered through another Florisil plug. The solution was diluted with ether to 25 mL, and 20 μL of n-dodecane was added as an internal standard. The sample was submitted for GC analysis, from which the conversion and the yield of recovered starting material and HDS products were calculated based on the calibration curves of DBT, 2-phenylthiophenol, and biphenyl. Specific experiments and results are detailed in Table 5.2.

Table 5.2 HDS of dibenzothiophene as a function of cobalt cluster under 1 atm H₂.

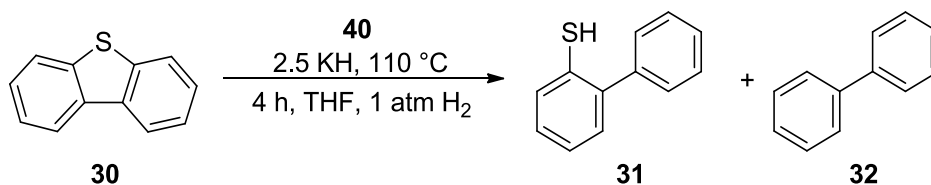
Entry	[Cat]	Time (h)	Solv	Conv. (%)	31 (%)	32 (%)	DBT recovered (%)	Unrecovered (%)
1	40	1.4	THF	63 ^a	29	14	37	20
2	40	2	THF	100	35	45	0	20
3	40	2	tol	39	18	7	61	14
4	60	2	THF	97	59	17	3	21
5	60	2	tol	16	0	2	84	14
6	69	2	THF	99	10	69	1	20
7	69	2	tol	59	38	17	42	3
8	61	2	THF	95	32	52	5	11
9	63	2	THF	91	16	64	9	11
10	62	2	THF	100	93	1	0	6
11	64	2	THF	100	87	1	0	12
12	53a	2	THF	100	3	96	0	1
13	53a	2	tol	44	12	13	56	19

^a6.8 equivalent of KH was used.

5.4.2 TOF vs. concentration of cobalt clusters **40** and **69**

The same general procedure described in section 5.4.1 was followed, using cobalt precatalyst mass as indicated in Tables **5.3** and **5.4**, along with DBT (0.13 g, 0.73 mmol), KH (0.072 g, 1.8 mmol), and THF (10 mL).

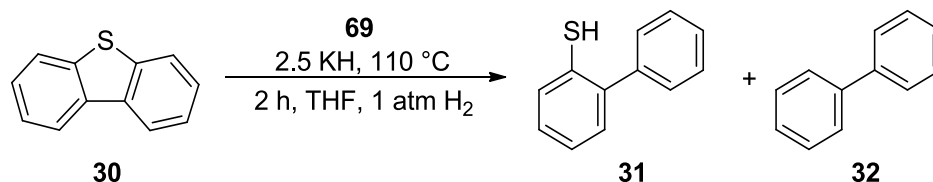
Table 5.3 Changes in turnover frequency for hydride-mediated HDS reactions as a function of precatalyst concentration.



Entry	Mole % 40	Mass of 40 (g, mmol)	TOF ^b (h ⁻¹)	31 (%)	32 (%)
1	0.1	0.0007, 0.0007	289	68	23
2	0.2	0.0014, 0.0014	169	34	50
3	0.3	0.0021, 0.0022	124	24	62
4	0.4	0.0028, 0.0029	95	30	60
5	0.5	0.0035, 0.0036	66	38	47

^aTOF is calculated as moles of C–S bond cleavage per mole of precatalyst cluster per hour.

Table 5.4 Turnover frequency of hydride-mediated HDS as a function of the concentration of precatalyst cluster **69**.



Entry	Mole % 69	Mass of 69 (g, mmol)	TOF ^b (h ⁻¹)	31 (%)	32 (%)
1	0.1	0.0009, 0.0007	590	37	38
2	0.2	0.0019, 0.0015	426	25	73
3	0.3	0.0028, 0.0022	205	58	32
4	0.4	0.0038, 0.0029	162	48	41
5	0.5	0.0047, 0.0036	135	52	41

^aTOF is calculated as moles of C–S bond cleavage per mole of precatalyst cluster per hour.

5.4.3 Solution molecular weight determinations for cobalt clusters **40** and **69** by the Signer method

The Signer method allows the molecular weight of an unknown solute to be calculated from comparison to the molecular weight of a standard.¹⁸⁰ Inside the dry box, two separate solutions of the same solvent, one containing the standard and one containing the unknown (see Tables 5.5 and 5.7), were placed in separate bulbs of the apparatus shown in Figure 5.2. The glass apparatus was sealed and brought outside the dry box. Then, the glass vessel was cooled using liquid nitrogen and evacuated for 10 min. In the closed system and at constant temperature, the two solutions were allowed to slowly come to vapor equilibrium. The volumes of the unknown and standard solutions were collected until constant volume was observed. The volumes were then used to calculate the molecular weight of the unknown using the following equation:

$$M_1 = \frac{W_1}{W} \times \frac{V}{V_1} \times M \quad (\text{a})$$

where M_1 and M are the molecular weights of the unknown and standard, respectively, W_1 and W are the masses in grams of the unknown and the standard, and V_1 and V are the final volumes in mL.¹⁸¹⁻¹⁸²

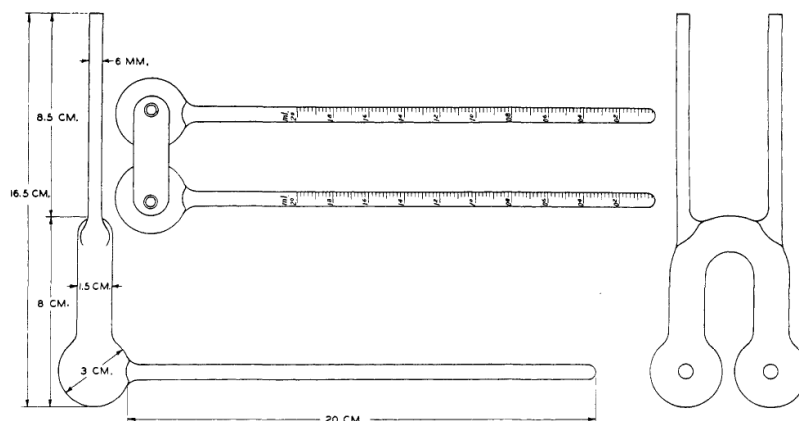


Figure 5.2 The apparatus for the Signer method.¹⁸¹

Table 5.5 Amounts of standard and cationic cluster **40** and volumes of solvent for determination of solution molecular weight.

	Ferrocene (standard)	40
Quantity (mg, mmol)	20, 0.11	20, 0.021
Initial volume (mL)	2.00	2.00
Final volume (mL)	2.87	1.15
MW (g/mol)	186	unknown

Table 5.6 Calculated and experimental molecular weights for **40** in solution.

	Molecular weight (g/mol)
Heterocubane (calculated)	969.5
Dimer (calculated)	484.7
Calculated from Signer data	464

Table 5.7 Amounts of standard and cationic cluster **69** and volumes of solvent for determination of solution molecular weight

	Ferrocene (standard)	69
Quantity (mg, mmol)	20, 0.11	20, 0.016
Initial volume (mL)	2.00	2.00
Final volume (mL)	2.50	0.75
MW (g/mol)	186	unknown

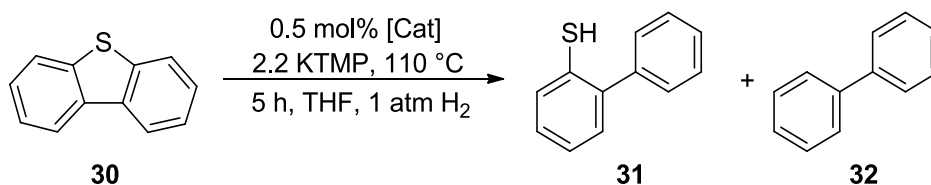
Table 5.8 Calculated and experimental molecular weights for **69** in solution.

	Molecular weight (g/mol)
Heterocubane (calculated)	1293.0
Dimer (calculated)	646.5
Calculated from Signer data	620

5.4.4 Homogeneity test for cobalt clusters **40**, **53a**, and **69**

The general procedure outlined in section 5.4.1 was followed, using cobalt cluster **40**, **53a**, or **69** (0.0036 mmol), DBT (0.13 g, 0.73 mmol), and THF (10 mL). Potassium hydride was substituted by potassium tetramethylpiperidide (KTMP) (0.26 g, 1.5 mmol). For selected experiments, elemental Hg (0.90 mg, 3.6 mmol, 950 eqivs of Hg per cluster) was added to the mixture. Results are given in Table 5.9.

Table 5.9 Homogeneity tests for clusters **40**, **53a**, and **69**.

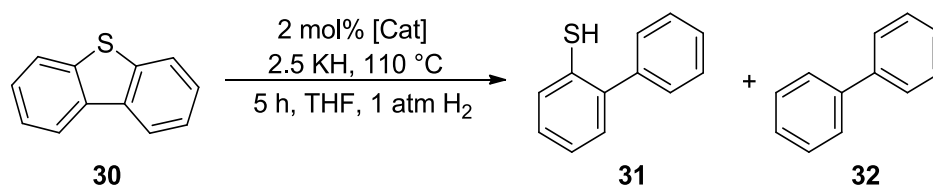


Entry	[Cat]	Eq. of Hg(0) per Co atom	Yield	
			31 (%)	32 (%)
1	40	0	13	16
2	40	300	6	8
3	53a	0	6	13
4	53a	300	3	10
5	69	0	14	15
6	69	300	10	5
7	-	0	0	2
8	-	300	0	3

5.4.5 HDS reactions with other transition metal halides, hydrogen, and KH

The general procedure outlined in section 5.4.1 was followed, using the indicated transition metal halide (2 mol% per metal, 0.0036 mmol), DBT (0.13 g, 0.73 mmol), KH (0.072 g, 1.8 mmol), and THF (10 mL). Results are provided in Table 5.10.

Table 5.10 HDS reactions with other transition metal halides as the precatalyst.

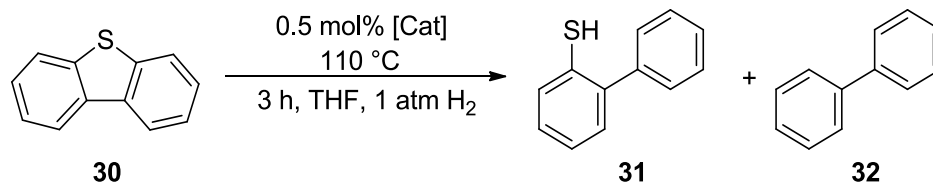


Entry	[Cat]	Conv. (%)	31 (%)	32 (%)	DBT recovered (%)	Unrecovered (%)
1	CoCl ₂	99	41	44	1	14
2	CoBr ₂	97	56	30	3	11
3	FeCl ₂	98	58	34	2	6
4	NiCl ₂	96	76	14	4	6
5	NiBr ₂	100	63	19	0	18
6	CuCl ₂	98	73	16	2	9
7	CuBr ₂	78	75	1	22	2

5.5 Experimental Procedures for Chapter 4

5.5.1 HDS reactions catalyzed by cobalt clusters 40, 53a, and 69

The general procedure detailed in section 5.4.1 was followed, using cobalt clusters 40, 53a, or 69 (0.0036 mmol), DBT (0.13 g, 0.73 mmol), and THF (10 mL); Table 5.11.

Table 5.11 HDS reactions in the absence of KH.

Entry	[Cat]	Conv. (%)	31 (%)	32 (%)	DBT recovered (%)	Unrecovered (%)
1	40	4.9	0.0	0.6	95.1	4.2
2	53a	30.7	0.0	0.7	69.0	30.0
3	69	4.5	0.0	0.7	95.5	3.8

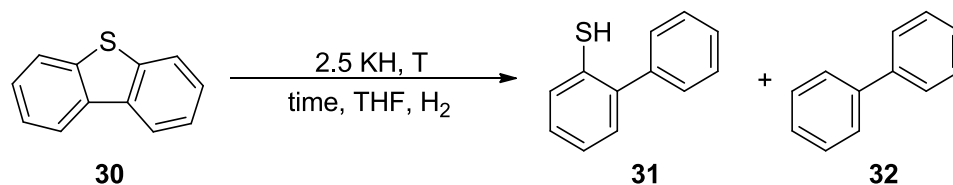
5.5.2 Dibenzothiophene HDS promoted by KH in the presence and absence of H₂

The general procedure detailed in section 5.4.1 was followed, using KH (0.072 g, 1.8 mmol) and DBT (0.13 g, 0.73 mmol) along with 10 mL THF. In each case, the suspension was heated (Table 5.12). For HDS reactions in the absence of H₂, after the glass vessel was charged with KH, DBT, and THF, the vessel was sealed with a Teflon cap, brought out of the glove box, and heated to the indicated temperature (Table 5.12).

For HDS reactions at high H₂ pressure (> 1 atm), a modified procedure was implemented. Inside the glove box, the reactor of a steel autoclave, equipped with a glass liner and Teflon-coated stir bar, was charged with DBT (0.13 g, 0.73 mmol), potassium hydride (0.072 g, 1.8 mmol), and THF (10 mL). The autoclave was sealed, brought out of the dry box, and pressurized with H₂. The reactor was then heated to the indicated temperature (Table 5.12). After the reaction time, the autoclave was cooled to room temperature and vented. Then, the glass liner was removed

from the autoclave, and the contents were quenched with 10% HCl until the solution became acidic. The products were extracted and characterized using the procedure outlined in section 5.4.1.

Table 5.12 Transition metal-free, potassium hydride mediated desulfurization of DBT.



Entry	T (°C)	Time (h)	H ₂ (atm)	Conv. (%)	31 (%)	32 (%)	DBT recovered (%)	Unrecovered (%)
1	110	5	1	74	58	0	27	15
2	110	16	1	93	89	2	7	2
3	130	5	1	91	82	4	9	5
4	110	16	34	93	81	1	7	11
5	110	5	0	72	63	1	28	8
6	110	16	0	99	78	10	1	11
7	130	5	0	100	79	11	0	10

5.5.3 H₂ production and detection during “hydrogen-free” HDS

Inside the glove box, KH and DBT were added to a medium-walled glass NMR tube along with 1.5 mL d⁸-THF, resulting in a grey suspension. The NMR tube was permanently sealed by melting the end of the glass tube in an open flame. A ¹H NMR spectrum was taken of the sample immediately after the NMR tube was sealed (Figure 5.3). The sample was heated for 1 h in a

paraffin oil bath at 80 °C. The ^1H NMR spectrum was taken immediately after heating (Figure 5.4), showing only peak broadening. Then, the sample was heated at 110 °C for 2 h and another ^1H NMR spectrum (Figure 5.5) was recorded immediately after removal from the oil bath.

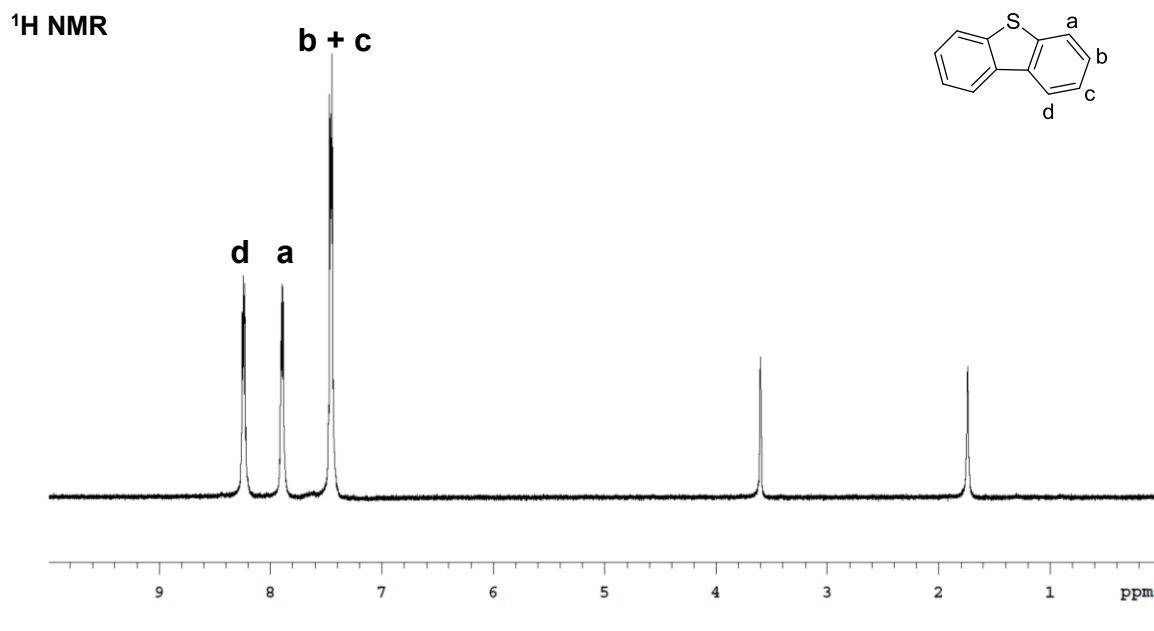


Figure 5.3 ^1H NMR spectrum of KH/DBT suspension prior to heating (room temperature).

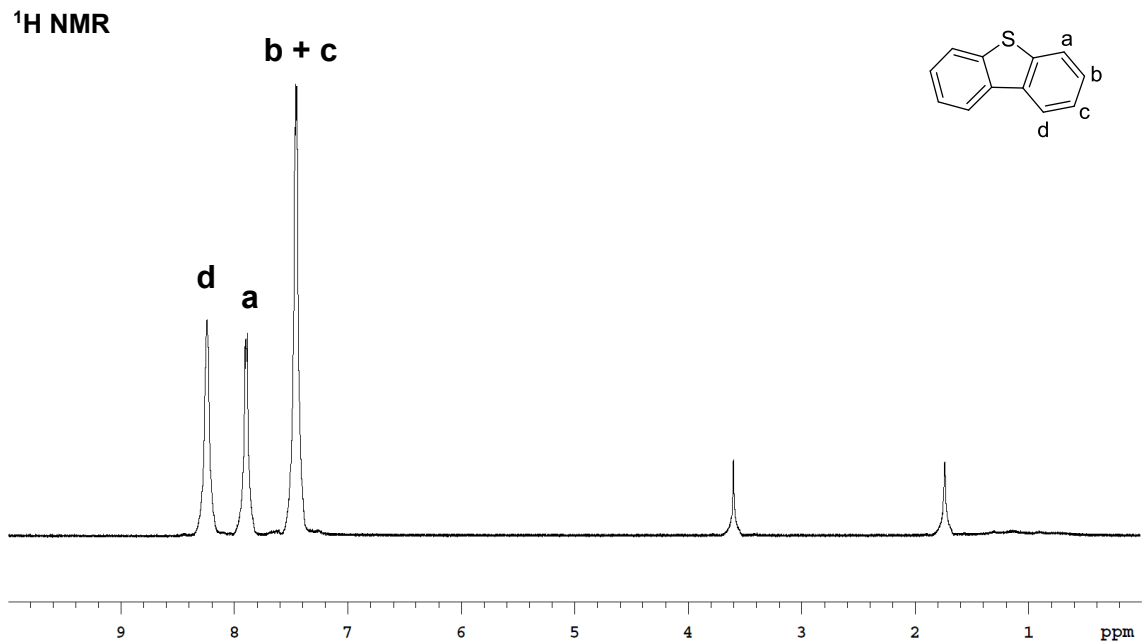


Figure 5.4 ¹H NMR spectrum of KH and DBT suspension after heating for 2 h at 80 °C.

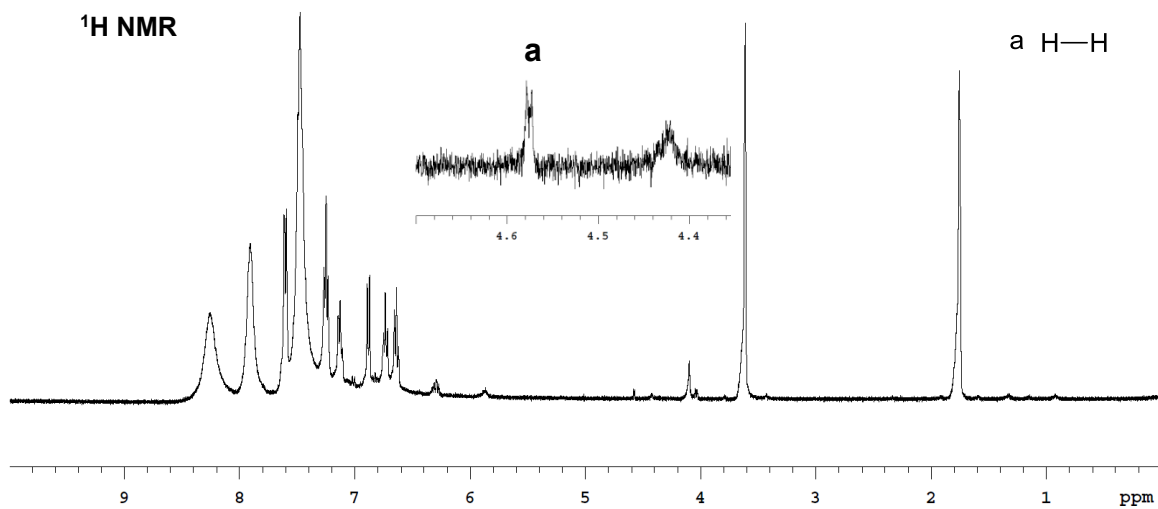


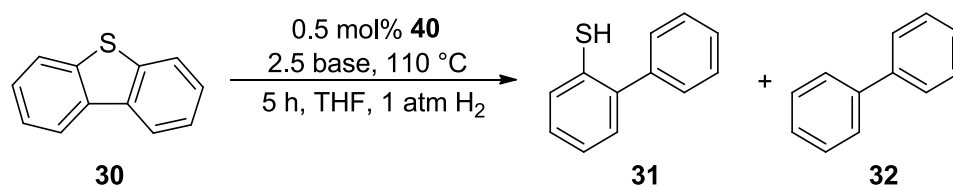
Figure 5.5 ¹H NMR spectrum of KH and DBT suspension after heating for 2 h at 110 °C.

5.5.4 Base-mediated HDS catalyzed by cationic cluster **40**: variation of the base

The general procedure outlined in section 5.4.1 was followed, using cationic cluster **40** (0.0035 g, 0.0036 mmol), DBT (0.13 g, 0.73 mmol), THF (10 mL), and a strong base (2.5 equivalents).

Results are provided in Table **5.13**.

Table 5.13 Catalytic HDS reactions under hydrogen, as a function of the base.

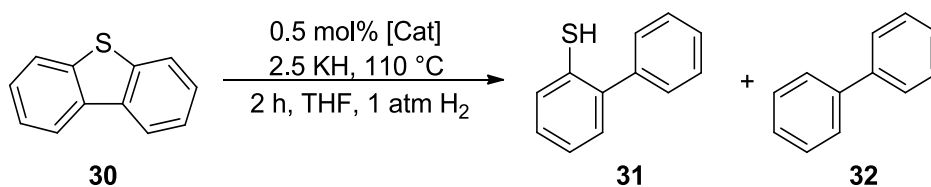


Entry	Base	Mass of base (g, mmol)	31 (%)	32 (%)
1	NaH	0.043, 1.8	0	2
2	KH	0.072, 1.8	27	58
3	LDA	0.19, 1.8	1	3
4	KDA	0.25, 1.8	37	11
5	LiTMP	0.27, 1.8	1	4
6	KTMP	0.32, 1.5	13	16
7	NaO'Bu	0.17, 1.5	0	0
8	KO'Bu	0.20, 1.8	0	0.6

5.5.5 Potassium-ion effect: HDS reactions in the presence of 18-crown-6

The general procedure detailed in section 5.4.1 was followed, using cluster **40** or **69** (0.0036 mmol), KH (0.072 g, 1.8 mmol), DBT (0.13 g, 0.73 mmol), 18-crown-6 (0.48 g, 1.8 mmol), and 10 mL THF. Results are provided in Table 5.14.

Table 5.14 18-crown-6 inhibits catalytic hydrodesulfurization by potassium hydride

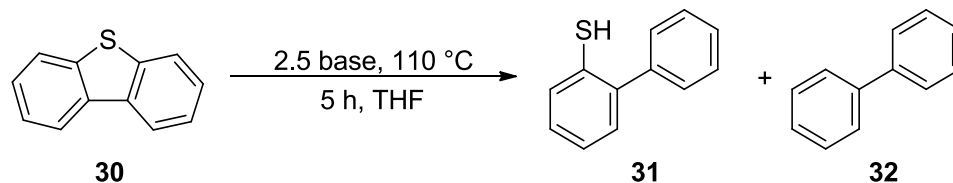


Entry	[Cat]	18-crown-6 (equiv.)	31 (%)	32 (%)
1	40	2.5	1	4
2	69	2.5	5	1

5.5.6 Potassium-ion effects. Catalyst-free HDS reactions using other potassium sources

The general procedure outlined in section 5.4.1 was followed, using DBT (0.13 g, 0.73 mmol) and 10 mL THF. For Entries 1 and 2 (Table 5.15), 2.5 equivalents of KH (0.072 g, 1.8 mmol) and NaH (0.043 g, 1.8 mmol) were used, respectively. In Entry 3, 2.5 equivalents of NaH (0.043 g, 1.8 mmol) and KO^tBu (0.20 g, 1.8 mmol) were added to the reactor.

Table 5.15 Comparison of HDS reactivity of sodium hydride and potassium hydride.



Entry	Base	KO ^t Bu (equiv.)	31 (%)	32 (%)
1	KH	0	63	1
2	NaH	0	0	1
3	NaH ^a	2.5	88	1

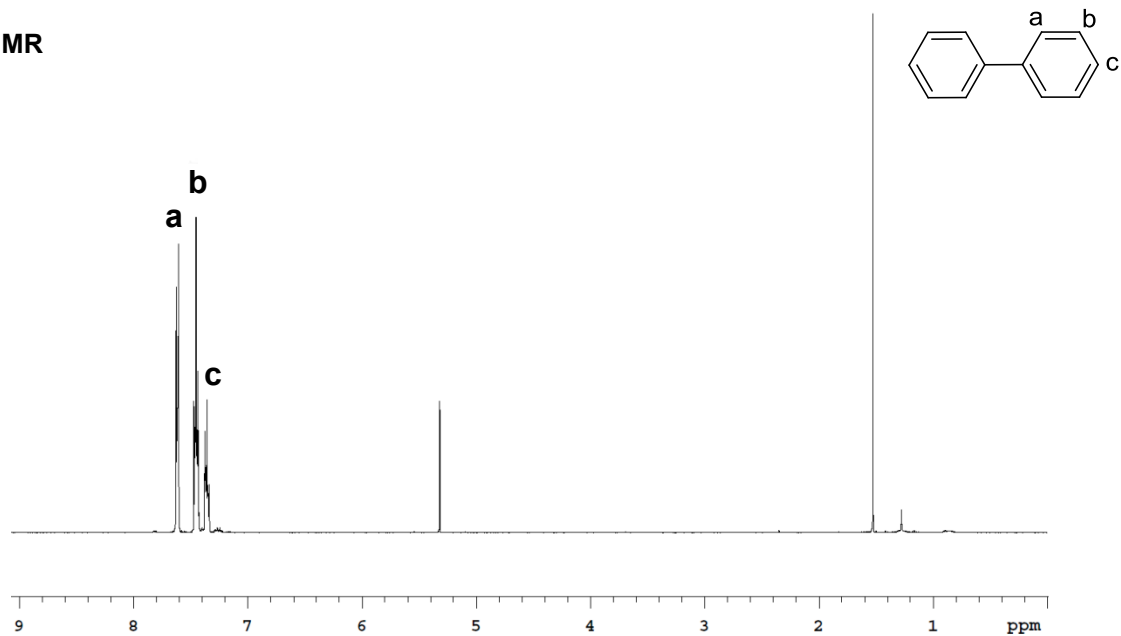
^aReaction time: 2 hours.

5.5.7 Isotopic labeling experiments: D₂ and KD.

5.5.7.1 Desulfurization under deuterium catalyzed by cobalt clusters **40**, **60**, and **69**

The general procedure outlined in section 5.4.1 was followed, using cobalt cluster **40**, **60**, or **69** (0.0036 mmol), KH (0.072 g, 1.8 mmol), DBT (0.13 g, 0.73 mmol), 10 mL THF, and 1 atm D₂ (at 99.7% purity). The reactions were heated at 110 °C for 5 h. Product extraction and work up were performed as detailed in section 5.4.1, but without the addition of n-dodecane. GC analysis revealed a mixture of biphenyl and 2-phenylthiophenol. Concentrated aqueous NaOH (5 mL) was added to the mixture, converting the 2-phenylthiophenol to the thiolate salt. The organic fraction was washed 3 times with 5 mL portions of the concentrated NaOH. Then, the organic layer was dried over MgSO₄ and filtered through a silica plug. GC analysis confirmed the presence of only biphenyl. After extraction, the solvent was removed, revealing a colorless, crystalline solid, biphenyl. About 10 mg of the biphenyl was dissolved in d²-CH₂Cl₂ for ¹H NMR spectroscopy and another 4 mg in CH₂Cl₂ (or diethyl ether) for ²H NMR spectroscopy.

^1H NMR



^2H NMR

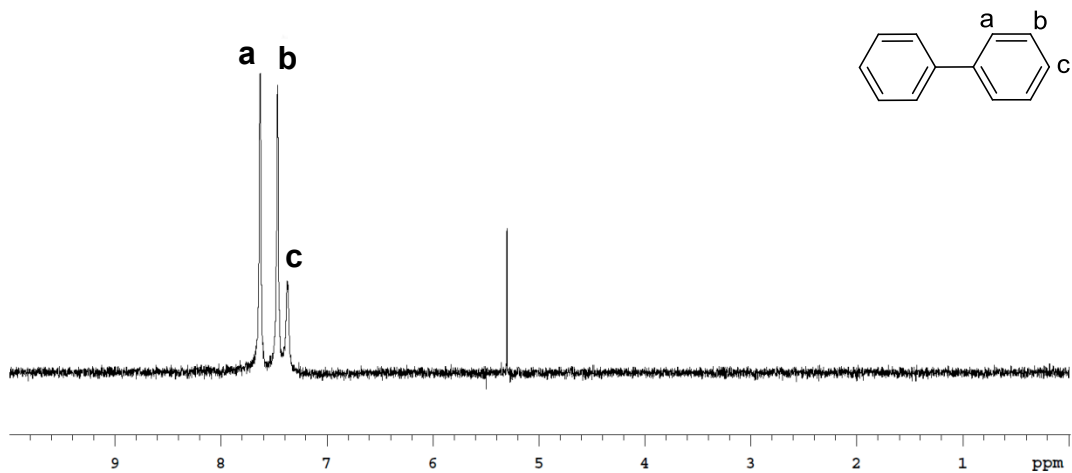


Figure 5.6 ^1H and ^2H NMR spectra of biphenyl from HDS reaction in the presence of KH, D_2 , and catalyst **53a**.

^2H NMR

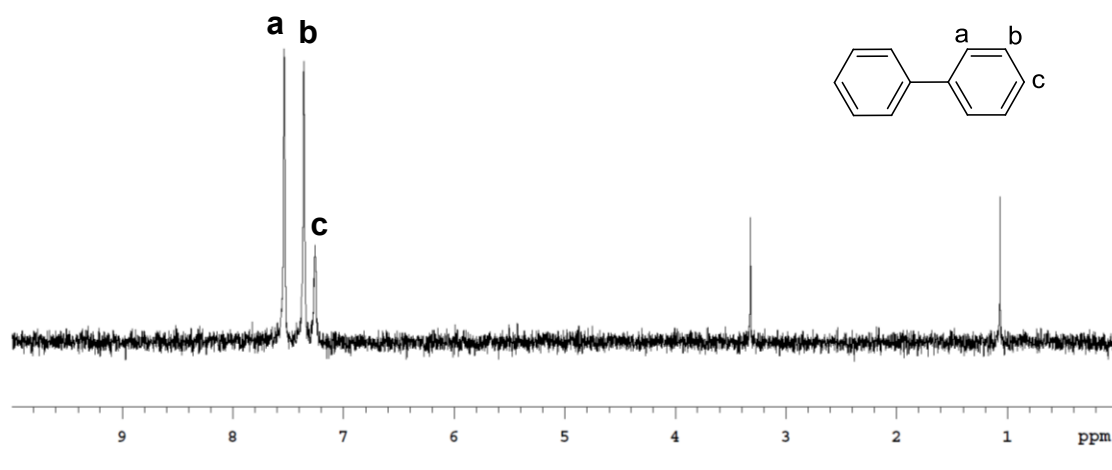


Figure 5.7 ^2H NMR spectrum of biphenyl from HDS reaction in the presence of KH, D_2 , and catalyst **69**.

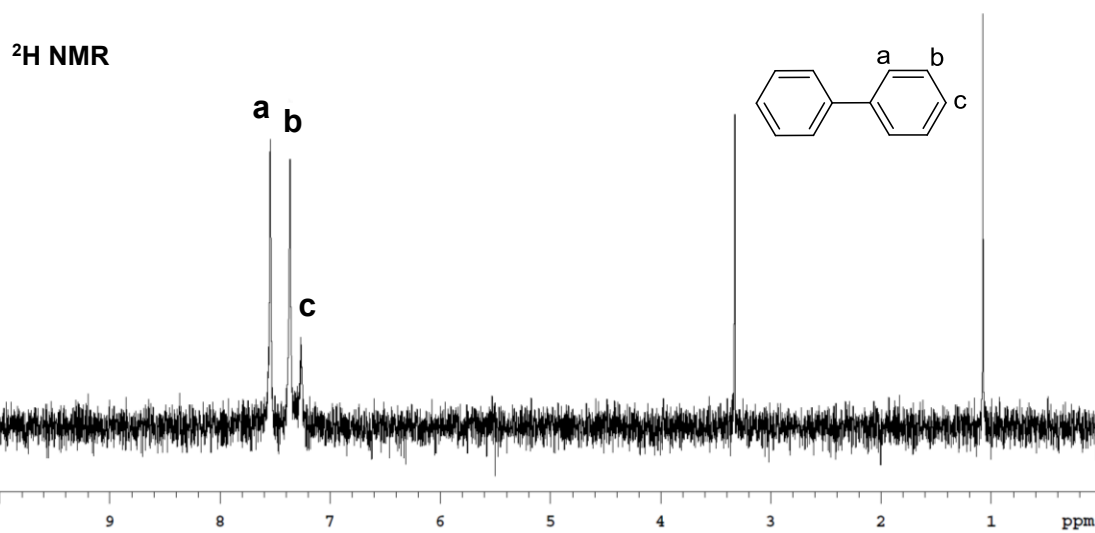
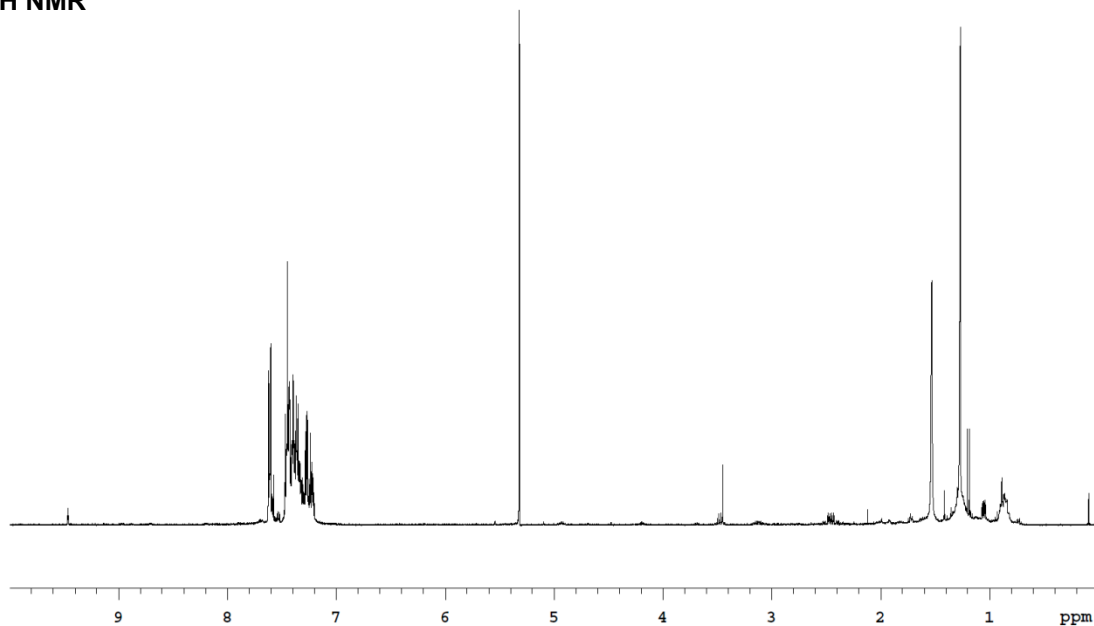


Figure 5.8 ^2H NMR spectrum of biphenyl from HDS reaction in the presence of KH, D_2 , and catalyst **40**.

5.5.7.2 Desulfurization under deuterium in the absence of transition metal source

The general procedure outlined in section 5.4.1 was followed, using KH (0.072 g, 1.8 mmol) and DBT (0.13 g, 0.72 mmol) along with 10 mL THF and 1 atm D₂ (at 99.7% purity). The suspension was heated for 29 hours at 110 °C. After the suspension was quenched with 10% HCl, the products were extracted as described. GC analysis revealed the presence of 2-phenylthiophenol and a trace amount of biphenyl. A total of 6 mL of concentrated NaOH was added to the mixture converting the 2-phenylthiophenol to the thiophenolate salt. The aqueous layer was separated from the organic layer. Then, 3 mL of diethyl ether and concentrated HCl (~5 mL) were added to the aqueous layer. The new organic layer was separated from the aqueous layer. Then, the new organic layer was dried with MgSO₄ and filtered through a Florisil plug. The solvent was removed under reduced pressure to yield yellow oil of 2-phenylthiophenol. A drop of the product was dissolved in d²-CH₂Cl₂ for ¹H NMR spectroscopy and another drop dissolved in CH₂Cl₂ for ²H NMR spectroscopy.

¹H NMR



²H NMR

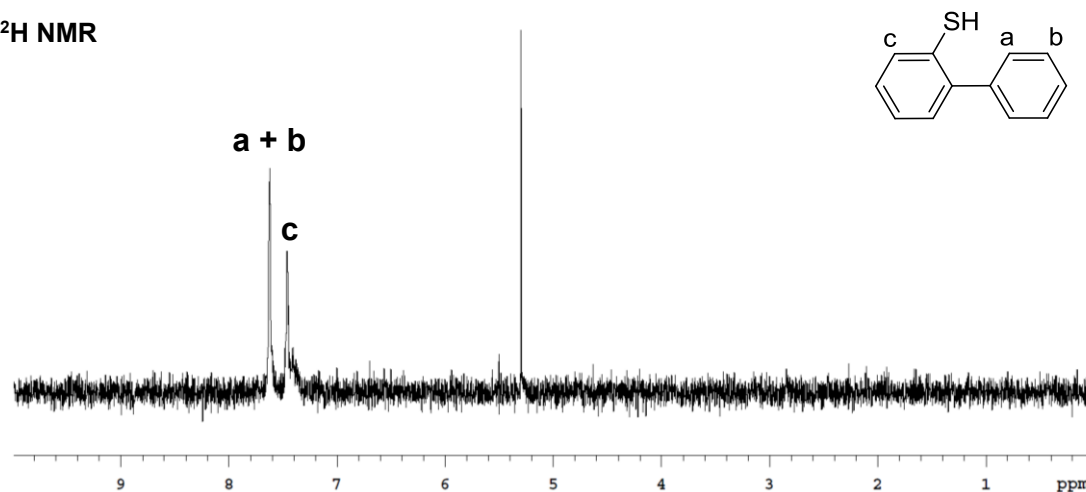
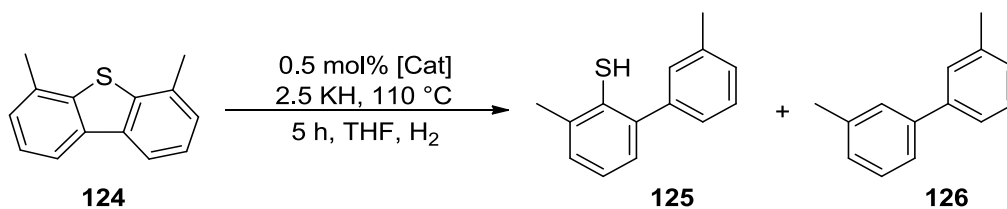


Figure 5.9 ¹H and ²H NMR spectra of 2-phenylthiophenol.

*5.5.8 HDS reactions of 4,6-dimethyl DBT promoted by KH in the presence and absence of homoleptic cluster **69***

The general procedure outlined in section 5.4.1 was followed, using cluster **69**, 4,6-dimethyl DBT, and KH, as specified in Table **5.16**.

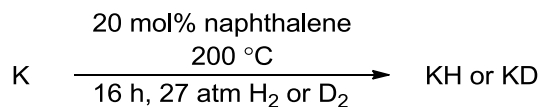
Table 5.16 KH-mediated desulfurization of 4,6-dimethyl DBT.

Entry	[69] (g, mmol)	2.5 KH (g, mmol)	124 (g, mmol)	Vol. (mL)	H ₂ (atm)	Conv. (%)	125 (%)	126 (%)
1	0.0013, 0.0010	0.020, 0.50	0.043, 0.20	7.0	1	100	31	69
2	0.0031, 0.0024	0.049, 1.2	0.10, 0.49	6.8	0	98	29	67
3	-	0.017, 0.42	0.036, 0.17	5.0	0	3	trace	0

5.5.9 Syntheses of KH and KD

Inside the glove box, clean potassium metal (3.2 g, 81 mmol), 20 mol% of naphthalene (2.1 g, 16 mmol), and a stir bar were added to the glass liner of the steel autoclave. The autoclave was sealed, brought out of the glove box, and pressurized with 27 atm D₂ (700 psi, full tank pressure). The reaction was heated at 200 °C for 16 hours, affording a mixture of black and tan solids. The solids were washed with toluene and THF (1 : 1), leaving only the tan powder. The powder was dried under high vacuum. The crude KD was purified by the general procedure outlined in section 5.1. The synthesis of KH proceeded identically, but using H₂ instead of D₂.

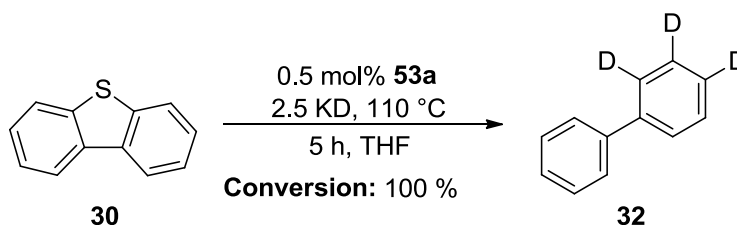
Table 5.17 Syntheses of KD and KH from potassium metal and naphthalene.



	K (g)	Naphthalene (g)	Yield (g, mmol)	Yield (%)
KD	3.2	2.1	2.7, 67	82
KH	2.1	1.4	1.6, 39	72

5.5.10 HDS reactions mediated by KD

5.5.10.1 KD-mediated HDS of DBT catalyzed by cobalt cluster **53a**



Inside the glove box, cobalt cluster **53a** (0.0032 g, 0.0036 mmol), DBT (0.13 g, 0.73 mmol), potassium deuteride (0.075 g, 1.8 mmol), and THF (10 mL) were added to a resealable, medium-walled glass vessel equipped with Teflon-coated magnetic stir bar. The glass vessel was sealed with a Teflon cap. Outside the glove box, the vessel was heated to 110 °C. After 5 hours, the vessel was cooled to room temperature, and the suspension was quenched with 10 % HCl solution until the solution was acidic. The product(s) was extracted with diethyl ether and filtered through a Florisil plug. The crude mixture was dried with MgSO₄ and filtered through another Florisil plug. GC analysis of the isolated products revealed 100 % conversion of DBT to biphenyl. About 10 mg of the biphenyl and n-dodecane (11 mg) were dissolved in d²-CH₂Cl₂ for ¹H NMR spectroscopy and another 4 mg in diethyl ether for ²H NMR spectroscopy.

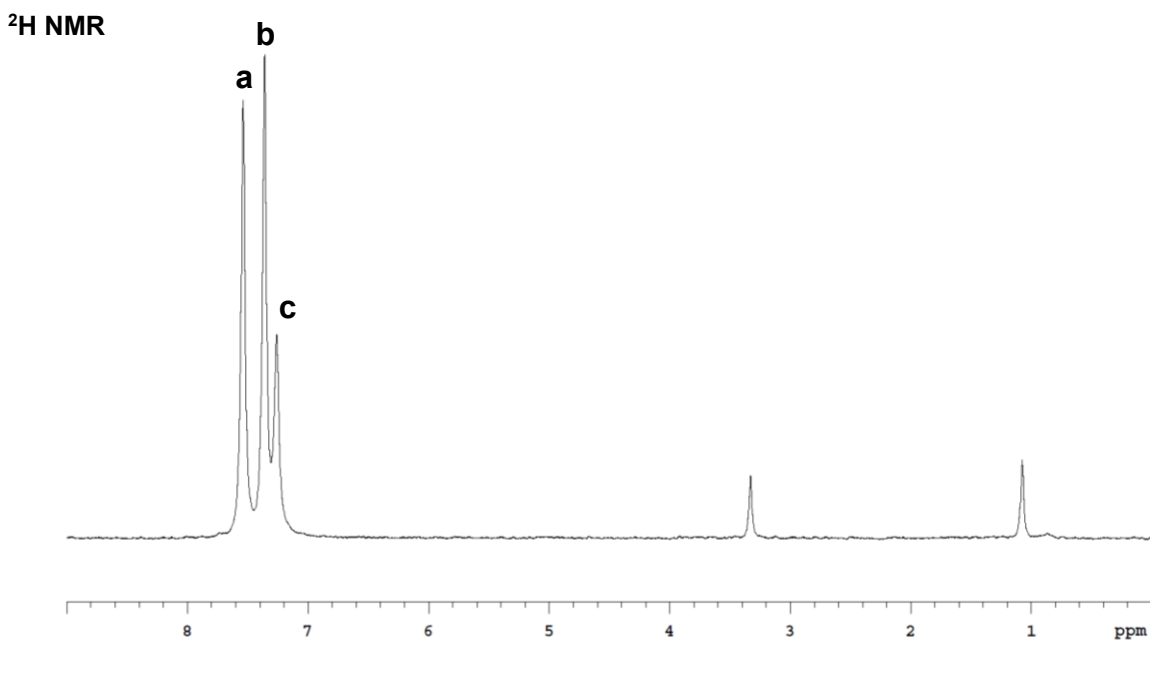
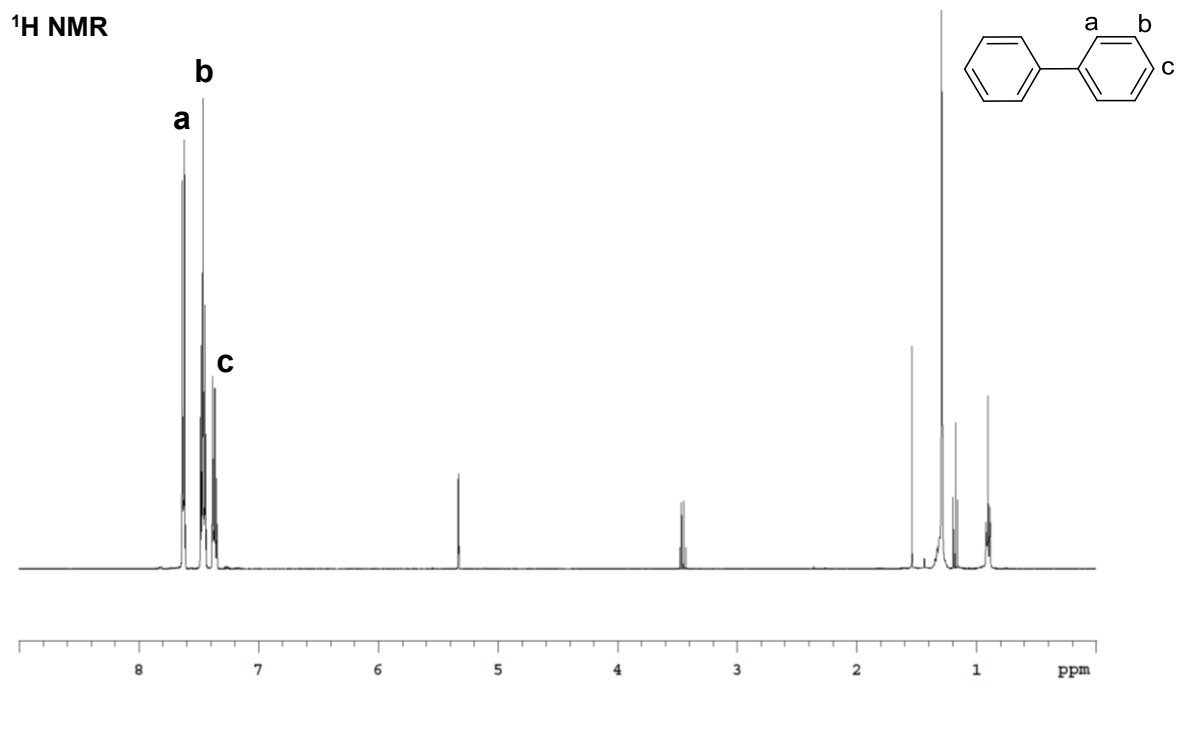
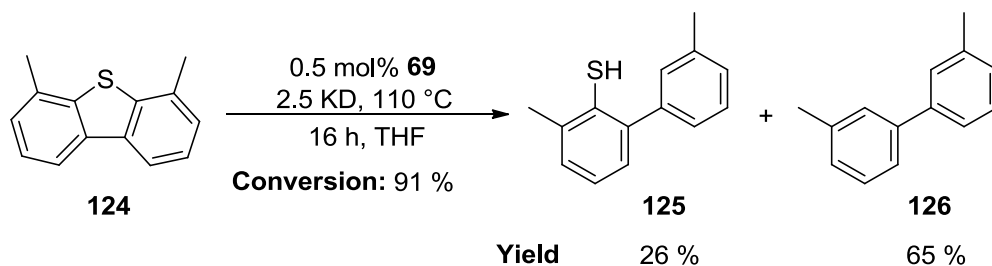


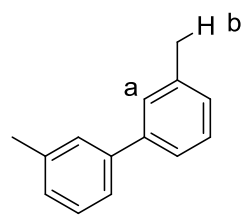
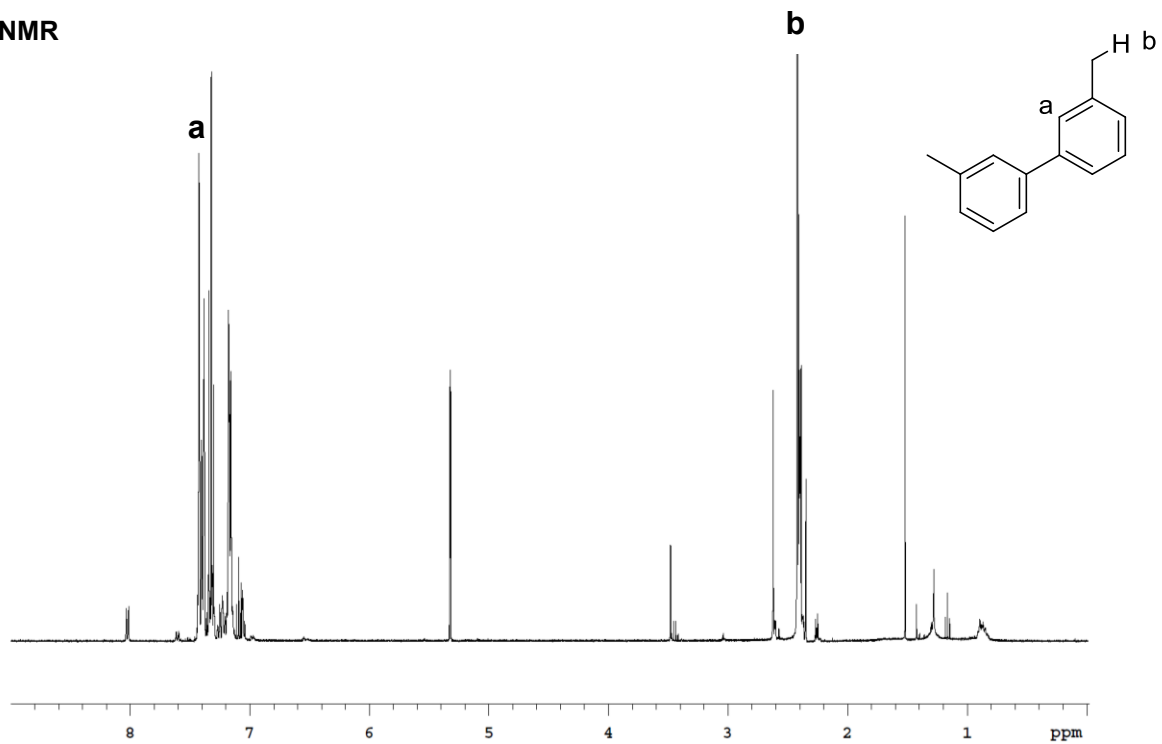
Figure 5.10 ¹H and ²H NMR spectra of biphenyl.

5.5.10.2 HDS reaction of 4,6-Me₂DBT catalyzed by cobalt cluster **69**



The procedure outlined in section 5.5.10.1 was followed, using cluster **69** (0.0016 g, 0.0012 mmol), KD (0.025 g, 0.61 mmol), commercial 4,6-Me₂DBT (0.052 g, 0.25 mmol), suspended in THF (4 mL). GC-MS analysis of the products after the work up revealed mixtures of the starting material and HDS products. A total of 3 mL of concentrated NaOH was added to the mixture to remove 3,3'-dimethyl-2-phenylthiophenol as the thiophenolate salt. The aqueous layer was separated from the organic layer. The organic layer was dried with MgSO₄ and filtered through a Florisil plug. The solvent was removed under reduced pressure to yield colorless oil. A drop of the product was dissolved in d²-CH₂Cl₂ for ¹H NMR spectroscopy and another drop dissolved in DCM for ²H NMR spectroscopy.

¹H NMR



²H NMR

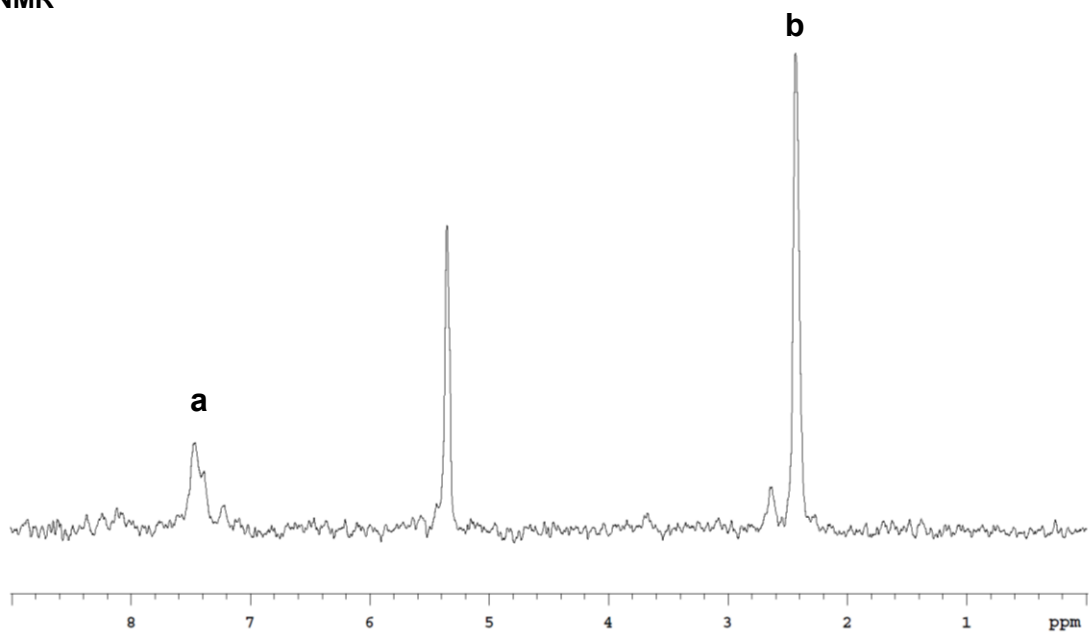
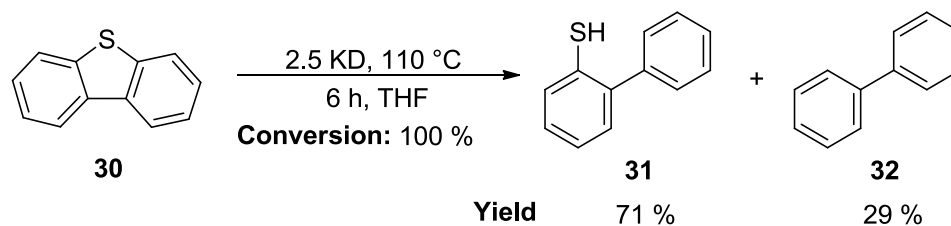


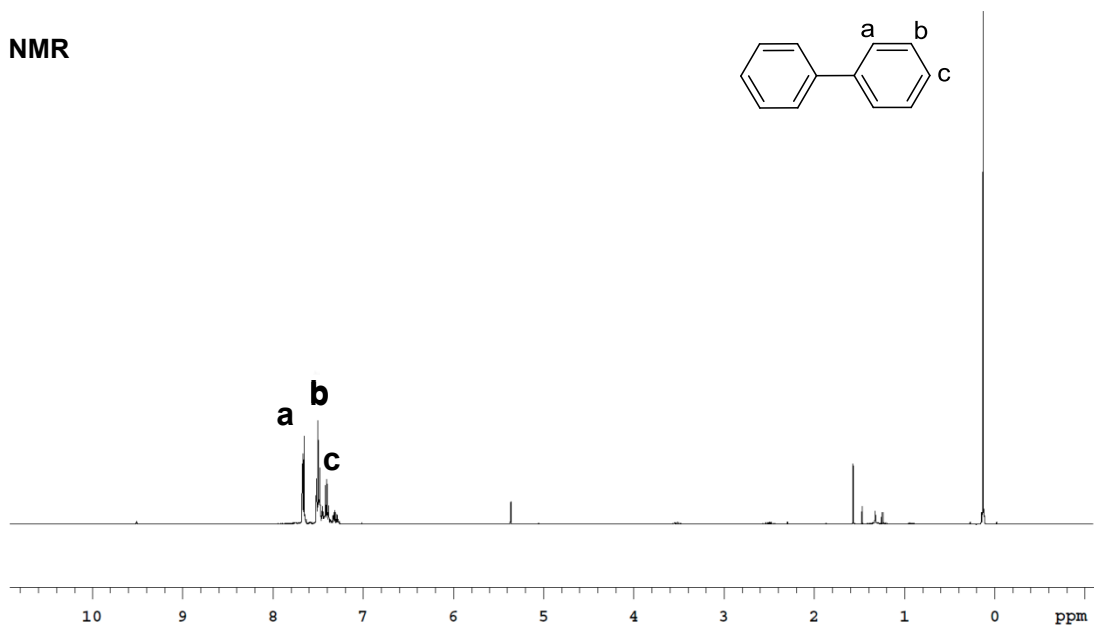
Figure 5.11 ¹H and ²H NMR spectra of 3,3'-dimethyl biphenyl.

5.5.10.3 HDS reaction of DBT with KD in the absence of catalyst and hydrogen



The procedure outlined in 5.5.10.1 was followed, using DBT (0.13 g, 0.73 mmol), KD (0.074 g, 1.8 mmol), and 10 mL THF. GC analysis of the products revealed a mixture of biphenyl and 2-phenylthiophenol. A total of 8 mL of concentrated NaOH solution was added to the mixture to remove 2-phenylthiophenol as the thiophenolate salt. The organic layer was separated from the aqueous layer, then, dried with MgSO₄. The organic layer was filtered through a silica gel plug and washed with 3 times with 1 mL portions of toluene. GC analysis of the solution gave exclusive biphenyl. The solvent was removed under reduced pressure to yield white, crystalline solid. About 4 mg of the product was dissolved in diethyl ether for ²H NMR spectroscopy. Deuterium incorporation was confirmed. Another portion of biphenyl (4.8 mg) and n-dodecane (5.5 mg) was dissolved in d²-CH₂Cl₂ for ¹H NMR spectroscopy. The ratio of the integral of the product and n-dodecane was used to determine the percentage of deuterium incorporation.

^1H NMR



^2H NMR

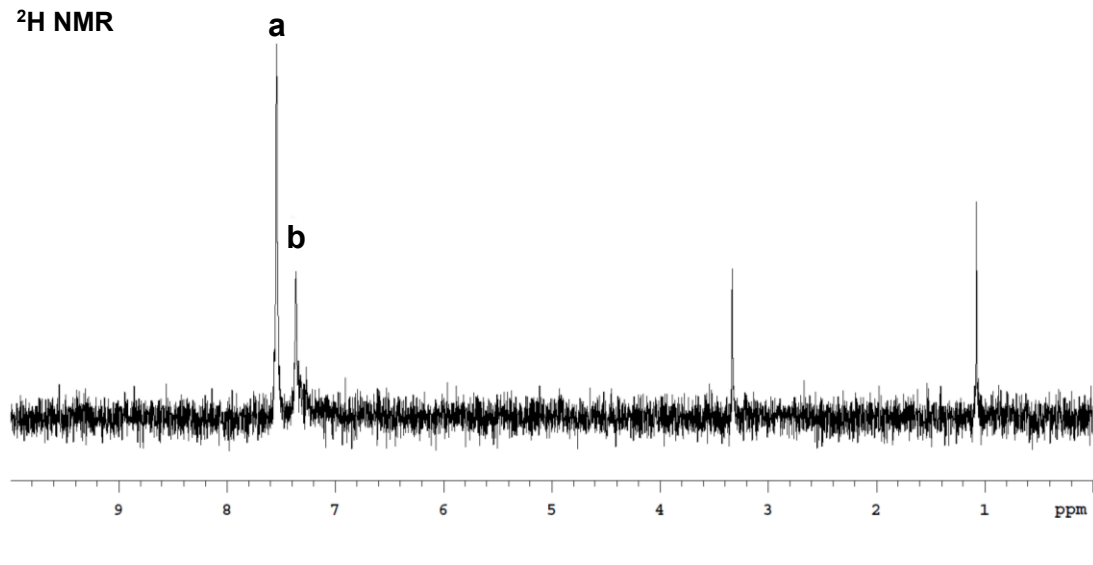
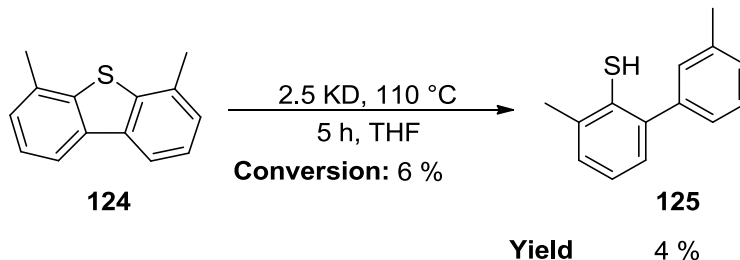


Figure 5.12 ^1H and ^2H NMR spectra of biphenyl.

5.5.10.4 KD-promoted HDS of 4,6-Me₂DBT in the absence of catalyst

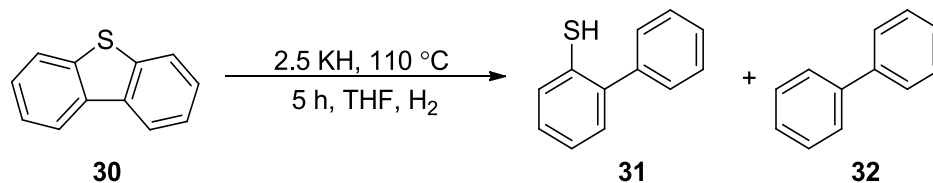


The procedure outlined in 5.5.10.1 was followed, using KD (0.018 g, 0.43 mmol) and 4,6-Me₂DBT (0.036 g, 0.17 mmol) in THF (3.5 mL). GC-MS analysis of the products after work-up revealed a mixture of starting material and low conversion to 3,3'-dimethyl-2-phenylthiophenol. No ¹H or ²H NMR spectrum was obtained.

5.5.11 Comparison of hexane-washed KH, purified KH, and synthetic KH

The general procedures outlined in section 5.5.2 were followed, using KH (0.072 g, 1.8 mmol), DBT (0.13 g, 0.73 mmol), and 10 mL THF. Hexane-washed KH was purchased from Sigma Aldrich and washed with excess anhydrous hexane to remove the paraffin oil. Synthetic KH was made as described in section 5.5.8. The results of KH-mediated HDS of DBT are provided in Table 5.18.

Table 5.18 Desulfurization of DBT with synthesized and commercial KH.



Entry	KH	H ₂ (atm)	Conv. (%)	31 (%)	32 (%)	DBT recovered (%)	Unrecovered (%)
1	Synthesized	0	100	77	20	0	3
2	Hex-washed	0	36	26	1	64	9
3	Synthesized	1	98	87	3	1	9
4	Hex-washed	1	33	24	1	67	8

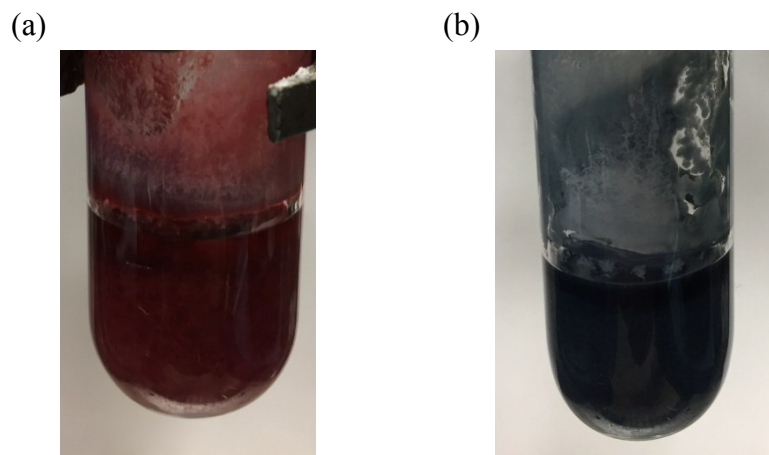


Figure 5.13 (a) The desulfurization of DBT using purified resulted in a red suspension. (b) When synthesized KH was used, the suspension has a blue color.

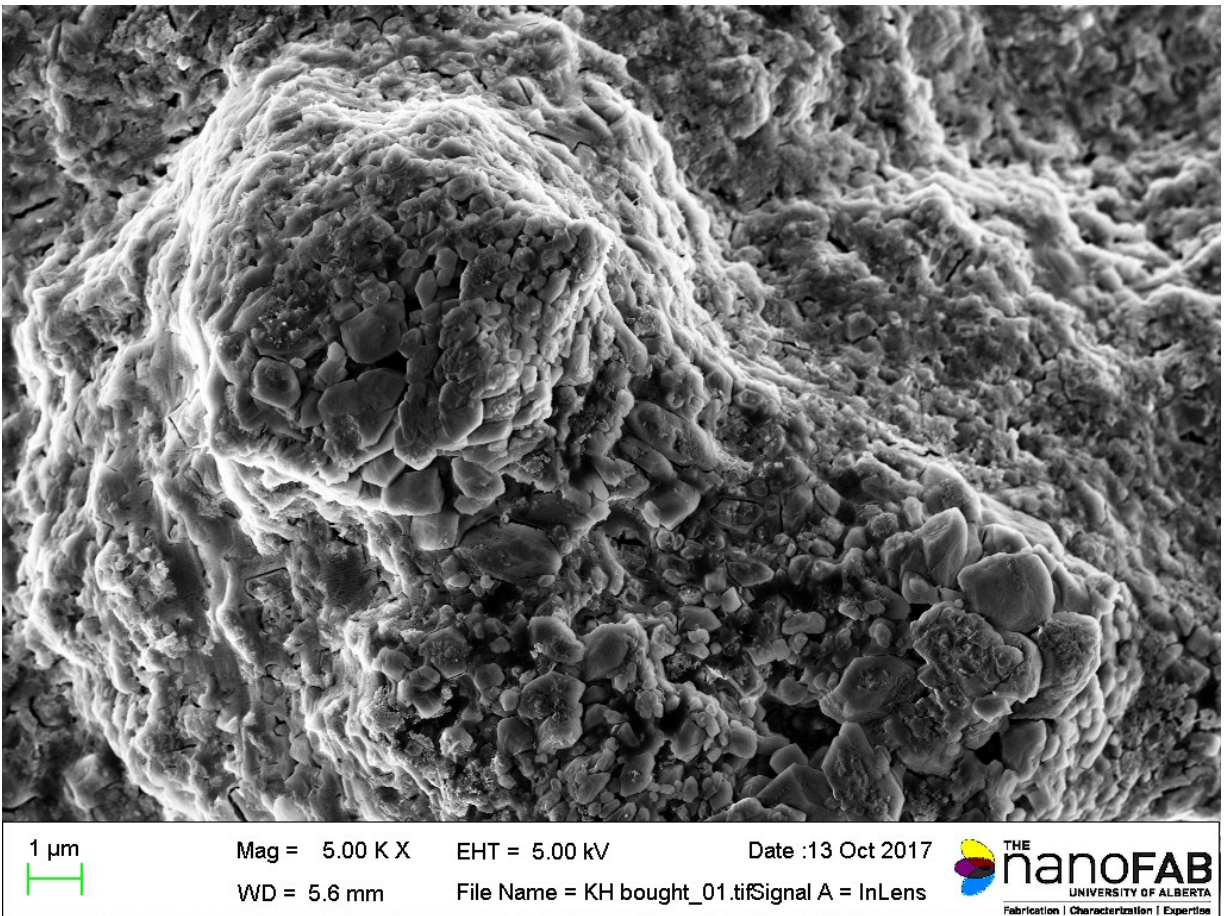


Figure 5.14 Secondary electrons SEM image of purified KH at magnification 5.00kx (scale: 1 μm).

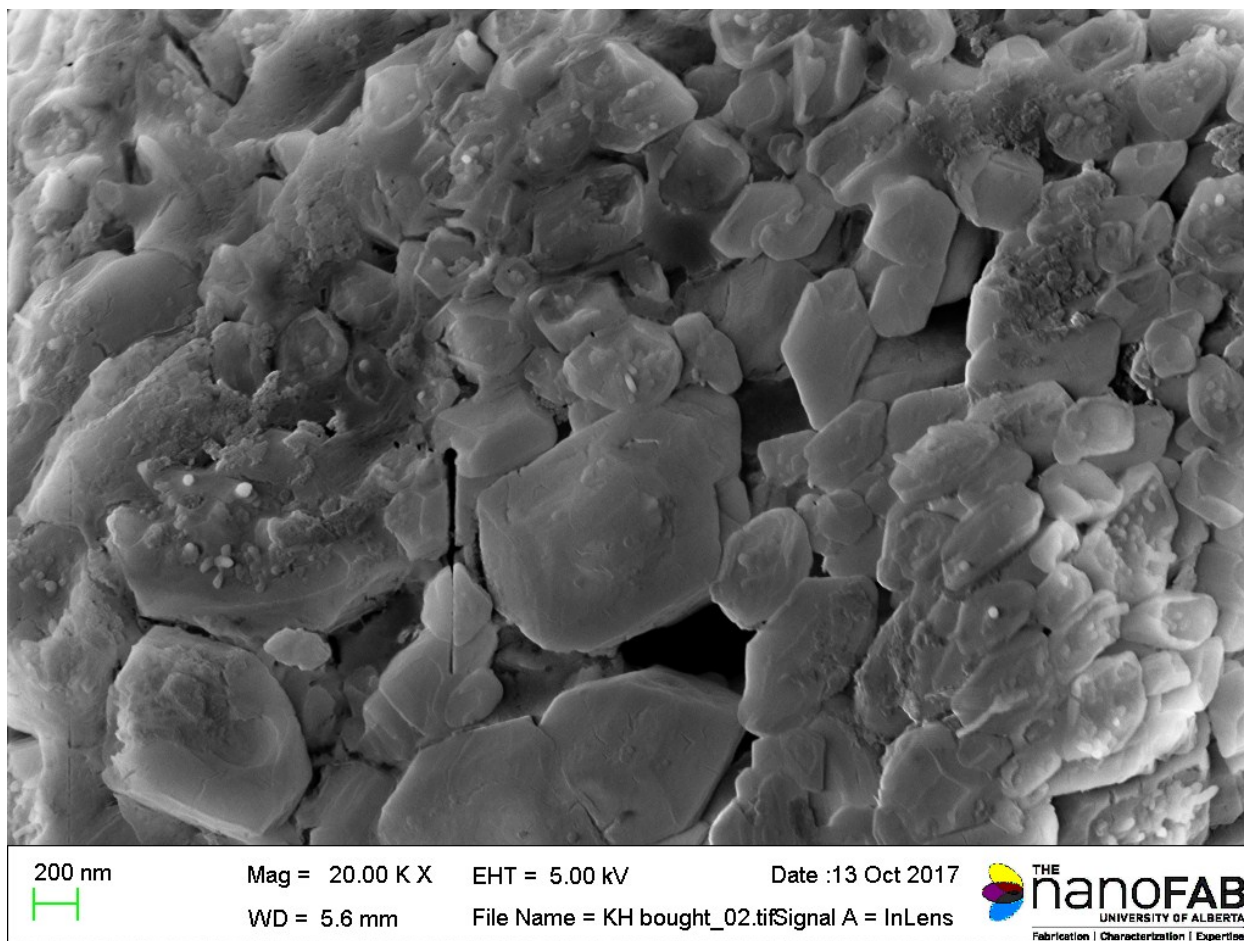


Figure 5.15 Secondary electrons SEM image of purified KH at magnification 20.00kx (scale: 200 nm).

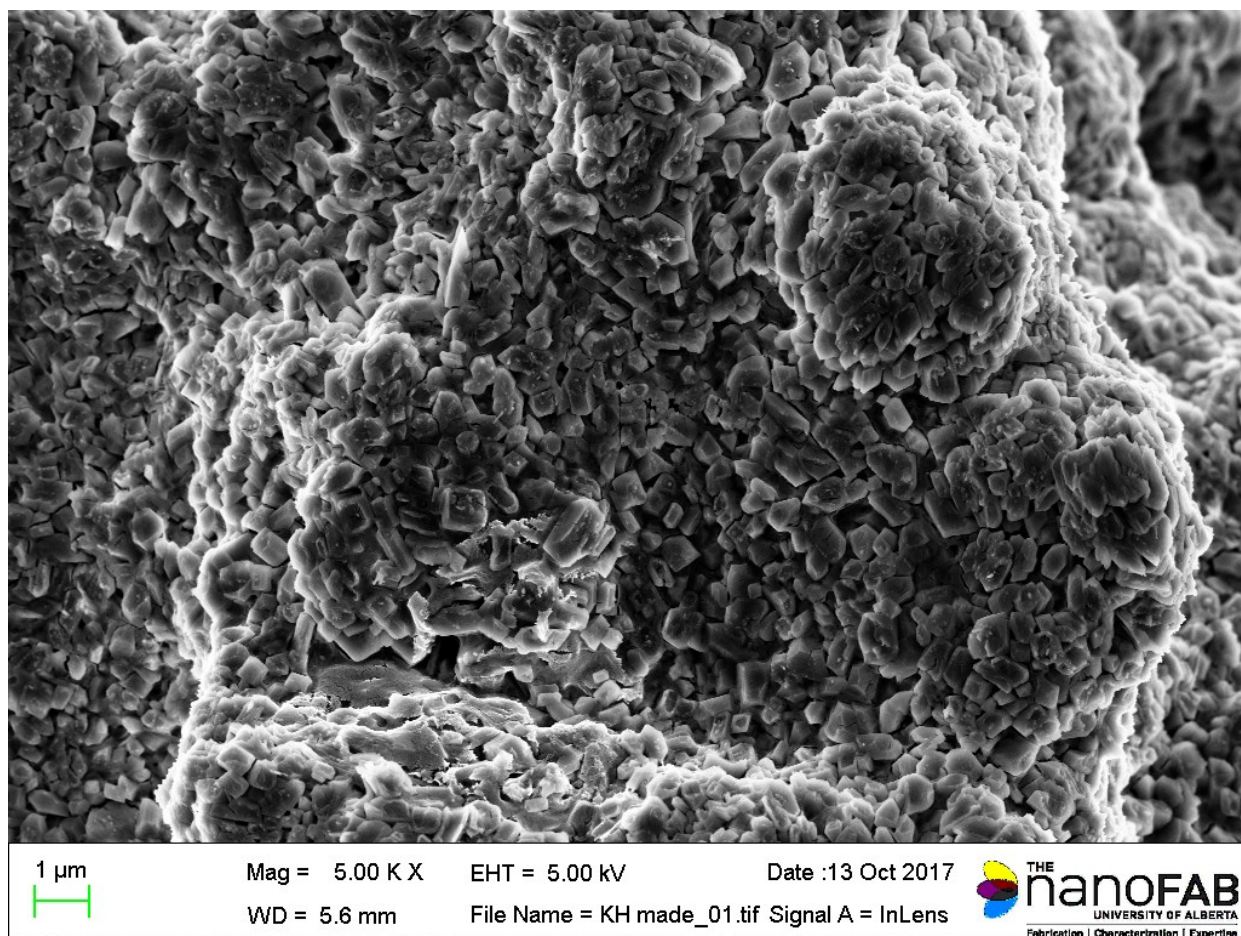


Figure 5.16 Secondary electrons SEM image of synthesized KH at magnification 5.00kx (scale: 1 μ m).

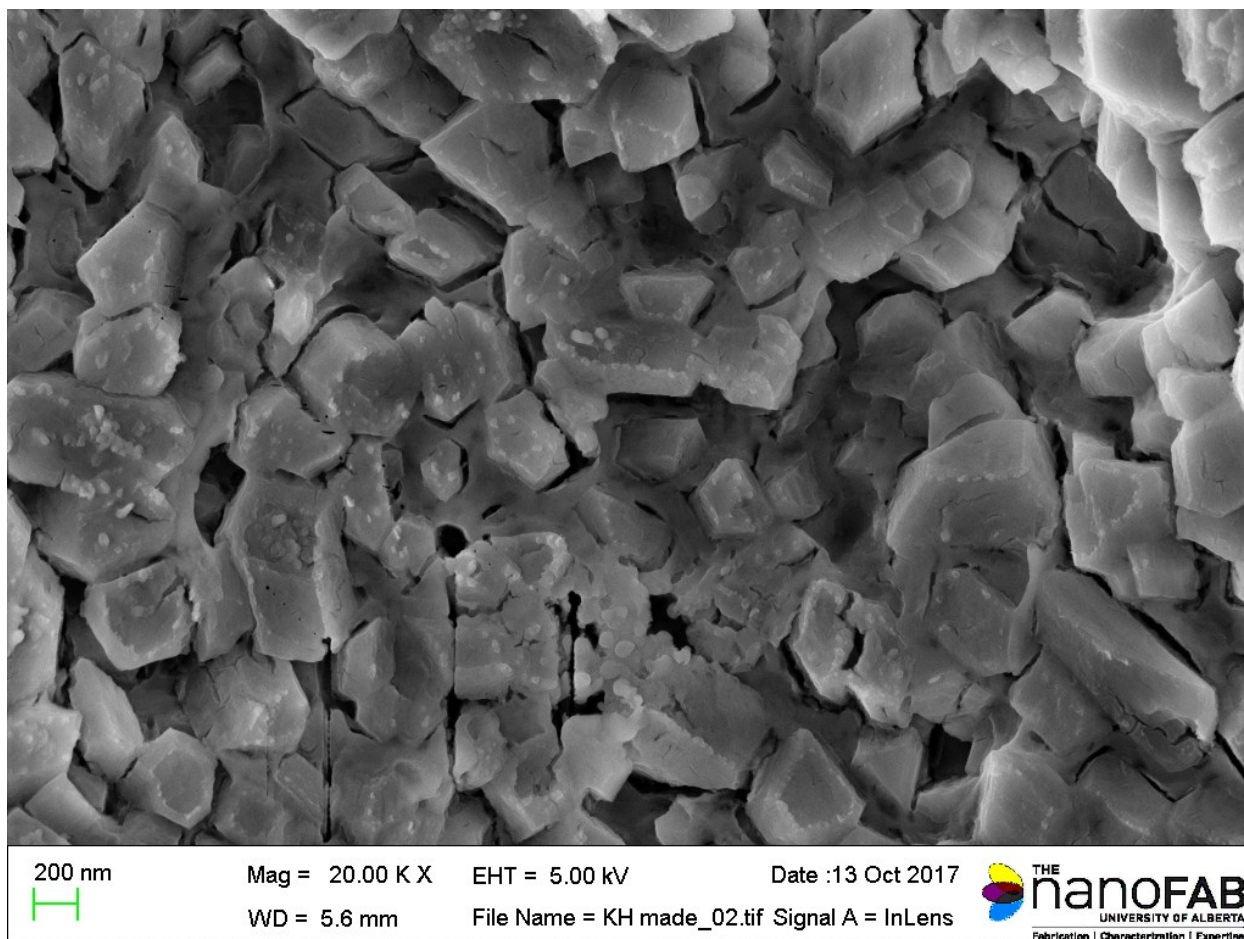


Figure 5.17 Secondary electrons SEM image of synthesized KH at magnification 20.00kx (scale: 200 nm).

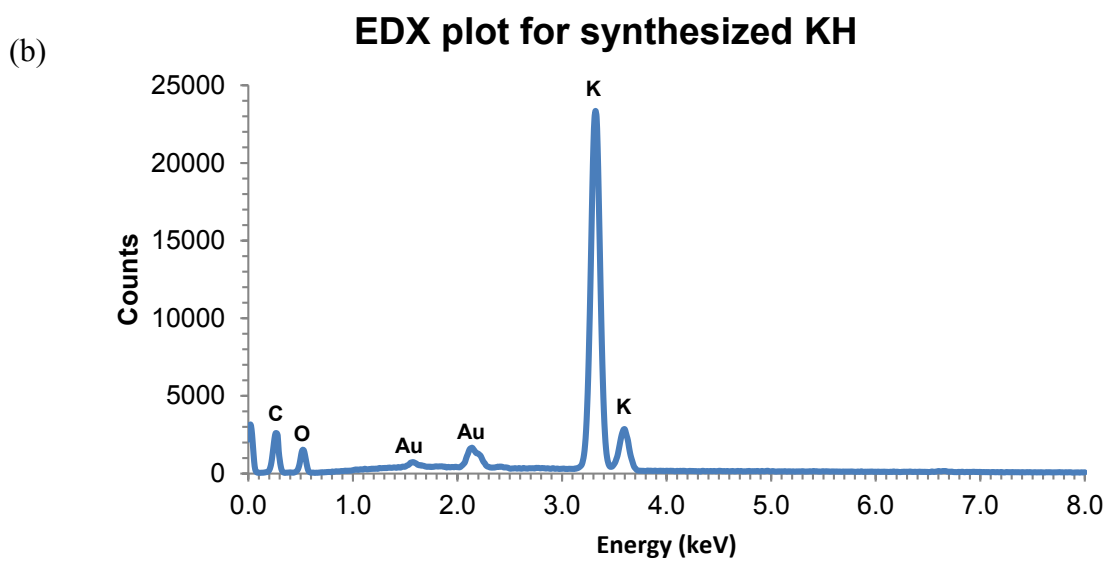
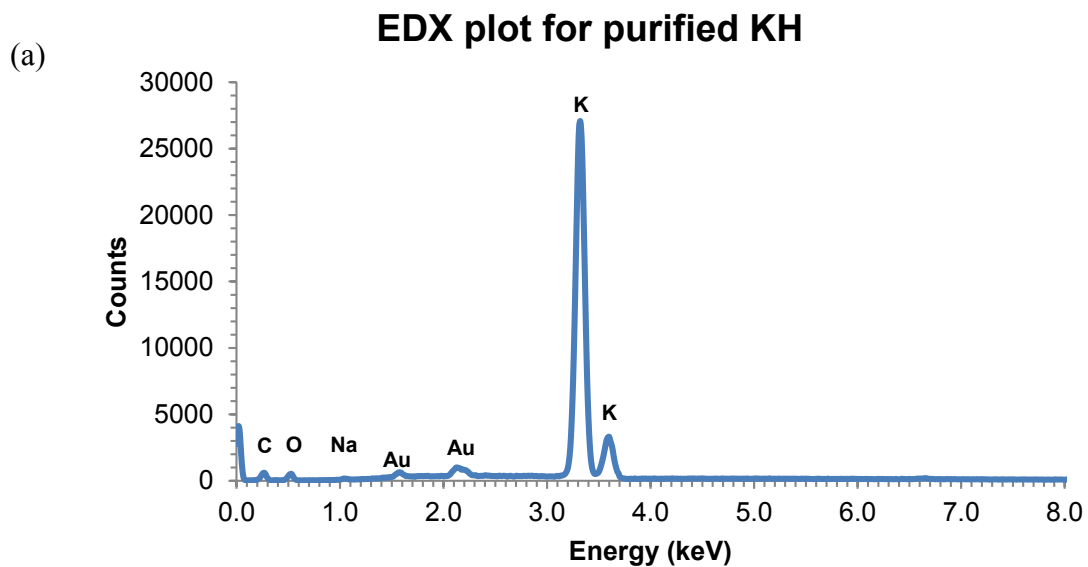
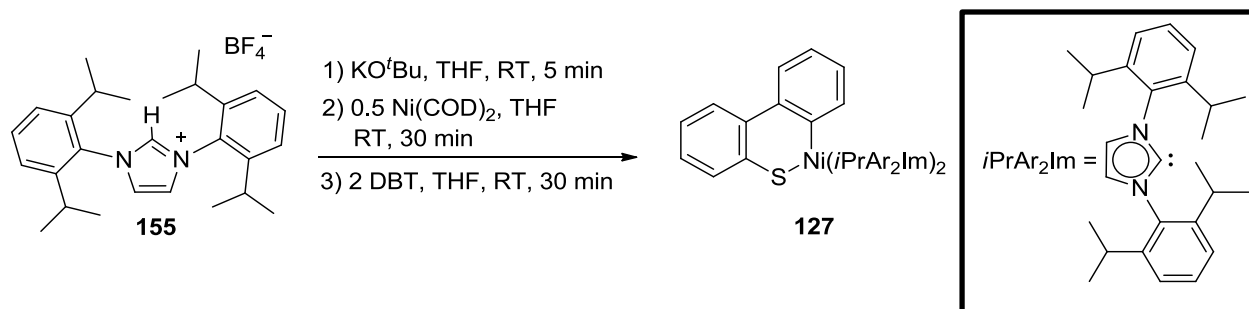


Figure 5.18 EDX plot of purified KH (a) vs. synthesized KH (b).

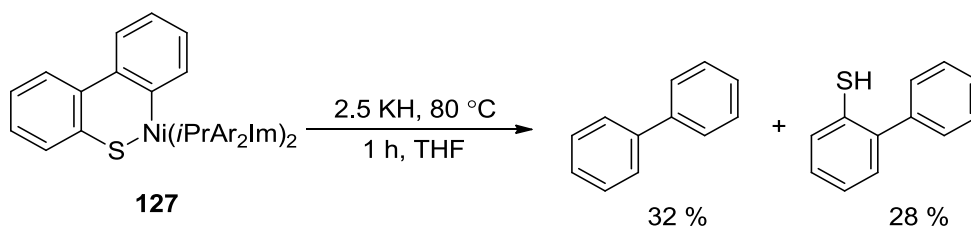
5.5.12 Role of the transition metal catalyst.

5.5.12.1 In situ synthesis of Ni(DBT)(iPrAr₂Im)₂ (**127**) and DBT desulfurization



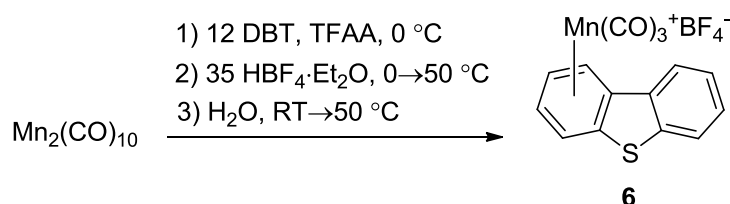
The synthesis was adapted from the published method.^{95, 216} Inside the glove box, a 5-dram vial was charged with a Teflon-coated stir bar, carbenium salt **155** (0.054 g, 0.11 mmol), and KO^tBu (0.013 g, 0.11 mmol). The mixture was dissolved in 1 mL of THF and stirred for 5 min to give a yellow solution. Then, Ni(COD)₂ (0.016 g, 0.057 mmol) in 1.5 mL THF was added to the mixture, yielding a dark green solution. After stirring 30 min, DBT (0.015 g, 0.083 mmol) was added to the solution, transforming the color to olive-green. The solution was stirred for 30 min and then used directly for desulfurization.

The reaction mixture and KH (7.9 mg, 0.20 mmol) were transferred into a medium-wall glass vessel and sealed with a Teflon cap. The vessel was heated at 80 °C for 1 h, after which the reactor was allowed to cool to room temperature and quenched with 10% HCl. The solution was filtered through a Florisil plug and washed with 3 times 1 mL portions of diethyl ether. The pale yellow solution was dried with MgSO₄ and filtered through another Florisil plug. GC analysis revealed 32% conversion to biphenyl and 28% conversion to 2-phenylthiophenol (Scheme 5.1).



Scheme 5.1

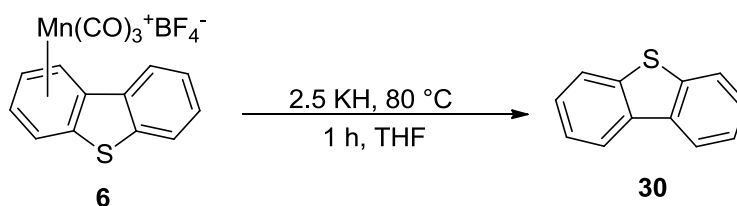
5.5.12.2 Synthesis of manganese complex **6**



The synthesis was adapted from the published method.²¹⁷ Inside the glove box, a 100-mL Schlenk flask equipped with a Teflon-coated stir bar was charged with $\text{Mn}_2(\text{CO})_{10}$ (0.14 g, 0.35 mmol) and dibenzothiophene (0.78 g, 4.2 mmol), then, sealed with a septum. Two mL of $\text{HBF}_4 \cdot \text{Et}_2\text{O}$ (35 equiv.) was added to a 20-mL round bottom flask and sealed with a septum. The two flasks were removed from the glove box, and cooled to 0 °C with an ice/water bath. Trifluoroacetic acid anhydride (10 mL) was added to the vigorously stirred mixture of manganese and DBT *via* cannula transfer, resulting in a yellow suspension. The suspension was stirred for 5 min at 0 °C and charged with $\text{HBF}_4 \cdot \text{Et}_2\text{O}$. The stirred suspension was allowed to warm to room temperature and then heated to reflux for 4 h. The resulting suspension of yellow and white solids was cooled to room temperature, exposed to air, and charged with 1 mL of H_2O . This suspension was heated to 50 °C overnight, affording golden-brown solution. After cooling to room temperature, the volatiles were removed under reduced pressure, giving a bright yellow

powder. This was triturated into 10 mL of a 1 : 1 mixture of CH₂Cl₂ and acetone, resulting in yellow solution. The manganese complex **6** was precipitated by the addition of diethyl ether (93 mL) and collected by vacuum filtration. The compound was purified by precipitation from acetone (4 mL) upon the addition of 50 mL diethyl ether. The pale yellow solid was collected by vacuum filtration, giving 12 g (41 %). The identity of the product was confirmed by IR spectroscopy.

5.5.12.3 Hydride-mediated HDS reaction of manganese complex **6**

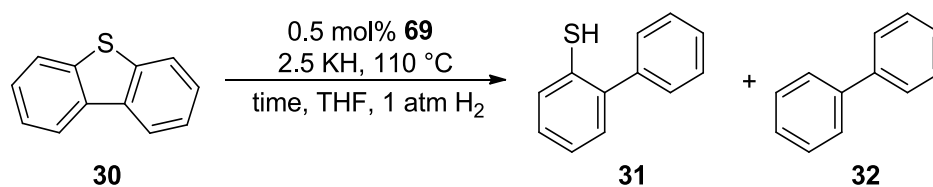


Inside the dry box, a medium-wall glass reactor equipped with a Teflon-coated stir bar was charged with complex **6** (0.028 g, 0.067 mmol) and KH (0.0065 g, 0.16 mmol), along with 5 mL of THF. The flask was sealed with a Teflon cap and brought outside the glove box. The yellow solution was heated for 1 h at 80 °C, cooled to room temperature, and quenched with 10 % HCl. The pale yellow solution was filtered through a Florisil plug, washed 3 times with 1 mL portions of diethyl ether, dried over MgSO₄, filtered through another Florisil plug washed with ether, to yield a yellow solution. GC analysis revealed only dibenzothiophene (100%).

5.5.13 Kinetic profile of hydride-mediated desulfurization of DBT catalyzed by cobalt cluster **69**

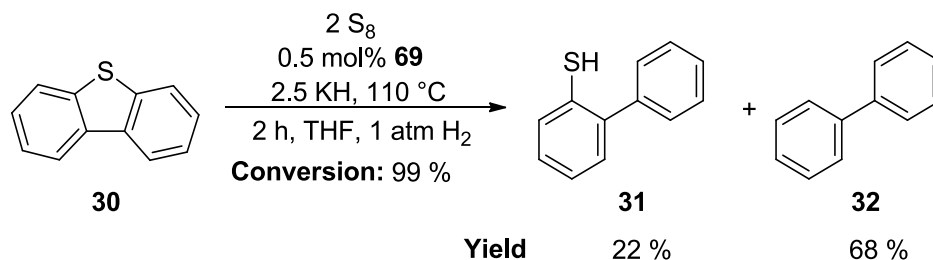
The general procedure outlined in section 5.4.1 was followed, using cluster **69** (0.0047 g, 0.0036 mmol), KH (0.072 g, 1.8 mmol), DBT (0.13 g, 0.73 mmol), and 10 mL THF. The reactions below were run in parallel for the reaction time indicated in Table **5.19**.

Table 5.19 Aliquot HDS reactions catalyzed by homoleptic cluster **69**.



Entry	Time (h)	Conv. (%)	31 (%)	32 (%)	DBT recovered (%)	Unrecovered (%)
1	0.00	65	36	3	35	26
2	0.083	82	56	5	18	21
3	0.17	98	67	12	1	20
4	0.25	99	68	13	2	17
5	0.33	99	21	66	1	12
6	1.00	99	15	74	1	10
7	1.25	99	10	82	1	7
8	1.5	100	17	69	0	14
9	1.92	100	10	75	0	15

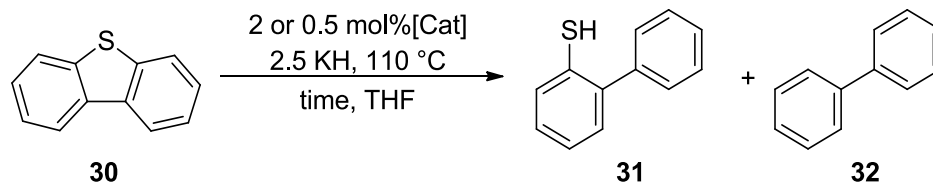
5.5.14 Hydride-mediated HDS of DBT in the presence of elemental sulfur



The general procedure outlined in section 5.4.1 was followed, using cluster **69** (0.0047 g, 0.0036 mmol), KH (0.072 g, 1.8 mmol), DBT (0.13 g, 0.73 mmol), S_8 (2.0 mg, 0.0009 mmol), suspended in 10 mL THF. GC analysis revealed a mixture of DBT (1 %), 2-phenylthiophenol (22 %), and biphenyl (68 %).

5.5.15 KH-promoted desulfurization of DBT catalyzed by various metal complex salts in the absence of hydrogen

The general procedure outlined in section 5.4.1 was followed, using the indicated transition metal source (0.0036 mmol), KH (0.072 g, 1.8 mmol), DBT (0.13 g, 0.73 mmol), and 10 mL THF. The vessel was sealed, removed from the glove box and heated to the specified temperature. Details and results are presented in Table **5.20**.

Table 5.20 Desulfurization of DBT in the absence of hydrogen.

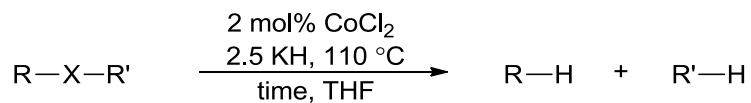
Entry	[Cat] ^a	Time (h)	Conv. (%)	31 (%)	32 (%)	DBT recovered (%)	Unrecovered (%)
1	40	2	99	39	38	1	22
2	53a	2	100	50	39	0	11
3	60	2	100	51	39	0	10
4	69	2	100	23	65	0	12
5	FeCl ₂	5	100	15	80	0	5
6	CoCl ₂	5	100	11	84	0	5
7	CoBr ₂	5	100	12	76	0	12
8	NiCl ₂	5	100	14	76	0	10
9	NiBr ₂	5	100	18	72	0	10
10	CuCl ₂	5	100	28	63	0	9
11	CuBr ₂	5	99	31	62	1	6

^a2 mol% metal halide or 0.5 mol% of phosphoramidate cobalt cluster.

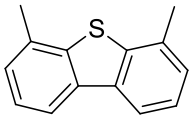
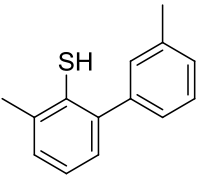
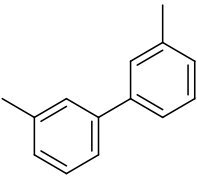
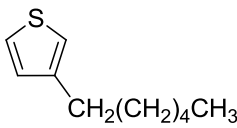
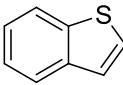
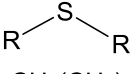
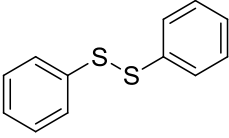
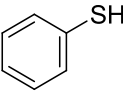
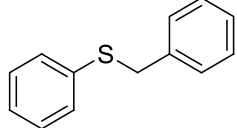
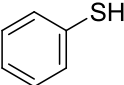
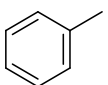
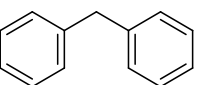
5.5.16 Substrate scope for CoCl₂/KH system

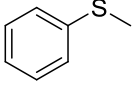
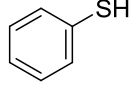
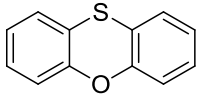
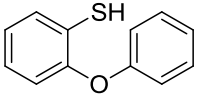
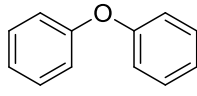
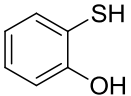
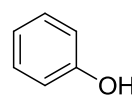
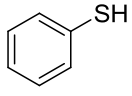
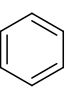
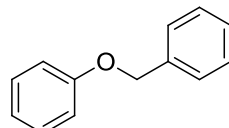
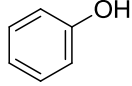
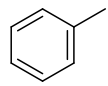
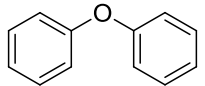
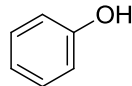
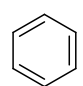
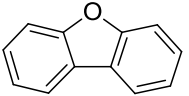
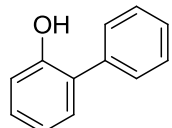
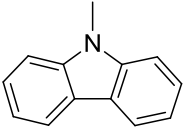
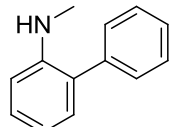
The same general procedure outlined in section 5.4.1 was followed, using CoCl₂ (0.0019 g, 0.0039 mmol), KH (0.072 g, 1.8 mmol), substrate (0.73 mmol), and 10 mL THF. The vessel was sealed, removed from the glove box, and heated to 110 °C. GC-MS analysis was used to determine the product(s), yield, and conversion. Details and results are shown in Table 5.21.

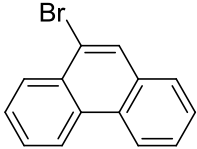
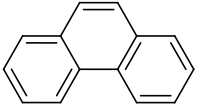
Table 5.21 Substrate scope for CoCl₂-KH system.



R, R' = aryl, alkyl
 X = S, O, N
 R = aryl when X = Br

Ent.	Substrate	Mass (g)	Time (h)	Conv. (%)	Product Selectivity (%)		
1	 124	0.1152	5	74	 125 71%	 126 29%	
2	 142	0.1229	5	0			
3	 143	0.0971	5	0			
4	 R = CH ₂ (CH ₂) ₁₀ CH ₃ 144	0.2695	5	5	CH ₃ (CH ₂) ₁₀ CH ₂ SH 144a 66%	CH ₃ (CH ₂) ₁₀ CH ₃ 144b 34%	
5	 145	0.1580	5	65	 145a 100%		
6	 146	0.1466	5	100	 146a 32%	 146b 10%	 146c 58%

Ent.	Substrate	Mass (g)	Time (h)	Conv. (%)	Product Selectivity (%)
7	 147	0.0967	5	100	 147a 100 %
8	 148	0.1454	16	100	 148a 15 %  148b 1 %  148c 72 %  148d 5 %  148e 4 %  148f 3 %
9	 149	0.1333	16	40	 149a 51 %  149b 49 %
10	 150	0.1247	16	86	 150a 55 %  150b 45 %
11	 151	0.1226	16	100	 151a 100 %
12	 152	0.1314	16	6	 152a 100 %

Ent.	Substrate	Mass (g)	Time (h)	Conv. (%)	Product Selectivity (%)
13	 153	0.1860	16	100	 153a 100 %

The conversion and product selectivity of each substrates are obtained using unstandardized GC-MS analysis.

References

- (1) Canada, E. a. C. C. Sulphur in Gasoline Regulations. <https://www.ec.gc.ca/energie-energy/default.asp?lang=En&n=BEA13229-1> (accessed August 27, 2017).
- (2) Minderhoud, J. K.; van Veen, J. A. R.; Hagan, A. P., *Hydrocracking in the year 2000: A strong interaction between technology development and market requirements*. 1999; Vol. 127, p 3-20.
- (3) Dusseault, M. B.; Shafiei, A., Oil Sands. In *Ullmann's Encyclopedia of Industrial Chemistry*, Wiley-VCH Verlag GmbH & Co. KGaA: 2011.
- (4) Javadli, R.; de Klerk, A. *Applied Petrochemical Research* **2012**, *1*, 3-19.
- (5) Gray, M. R., *Upgrading Oilsands Bitumen and Heavy Oil*. First edition. ed.; University of Alberta Press: 2014; p xi, 499 pages.
- (6) Yu, Z. K., Catalytic Carbon-Sulfur Bond Activation and Transformations. In *Homogeneous Catalysis for Unreactive Bond Activation*, 2015; pp 317-345.
- (7) Sanchez-Delgado, R. A., *Organometallic modeling of the hydrodesulfurization and hydrodenitrogenation reactions*. Kluwer Academic Publishers: Dordrecht ; Boston, 2002; p xii, 209 p.
- (8) Dong, L. Z.; Duckett, S. B.; Ohman, K. F.; Jones, W. D. *J. Am. Chem. Soc.* **1992**, *114*, 151-160.
- (9) Jones, W. D.; Chin, R. M. *J. Organomet. Chem.* **1994**, *472*, 311-316.
- (10) Sánchez-Delgado, R. A. *J. Mol. Catal.* **1994**, *86*, 287-307.
- (11) Vicic, D. A.; Jones, W. D. *Organometallics* **1998**, *17*, 3411-3413.
- (12) Zhang, X.; Dullaghan, C. A.; Watson, E. J.; Carpenter, G. B.; Sweigart, D. A. *Organometallics* **1998**, *17*, 2067-2075.
- (13) Baird, J., William C.; Bearden, J., Roby Desulfurization and Hydroconversion of Residua with Sodium Hydride and Hydrogen. U.S. Patent 4,003,824, January 18, 1977.
- (14) Baird, J., William C.; Bearden, J., Roby Desulfurization and Hydroconversion of Residua with Alkaline Earth Metal Compounds and Hydrogen. U.S. Patent 4,087,348, May 2, 1978.
- (15) Baird, J., William C. Hydroconversion and Desulfurization Process U.S. Patent 4,087,349, May 2, 1978.
- (16) Vann, W. D.; Leta, D. P.; Mcconnachie, J. M.; Demmin, R. A.; Hisson, D. W.; Baird, J., William C.; ; Bearden, J., Roby; ; Bielenberg, J. R.; Freund, H.; Wright, C. A.; Raterman, M. F.; Rigby, J. R.; Stone, B. T. Alkali Metal Hydroprocessing of Heavy Oils with Enhanced Removal of Coke Products. U.S. Patent 8,894,845, November 25, 2014.
- (17) Soto, J. L.; Raterman, M.; Leta, D. P.; Vann, W. D.; Han, L.; McConnachie, J. M.; Bielenberg, J. R.; Baird, J., William C.; ; Bearden, J., Roby; Desulfurization Process Using Alkali Metal Reagent. U.S. Patent 8,696,890, April 15, 2014.
- (18) Bearden, R.; Fink, T. Alkali Metal Desulfurization Process for Petroleum Oil Stocks Using Low Pressure Hydrogen U.S. Patent 3,787,315, January 22, 1974.
- (19) Hardesty, D. E.; Rodgers, T. A. Molten Salt Hydroconversion Process U.S. Patent 3,677,932, July 18, 1972.
- (20) Baird Jr., W. C.; Bearden Jr., R.; Ledford, T. H. Hydroconversion with Group IA, IIA Metal Compounds U.S. Patent 4,127,470, November 28, 1978.

- (21) Toutov, A. A.; Salata, M.; Fedorov, A.; Yang, Y.-F.; Liang, Y.; Cariou, R.; Betz, K. N.; Couzijn, E. P. A.; Shabaker, J. W.; Houk, K. N.; Grubbs, R. H. *Nat. Energy*. **2017**, *2*, 17008-17015.
- (22) Bunquin, J. C.; Stryker, J. M. Transition metal catalysts for hydrodesulfurization. U.S. Patent 9,120,984, September 1, 2015.
- (23) Brown, H. J. S.; Stryker, J. M.; Hebert, D. M. Catalysts for hydrodesulfurization. U.S. Patent 9,458,395, October 4, 2016.
- (24) Brown, O. First-Row Metal Catalysts for Hydrogenolysis of Carbon-Sulfur and Carbon-Oxygen Bonds. Ph.D. Thesis, University of Alberta, Edmonton, Alberta, 2017.
- (25) Zhao, T. Phosphoranimide-supported Nickel Clusters for Hydrotreatment. Ph.D. Thesis, University of Alberta, Edmonton, Alberta, 2017.
- (26) World Motor Gasoline Consumption by Year. <http://www.indexmundi.com/energy/?product=gasoline&> (accessed November 21, 2017).
- (27) Administration, U. S. E. I. Gasoline Explained: Use of Gasoline. https://www.eia.gov/energyexplained/index.cfm?page=gasoline_use (accessed November 21).
- (28) Administration, U. S. E. I. Energy and the Environment Explained: Greenhouse Gases' Effect on the Climate. https://www.eia.gov/energyexplained/index.cfm?page=environment_how_ghg_affect_climate (accessed August 27, 2017).
- (29) Agency, U. S. E. P. Sulfur Dioxide (SO₂) Pollution <https://www.epa.gov/so2-pollution/sulfur-dioxide-basics#what%20is%20so2> (accessed August 27, 2017).
- (30) Agency, U. S. E. P. What is Acid Rain? <https://www.epa.gov/acidrain/what-acid-rain> (accessed August 27).
- (31) Agency, U. S. E. P. Gasoline Sulfur. <https://www.epa.gov/gasoline-standards/gasoline-sulfur> (accessed August 27, 2017).
- (32) Topsøe, H.; Clausen, B. S.; Massoth, F. E., *Hydrotreating Catalysis*. Springer-Verlag Berlin Heidelberg: 1996; Vol. 11, p 312.
- (33) Babich, I. V.; Moulijn, J. A. *Fuel* **2003**, *82*, 607-631.
- (34) Vanrysselberghe, V.; Froment, G. F., Hydrodesulfurization - Heterogeneous. In *Encyclopedia of catalysis*, Horváth, I. T., Ed. Wiley-Interscience: Hoboken, N.J., 2003; Vol. 3, pp 667-733.
- (35) Sanchez-Delgado, R. A., Hydrodesulfurization - Homogeneous. In *Encyclopedia of catalysis*, Horváth, I. T., Ed. Wiley-Interscience: Hoboken, N.J., 2003; Vol. 3, pp 636-666.
- (36) Western Canadian Select Explained. <http://www.oilsandsmagazine.com/technical/western-canadian-select-wcs> (accessed March 3, 2017).
- (37) Ancheyta, J.; Rana, M. S.; Furimsky, E. *Catal. Today*. **2005**, *109*, 3-15.
- (38) BDEs of S-, Se-, Te-, Po-X bonds. In *Comprehensive Handbook of Chemical Bond Energies*, CRC Press: 2007; pp 424-454.
- (39) Stanislaus, A.; Cooper, B. H. *Catal. Rev.* **1994**, *36*, 75-123.
- (40) Vanrysselberghe, V.; Le Gall, R.; Froment, G. F. *Ind. Eng. Chem. Res.* **1998**, *37*, 1235-1242.

- (41) Resources, R. Sulfiding 101: An introduction to sulfiding of hydrotreating catalyst. <http://www.reactor-resources.com/sulfiding-services/sulfiding-101.html> (accessed January 1).
- (42) Hagen, J., Heterogeneous Catalysis: Fundamentals. In *Industrial Catalysis*, Wiley-VCH Verlag GmbH & Co. KGaA: 2015; pp 99-210.
- (43) Karroua, M.; Centeno, A.; Matralis, H. K.; Grange, P.; Delmon, B. *Appl. Catal.* **1989**, *51*, L21-L26.
- (44) Schuit, G. C. A.; Gates, B. C. *AIChE J.* **1973**, *19*, 417-438.
- (45) Voorhoeve, R. J. H.; Stuiver, J. C. M. *J. Catal.* **1971**, *23*, 228-235.
- (46) Topsøe, H.; Clausen, B. S. *Catal. Rev.* **1984**, *26*, 395-420.
- (47) Okamoto, Y.; Kawano, M.; Kawabata, T.; Kubota, T.; Hiromitsu, I. *J. Phys. Chem. B* **2005**, *109*, 288-296.
- (48) Lipsch, J. M. J. G.; Schuit, G. C. A. *J. Catal.* **1969**, *15*, 179-189.
- (49) O'Brien, W. S.; Chen, J. W.; Nayak, R. V.; Carr, G. S. *Ind. Eng. Chem. Proc. D.D.* **1986**, *25*, 221-229.
- (50) Whitehurst, D. D.; Isoda, T.; Mochida, I. *Advances in Catalysis* **1998**, *42*, 345-471.
- (51) Kwart, H.; Schuit, G. C. A.; Gates, B. C. *J. Catal.* **1980**, *61*, 128-134.
- (52) Harris, S.; Chianelli, R. R. *J. Catal.* **1984**, *86*, 400-412.
- (53) Deutschmann, O.; Knözinger, H.; Kochloefl, K.; Turek, T., Heterogeneous Catalysis and Solid Catalysts, 2. Development and Types of Solid Catalysts. In *Ullmann's Encyclopedia of Industrial Chemistry*, Wiley-VCH Verlag GmbH & Co. KGaA: 2000.
- (54) Pecoraro, T. A.; Chianelli, R. R. *J. Catal.* **1981**, *67*, 430-445.
- (55) Vissers, J. P. R.; Groot, C. K.; van Oers, E. M.; de Beer, V. H. J.; Prins, R. *Bull. Soc. Chim. Belg.* **1984**, *93*, 813.
- (56) Ledoux, M. J.; Michaux, O.; Agostini, G.; Panissod, P. *J. Catal.* **1986**, *102*, 275-288.
- (57) Raybaud, P.; Kresse, G.; Hafner, J.; Toulhoat, H. *J. Phys.-Condens. Mat.* **1997**, *9*, 11085-11106.
- (58) Chianelli, R. R. *Oil Gas Sci Technol.* **2006**, *61*, 503-513.
- (59) Sun, M.; Nicosia, D.; Prins, R. *Catal. Today.* **2003**, *86*, 173-189.
- (60) Al-Dalama, K.; Stanislaus, A. *Energ. Fuel* **2006**, *20*, 1777-1783.
- (61) Adams, R. D.; Kwon, O. S.; Perrin, J. L. *J. Organomet. Chem.* **1999**, *584*, 223-229.
- (62) Breyse, M.; Afanasiev, P.; Geantet, C.; Vrinat, M. *Catal. Today.* **2003**, *86*, 5-16.
- (63) Dhar, G. M.; Srinivas, B. N.; Rana, M. S.; Kumar, M.; Maity, S. K. *Catal. Today.* **2003**, *86*, 45-60.
- (64) Venezia, A. M.; La Parola, V.; Liotta, L. F. *Catal. Today.* **2017**, *285*, 114-124.
- (65) Chianelli, R. R. *Catal. Rev.* **1984**, *26*, 361-393.
- (66) King, R. B.; Stone, F. G. A. *J. Am. Chem. Soc.* **1960**, *82*, 4557-4562.
- (67) King, R. B.; Treichel, P. M.; Stone, F. G. A. *J. Am. Chem. Soc.* **1961**, *83*, 3600-3604.
- (68) Jones, W. D.; Dong, L. *J. Am. Chem. Soc.* **1991**, *113*, 559-564.
- (69) Bianchini, C.; Meli, A.; Peruzzini, M.; Vizza, F.; Frediani, P.; Herrera, V.; Sanchez-Delgado, R. A. *J. Am. Chem. Soc.* **1993**, *115*, 2731-2742.
- (70) Jones, W. D.; Chin, R. M.; Crane, T. W.; Baruch, D. M. *Organometallics* **1994**, *13*, 4448-4452.
- (71) Riaz, U.; Curnow, O. J.; Curtis, M. D. *J. Am. Chem. Soc.* **1994**, *116*, 4357-4363.
- (72) Bianchini, C.; Jiménez, M. V.; Mealli, C.; Meli, A.; Moneti, S.; Patinec, V.; Vizza, F. *Angew. Chem. Int. Edit.* **1996**, *35*, 1706-1708.

- (73) Garcia, J. J.; Mann, B. E.; Adams, H.; Bailey, N. A.; Maitlis, P. M. *J. Am. Chem. Soc.* **1995**, *117*, 2179-2186.
- (74) Vicic, D. A.; Jones, W. D. *J. Am. Chem. Soc.* **1999**, *121*, 7606-7617.
- (75) Churchill, D. G.; Bridgewater, B. M.; Parkin, G. *J. Am. Chem. Soc.* **2000**, *122*, 178-179.
- (76) Sattler, A.; Janak, K. E.; Parkin, G. *Inorg. Chim. Acta.* **2011**, *369*, 197-202.
- (77) Mills, R. C.; Abboud, K. A.; Boncella, J. M. *Chem. Commun.* **2001**, 1506-1507.
- (78) Sattler, A.; Parkin, G. *J. Am. Chem. Soc.* **2011**, *133*, 3748-3751.
- (79) Rosini, G. P.; Jones, W. D. *J. Am. Chem. Soc.* **1992**, *114*, 10767-10775.
- (80) Reynolds, M. A.; Guzei, I. A.; Angelici, R. J. *Chem. Commun.* **2000**, 513-514.
- (81) Arce, A. J.; Arrojo, P.; Deeming, A. J.; De Sanctis, Y. *J. Chem. Soc. Dalton Trans.* **1992**, 2423-2424.
- (82) Bianchini, C.; Jiménez, M. V.; Meli, A.; Moneti, S.; Patinec, V.; Vizza, F. *Organometallics* **1997**, *16*, 5696-5705.
- (83) Myers, A. W.; Jones, W. D. *Organometallics* **1996**, *15*, 2905-2917.
- (84) Bianchini, C.; Meli, A.; Peruzzini, M.; Vizza, F.; Moneti, S.; Herrera, V.; Sanchez-Delgado, R. A. *J. Am. Chem. Soc.* **1994**, *116*, 4370-4381.
- (85) Bianchini, C.; Jimenez, M. V.; Meli, A.; Moneti, S.; Vizza, F.; Herrera, V.; Sanchez-Delgado, R. A. *Organometallics* **1995**, *14*, 2342-2352.
- (86) Garcia, J. J.; Maitlis, P. M. *J. Am. Chem. Soc.* **1993**, *115*, 12200-12201.
- (87) Vicic, D. A.; Jones, W. D. *Organometallics* **1997**, *16*, 1912-1919.
- (88) Matsubara, K.; Okamura, R.; Tanaka, M.; Suzuki, H. *J. Am. Chem. Soc.* **1998**, *120*, 1108-1109.
- (89) Egorova, K. S.; Ananikov, V. P. *Organometallics* **2017**, *36*, 4071-4090.
- (90) Market Data: Commodity Prices. <http://www.mining.com/market-data/> (accessed May 5, 2017S).
- (91) Zhang, X.; A. Dullaghan, C.; B. Carpenter, G.; A. Sweigart, D.; Zhang, X.; B. Carpenter, G.; Meng, Q. *Chem. Commun.* **1998**, 93-94.
- (92) Yu, K.; Li, H.; Watson, E. J.; Virkaitis, K. L.; Carpenter, G. B.; Sweigart, D. A. *Organometallics* **2001**, *20*, 3550-3559.
- (93) Jones, W. D.; Chin, R. M. *Organometallics* **1992**, *11*, 2698-2700.
- (94) Vicic, D. A.; Jones, W. D. *J. Am. Chem. Soc.* **1999**, *121*, 4070-4071.
- (95) Schaub, T.; Backes, M.; Plietzsch, O.; Radius, U. *Dalton T.* **2009**, 7071-7079.
- (96) Vicic, D. A.; Jones, W. D. *J. Am. Chem. Soc.* **1997**, *119*, 10855-10856.
- (97) Shoshani, M. M.; Johnson, S. A. *Inorg. Chem.* **2015**, *54*, 11977-11985.
- (98) Curtis, M. D.; Druker, S. H. *J. Am. Chem. Soc.* **1997**, *119*, 1027-1036.
- (99) Bianchini, C.; Herrera, V.; Jimenez, M. V.; Meli, A.; Sanchez-Delgado, R.; Vizza, F. *J. Am. Chem. Soc.* **1995**, *117*, 8567-8575.
- (100) Bianchini, C.; Casares, J. A.; Meli, A.; Sernau, V.; Vizza, F.; Sánchez-Delgado, R. A. *Polyhedron* **1997**, *16*, 3099-3114.
- (101) InfoMine Commodity and Metal Prices. <http://www.infomine.com/investment/metal-prices/> (accessed October 15, 2017).
- (102) Torres-Nieto, J.; Arévalo, A.; García, J. J. *Organometallics* **2007**, *26*, 2228-2233.
- (103) Brown, H. J. S. Mixed-Valence First-Row Metal Clusters for Catalytic Hydrodesulfurization and Hydrodeoxygenation. Ph.D. Thesis, University of Alberta, Edmonton, Alberta, 2013.

- (104) Camacho-Bunquin, J. Empowering the Base Metals: Rational Design of High-Activity Homogeneous Catalysts for Reduction of Organic Unsaturates and Mild-Condition Hydrotreatment. Ph.D. Thesis, University of Alberta, Edmonton, Alberta, 2013.
- (105) Brown, H. J. S.; Stryker, J. M.; Hebert, D. M. Mixed-valent transition metal-phosphoranimide catalysts. U.S. Patent 9,000,198, April 7, 2015.
- (106) Muetterties, E. L.; Krause, M. J. *Angew. Chem. Int. Edit.* **1983**, *22*, 135-148.
- (107) Bartholomew, C. H.; Farrauto, R. J., Introduction and Fundamentals. In *Fundamentals of Industrial Catalytic Processes*, John Wiley & Sons, Inc.: 2005; pp 1-1.
- (108) Bartholomew, C. H.; Farrauto, R. J., Petroleum Refining and Processing. In *Fundamentals of Industrial Catalytic Processes*, John Wiley & Sons, Inc.: 2005; pp 635-704.
- (109) Brasted, R. C. Sulfur (S). <https://www.britannica.com/science/sulfur> (accessed Nov. 1, 2017).
- (110) Ashar, N. G.; Golwalkar, K. R., A practical guide to the manufacture of sulfuric acid, oleums, and sulfonating agents. Golwalkar, K. R., Ed. Springer International Publishing Switzerland 2013.
- (111) Muetterties, E. L. *Science* **1977**, *196*, 839-848.
- (112) Norton, J. R., Metal Clusters in Catalysis. In *Fundamental Research in Homogeneous Catalysis*, Tsutsui, M.; Ugo, R., Eds. Springer US: Boston, MA, 1977; pp 99-114.
- (113) Lauher, J. W. *J. Am. Chem. Soc.* **1978**, *100*, 5305-5315.
- (114) Boudart, M. *J. Mol. Catal.* **1985**, *30*, 27-38.
- (115) González-Moraga, G., *Cluster chemistry : Introduction to the Chemistry of Transition Metal and Main Group Element Molecular Clusters*. Springer-Verlag: Berlin ;, 1993.
- (116) Chisholm, M. H., Molecular Clusters – An Overview. In *Metal Clusters in Chemistry*, Wiley-VCH Verlag GmbH: 2008; pp 8-9.
- (117) Cotton, F. A., General Introduction. In *Metal Clusters in Chemistry*, Wiley-VCH Verlag GmbH: 2008; pp 2-7.
- (118) Cotton, F. A. *Inorg. Chem.* **1964**, *3*, 1217-1220.
- (119) Huttner, G.; Knoll, K. *Angew. Chem. Int. Edit.* **1987**, *26*, 743-760.
- (120) Fenske, D.; Ohmer, J.; Hachgenei, J.; Merzweiler, K. *Angew. Chem. Int. Edit.* **1988**, *27*, 1277-1296.
- (121) Whitmire, K. H. *J. Coord. Chem.* **1988**, *17*, 095-203.
- (122) Gates, B. C. *Chem. Rev.* **1995**, *95*, 511-522.
- (123) Brown, R. K.; Williams, J. M.; Fredrich, M. F.; Day, V. W.; Sivak, A. J.; Muetterties, E. L. *P. Natl. Acad. Sci. USA* **1979**, *76*, 2099 - 2102.
- (124) Kaesz, H. D.; King, R. B.; Manuel, T. A.; Nichols, L. D.; Stone, F. G. A. *J. Am. Chem. Soc.* **1960**, *82*, 4749-4750.
- (125) Ogilvy, A. E.; Draganjac, M.; Rauchfuss, T. B.; Wilson, S. R. *Organometallics* **1988**, *7*, 1171-1177.
- (126) Smith, A. K.; Basset, J. M. *J. Mol. Catal.* **1977**, *2*, 229-241.
- (127) Lee, S. C.; Holm, R. H. *Chem. Rev.* **2004**, *104*, 1135-1158.
- (128) Zhao, Q.; Betley, T. A. *Angew. Chem. Int. Edit.* **2011**, *50*, 709-712.
- (129) Staudinger, H.; Meyer, J. *Helv. Chim. Acta* **1919**, *2*, 635-646.
- (130) Dehnicke, K.; Strahle, J. *Polyhedron* **1989**, *8*, 707-726.
- (131) Dehnicke, K.; Krieger, M.; Massa, W. *Coordin. Chem. Rev.* **1999**, *182*, 19-65.
- (132) Sundermann, A.; Schoeller, W. W. *J. Am. Chem. Soc.* **2000**, *122*, 4729-4734.

- (133) Riese, U.; Harms, K.; Neumüller, B.; Dehnicke, K. *Z. Anorg. Allg. Chem.* **1998**, *624*, 1279-1284.
- (134) Mai, H. J.; Kang, H. C.; Wocadlo, S.; Massa, W.; Dehnicke, K. *Z. Anorg. Allg. Chem.* **1995**, *621*, 1963-1968.
- (135) Mai, H.-J.; zu Köcker, R. M.; Wocadlo, S.; Massa, W.; Dehnicke, K. *Angew. Chem.* **1995**, *107*, 1349-1350.
- (136) Riese, U.; Faza, N.; Harms, K.; Massa, W.; Neumüller, B.; Dehnicke, K. *Phosphorus Sulfur* **1997**, *124*, 315-321.
- (137) Krieger, M.; Gould, R. O.; Pebler, J.; Dehnicke, K. *Z. Anorg. Allg. Chem.* **1998**, *624*, 781-786.
- (138) Honeyman, C. H.; Lough, A. J.; Manners, I. *Inorg. Chem.* **1994**, *33*, 2988-2993.
- (139) Hawkeswood, S. B.; Stephan, D. W. *Inorg. Chem.* **2003**, *42*, 5429-5433.
- (140) Stephan, D. W.; Stewart, J. C.; Guérin, F.; Courtenay, S.; Kickham, J.; Hollink, E.; Beddie, C.; Hoskin, A.; Graham, T.; Wei, P.; Spence, R. E. v. H.; Xu, W.; Koch, L.; Gao, X.; Harrison, D. G. *Organometallics* **2003**, *22*, 1937-1947.
- (141) Hebert, D. M.; Hamilton, R. J.; Stryker, J. M. Unpublished Work.
- (142) LePichon, L.; Stephan, D. W.; Gao, X.; Wang, Q. *Organometallics* **2002**, *21*, 1362-1366.
- (143) Bai, T.; Janes, T.; Song, D. *Dalton T.* **2017**, *46*, 12408-12412.
- (144) Camacho-Bunquin, J.; Ferguson, M. J.; Stryker, J. M. *J. Am. Chem. Soc.* **2013**, *135*, 5537-5540.
- (145) Gauthier, J. Titanacyclobutene and Cobalt(II) phosphinimide Complexes. Ph.D. Thesis, University of Alberta, Edmonton, Alberta, 2012.
- (146) Grob, T.; Harms, K.; Dehnicke, K. *Z. Anorg. Allg. Chem.* **2000**, *626*, 1065-1072.
- (147) Hamilton, R. J.; Hebert, D. M.; Reaugh, D.; Zhao, T.; Yu, S.; Stryker, J. M. Unpublished Work.
- (148) Trimethylsilylazide; Thermo Fisher Scientific. United Kingdom, 2017.
- (149) Birkofer, L.; Kim, S. M. *Chem. Ber.* **1964**, *97*, 2100-2101.
- (150) Hamilton, R. J.; Hebert, D. M.; Stryker, J. M. Unpublished Work.
- (151) Hebert, D. M.; Stryker, J. M. Unpublished Work.
- (152) Riese, U. Phosphaniminato-Komplexe Elektronenreicher Übergangsmetalle. Philipps-Universität Marburg, 1998.
- (153) Nkala, F. M. A New Approach to Molecular Hydrodesulfurization Catalysts: Allyl-capped Trialkylphosphoranimide-bridged Late First-row Transition Metal Clusters. University of Alberta, Edmonton, Alberta, 2017.
- (154) Hartwig, J. F., *Organotransition Metal Chemistry : From Bonding to Catalysis*. University Science Books: Sausalito, California, 2010.
- (155) Kaesz, H. D.; Saillant, R. B. *Chem. Rev.* **1972**, *72*, 231-281.
- (156) Spilebout, F.; Stoyanov, S.; Kovalenko, A. Unpublished Work.
- (157) Sellmann, D.; Rackelmann, G. H.; Heinemann, F. W. *Chem. Eur. J.* **1997**, *3*, 2071-2080.
- (158) Ohki, Y.; Sakamoto, M.; Tatsumi, K. *J. Am. Chem. Soc.* **2008**, *130*, 11610-11611.
- (159) Corwin, D. T.; Fikar, R.; Koch, S. A. *Inorg. Chem.* **1987**, *26*, 3079-3080.
- (160) Solomon, E. I.; Gorelsky, S. I.; Dey, A. *J. Comput. Chem.* **2006**, *27*, 1415-1428.
- (161) Pauling, L. *P. Natl. Acad. Sci. USA* **1976**, *73*, 4290-4293.
- (162) Mondal, K. C.; Samuel, P. P.; Roesky, H. W.; Carl, E.; Herbst-Irmer, R.; Stalke, D.; Schwederski, B.; Kaim, W.; Ungur, L.; Chibotaru, L. F.; Hermann, M.; Frenking, G. *J. Am. Chem. Soc.* **2014**, *136*, 1770-1773.

- (163) Moore, E. J.; Sullivan, J. M.; Norton, J. R. *J. Am. Chem. Soc.* **1986**, *108*, 2257-2263.
- (164) Fulmer, G. R.; Muller, R. P.; Kemp, R. A.; Goldberg, K. I. *J. Am. Chem. Soc.* **2009**, *131*, 1346-1347.
- (165) Brothers, P. J., Heterolytic Activation of Hydrogen by Transition Metal Complexes. In *Progress in Inorganic Chemistry*, John Wiley & Sons, Inc.: 2007; pp 1-61.
- (166) Kubas, G. J. *J. Organomet. Chem.* **2009**, *694*, 2648-2653.
- (167) Hawkeswood, S.; Wei, P.; Gault, J. W.; Stephan, D. W. *Inorg. Chem.* **2005**, *44*, 4301-4308.
- (168) Holthausen, M. H.; Mallov, I.; Stephan, D. W. *Dalton T.* **2014**, *43*, 15201-15211.
- (169) Hartmann, N. J.; Wu, G.; Hayton, T. W. *Angew. Chem. Int. Edit.* **2015**, *54*, 14956-14959.
- (170) Waterman, R. *Organometallics* **2013**, *32*, 7249-7263.
- (171) Perutz, R. N.; Sabo-Etienne, S. *Angew. Chem. Int. Edit.* **2007**, *46*, 2578-2592.
- (172) Niu, S.; Thomson, L. M.; Hall, M. B. *J. Am. Chem. Soc.* **1999**, *121*, 4000-4007.
- (173) Fagnou, K.; Lautens, M. *Angew. Chem. Int. Edit.* **2002**, *41*, 26-47.
- (174) BDEs of Co(Co ±)-, Rh(Rh +)-, and Ir(Ir +)-X bonds. In *Comprehensive Handbook of Chemical Bond Energies*, CRC Press: 2007; pp 855-902.
- (175) Brown, C. A. *J. Org. Chem.* **1974**, *39*, 3913-3918.
- (176) Laine, R. M. *J. Mol. Catal.* **1982**, *14*, 137-169.
- (177) Thomson, W. J.; Laine, R. M., Homogeneous Catalytic Reduction of Benzaldehyde with Carbon Monoxide and Water. In *Catalytic Activation of Carbon Monoxide*, AMERICAN CHEMICAL SOCIETY: 1981; Vol. 152, pp 133-145.
- (178) Fumagalli, A.; Koetzle, T. F.; Takusagawa, F.; Chini, P.; Martinengo, S.; Heaton, B. T. *J. Am. Chem. Soc.* **1980**, *102*, 1740-1742.
- (179) Vidal, J. L.; Walker, W. E. *Inorg. Chem.* **1980**, *19*, 896-903.
- (180) Signer, R. *Liebigs Ann. Chem.* **1930**, *478*, 246-266.
- (181) Clark, E. P. *Anal. Chem* **1941**, *13*, 820-821.
- (182) Rush, C. A.; Cruikshank, S. S.; Schrock, J. J.; Rosenblatt, D. H. *Microchem. J.* **1966**, *10*, 522-528.
- (183) Lin, Y.; Finke, R. G. *Inorg. Chem.* **1994**, *33*, 4891-4910.
- (184) Widegren, J. A.; Finke, R. G. *J. Mol. Catal. A-Chem.* **2003**, *198*, 317-341.
- (185) Jones, R. A.; Real, F. M.; Wilkinson, G.; Galas, A. M. R.; Hursthouse, M. B. *J. Chem. Soc. Dalton Trans.* **1981**, 126-131.
- (186) van Asselt, R.; Elsevier, C. J. *J. Mol. Catal.* **1991**, *65*, L13-L19.
- (187) Stein, J.; Lewis, L. N.; Gao, Y.; Scott, R. A. *J. Am. Chem. Soc.* **1999**, *121*, 3693-3703.
- (188) Pinnick, H. W. *Org. Prep. Proced. Int.* **1983**, *15*, 199-223.
- (189) Gawley, R. E.; Zhang, X.; Wang, Q., Potassium Hydride. In *Encyclopedia of Reagents for Organic Synthesis*, John Wiley & Sons, Ltd: 2001.
- (190) Gamero-Melo, P.; Villanueva-García, M.; Robles, J.; Contreras, R.; Paz-Sandoval, M. A. *J. Organomet. Chem.* **2005**, *690*, 1379-1395.
- (191) Fulmer, G. R.; Miller, A. J. M.; Sherden, N. H.; Gottlieb, H. E.; Nudelman, A.; Stoltz, B. M.; Bercaw, J. E.; Goldberg, K. I. *Organometallics* **2010**, *29*, 2176-2179.
- (192) Ripin, D. H.; Evans, D. A. Evans pKa.
http://evans.rc.fas.harvard.edu/pdf/evans_pKa_table.pdf (accessed Sept. 6, 2017).
- (193) Sam, D. J.; Simmons, H. E. *J. Am. Chem. Soc.* **1974**, *96*, 2252-2253.
- (194) Schlosser, M., Superbases for organic synthesis. In *Pure Appl. Chem.*, 1988; Vol. 60, p 1627.

- (195) Banerjee, S.; Yang, Y.-F.; Jenkins, I. D.; Liang, Y.; Toutov, A. A.; Liu, W.-B.; Schuman, D. P.; Grubbs, R. H.; Stoltz, B. M.; Krenske, E. H.; Houk, K. N.; Zare, R. N. *J. Am. Chem. Soc.* **2017**, *139*, 6880-6887.
- (196) Unkelbach, C.; Rosenbaum, H. S.; Strohmamm, C. *Chem. Commun.* **2012**, *48*, 10612-10614.
- (197) Zhang, W.; Liao, S.; Xu, Y.; Zhang, Y. *Synthetic Commun.* **1997**, *27*, 3977-3983.
- (198) Terrier, F. *Chem. Rev.* **1982**, *82*, 77-152.
- (199) Senger, N. A.; Bo, B.; Cheng, Q.; Keeffe, J. R.; Gronert, S.; Wu, W. *J. Org. Chem.* **2012**, *77*, 9535-9540.
- (200) Goldstein, S. W.; Bill, A.; Dhuguru, J.; Ghoneim, O. *J. Chem. Educ.* **2017**.
- (201) Brown, D. A.; Raju, J. R. *J. Chem. Soc. A* **1966**, 40-43.
- (202) Bhanuchandra, M.; Murakami, K.; Vasu, D.; Yorimitsu, H.; Osuka, A. *Angew. Chem. Int. Edit.* **2015**, *54*, 10234-10238.
- (203) Angelici, R. J. *Accounts Chem. Res.* **1988**, *21*, 387-394.
- (204) Bank, S.; Lois, T. A. *J. Am. Chem. Soc.* **1968**, *90*, 4505-4506.
- (205) Ito, O.; Aruga, T.; Matsuda, M. *J. Chem. Soc., Perkin. Trans. 2* **1982**, 1113-1115.
- (206) Bank, S.; Prislowski, M. C. *J. Chem. Soc. Chem. Comm.* **1970**, 1624-1625.
- (207) Yiping, Z.; Shijian, L.; Yun, X. *J. Mol. Catal.* **1993**, *84*, 211-221.
- (208) Sauer, N. N.; Angelici, R. J. *Organometallics* **1987**, *6*, 1146-1150.
- (209) Shen, K.; Fu, Y.; Li, J.-N.; Liu, L.; Guo, Q.-X. *Tetrahedron* **2007**, *63*, 1568-1576.
- (210) Bennett, M. A.; Hambley, T. W.; Roberts, N. K.; Robertson, G. B. *Organometallics* **1985**, *4*, 1992-2000.
- (211) Lesch, D. A.; Richardson, J. W.; Jacobson, R. A.; Angelici, R. J. *J. Am. Chem. Soc.* **1984**, *106*, 2901-2906.
- (212) Kane-Maguire, L. A. P.; Honig, E. D.; Sweigart, D. A. *Chem. Rev.* **1984**, *84*, 525-543.
- (213) Hachgenei, J. W.; Angelici, R. J. *Angew. Chem. Int. Edit.* **1987**, *26*, 909-910.
- (214) Arce, A. J.; De Sanctis, Y.; Karam, A.; Deeming, A. J. *Angew. Chem. Int. Edit.* **1994**, *33*, 1381-1383.
- (215) Cope, A. C. *J. Am. Chem. Soc.* **1935**, *57*, 2238-2240.
- (216) Kirmse, W. *Angew. Chem. Int. Edit.* **2004**, *43*, 1767-1769.
- (217) Jackson, J. D.; Villa, S. J.; Bacon, D. S.; Pike, R. D.; Carpenter, G. B. *Organometallics* **1994**, *13*, 3972-3980.

Appendix

Appendix I: Crystal structure report for cobalt cluster **61**

STRUCTURE REPORT

XCL Code: JMS1523

Date: 17 November 2017

Compound: $[\text{Co}_4(\text{Si}^i\text{Pr})_4(\text{NPET}_3)_4]$

Formula: $\text{C}_{36}\text{H}_{88}\text{Co}_4\text{N}_4\text{P}_4\text{S}_4$

Supervisor: J. M. Stryker

Crystallographer: M. J. Ferguson

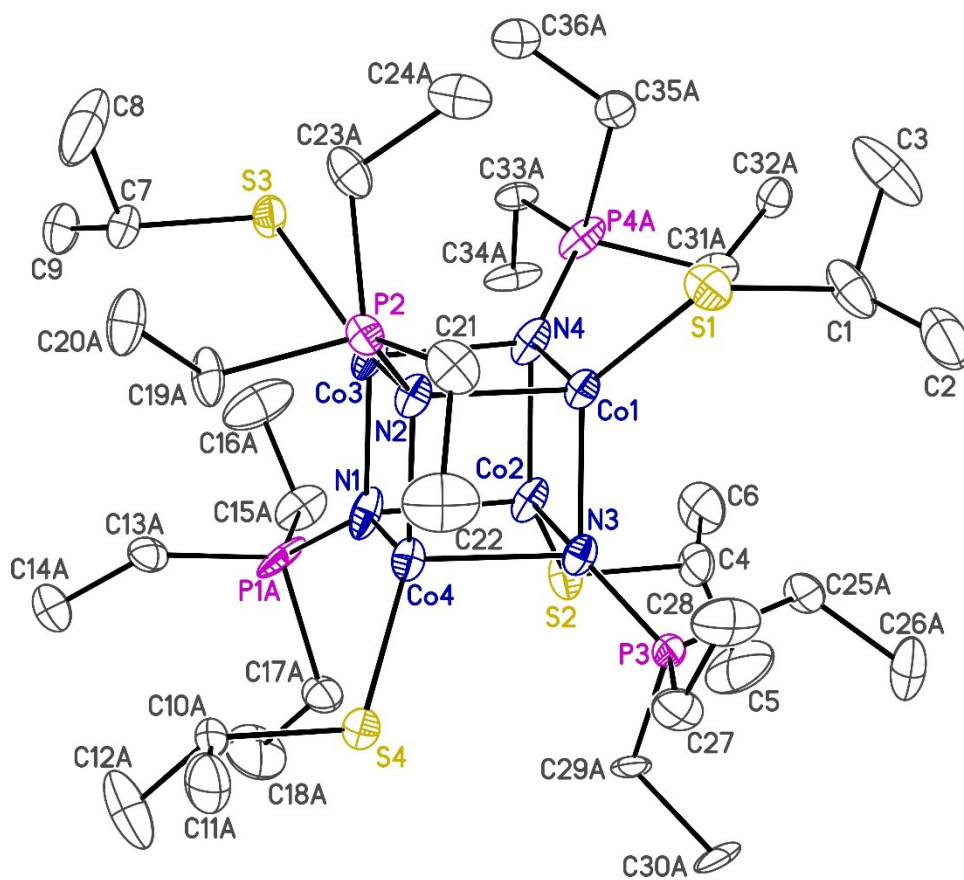
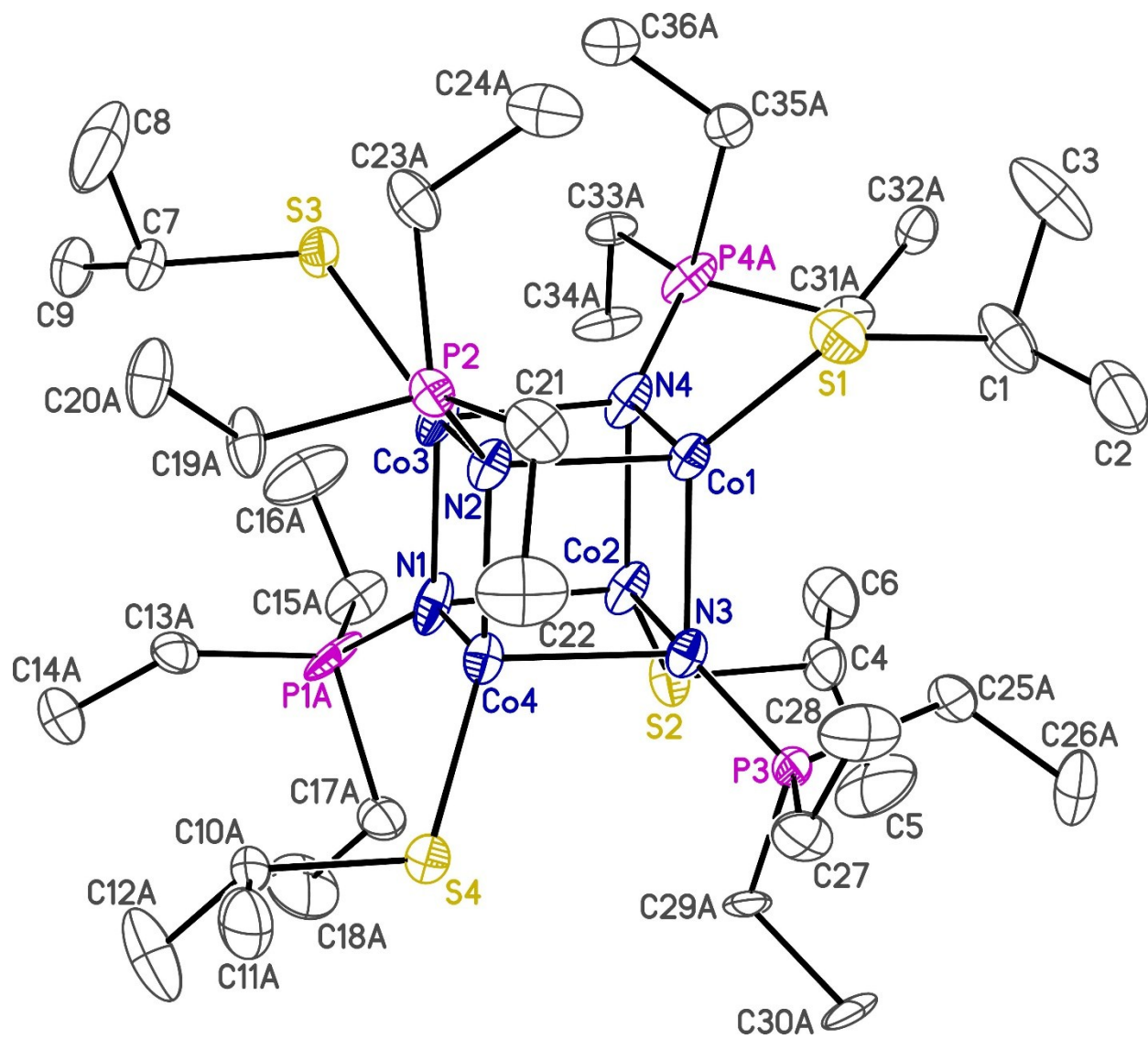


Figure Legends

- Figure 1.** Perspective view of the $[\text{Co}_4(\text{Si}^i\text{Pr})_4(\text{NPEt}_3)_4]$ molecule showing the atom labelling scheme. Non-hydrogen atoms are represented by Gaussian ellipsoids at the 30% probability level. Only one orientation of the disordered groups is shown for clarity. Hydrogen atoms are not shown.
- Figure 2.** Same view of the molecule showing the alternate orientation for the disordered groups.



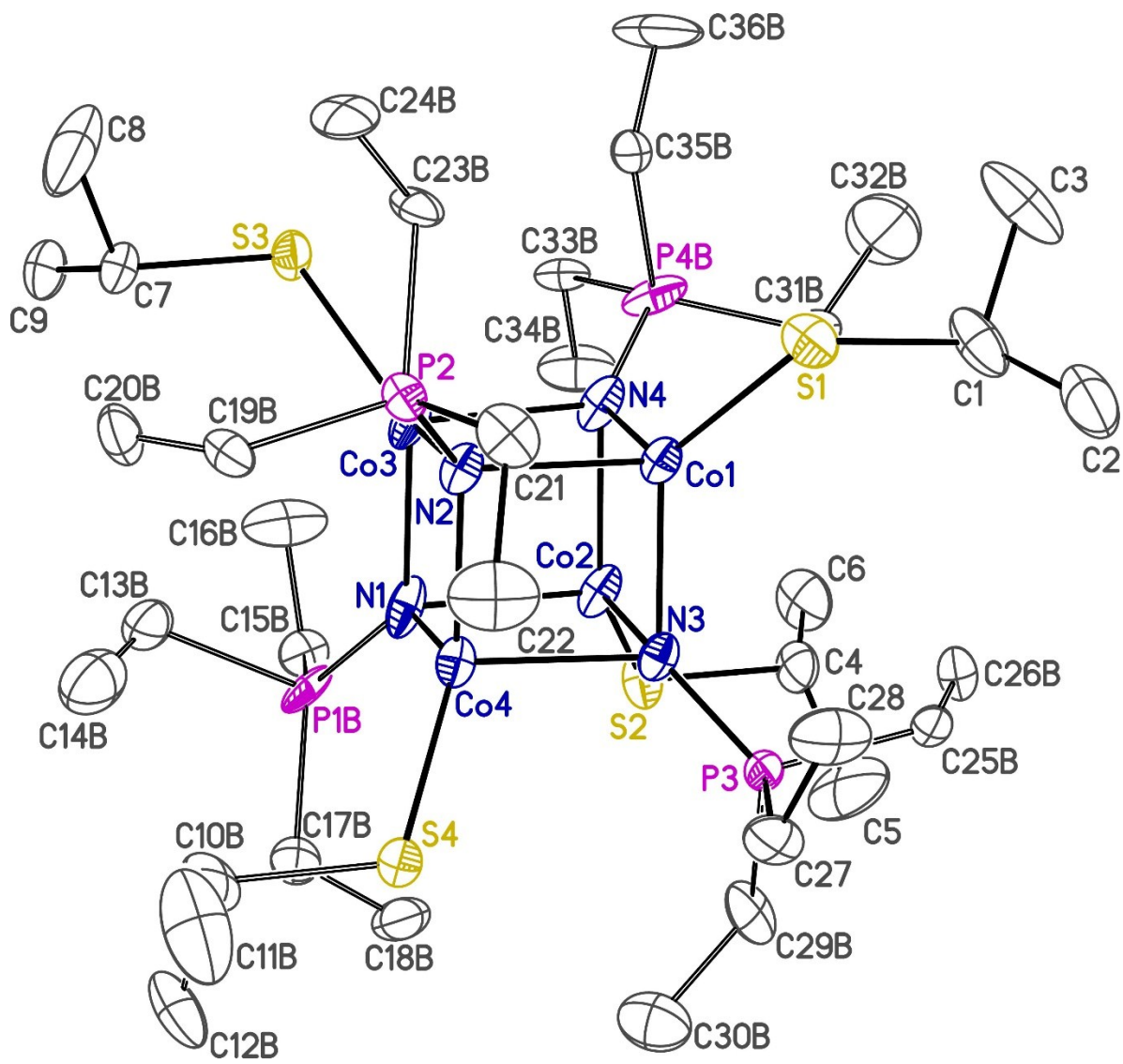


Table 1. Crystallographic Experimental Details*A. Crystal Data*

formula	C ₃₆ H ₈₈ Co ₄ N ₄ P ₄ S ₄
formula weight	1064.94
crystal dimensions (mm)	0.21 × 0.15 × 0.08
crystal system	triclinic
space group	$P\bar{1}$ (No. 2)
unit cell parameters ^a	
<i>a</i> (Å)	11.3112(7)
<i>b</i> (Å)	12.2885(7)
<i>c</i> (Å)	19.9296(12)
<i>α</i> (deg)	77.1442(7)
<i>β</i> (deg)	89.4206(8)
<i>γ</i> (deg)	76.1679(7)
<i>V</i> (Å ³)	2619.7(3)
<i>Z</i>	2
ρ_{calcd} (g cm ⁻³)	1.350
μ (mm ⁻¹)	1.554

B. Data Collection and Refinement Conditions

diffractometer	Bruker D8/APEX II CCD ^b
radiation (λ [Å])	graphite-monochromated Mo K α (0.71073)
temperature (°C)	-100
scan type	ω scans (0.3°) (20 s exposures)
data collection 2θ limit (deg)	52.88
total data collected	10744 ($-14 \leq h \leq 14$, $-14 \leq k \leq 15$, $0 \leq l \leq 24$)
independent reflections	10744 ($R_{\text{int}} = 0.0524$)
number of observed reflections (<i>NO</i>)	7840 [$F_o^2 \geq 2\sigma(F_o^2)$]
structure solution method	intrinsic phasing (<i>SHELXT-2014</i> ^c)
refinement method	full-matrix least-squares on F^2 (<i>SHELXL-2014</i> ^d)
absorption correction method	multi-scan (<i>TWINABS</i>)
range of transmission factors	0.7453–0.6305
data/restraints/parameters	10744 / 439 ^e / 689
goodness-of-fit (<i>S</i>) ^f [all data]	1.096
final <i>R</i> indices ^g	
<i>R</i> ₁ [$F_o^2 \geq 2\sigma(F_o^2)$]	0.0438
<i>wR</i> ₂ [all data]	0.1185
largest difference peak and hole	0.801 and -0.605 e Å ⁻³

(continued)

Table 1. Crystallographic Experimental Details (continued)

^aObtained from least-squares refinement of 8599 reflections with $4.34^\circ < 2\theta < 51.58^\circ$.

^bPrograms for diffractometer operation, data collection, data reduction and absorption correction were those supplied by Bruker. The crystal used for data collection was found to display non-merohedral twinning. Both components of the twin were indexed with the program *CELL_NOW* (Bruker AXS Inc., Madison, WI, 2004). The second twin component can be related to the first component by 180° rotation about the [1 0 0] axis in real space and about the [1 0.256 0] axis in reciprocal space. Integrated intensities for the reflections from the two components were written into a *SHELXL-2016* HKLF 5 reflection file with the data integration program *SAINTE* (version 8.34A), using all reflection data (exactly overlapped, partially overlapped and non-overlapped). The refined value of the twin fraction (*SHELXL-2016* BASF parameter) was 0.3726(13).

^cSheldrick, G. M. *Acta Crystallogr.* **2015**, *A71*, 3–8. (*SHELXT-2014*)

^dSheldrick, G. M. *Acta Crystallogr.* **2015**, *C71*, 3–8. (*SHELXL-2016*)

^eThe disordered components of the Et₃PN ligands had the following bond lengths restrained by use of the *SHELXL SADI* instruction: P–C, P–N, and C–C; further, the rigid-bond restraint (**RIGU**) was applied to the Et₃P groups that included phosphorus atoms, P1A, P1B, P4A and P4B, and also to the ethyl groups that included carbon atoms C29A, C30A, C29B and C30B, in an effort to improve their respective anisotropic displacement parameters. Similarly, the disordered isopropylsulfide ligand had the S–C and C–C distances and displacement parameters restrained. In total, there were 253 **SADI** and 186 **RIGU** restraints applied during the refinement.

$$fS = [\sum w(F_o^2 - F_c^2)^2 / (n - p)]^{1/2} \quad (n = \text{number of data; } p = \text{number of parameters varied; } w = [\sigma^2(F_o^2) + (0.0642P)^2]^{-1} \text{ where } P = [\text{Max}(F_o^2, 0) + 2F_c^2]/3).$$

$$gR_1 = \sum ||F_o| - |F_c|| / \sum |F_o|; \quad wR_2 = [\sum w(F_o^2 - F_c^2)^2 / \sum w(F_o^4)]^{1/2}.$$

STRUCTURE REPORT

XCL Code: JMS1524

Date: 28 October 2015

Compound: $[\text{Co}_4(\text{SC}_6\text{H}_4\text{Me})_4(\text{NPEt}_3)_4]$

Formula: $\text{C}_{52}\text{H}_{88}\text{Co}_4\text{N}_4\text{P}_4\text{S}_4$

Supervisor: J. M. Stryker

Crystallographer: R. McDonald

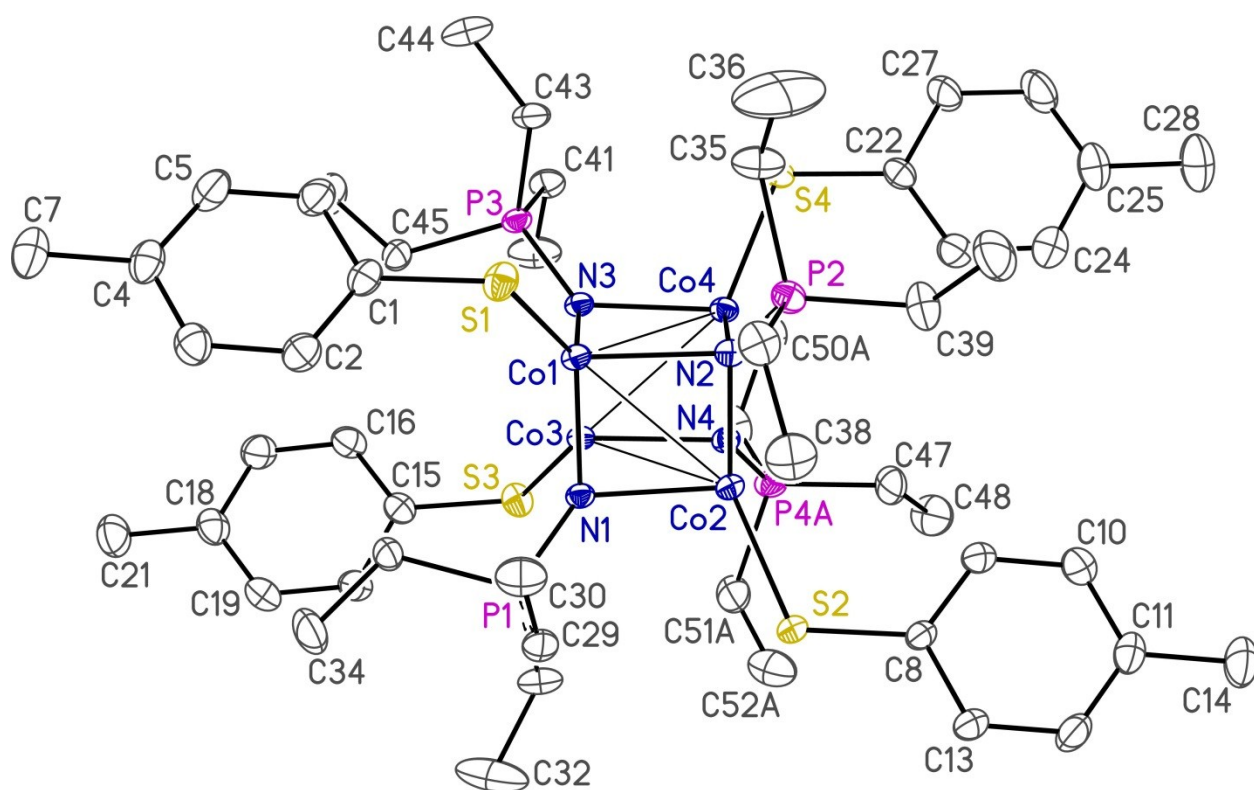
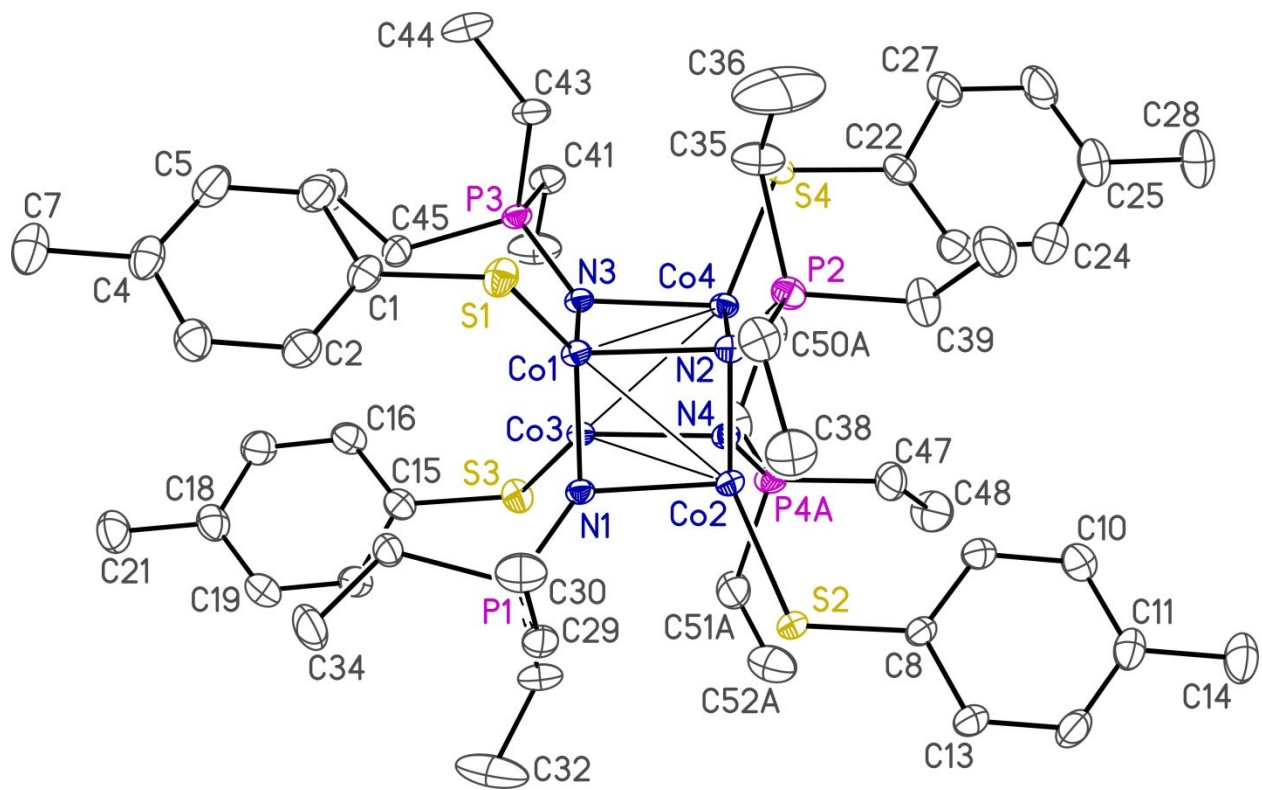


Figure Legends

- Figure 1.** Perspective view of the $[\text{Co}_4(\text{SC}_6\text{H}_4\text{Me})_4(\text{NPEt}_3)_4]$ molecule showing the atom labelling scheme. Non-hydrogen atoms are represented by Gaussian ellipsoids at the 30% probability level. Hydrogen atoms are not shown.
- Figure 2.** Alternate view of the molecule.



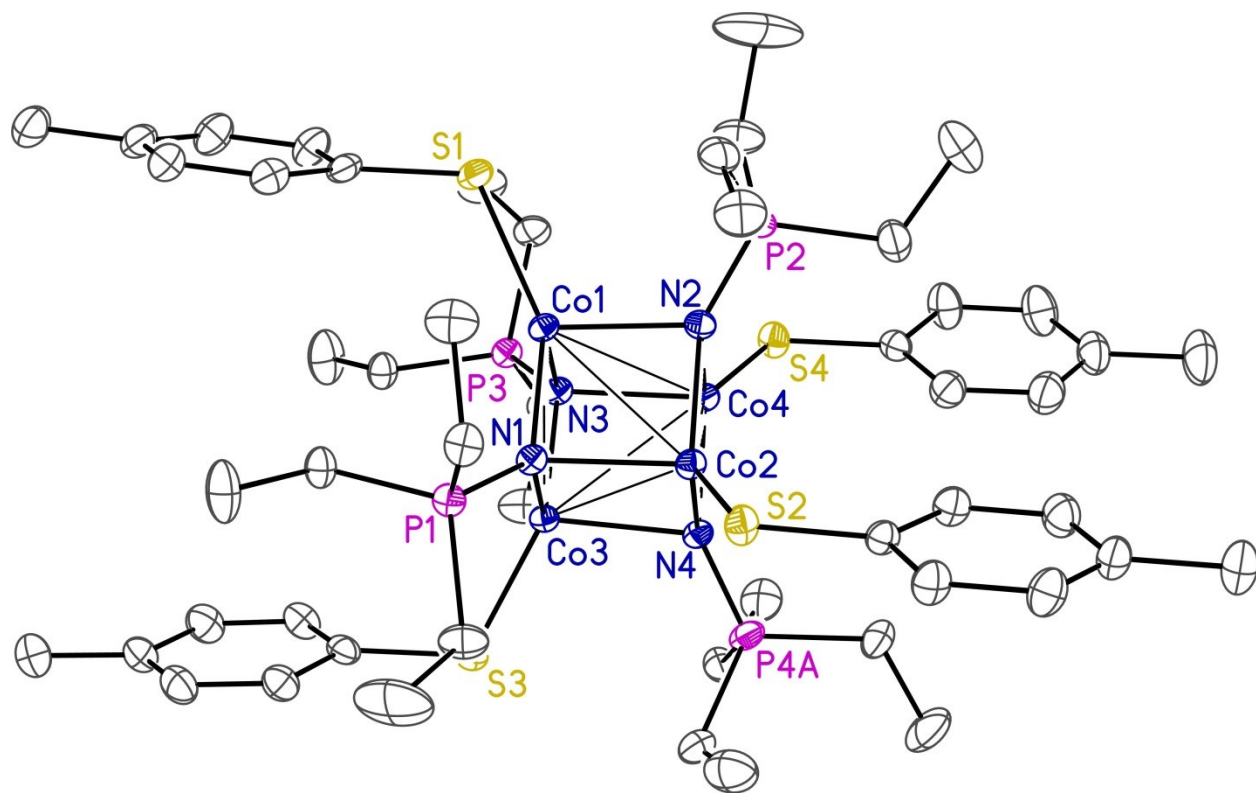


Table 1. Crystallographic Experimental Details*A. Crystal Data*

formula	C ₅₂ H ₈₈ Co ₄ N ₄ P ₄ S ₄
formula weight	1257.10
crystal dimensions (mm)	0.59 × 0.42 × 0.18
crystal system	triclinic
space group	$P\bar{1}$ (No. 2)
unit cell parameters ^a	
<i>a</i> (Å)	11.3098 (8)
<i>b</i> (Å)	15.6320 (11)
<i>c</i> (Å)	19.0569 (13)
<i>α</i> (deg)	67.6391 (7)
<i>β</i> (deg)	82.0196 (8)
<i>γ</i> (deg)	81.4431 (8)
<i>V</i> (Å ³)	3068.7 (4)
<i>Z</i>	2
ρ_{calcd} (g cm ⁻³)	1.361
μ (mm ⁻¹)	1.339

B. Data Collection and Refinement Conditions

diffractometer	Bruker D8/APEX II CCD ^b
radiation (λ [Å])	graphite-monochromated Mo K α (0.71073)
temperature (°C)	-100
scan type	ω scans (0.3°) (15 s exposures)
data collection 2θ limit (deg)	56.63
total data collected	28755 ($-15 \leq h \leq 15$, $-20 \leq k \leq 20$, $-24 \leq l \leq 25$)
independent reflections	14864 ($R_{\text{int}} = 0.0143$)
number of observed reflections (<i>NO</i>)	13015 [$F_o^2 \geq 2\sigma(F_o^2)$]
structure solution method	intrinsic phasing (<i>SHELXT-2014</i> ^c)
refinement method	full-matrix least-squares on F^2 (<i>SHELXL-2014</i> ^d)
absorption correction method	Gaussian integration (face-indexed)
range of transmission factors	0.8099–0.5668
data/restraints/parameters	14864 / 8 ^e / 640
goodness-of-fit (<i>S</i>) ^f [all data]	1.054
final <i>R</i> indices ^g	
<i>R</i> ₁ [$F_o^2 \geq 2\sigma(F_o^2)$]	0.0351
<i>wR</i> ₂ [all data]	0.1008
largest difference peak and hole	1.104 and -0.592 e Å ⁻³

(continued)

Table 1. Crystallographic Experimental Details (continued)

^aObtained from least-squares refinement of 9934 reflections with $4.38^\circ < 2\theta < 54.76^\circ$.

^bPrograms for diffractometer operation, data collection, data reduction and absorption correction were those supplied by Bruker.

^cSheldrick, G. M. *Acta Crystallogr.* **2015**, *A71*, 3–8.

^dSheldrick, G. M. *Acta Crystallogr.* **2015**, *C71*, 3–8.

^eThe following constraints were applied to distances involving atoms within the disordered triethylphosphoranimide group: (a) $d(\text{P4B}-\text{C49B}) = d(\text{P4B}-\text{C51B}) = 1.82(1) \text{ \AA}$; (b) $d(\text{C51A}-\text{C52A}) = d(\text{C49B}-\text{C50B}) = d(\text{C51B}-\text{C52B}) = 1.52(1) \text{ \AA}$; (c) $d(\text{P4B}\cdots\text{C50B}) = d(\text{P4B}\cdots\text{C52B}) = 2.85(1) \text{ \AA}$; (d) $d(\text{H42B}\cdots\text{H50F}) \geq 2.10(1) \text{ \AA}$.

$fS = [\sum w(F_o^2 - F_c^2)^2 / (n - p)]^{1/2}$ (n = number of data; p = number of parameters varied; $w = [\sigma^2(F_o^2) + (0.0595P)^2 + 1.2985P]^{-1}$ where $P = [\text{Max}(F_o^2, 0) + 2F_c^2]/3$).

$gR_1 = \sum ||F_o| - |F_c|| / \sum |F_o|$; $wR_2 = [\sum w(F_o^2 - F_c^2)^2 / \sum w(F_o^4)]^{1/2}$.

STRUCTURE REPORT

XCL Code: JMS1637

Date: 18 October 2016

Compound: $[\text{Ni}_4(\text{S}^i\text{Pr})_4(\text{NPEt}_3)_4]$

Formula: $\text{C}_{36}\text{H}_{88}\text{N}_4\text{Ni}_4\text{P}_4\text{S}_4$

Supervisor: J. M. Stryker

Crystallographer: R. McDonald

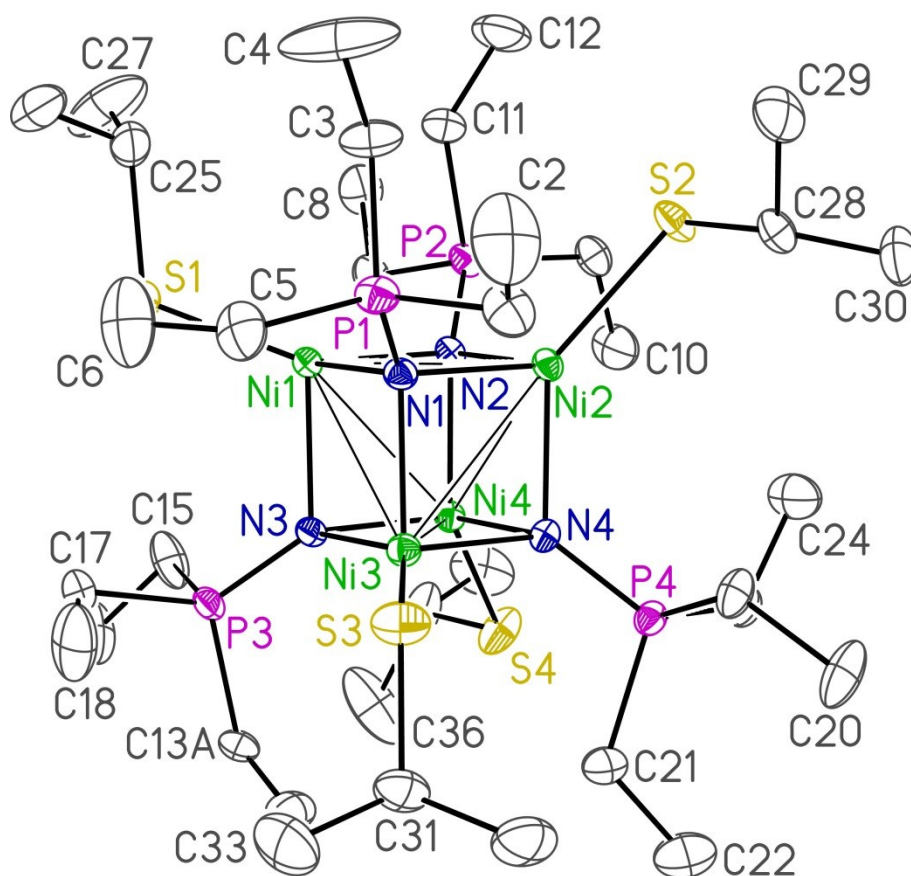
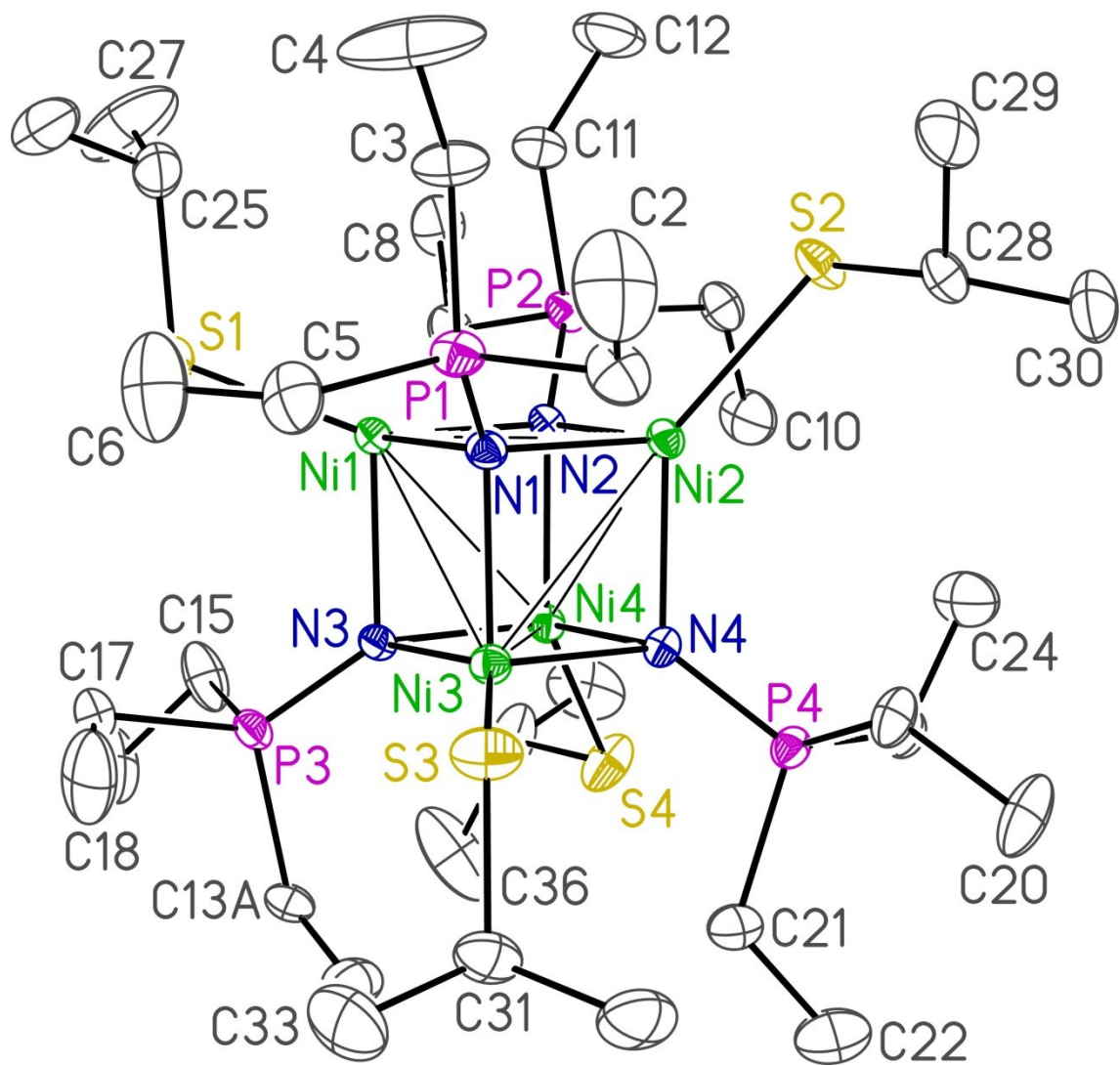


Figure Legends

- Figure 1.** Perspective view of the $[\text{Ni}_4(\text{S}^i\text{Pr})_4(\text{NPEt}_3)_4]$ molecule showing the atom labelling scheme. Non-hydrogen atoms are represented by Gaussian ellipsoids at the 30% probability level. Hydrogen atoms are not shown.
- Figure 2.** Alternate view of the molecule.



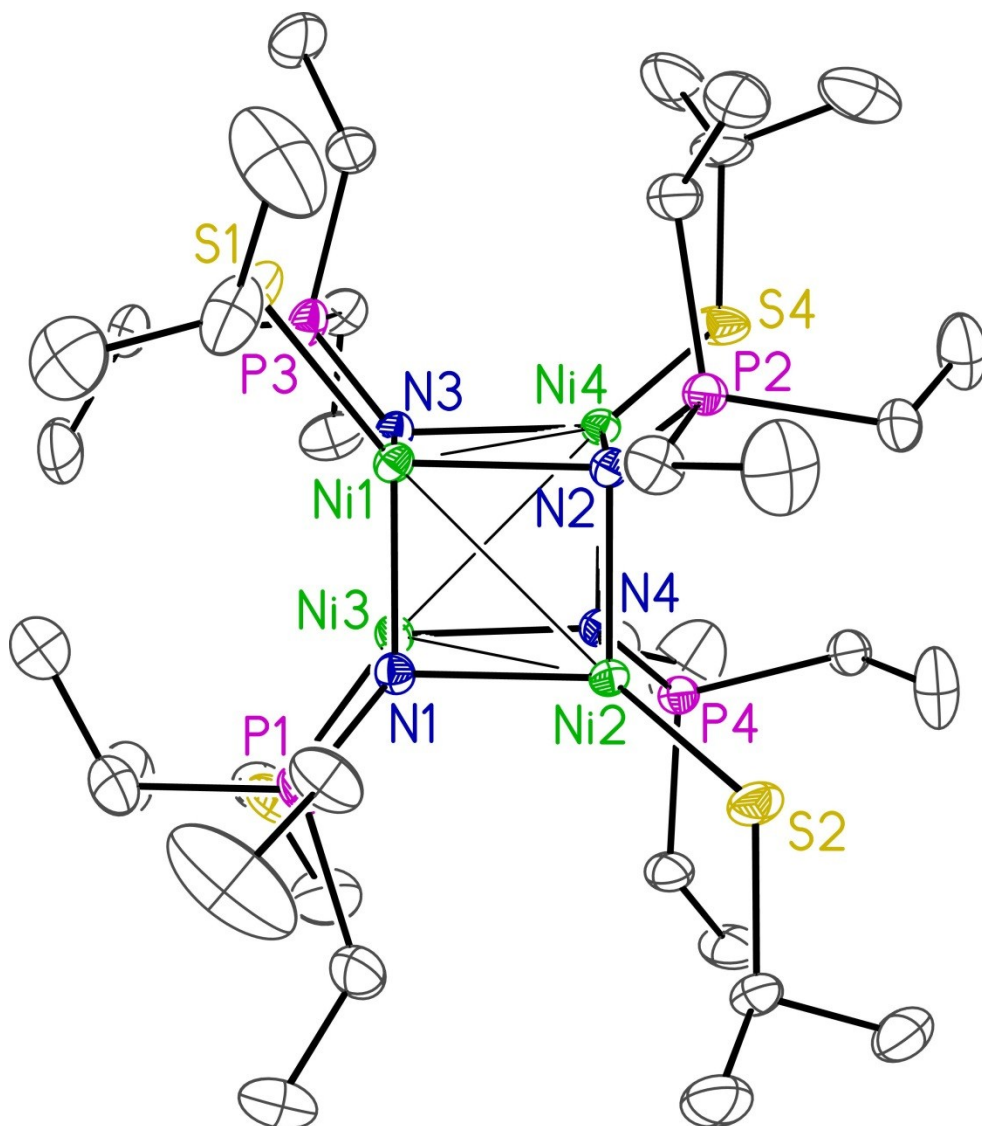


Table 1. Crystallographic Experimental Details*A. Crystal Data*

formula	C ₃₆ H ₈₈ N ₄ Ni ₄ P ₄ S ₄
formula weight	1064.06
crystal dimensions (mm)	0.16 × 0.14 × 0.07
crystal system	triclinic
space group	<i>P</i> $\bar{1}$ (No. 2)
unit cell parameters ^a	
<i>a</i> (Å)	11.6514 (2)
<i>b</i> (Å)	11.8624 (2)
<i>c</i> (Å)	20.3983 (4)
α (deg)	96.0579 (12)
β (deg)	104.6906 (11)
γ (deg)	102.7828 (11)
<i>V</i> (Å ³)	2620.23 (8)
<i>Z</i>	2
ρ_{calcd} (g cm ⁻³)	1.349
μ (mm ⁻¹)	4.460

B. Data Collection and Refinement Conditions

diffractometer	Bruker D8/APEX II CCD ^b
radiation (λ [Å])	Cu K α (1.54178) (microfocus source)
temperature (°C)	-100
scan type	ω and ϕ scans (1.0°) (5 s exposures)
data collection 2θ limit (deg)	148.15
total data collected	217159 ($-14 \leq h \leq 14$, $-13 \leq k \leq 14$, $-25 \leq l \leq 25$)
independent reflections	10211 ($R_{\text{int}} = 0.1252$)
number of observed reflections (<i>NO</i>)	8402 [$F_o^2 \geq 2\sigma(F_o^2)$]
structure solution method	direct methods/dual space (<i>SHELXD</i> ^c)
refinement method	full-matrix least-squares on F^2 (<i>SHELXL-2014</i> ^d)
absorption correction method	multi-scan (<i>TWINABS</i>)
range of transmission factors	0.6495–0.4903
data/restraints/parameters	10211 / 2 ^e / 478
goodness-of-fit (<i>S</i>) ^f [all data]	1.040
final <i>R</i> indices ^g	
<i>R</i> ₁ [$F_o^2 \geq 2\sigma(F_o^2)$]	0.0513
<i>wR</i> ₂ [all data]	0.1512
largest difference peak and hole	1.124 and -0.840 e Å ⁻³

(continued)

Table 1. Crystallographic Experimental Details (continued)

^aObtained from least-squares refinement of 9781 reflections with $8.10^\circ < 2\theta < 146.78^\circ$.

^bPrograms for diffractometer operation, data collection, data reduction and absorption correction were those supplied by Bruker. The crystal used for data collection was found to display non-merohedral twinning. Both components of the twin were indexed with the program *CELL_NOW* (Bruker AXS Inc., Madison, WI, 2004). The second twin component can be related to the first component by a 3.5° rotation about the $[1 \ -0.45 \ -0.35]$ axis in real space and about the $[-0.9 \ 0.45 \ 1]$ axis in reciprocal space. Integrated intensities for the reflections from the two components were written into a *SHELXL-2014* HKLF 5 reflection file with the data integration program *SAINTE* (version 8.37A), using all reflection data (exactly overlapped, partially overlapped and non-overlapped). The refined value of the twin fraction (*SHELXL-2014* BASF parameter) was 0.456(2).

^cSchneider, T. R.; Sheldrick, G. M. *Acta Crystallogr.* **2002**, *D58*, 1772-1779.

^dSheldrick, G. M. *Acta Crystallogr.* **2015**, *C71*, 3–8.

^eDistances involving carbons belonging to components of a disordered ethyl group were constrained to be equal (within 0.03 Å) during refinement: $d(\text{P3-C13A}) = d(\text{P3-C13B})$; $d(\text{C13A-C14A}) = d(\text{C13B-C14B})$.

$fS = [\sum w(F_o^2 - F_c^2)^2 / (n - p)]^{1/2}$ (n = number of data; p = number of parameters varied; $w = [\sigma^2(F_o^2) + (0.0857P)^2 + 2.0314P]^{-1}$ where $P = [\text{Max}(F_o^2, 0) + 2F_c^2]/3$).

$gR_1 = \sum ||F_o| - |F_c|| / \sum |F_o|$; $wR_2 = [\sum w(F_o^2 - F_c^2)^2 / \sum w(F_o^4)]^{1/2}$.

STRUCTURE REPORT

XCL Code: JMS1725

Date: 23 January 2018

Compound: {Hydridobis(9-borabicyclo[3.3.1]nonan-9-yl)}triethylphosphoranimine

Formula: C₂₂H₄₄B₂NP

Supervisor: J. M. Stryker

Crystallographer: R. McDonald

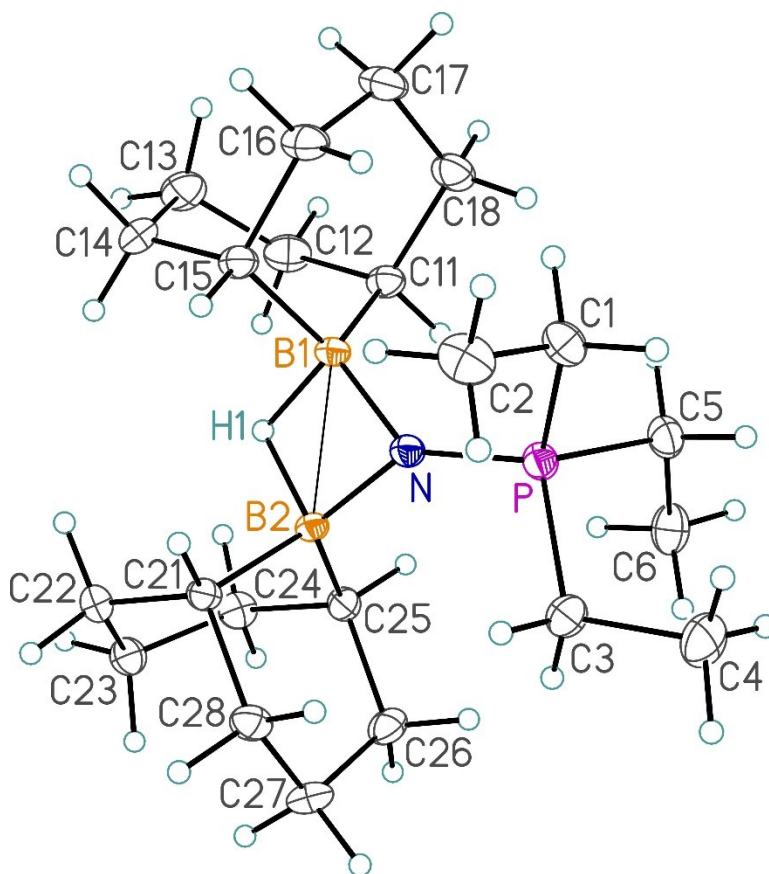
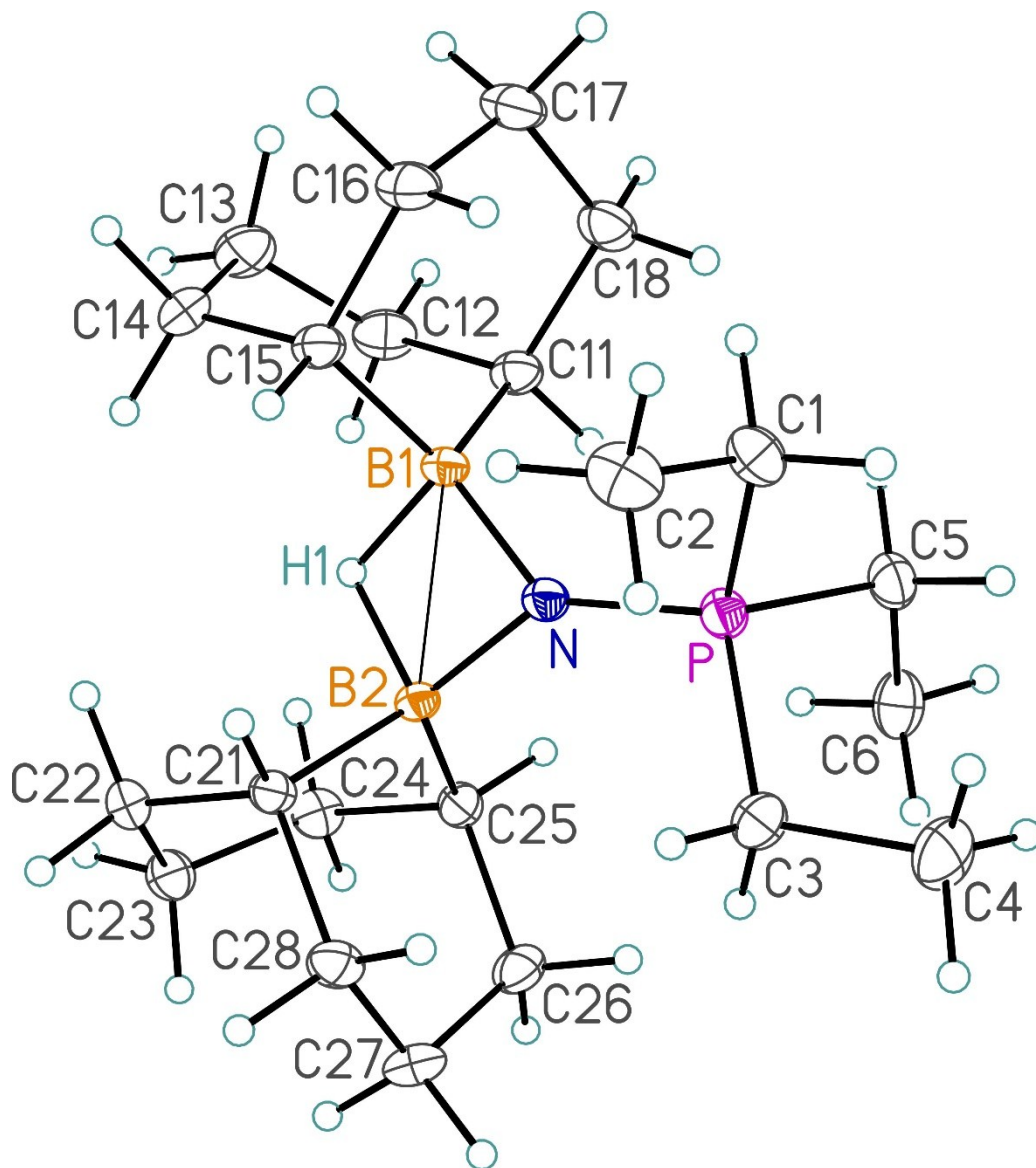


Figure Legends

- Figure 1.** Perspective view of the {hydridobis(9-borabicyclo[3.3.1]nonan-9-yl)}triethylphosphoranimine molecule showing the atom labelling scheme. Non-hydrogen atoms are represented by Gaussian ellipsoids at the 30% probability level. Hydrogen atoms are shown with arbitrarily small thermal parameters.
- Figure 2.** Alternate view of the molecule. All hydrogen atoms except for H1 have been omitted.



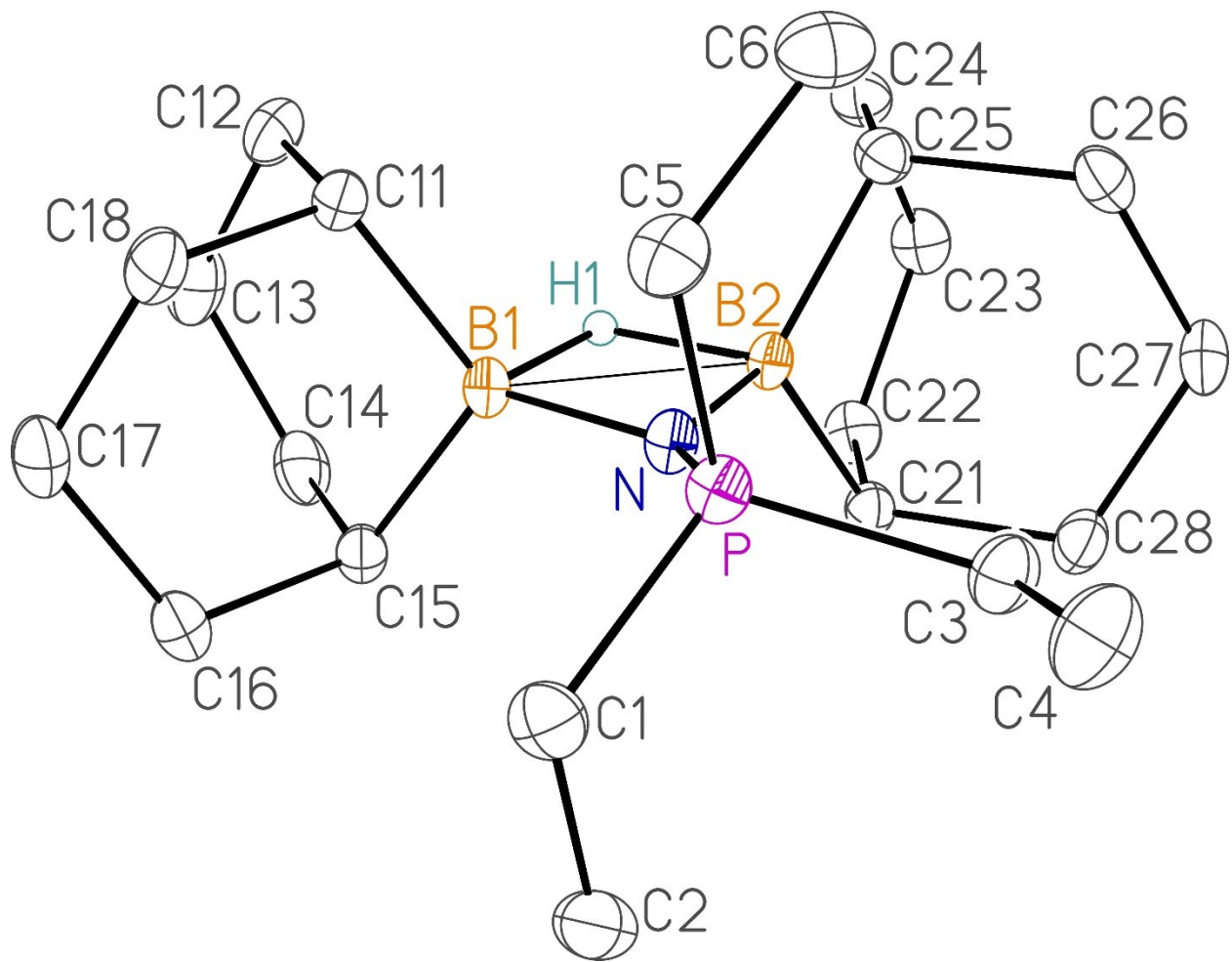


Table 1. Crystallographic Experimental Details*A. Crystal Data*

formula	C ₂₂ H ₄₄ B ₂ NP
formula weight	375.17
crystal dimensions (mm)	0.43 × 0.25 × 0.09
crystal system	triclinic
space group	$P\bar{1}$ (No. 2)
unit cell parameters ^a	
<i>a</i> (Å)	10.1753(12)
<i>b</i> (Å)	10.3881(12)
<i>c</i> (Å)	13.3146(16)
α (deg)	68.4938(14)
β (deg)	68.2605(14)
γ (deg)	61.0070(14)
<i>V</i> (Å ³)	1112.7(2)
<i>Z</i>	2
ρ_{calcd} (g cm ⁻³)	1.120
μ (mm ⁻¹)	0.130

B. Data Collection and Refinement Conditions

diffractometer	Bruker D8/APEX II CCD ^b
radiation (λ [Å])	graphite-monochromated Mo K α (0.71073)
temperature (°C)	-100
scan type	ω scans (0.3°) (20 s exposures)
data collection 2θ limit (deg)	55.42
total data collected	9879 ($-13 \leq h \leq 13$, $-13 \leq k \leq 13$, $-17 \leq l \leq 17$)
independent reflections	5155 ($R_{\text{int}} = 0.0344$)
number of observed reflections (<i>NO</i>)	3767 [$F_o^2 \geq 2\sigma(F_o^2)$]
structure solution method	intrinsic phasing (<i>SHELXT-2014</i> ^c)
refinement method	full-matrix least-squares on F^2 (<i>SHELXL-2014</i> ^d)
absorption correction method	Gaussian integration (face-indexed)
range of transmission factors	1.0000–0.8455
data/restraints/parameters	5155 / 0 / 239
goodness-of-fit (<i>S</i>) ^e [all data]	1.048
final <i>R</i> indices ^f	
<i>R</i> ₁ [$F_o^2 \geq 2\sigma(F_o^2)$]	0.0512
<i>wR</i> ₂ [all data]	0.1447
largest difference peak and hole	0.351 and -0.496 e Å ⁻³

(continued)

Table 1. Crystallographic Experimental Details (continued)

^aObtained from least-squares refinement of 2787 reflections with $4.60^\circ < 2\theta < 53.42^\circ$.

^bPrograms for diffractometer operation, data collection, data reduction and absorption correction were those supplied by Bruker.

^cSheldrick, G. M. *Acta Crystallogr.* **2015**, *A71*, 3–8.

^dSheldrick, G. M. *Acta Crystallogr.* **2015**, *C71*, 3–8.

^e $S = [\Sigma w(F_o^2 - F_c^2)^2 / (n - p)]^{1/2}$ (n = number of data; p = number of parameters varied; $w = [\sigma^2(F_o^2) + (0.0675P)^2 + 0.2031P]^{-1}$ where $P = [\text{Max}(F_o^2, 0) + 2F_c^2]/3$).

^f $R_1 = \Sigma ||F_o| - |F_c|| / \Sigma |F_o|$; $wR_2 = [\Sigma w(F_o^2 - F_c^2)^2 / \Sigma w(F_o^4)]^{1/2}$.

PRELIMINARY STRUCTURE REPORT – NOT FOR PUBLICATION

XCL Code: JMS1615

Date: 13 February 2018

Compound: [Co₄(OBO₂C₂Me₄)₄(NPt₃)₄]

Formula: C₄₈H₁₀₈B₄Co₄N₄O₁₂P₄

Supervisor: J. M. Stryker

Crystallographer: R. McDonald

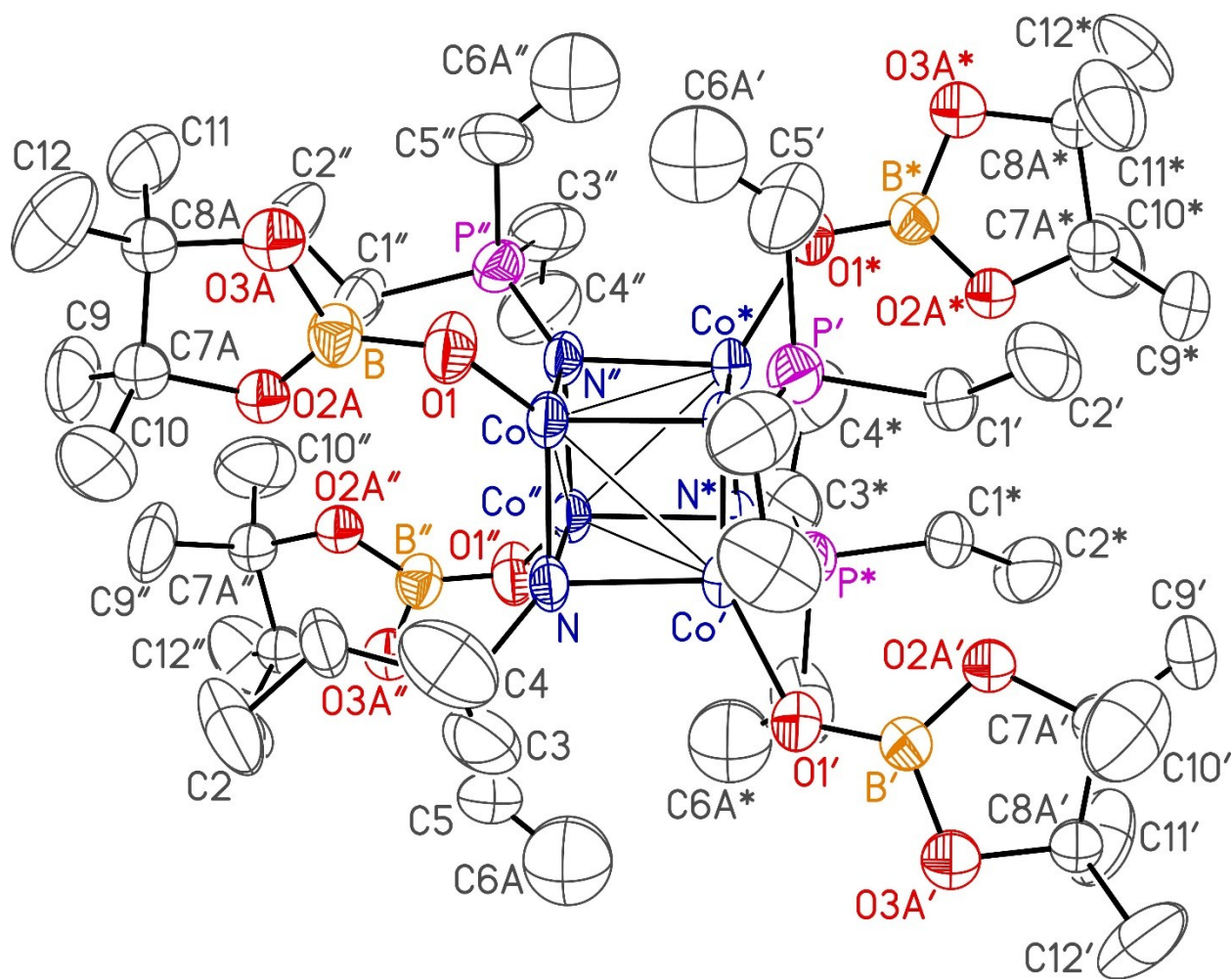
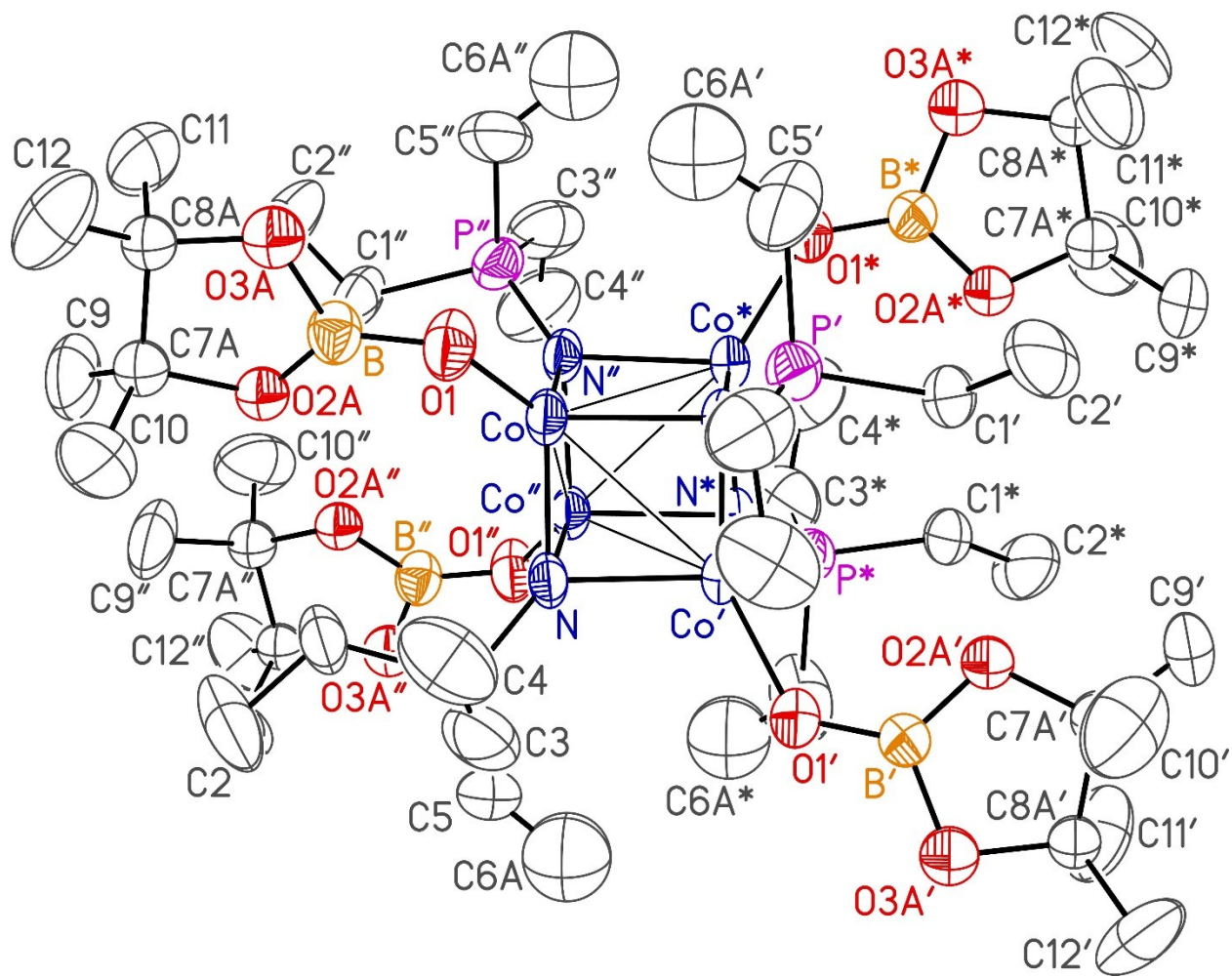


Figure Legends

- Figure 1.** Perspective view of the $[\text{Co}_4(\text{OBO}_2\text{C}_2\text{Me}_4)_4(\text{NPEt}_3)_4]$ molecule showing the atom labelling scheme. Non-hydrogen atoms are represented by Gaussian ellipsoids at the 30% probability level. Hydrogen atoms are not shown. Primed atoms are related to unprimed ones via the crystallographic twofold rotational axis $(x, 1/4, 1/4)$. Double-primed atoms are related to unprimed ones via the crystallographic twofold axis $(0, y, 1/4)$. Starred (*) atoms are related to unstarred ones via the crystallographic twofold axis $(0, 1/4, z)$.
- Figure 2.** Alternate view of the molecule. The phosphine ethyl groups have been omitted.



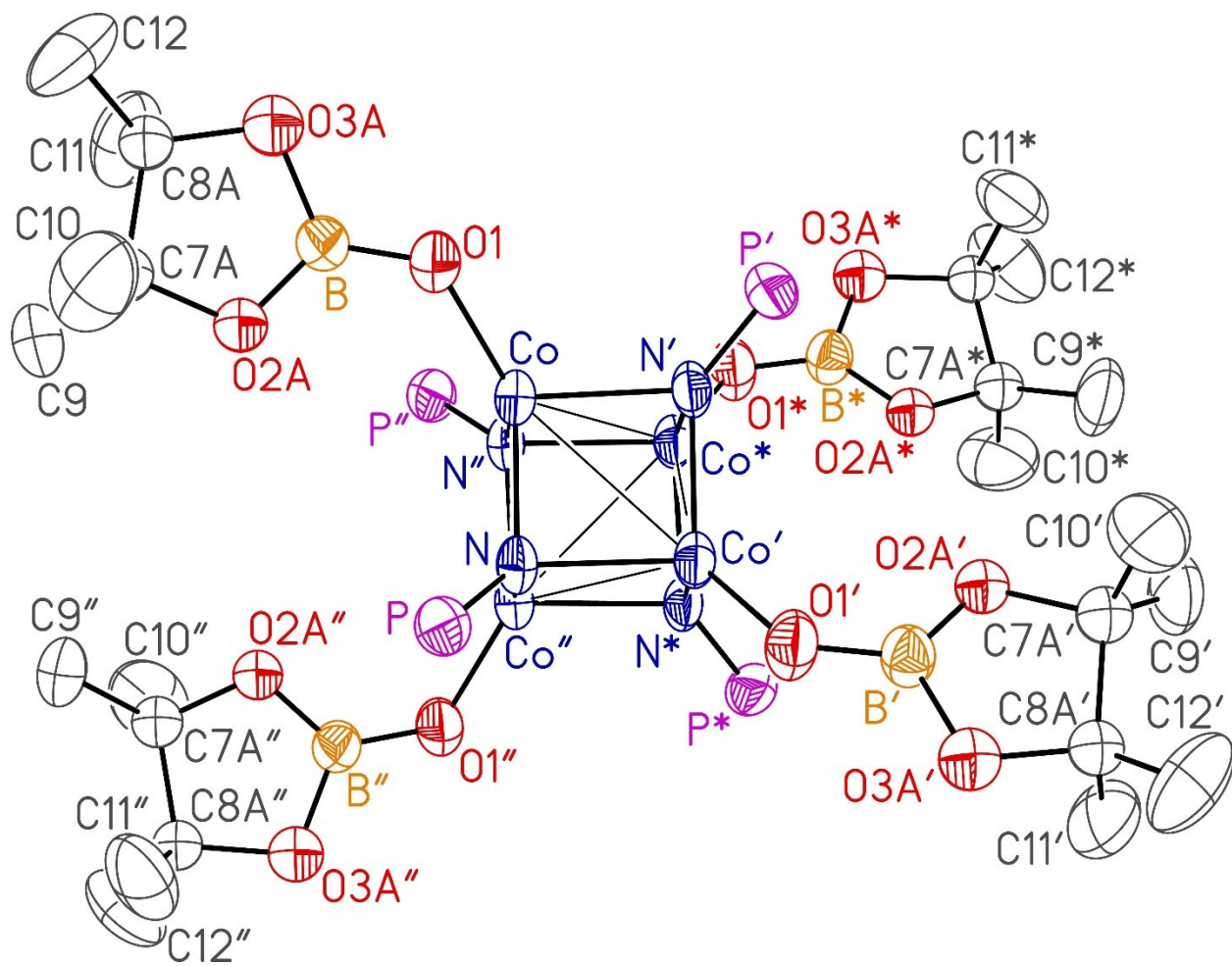


Table 1. Crystallographic Experimental Details

<i>A. Crystal Data</i>	
formula	C ₄₈ H ₁₀₈ B ₄ Co ₄ N ₄ O ₁₂ P ₄
formula weight	1336.22
crystal dimensions (mm)	0.23 × 0.12 × 0.06
crystal system	orthorhombic
space group	<i>Ccca</i> (No. 68)
unit cell parameters ^a	
<i>a</i> (Å)	19.9528(4)
<i>b</i> (Å)	30.0697(4)
<i>c</i> (Å)	11.0213(2)
<i>V</i> (Å ³)	6612.5(2)
<i>Z</i>	4
ρ_{calcd} (g cm ⁻³)	1.342
μ (mm ⁻¹)	9.074
<i>B. Data Collection and Refinement Conditions</i>	
diffractometer	Bruker D8/APEX II CCD ^b
radiation (λ [Å])	Cu K α (1.54178) (microfocus source)
temperature (°C)	-100
scan type	ω and ϕ scans (1.0°) (15 s exposures)
data collection 2θ limit (deg)	141.03
total data collected	20994 ($-24 \leq h \leq 24$, $-36 \leq k \leq 36$, $-13 \leq l \leq 13$)
independent reflections	3170 ($R_{\text{int}} = 0.0754$)
number of observed reflections (<i>NO</i>)	1993 [$F_o^2 \geq 2\sigma(F_o^2)$]
structure solution method	intrinsic phasing (<i>SHELXT-2014</i> ^c)
refinement method	full-matrix least-squares on F^2 (<i>SHELXL-2014</i> ^d)
absorption correction method	Gaussian integration (face-indexed)
range of transmission factors	0.7046–0.2451
data/restraints/parameters	3170 / 0 / 167
goodness-of-fit (<i>S</i>) ^e [all data]	1.056
final <i>R</i> indices ^f	
<i>R</i> ₁ [$F_o^2 \geq 2\sigma(F_o^2)$]	0.0794
<i>wR</i> ₂ [all data]	0.2562
largest difference peak and hole	1.086 and -0.488 e Å ⁻³

(continued)

Table 1. Crystallographic Experimental Details (continued)

^aObtained from least-squares refinement of 8465 reflections with $5.88^\circ < 2\theta < 138.58^\circ$.

^bPrograms for diffractometer operation, data collection, data reduction and absorption correction were those supplied by Bruker.

^cSheldrick, G. M. *Acta Crystallogr.* **2015**, *A71*, 3–8.

^dSheldrick, G. M. *Acta Crystallogr.* **2015**, *C71*, 3–8.

^e $S = [\Sigma w(F_o^2 - F_c^2)^2 / (n - p)]^{1/2}$ (n = number of data; p = number of parameters varied; $w = [\sigma^2(F_o^2) + (0.1416P)^2 + 11.4877P]^{-1}$ where $P = [\text{Max}(F_o^2, 0) + 2F_c^2]/3$).

^f $R_1 = \Sigma ||F_o| - |F_c|| / \Sigma |F_o|$; $wR_2 = [\Sigma w(F_o^2 - F_c^2)^2 / \Sigma w(F_o^4)]^{1/2}$.

STRUCTURE REPORT

XCL Code: JMS1726

Date: 6 February 2018

Compound: $[\text{Co}_4\text{Cl}_2(\text{SCPh}_3)_2(\text{NPEt}_3)_4]$

Formula: $\text{C}_{62}\text{H}_{90}\text{Cl}_2\text{Co}_4\text{N}_4\text{P}_4\text{S}_2$

Supervisor: J. M. Stryker

Crystallographer: R. McDonald

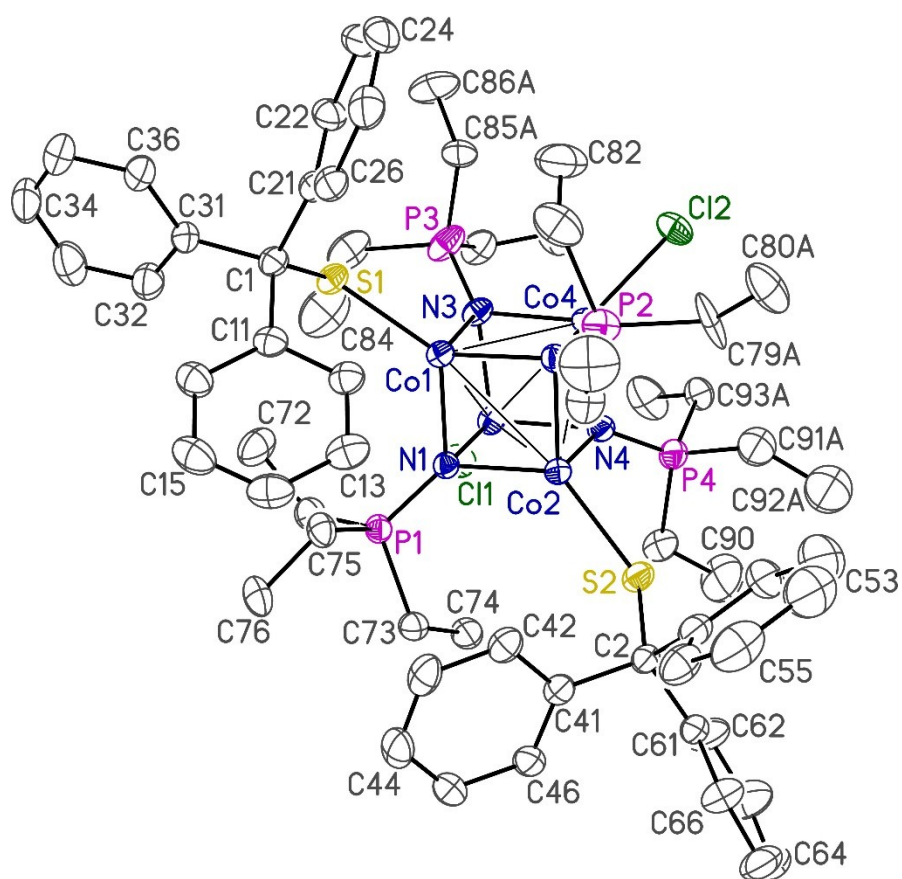
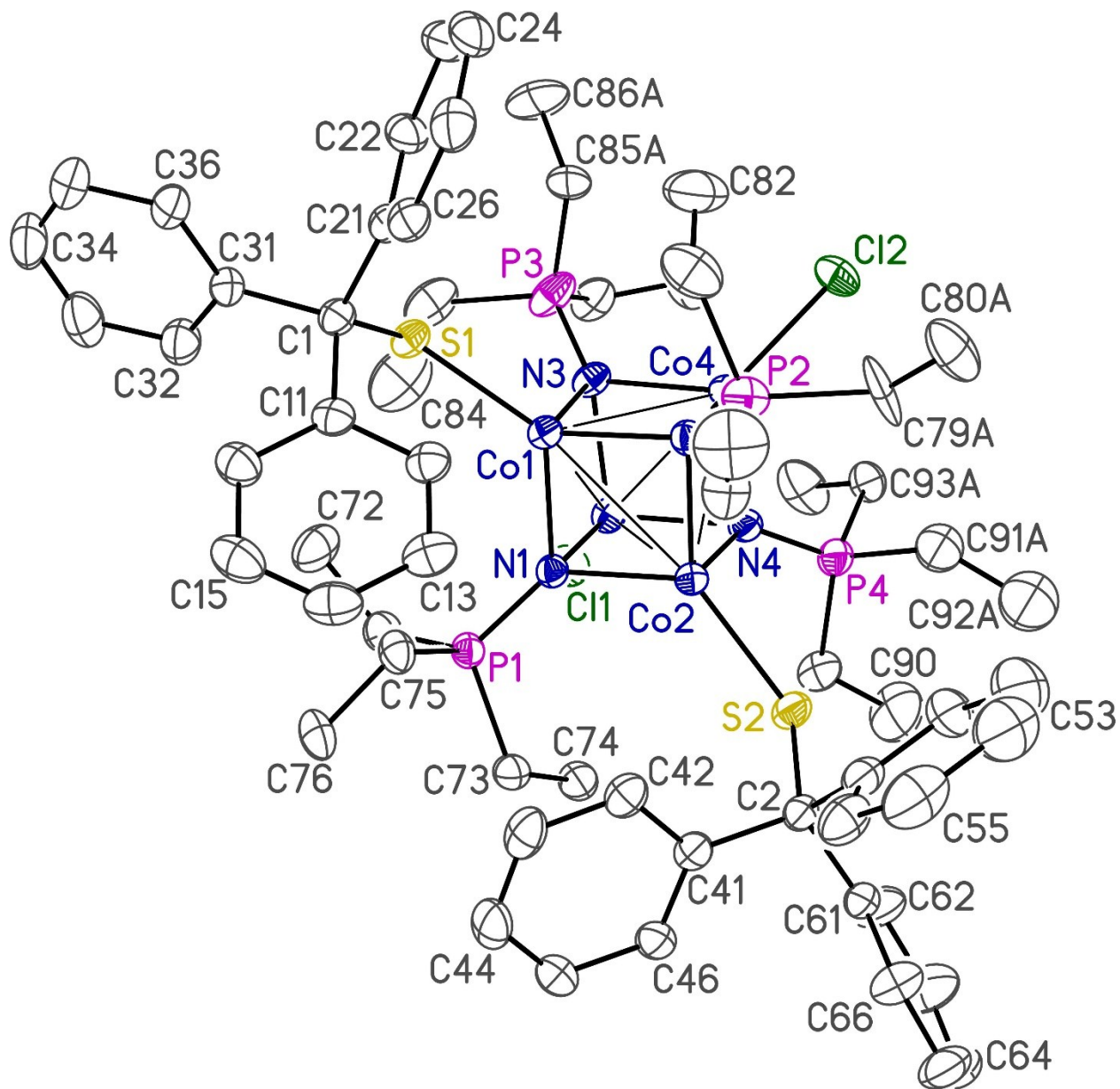
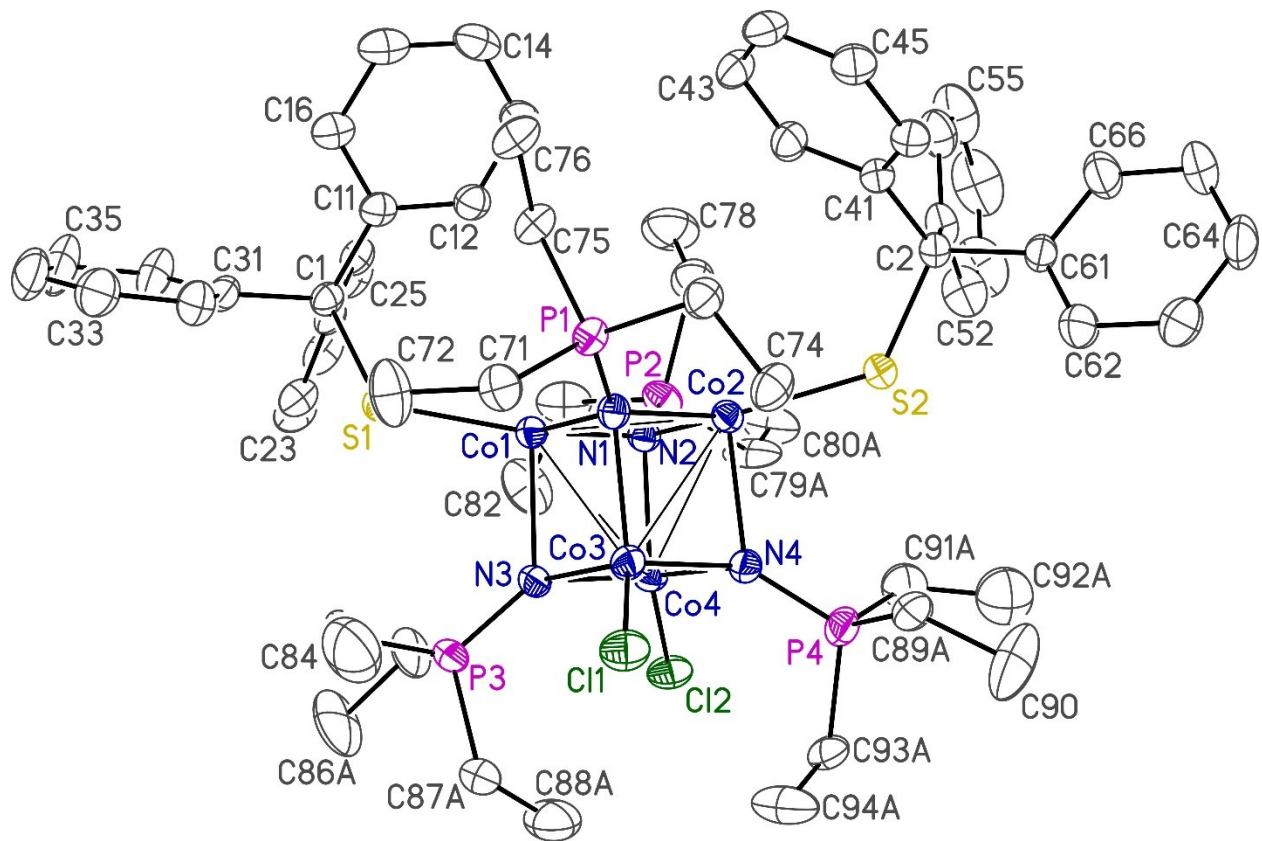


Figure Legends

- Figure 1.** Perspective view of the $[\text{Co}_4\text{Cl}_2(\text{SCPh}_3)_2(\text{NPEt}_3)_4]$ molecule showing the atom labelling scheme. Non-hydrogen atoms are represented by Gaussian ellipsoids at the 30% probability level. Hydrogen atoms are not shown.
- Figure 2.** Alternate view of the molecule.





List of Tables

- Table 1.** Crystallographic Experimental Details
- Table 2.** Atomic Coordinates and Equivalent Isotropic Displacement Parameters
- Table 3.** Selected Interatomic Distances
- Table 4.** Selected Interatomic Angles
- Table 5.** Torsional Angles
- Table 6.** Anisotropic Displacement Parameters
- Table 7.** Derived Atomic Coordinates and Displacement Parameters for Hydrogen Atoms

Table 1. Crystallographic Experimental Details*A. Crystal Data*

formula	C ₆₂ H ₉₀ Cl ₂ Co ₄ N ₄ P ₄ S ₂
formula weight	1385.99
crystal dimensions (mm)	0.41 × 0.32 × 0.18
crystal system	monoclinic
space group	<i>P</i> 2 ₁ / <i>c</i> (No. 14)
unit cell parameters ^a	
<i>a</i> (Å)	19.9270(11)
<i>b</i> (Å)	13.2584(8)
<i>c</i> (Å)	25.6507(15)
β (deg)	92.7739(8)
<i>V</i> (Å ³)	6769.0(7)
<i>Z</i>	4
ρ _{calcd} (g cm ⁻³)	1.360
μ (mm ⁻¹)	1.238

B. Data Collection and Refinement Conditions

diffractometer	Bruker D8/APEX II CCD ^b
radiation (λ [Å])	graphite-monochromated Mo Kα (0.71073)
temperature (°C)	-100
scan type	ω scans (0.3°) (45 s exposures)
data collection 2θ limit (deg)	52.76
total data collected	51359 (-24 ≤ <i>h</i> ≤ 24, -16 ≤ <i>k</i> ≤ 16, -31 ≤ <i>l</i> ≤ 31)
independent reflections	13824 (<i>R</i> _{int} = 0.0426)
number of observed reflections (<i>NO</i>)	10381 [<i>F</i> _o ² ≥ 2σ(<i>F</i> _o ²)]
structure solution method	direct methods/dual space (<i>SHELXD</i> ^c)
refinement method	full-matrix least-squares on <i>F</i> ² (<i>SHELXL-2014</i> ^d)
absorption correction method	Gaussian integration (face-indexed)
range of transmission factors	0.9271–0.7182
data/restraints/parameters	13824 / 12 ^e / 735
goodness-of-fit (<i>S</i>) ^f [all data]	1.027
final <i>R</i> indices ^g	
<i>R</i> ₁ [<i>F</i> _o ² ≥ 2σ(<i>F</i> _o ²)]	0.0515
<i>wR</i> ₂ [all data]	0.1511
largest difference peak and hole	1.446 and -0.745 e Å ⁻³

^aObtained from least-squares refinement of 9924 reflections with 4.42° < 2θ < 48.94°.

^bPrograms for diffractometer operation, data collection, data reduction and absorption correction were those supplied by Bruker.

(continued)

Table 1. Crystallographic Experimental Details (continued)

^cSchneider, T. R.; Sheldrick, G. M. *Acta Crystallogr.* **2002**, *D58*, 1772-1779.

^dSheldrick, G. M. *Acta Crystallogr.* **2015**, *C71*, 3–8.

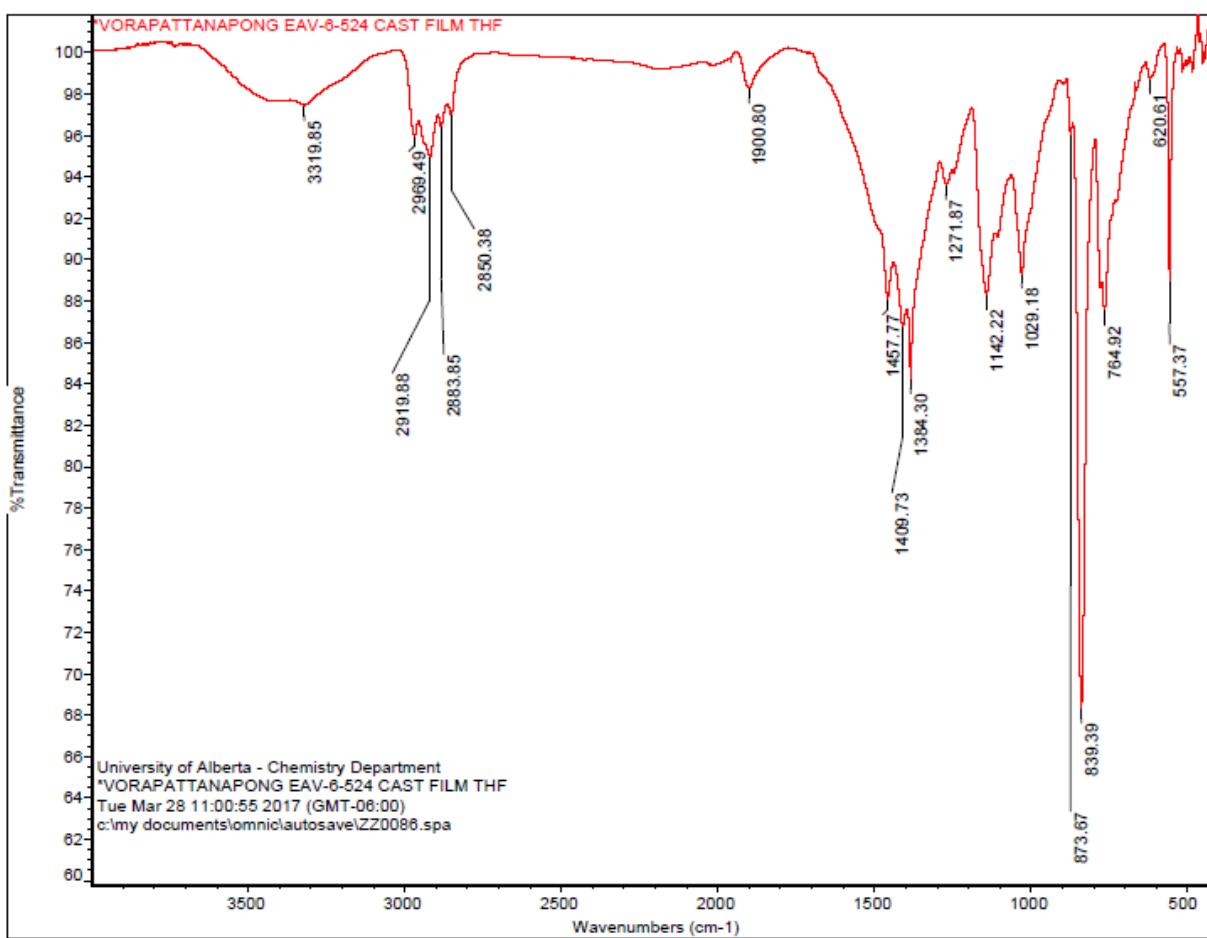
^eThe following distances involving disordered Pet3 ethyl groups were constrained during refinement: (a) $d(\text{P2-C79A}) = d(\text{P2-C79B}) = d(\text{P3-C85A}) = d(\text{P3-C85B}) = d(\text{P4-C91A}) = d(\text{P4-C91B}) = d(\text{P4-C93A}) = d(\text{P4-C93B}) = 1.82(1) \text{ \AA}$; (b) $d(\text{C85A-C86A}) = d(\text{C85B-C86B}) = d(\text{C91A-C92A}) = d(\text{C91B-C92B}) = 1.52(1) \text{ \AA}$.

^f $S = [\sum w(F_o^2 - F_c^2)^2 / (n - p)]^{1/2}$ (n = number of data; p = number of parameters varied; $w = [\sigma^2(F_o^2) + (0.0796P)^2 + 8.0010P]^{-1}$ where $P = [\text{Max}(F_o^2, 0) + 2F_c^2]/3$).

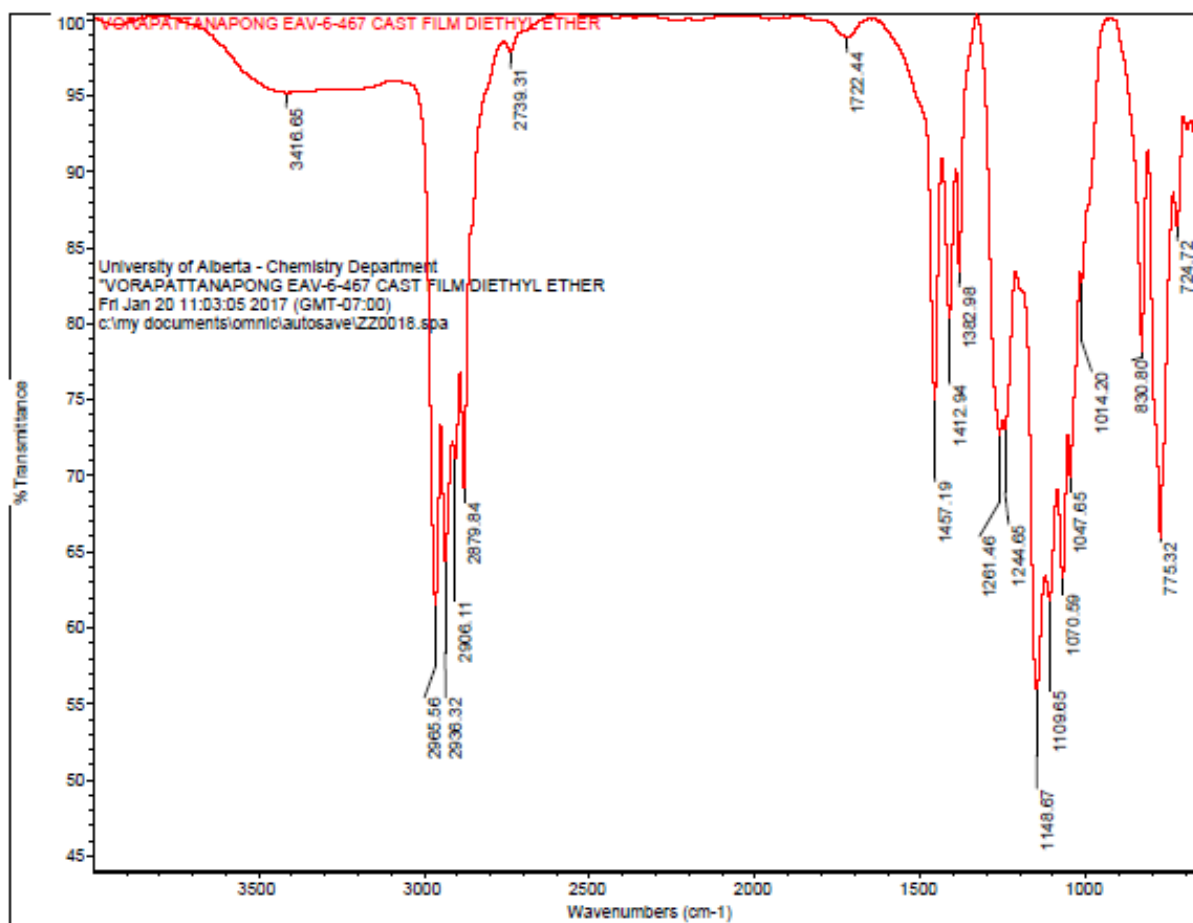
^g $R_1 = \sum ||F_o| - |F_c|| / \sum |F_o|$; $wR_2 = [\sum w(F_o^2 - F_c^2)^2 / \sum w(F_o^4)]^{1/2}$.

Appendix VII: FT-IR Spectra

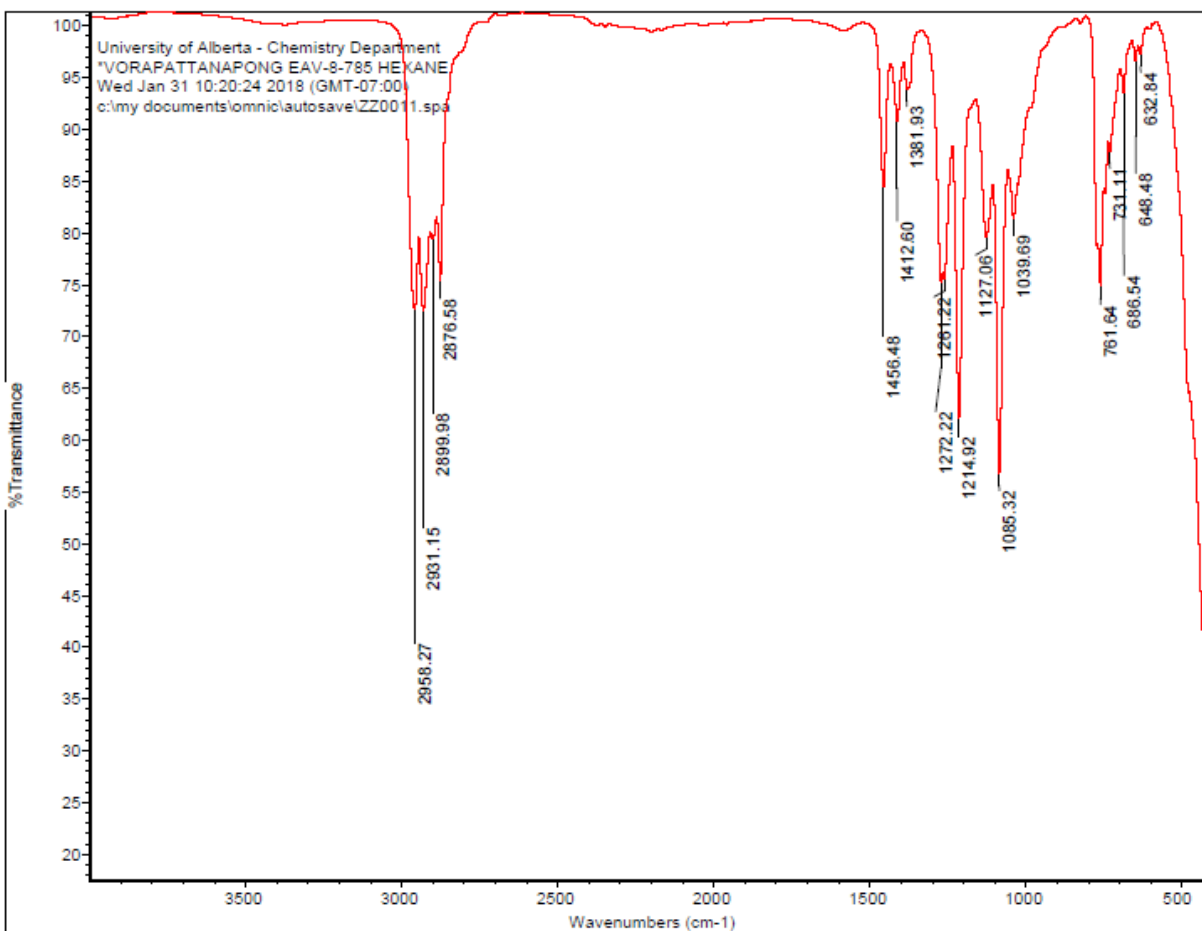
Section 5.3.6.2



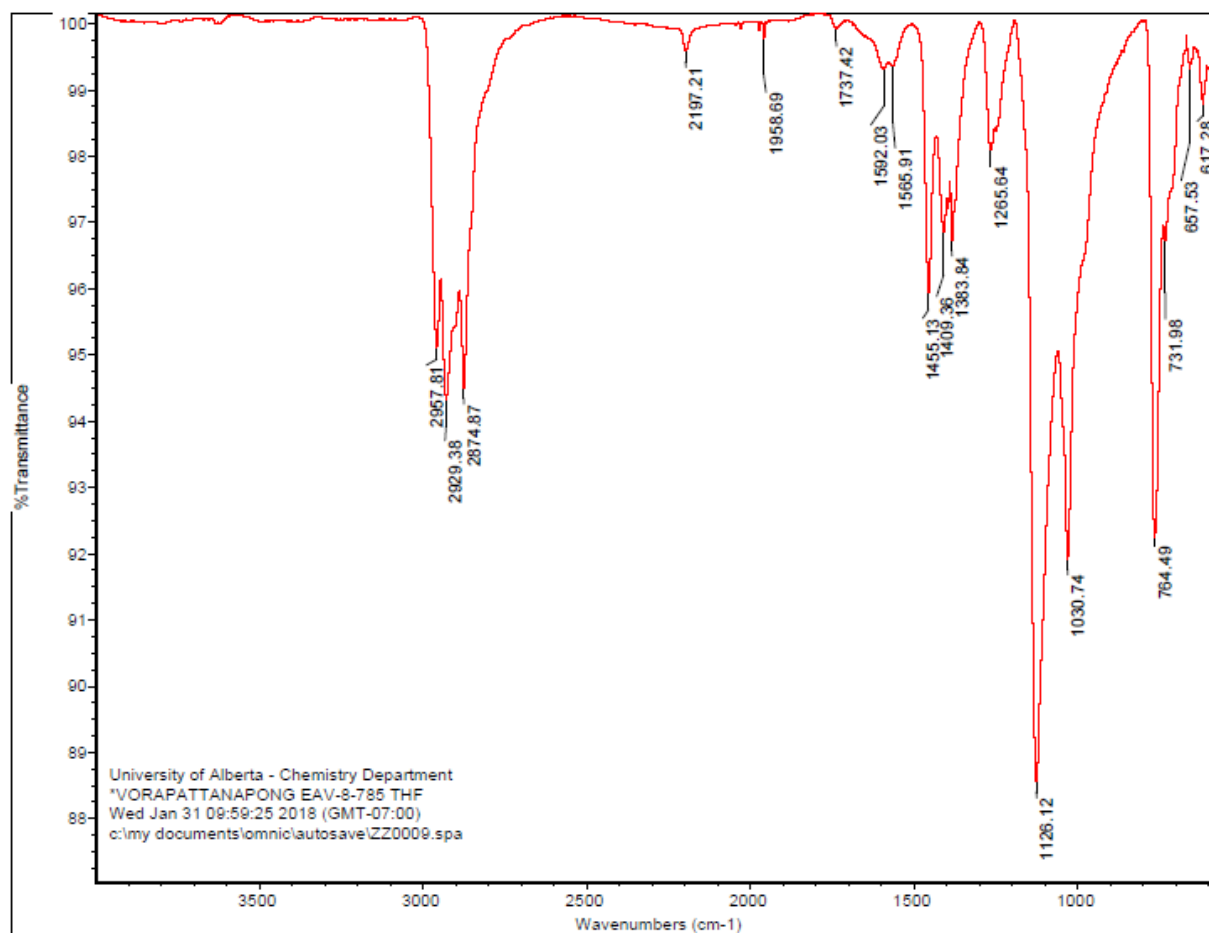
Section 5.3.6.3



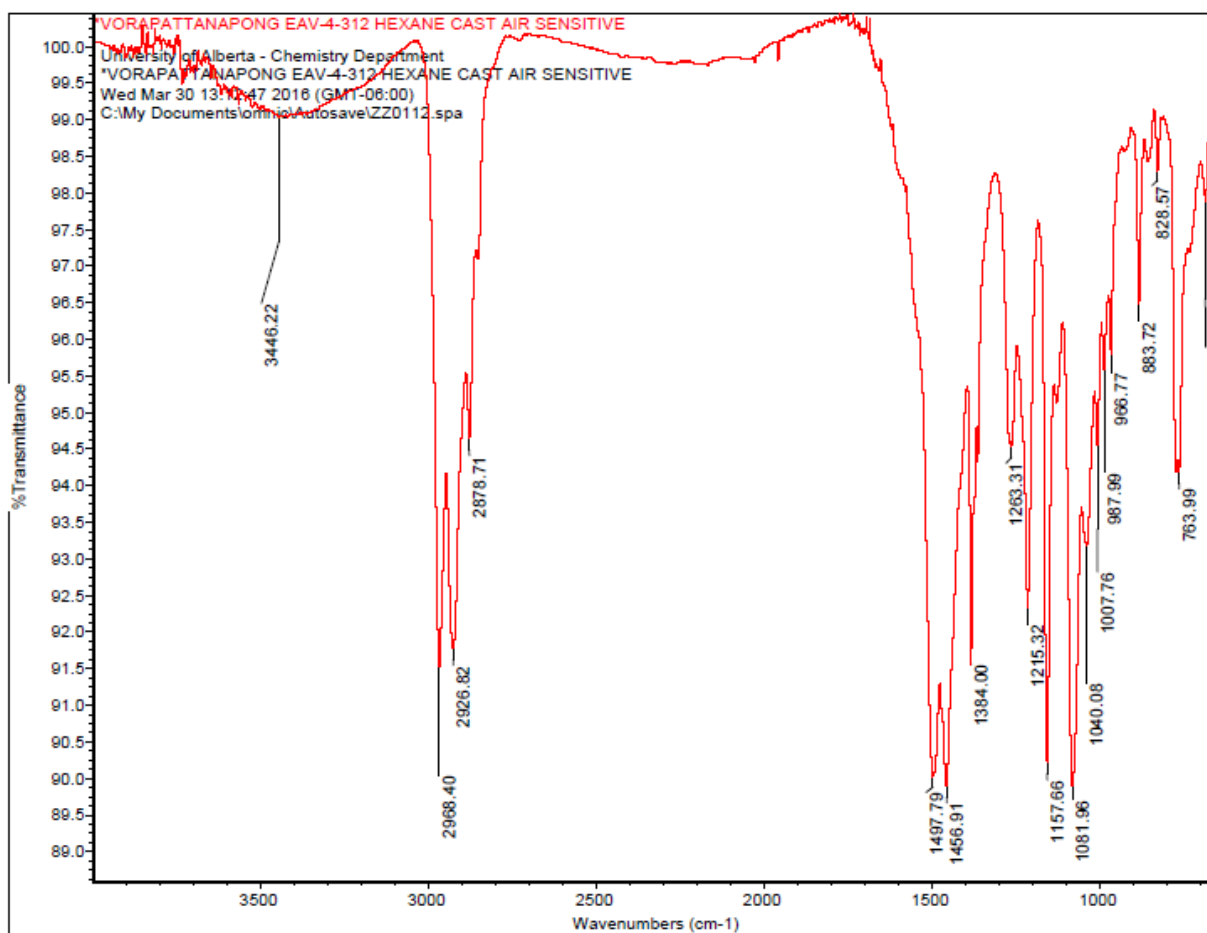
Section 5.3.7 – Hexane-soluble fraction



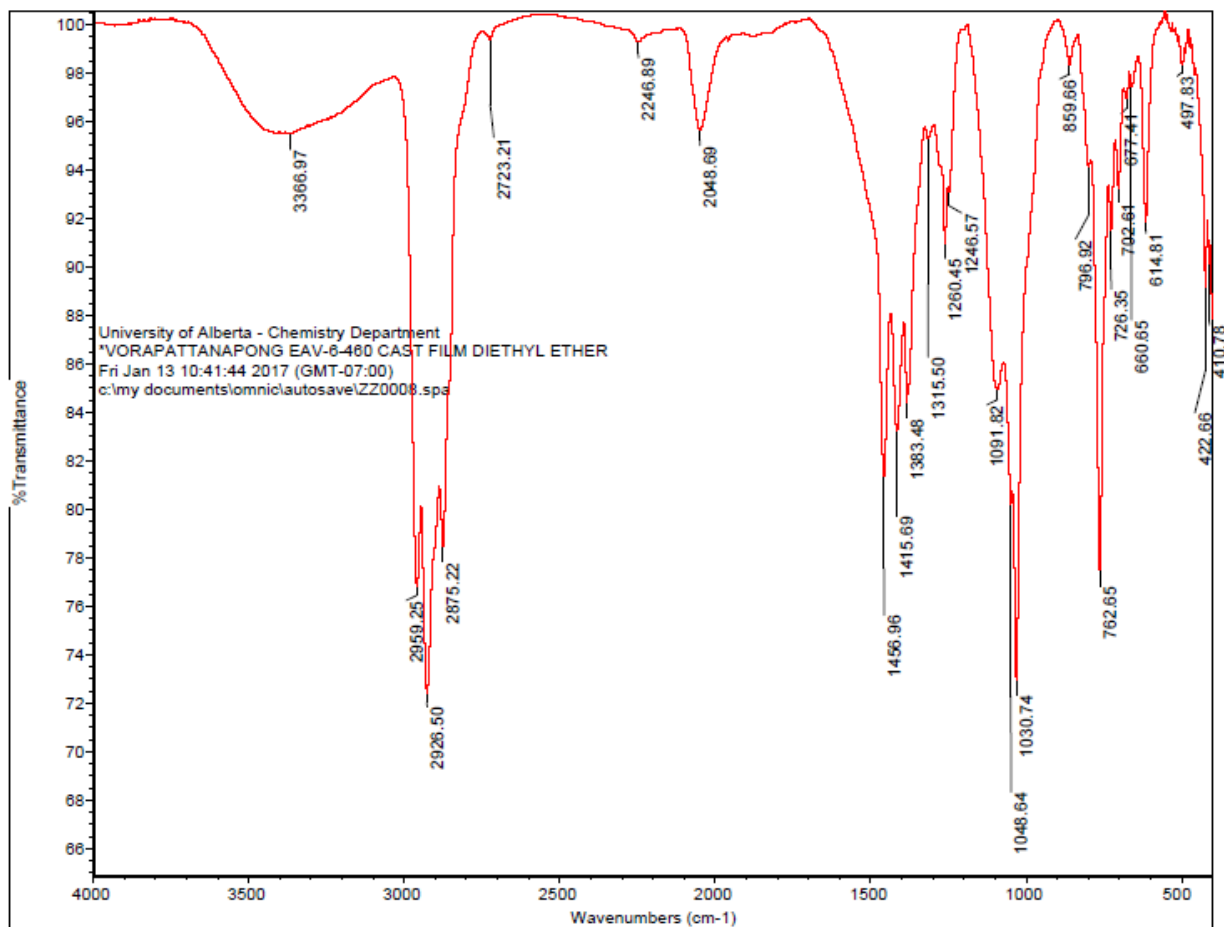
Section 5.3.7 – THF-soluble fraction



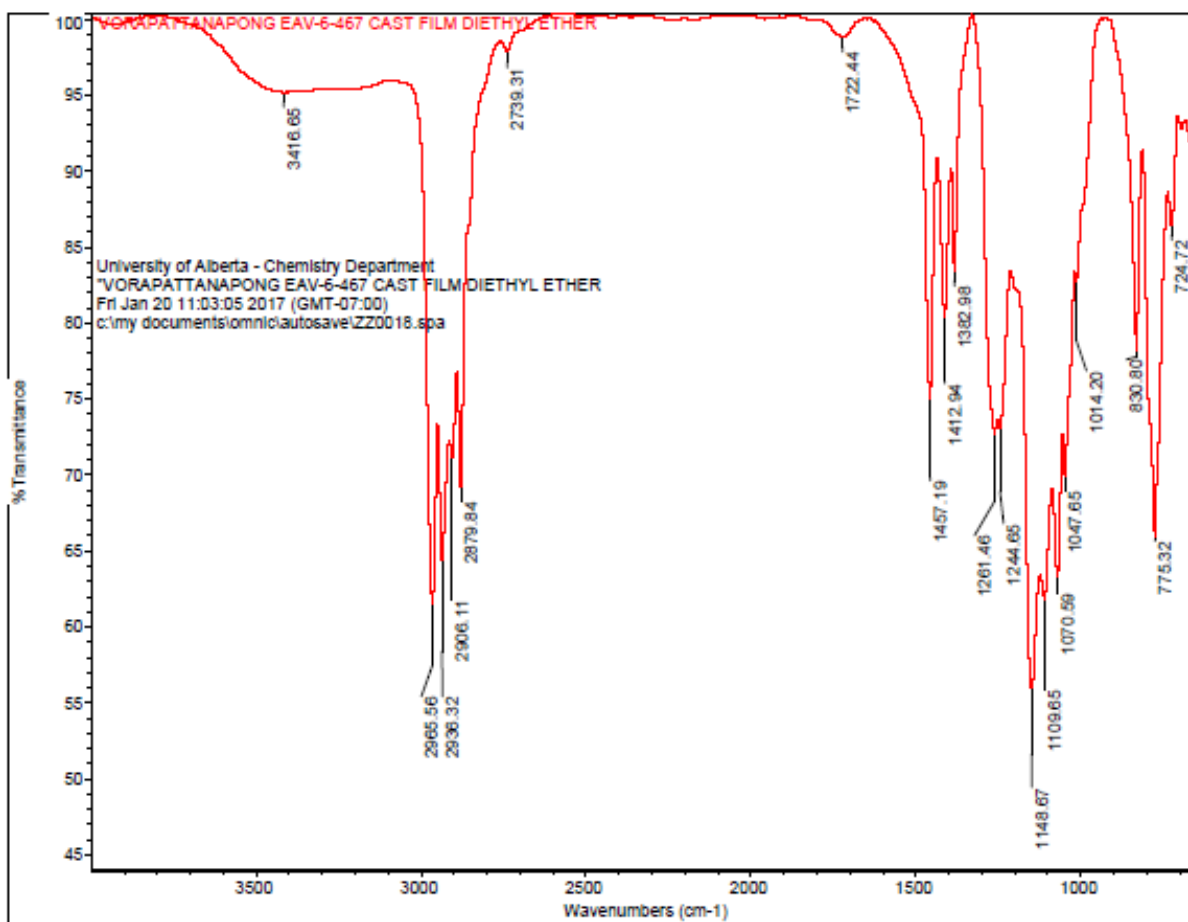
Section 5.3.9



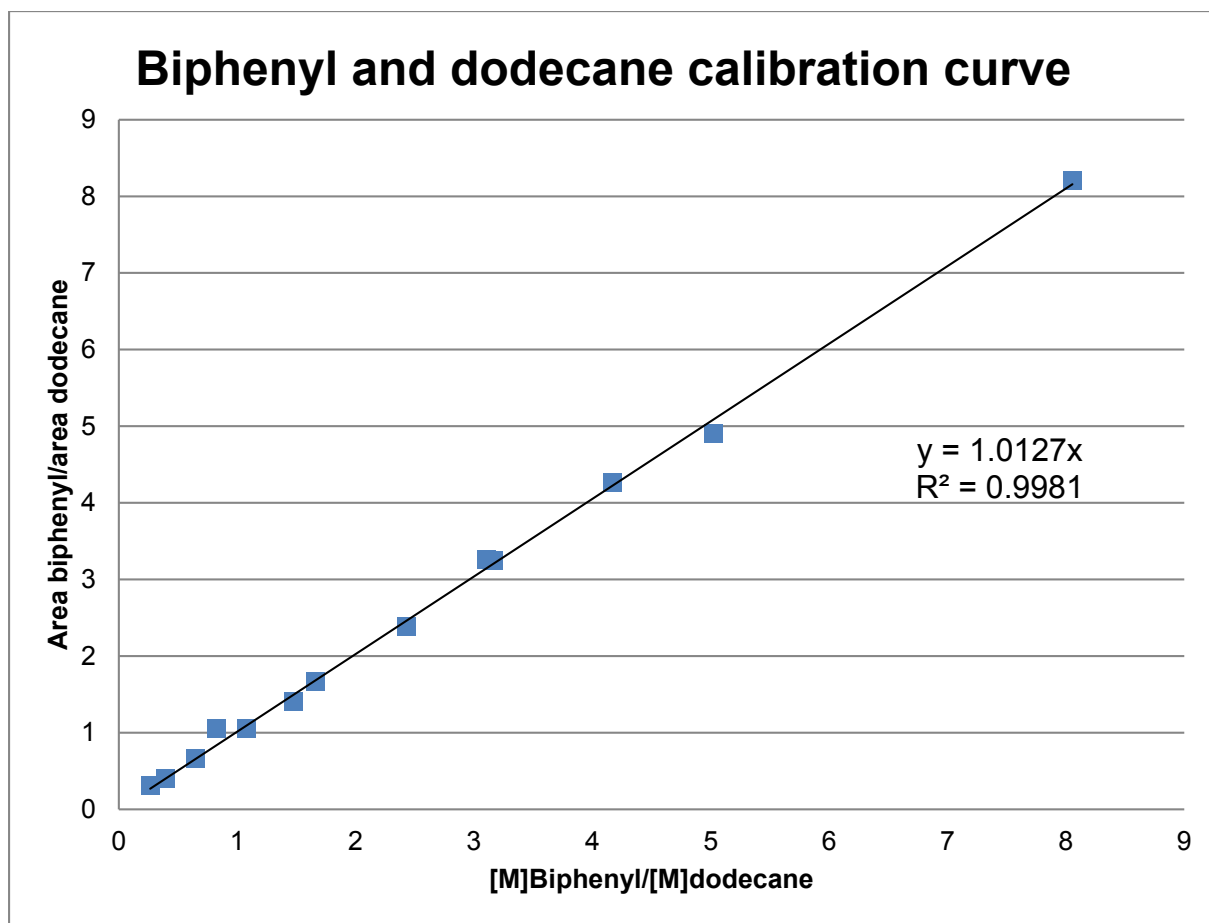
Section 5.3.10



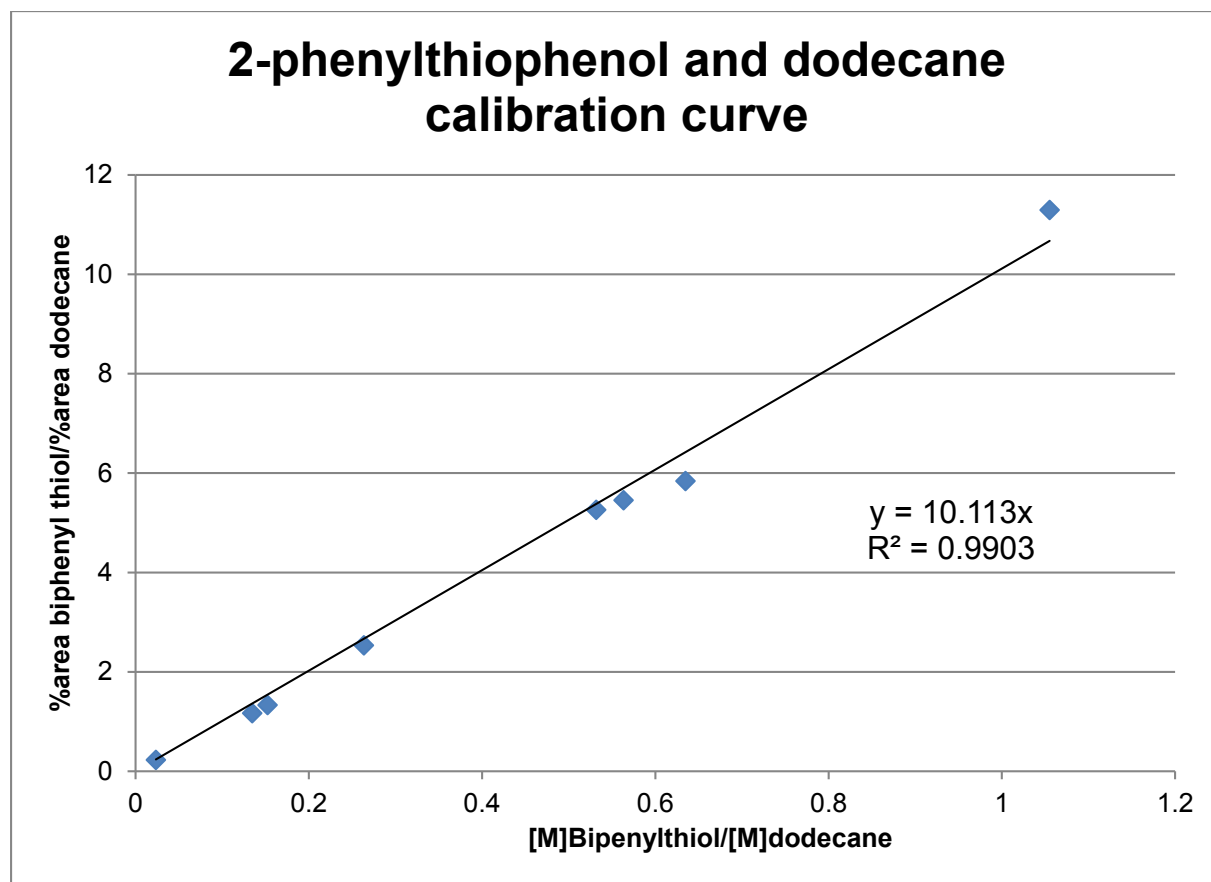
Section 5.3.11



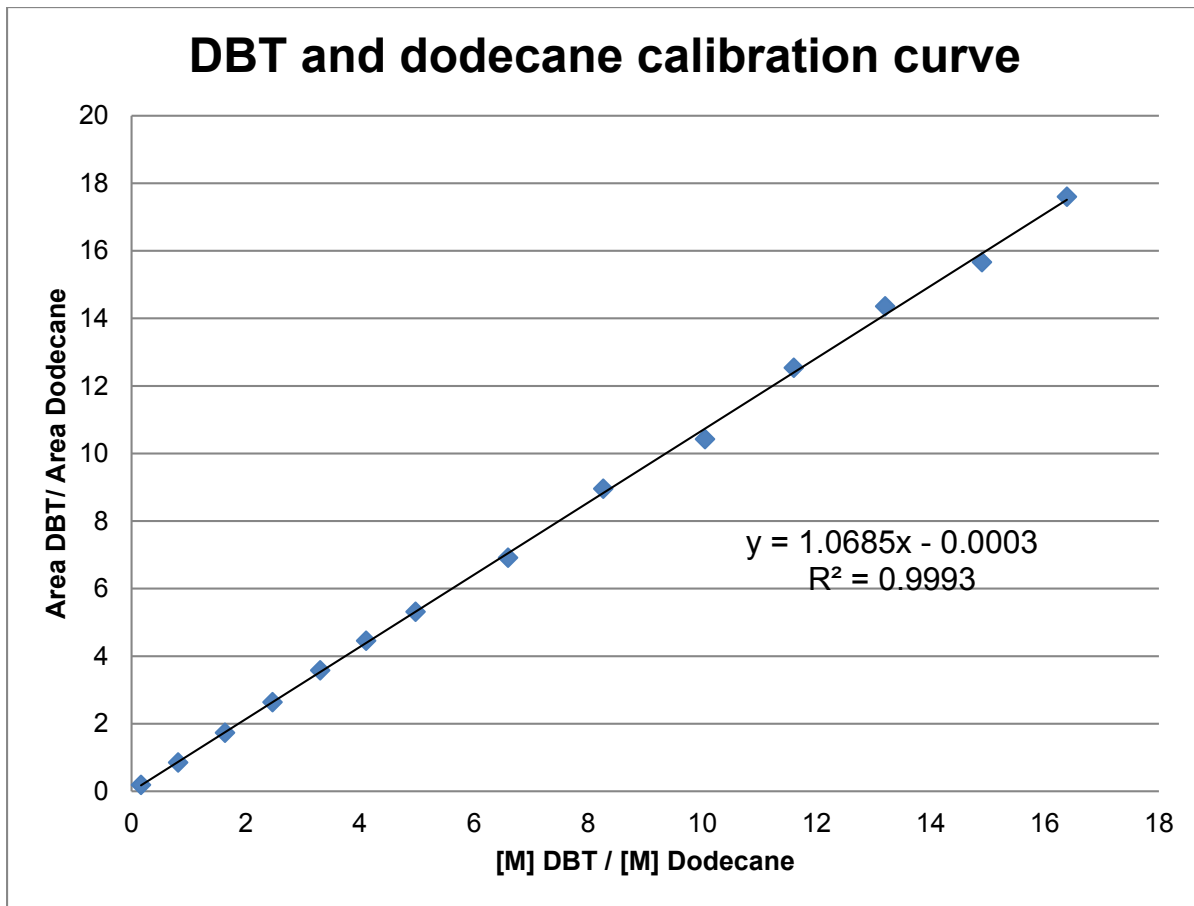
Appendix VIII: Calibration curve for biphenyl: from Dr. Samuel Mitton



Appendix IX: Calibration curve for 2-phenylthiophenol: from Dr. Samuel Mitton



Appendix X: Calibration curve for dibenzothiophene:



Appendix XI: Sample GC-MS analysis: chromatogram and mass spectrometry spectra of products from a HDS reaction.

Area Percent Report

Data File : E:\20180215\0401004.D Vial: 4
Acq On : 15 Feb 2018 13:20 Operator: JMJ
Sample : VORAPATTANAPONG EAV-8-788 Inst : GCMS1
Misc : THF/ETHER Multiplr: 1.00
Sample Amount: 0.00

MS Integration Params: autoint1.e

Method : C:\HPCHEM\1\METHODS\DEFAULT.M (Chemstation Integrator)
Title :

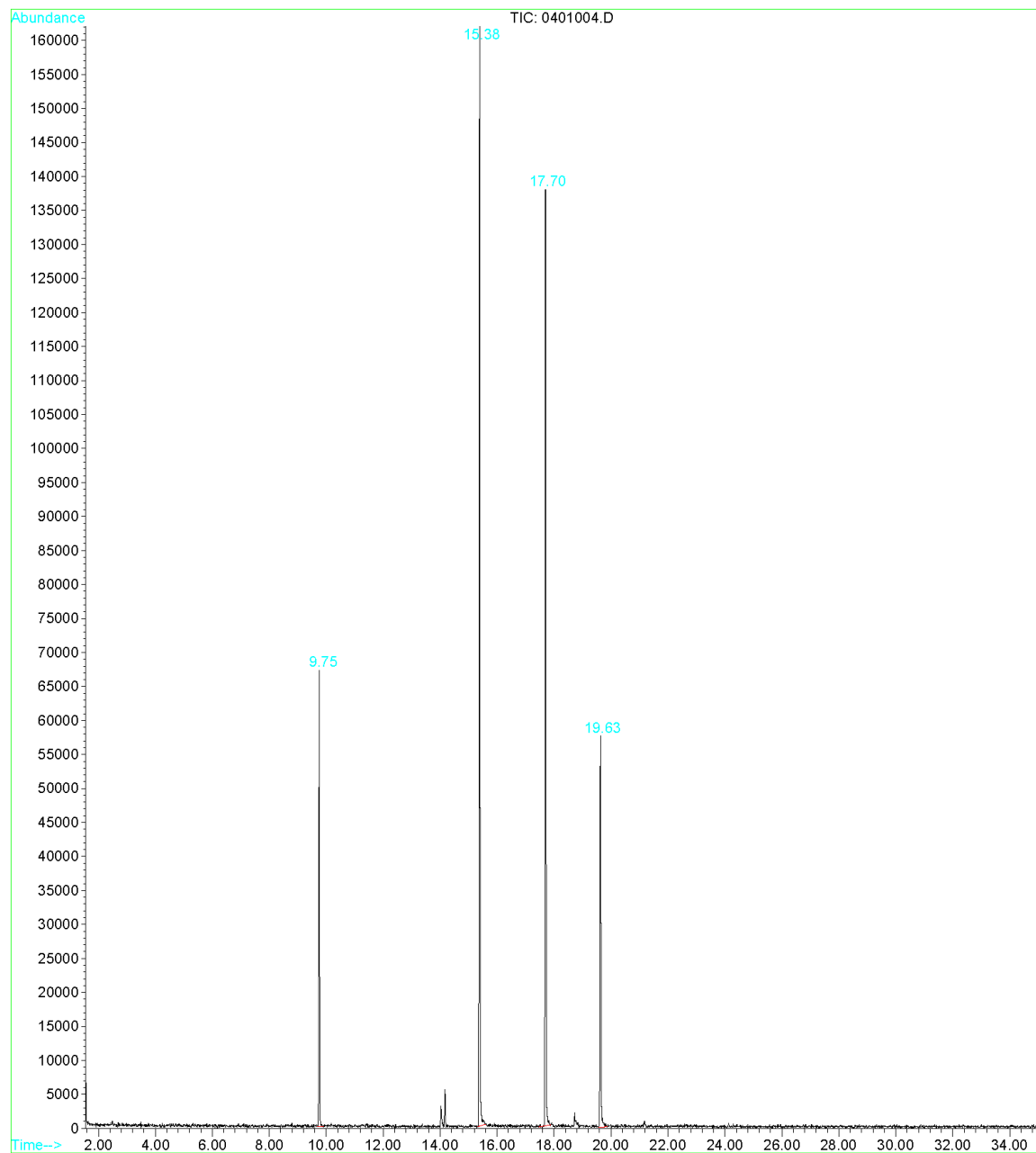
Signal : TIC

peak #	R.T. min	first scan	max scan	last scan	PK TY	peak height	peak area	peak % max.	% of total
1	9.747	717	721	735	BB	62450	1061422	32.54%	12.584%
2	15.386	1209	1215	1233	BB	160533	3261716	100.00%	38.670%
3	17.707	1398	1418	1433	BB	138563	2842395	87.14%	33.698%
4	19.631	1580	1586	1607	BB	56479	1269290	38.91%	15.048%

Sum of corrected areas: 8434824

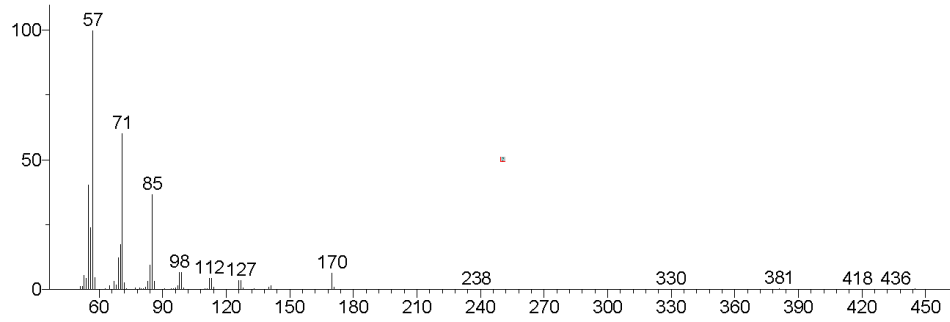
0401004.D DEFAULT.M Thu Feb 15 13:48:05 2018

File : E:\20180215\0401004.D
Operator : JMJ
Acquired : 15 Feb 2018 13:20 using AcqMethod GCMS-DB5
Instrument : GCMS1
Sample Name: VORAPATTANAPONG EAV-8-788
Misc Info : THF/ETHER
Vial Number: 4

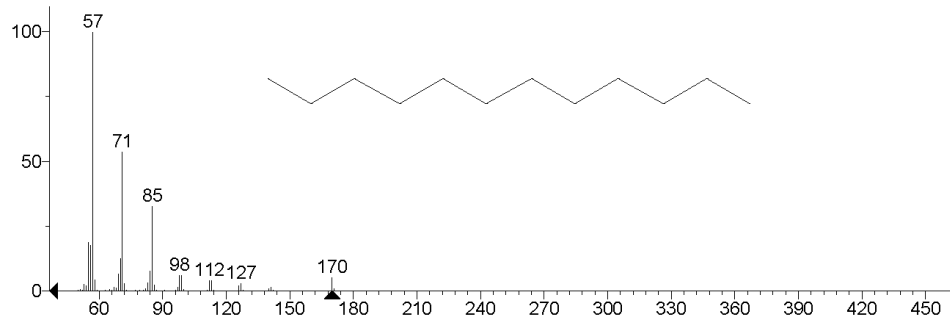


** Search Report Page 1 of 1 **

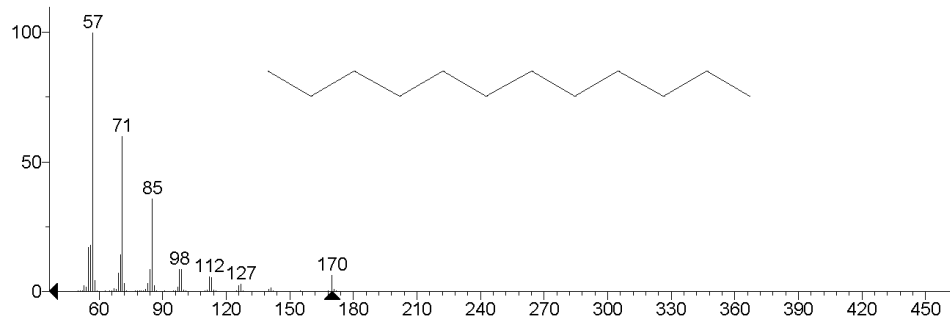
Unknown: Scan 721 (9.747 min); 0401004.D
Compound in Library Factor = 177



Hit 1 : Dodecane
C₁₂H₂₆; MF: 924; RMF: 929; Prob 38.3%; CAS: 112-40-3; Lib: mainlib; ID: 22550.

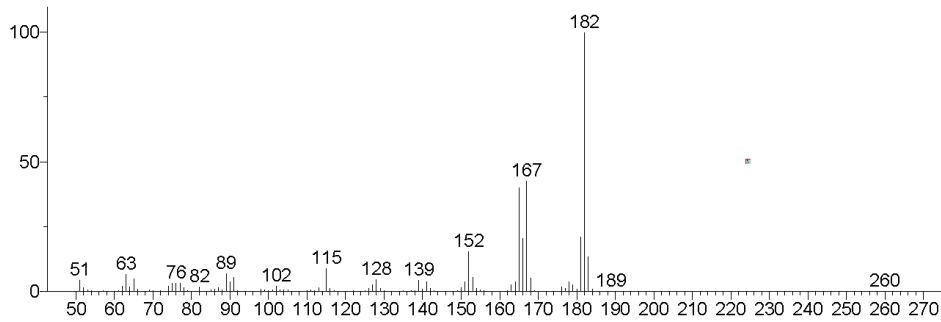


Hit 2 : Dodecane
C₁₂H₂₆; MF: 916; RMF: 922; Prob 38.3%; CAS: 112-40-3; Lib: replib; ID: 5782.

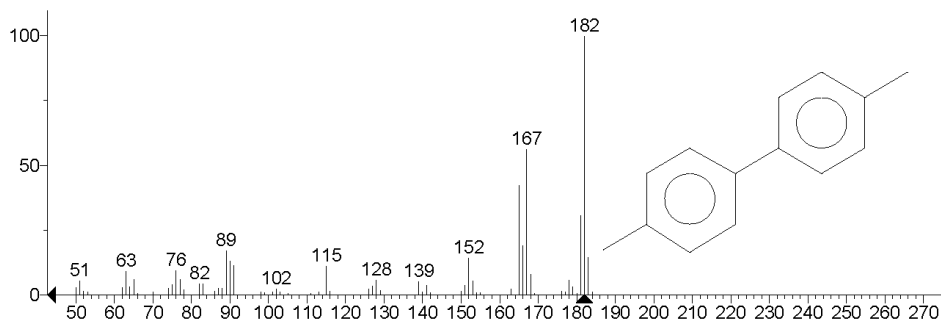


** Search Report Page 1 of 1 **

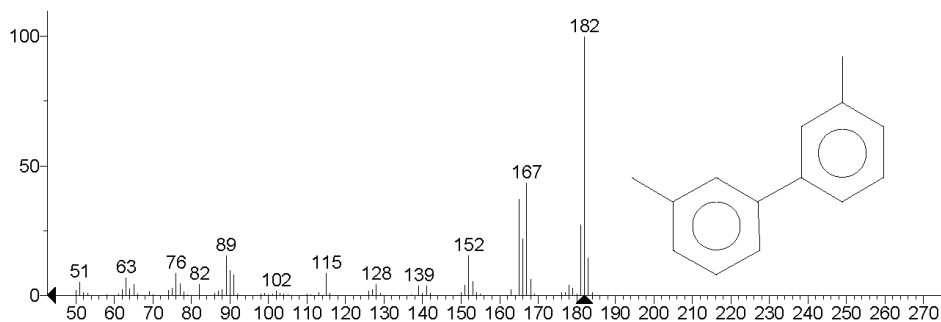
Unknown: Scan 1215 (15.386 min): 0401004.D
Compound in Library Factor = -113



Hit 1 : 4,4'-Dimethylbiphenyl
C₁₄H₁₄; MF: 918; RMF: 928; Prob 25.8%; CAS: 613-33-2; Lib: replib; ID: 25162.

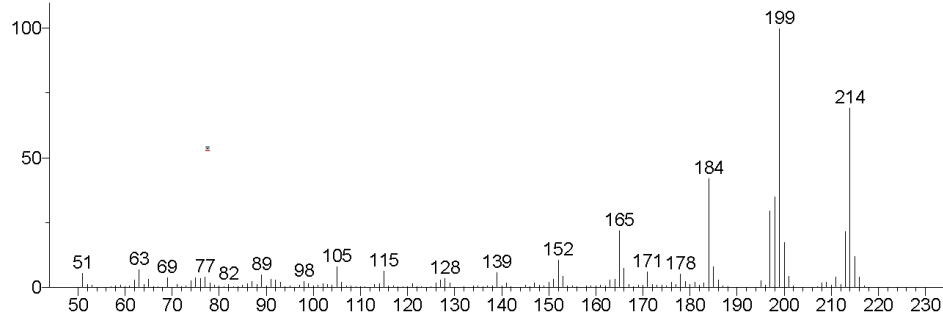


Hit 2 : 3,3'-Dimethylbiphenyl
C₁₄H₁₄; MF: 908; RMF: 916; Prob 18.2%; CAS: 612-75-9; Lib: replib; ID: 25161.

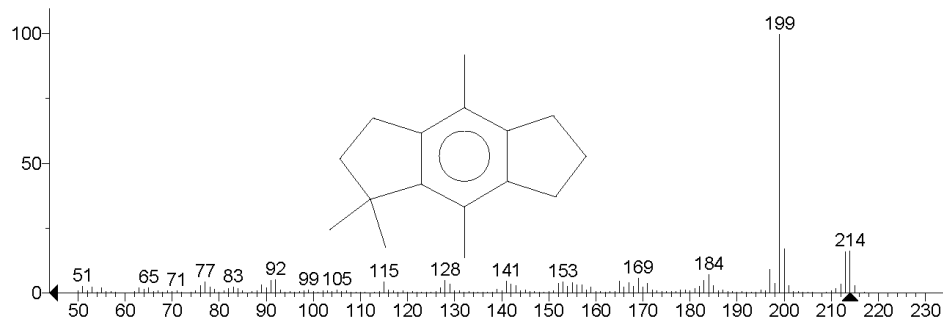


** Search Report Page 1 of 1 **

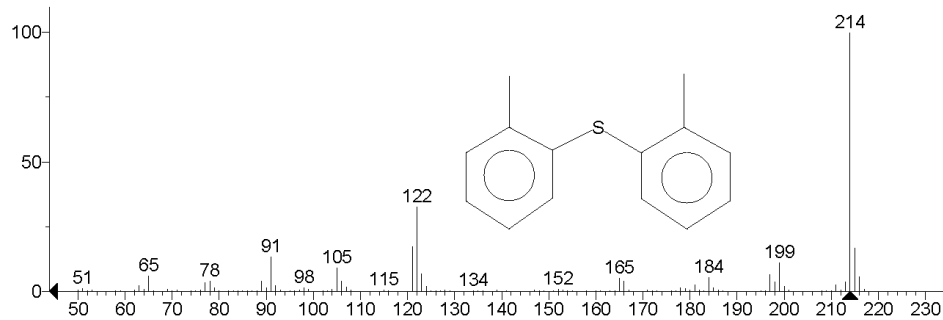
Unknown: Average of 17.684 to 17.707 min.: 0401004.D
Compound in Library Factor = -695



Hit 1 : s-Indacene, 1,2,3,5,6,7-hexahydro-1,1,4,8-tetramethyl-
C16H22; MF: 719; RMF: 725; Prob 54.6%; CAS: 55030-60-9; Lib: mainlib; ID: 162198.

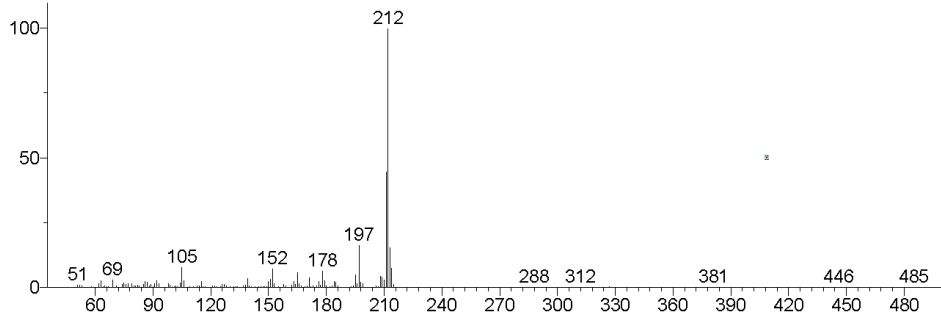


Hit 2 : Benzene, 1,1'-thiobis[2-methyl-
C14H14S; MF: 688; RMF: 696; Prob 14.9%; CAS: 4537-05-7; Lib: mainlib; ID: 169619.

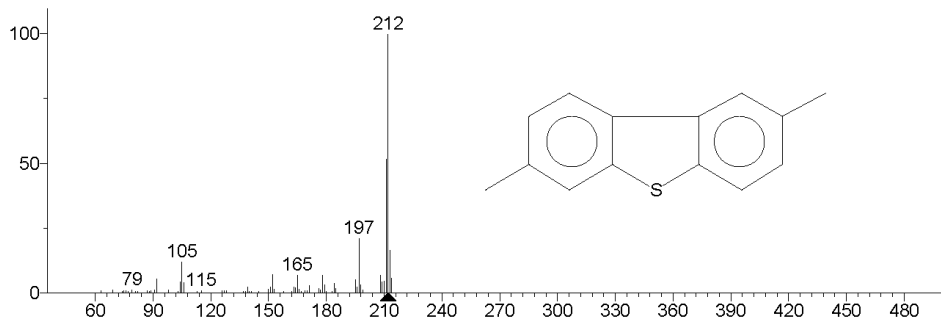


** Search Report Page 1 of 1 **

Unknown: Scan 1586 (19.631 min): 0401004.D
Compound in Library Factor = 367



Hit 1 : 2,7-Dimethyldibenzothiophene
C₁₄H₁₂S; MF: 894; RMF: 918; Prob 26.9%; CAS: 31317-19-8; Lib: mainlib; ID: 168891.



Hit 2 : 2,6-Dimethyldibenzothiophene
C₁₄H₁₂S; MF: 880; RMF: 902; Prob 16.8%; CAS: 89816-75-1; Lib: mainlib; ID: 168880.

